NASA Contractor Report 195469

Propulsion System Assessment for Very High Altitude UAV Under ERAST

James L. Bettner, Craig S. Blandford, and Bernie J. Rezy
Allison Engine Company
Indianapolis, Indiana

May 1995

Prepared for
Lewis Research Center
Under Contract NAS3–25950

National Aeronautics and
Space Administration

NASA CR-195469
EDR 17199

Propulsion System Assessment for Very High Altitude UAV under ERAST

James L. Bettner, Craig S. Blandford, and Bernie J. Rezy
Allison Engine Company
Indianapolis, Indiana

Final Report

May 1995

Prepared for
NATIONAL AERONAUTICS AND SPACE ADMINISTRATION
Lewis Research Center
Under Contract NAS3-25950
Task Order No. 21

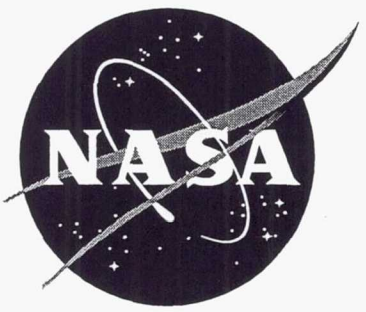

TABLE OF CONTENTS

TABLE OF CONTENTS (cont)

TABLE OF CONTENTS (cont)

LIST OF ILLUSTRATIONS

LIST OF ILLUSTRATIONS (cont)

LIST OF ILLUSTRATIONS (cont)

LIST OF ILLUSTRATIONS (cont)

LIST OF TABLES

1.0 INTRODUCTION

NASA is embarking on an initiative called the Environmental Research Aircraft and Sensor Technology (ERAST) program. This program will focus on the study and development of technology for advanced, unmanned aerial vehicles (UAVs) that can meet the altitude and endurance needs of the environmental science community. This very high altitude class of UAV will be used primarily to collect air samples in the stratosphere; these samples would then be analyzed to determine the presence and concentrations of particular chemical species (ozone, CFCs, nitrogen oxides, etc). The very high altitude UAVs are considered to be of great national importance and are essential for the investigation and modeling of global atmospheric change.

A series of propulsion systems employing state-of-the-art (SOA), near-term (NT), and advanced technologies was configured to power a sensor platform to very high altitudes. Its requirements were to carry a 100 kg instrument package to 90,000 ft altitude, collect samples, make scientific measurements for 4 hr, and then return to base.

Allison's product line includes turboshaft, turboprop, and turbofan propulsion systems. Also, Allison has developed a series of spark ignition, diesel, rotary, and fuel cell engine performance models. Allison was selected to conduct this propulsion system screening study, which examined a wide range of propulsion system concepts, applied a consistent set of requirements and a design philosophy to all concepts, and provided a ranking of the concepts. Aircraft takeoff gross weight (TOGW) was selected as the principal evaluation metric.

For this high altitude mission, a preliminary design performance screening evaluation of 11 propulsion systems was conducted in terms of mission suitability, risk, and cost. The propulsion system employing SOA technology that was best matched for this very high altitude mission was identified as the four-stroke, non-turbo-compounded diesel. The best-matched NT technology concept was the Coleman engine and the best advanced concept was the two-stroke, non-turbo-compounded diesel engine. It is recommended that these concepts be further investigated to optimize performance, size, power, and aircraft installation requirements.

2.0 SUMMARY

The overall objectives of this study were: to interrogate a variety of propulsion systems of varying technology levels with high potential for powering an aircraft to 90,000 ft and loitering there before returning to base; to provide preliminary designs of these candidates sized to 300 shp at mission altitude for use in follow-on mission studies; and to make a first pass at how these engines might fare against one another in powering a representative environmental science aircraft with the aforementioned goals.

State-of-the-art (SOA), near-term (NT), and advanced technology concepts were considered. SOA technology was defined as demonstrable today to fixed price and performance. NT was defined as needing only minor hardware technology development before demonstration, and advanced concepts required technology development before concept demonstration. Eleven engine configurations ranging from turboprop, spark ignition, two- and four-stroke diesel, rotary, and fuel cell concepts were analyzed. A twelfth powerplant candidate was evaluated by running the Rc = 20 turboshaft on hydrogen fuel. This was not a new configuration though, because none of the engine hardware was changed. Turbo- and non-turbo-compounded, recuperated, and nonrecuperated arrangements, along with regular JP, hydrogen fuels, and Avgas were interrogated. Each configuration was carried through a preliminary design where all turbomachinery, heat exchangers, and engine core components were sized and weighed for near optimum design point performance.

All of the engine concepts, except the turboshaft configurations, required high levels of turbocharging with subsequent intercooling. This was necessary to present acceptable thermodynamic conditions to the inlet of the respective engine concept. All propulsion systems (engine, reduction gearbox, and propeller) were designed to produce 300 shp at design altitude cruise flight conditions. All of the configurations analyzed are presented in Figure 1.

Finally, mission analysis was conducted with each resulting concept using a NASA Ames supplied baseline aircraft description. The intention of this part of the study was to provide a first pass at the applicability, takeoff gross weight (TOGW), scaling trends, and initial ranking of all propulsion systems considered. All mission analysis was completed using aircraft lift/drag characteristics that were provided by NASA Ames Laboratory and scaled from the Stratolite high altitude UAV presented in Figure 2.

Aircraft geometry and weight, fuel volume, and propulsion system geometry and weight were varied together to meet the mission requirements. A summary of the mission analysis results for all engine concepts investigated is illustrated in Table 1. The results of Table 1 show the variation of aircraft TOGW, aircraft overall dimensions, power levels, engine/propulsion system weight requirements for the aircraft to takeoff, climb to altitude, cruise at 90,000 ft for 4 hr with the designated payload, and then return to base. No converged solution was obtained with the 16:1 Rc recuperated turboshaft configuration. Also, a design point fuel cell engine configuration was developed, but no off-design point and, therefore, no mission analysis was completed for the fuel cell concept.

All of the propulsion system concepts investigated in each of the three technology categories were ranked with respect to their mission suitability, risk, and cost. In addition, a weighting factor philosophy was applied that allowed the ranking process to reflect a larger importance to mission suitability, followed by risk, and finally propulsion system cost. The following considerations were applied in the ranking process:

- The ERAST mission had to be accomplished in terms of attaining altitude and duration with required payload.
- Aircraft TOGW was the principal evaluation metric.
- Risk ranking was strongly influenced by system complexity, engine technology level, prior demonstration of the basic cycle concept, and past experience of engine concept operation at relatively high altitudes.

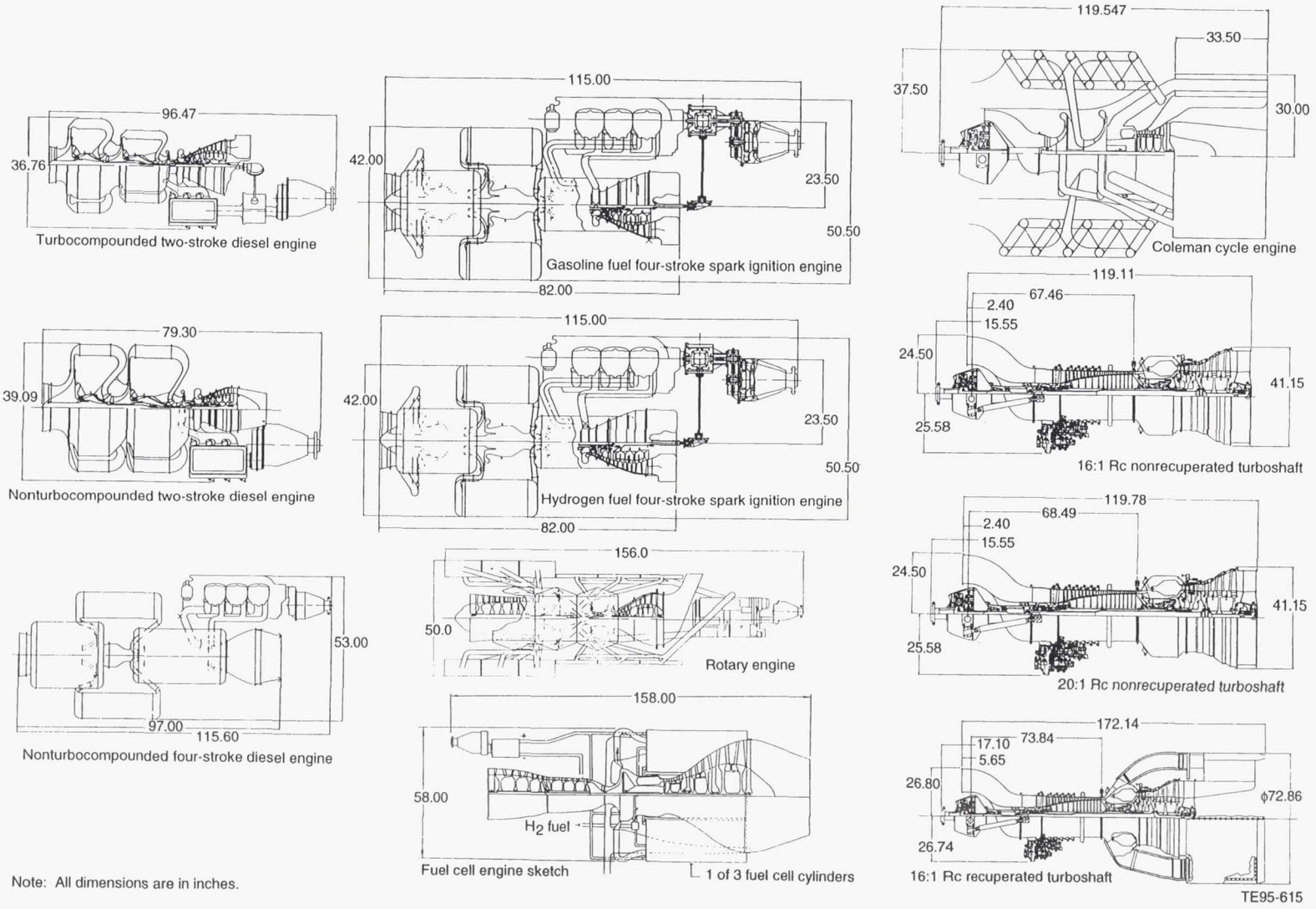

Figure 1. ERAST candidate propulsion systems.

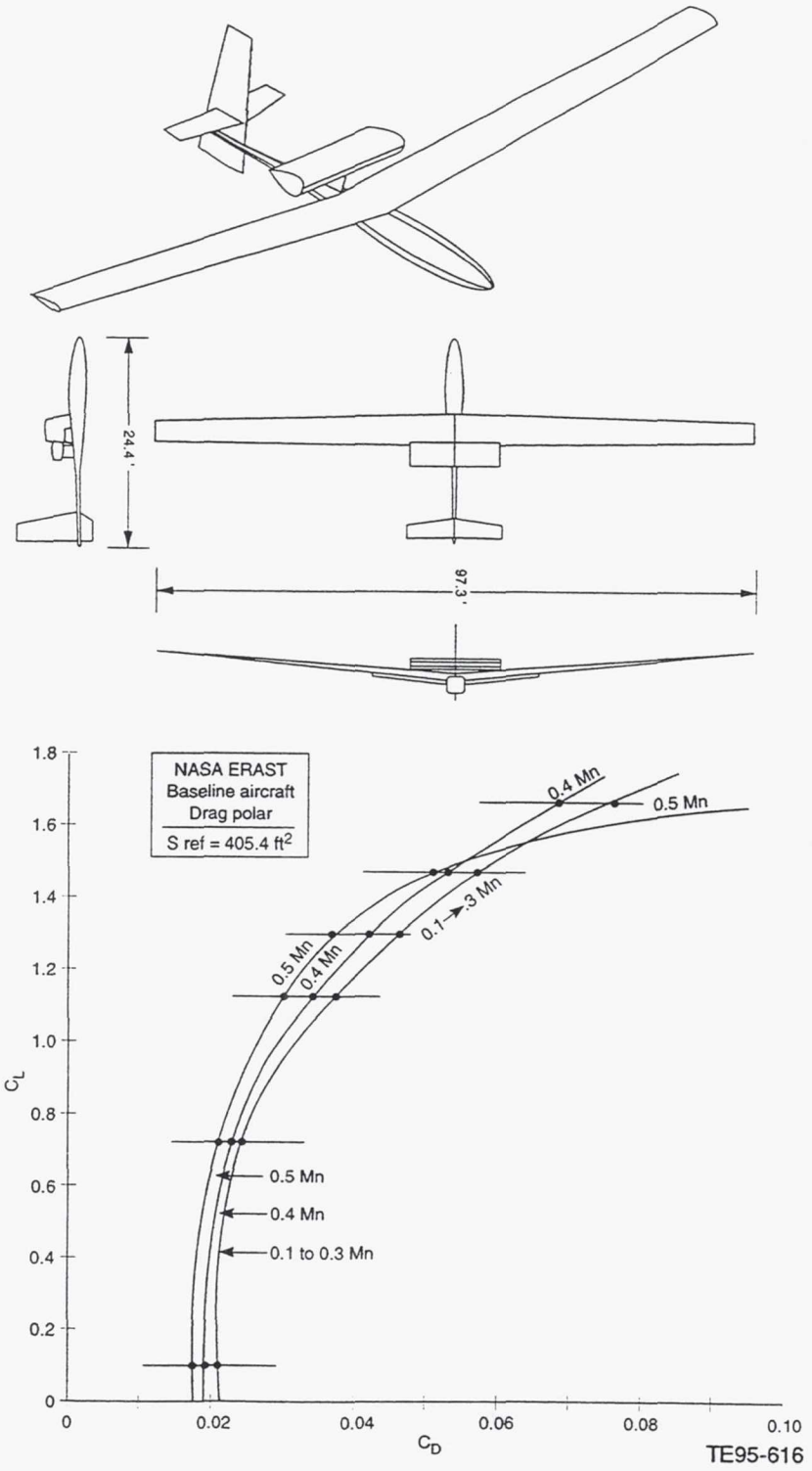

Figure 2. Stratolite reference airplane.

Table 1.
Mission analysis summary.

Technology Level	ADV	ADV	SOA	SOA	NT	NT	NT	SOA	NT	NT	NT	ADV
Engine Description	2 Stroke Diesel Turbo	2 Stroke Diesel	4 Stroke Diesel	4 Stroke Spark Turbo	4 Stroke Spark Turbo	Rotary	Coleman Recup	Turboshaft Rc = 16	Turboshaft Rc = 20	Turboshaft Rc = 20	Turboshaft Rc = 16 Recup	Fuel Cell
Fuel Type	Diesel	Diesel	Diesel	Avgas	H2	Diesel	JP-5	JP-5	JP-5	H2	JP-5	H2
											No solution	No solution
Aircraft Characteristics :												
Aircraft TOGW, lb	1956	1532	2639	2656	3325	3203	2486	3302	3166	4069		
Wing Area, sq ft	264	207	356	359	449	433	336	446	428	550		
Fuselage Length, ft	22.0	21.7	24.4	24.0	24.6	26.1	25.2	23.6	23.5	24.1		
Fuselage Diameter, ft	2.7	2.7	3.0	3.0	3.0	3.2	3.1	2.9	2.9	3.0		
Powerplant Characteristics :												
Engine Scale (Sized SHP/Unity SHP)	0.297	0.220	0.410	0.399	0.506	0.500	0.294	0.344	0.334	0.447		
Sized SHP (@0.4M/90K), hp	89	66	123	120	152	150	98	103	100	134		
Max Power Level, hp	256	140	125	190	286	150	470	551	534	716		
Engine Weight, lb	246	170	637	516	631	785	442	865	823	1106		
Reduction Gearbox Weight, lb	214	61	94	227	290	73	96	121	118	150		
Propeller Weight, lb	202	173	150	174	194	156	245	256	254	269		
Total Propulsion System Weight, lb	662	404	881	917	1115	1014	783	1242	1195	1525		
Propeller Diameter, ft	15.2	13.1	17.9	17.7	19.9	19.8	15.9	16.4	16.2	18.7		
Max Endurance Cruise @ 90K (4 hrs) :												
Initial Mn	0.49	0.48	0.48	0.49	0.50	0.46	0.48	0.51	0.51	0.52		
Final Mn	0.48	0.47	0.46	0.47	0.50	0.44	0.46	0.49	0.49	0.51		
Percent Thrust, %	83	84	87	83	84	85	96	100	100	100		
TSFCavg, lb/hr/hp	0.258	0.274	0.355	0.374	0.107	0.410	0.422	0.489	0.473	0.167		
Mission Fuel Burn, lb	128	114	274	261	94	430	255	344	313	148		

- Cost ranking was influenced principally by propulsion system complexity and engine weight.
- Weighting factors were established to illustrate the relative importance of the three ranked categories. Weighting factors were as follows:
  - mission suitability 0.5
  - risk 0.3
  - cost 0.2
  - 1.0

Results of the ranking process are summarized in Table 2. The propulsion system employing SOA technology that was best matched for this mission was the four-stroke, non-turbo-compounded diesel. The best matched NT technology concept was the Coleman engine and the best advanced concept was the two-stroke, non-turbo-compounded diesel engine. It is recommended that these concepts be further investigated for improved performance, detailed installation size, and arrangement limitations and subsequent weight analysis.

Table 2.
ERAST propulsion system concept ranking.

Technology Level Engine Description		SOA 4 Stroke Diesel	SOA 4 Stroke Spark Turbo	SOA Turboshaft Rc=16	NT Coleman	NT Rotary	NT Turboshaft Rc=20	NT 4 Stroke Spark Turbo	NT Turboshaft Rc=20	NT Turboshaft Rc=16 Recup	ADV 2 Stroke Diesel	ADV 2 Stroke Diesel Turbo	ADV Fuel Cell
Fuel Type		Diesel	Avgas	JP-5	JP-5	Diesel	JP-5	H2	H2	JP-5	Diesel	Diesel	H2
Mission Suitability (Weighting Factor=0.5)	Rank	7	7	5	8	6	6	5	3	1	10	9	1
	Sub Total	3.5	3.5	2.5	4	3	3	2.5	1.5	0.5	5	4.5	0.5
Risk (Weighting Factor=0.3)	Rank	8	7	10	6	7	9	5	6	9	6	5	1
	Sub Total	2.4	2.1	3	1.8	2.1	2.7	1.5	1.8	2.7	1.8	1.5	0.3
Cost (Weighting Factor=0.2)	Rank	9	10	4	7	8	4	6	4	4	7	6	1
	Sub Total	1.8	2	0.8	1.4	1.6	0.8	1.2	0.8	0.8	1.4	1.2	0.2
	Total	7.7	7.6	6.3	7.2	6.7	6.5	5.2	4.1	4	8.2	7.2	1
	Group Ranking	1	2	3	1	2	3	4	5	6	1	2	3
	Overall Ranking	2	3	7	4	5	6	8	9	10	1	4	11
		I<------- SOA = State of the Art ------->			I<---------- NT = Near Term technology ---------->						I<--- ADV = Advanced tech -->		

3.0 TECHNICAL APPROACH

3.1 CYCLE ANALYSIS

3.1.1 Two Stroke Opposed-Piston Diesel Engine - Advanced Technology

A computer program was developed to simulate two- and four-stroke diesel engine performance. The Benson ideal Dual Combustion/Diesel Cycle Program (presented in Reference 1) was updated to include engine block heat loss and piston friction loss modeling so that a more realistic diesel engine could be simulated. This program was then further calibrated with actual engine data.

The program used at Allison Engine Company to conduct engine cycle performance analysis is identified as TERMAP (Turbine Engine Reverse Modeling Aid Program). Because of its building block structure, TERMAP is easily adapted to new applications by the addition of new routines. Modeling of a turbocharged diesel was accomplished by replacing TERMAP's BURNER building block subroutine with the DIESEL program. These two programs were then run simultaneously to perform design point cycle analysis for turbocharged diesel engines.

The baseline two-stroke opposed-piston diesel used in this study is from a previously combined Allison/Detroit Diesel study conducted for potential Army and NASA funding. The engine is a horizontally opposed-piston configuration, highly turbocharged and turbo-compounded. Opposed-piston engines are not new; Fairbanks-Morse produced them for the Navy during World War II and still produce them today for marine applications. Likewise, turbo-compounding is not new; the Napier-Nomad engine very successfully used this concept.

The opposed-piston two-stroke diesel baseline uses the basic concept of the previously mentioned engines combined with increased engine speed, today's turbomachinery, advanced technology materials, and design concepts aimed at reducing weight and increasing specific power. Sea level, standard day performance, and configuration sizing are presented in Table 3.

Table 3.
Baseline opposed-piston two-stroke diesel.

Bore, in.	3.101
Stroke, in.	2.94
Number of cylinders/pistons	3/6
Displacement, $in.^3$	133.2
Engine speed, rpm	6122
Compression ratio	9.2
Turbocharger boost pressure, psia	140
Shaft horsepower	1000
Diesel % power	78
Turbine % power	22
BSFC, lb/hp-hr	0.316
Peak firing pressure, psia	2950
Brake mean effective pressure, psia	400
Piston speed, ft/min	3000

This compact design offers excellent diesel core power density (5.86 $hp/in.^3$) and fuel efficiency sufficient to be very competitive with gas turbine engines in some applications, such as helicopters.

The baseline diesel concept was modified as discussed in this section for high altitude applications. Peak cylinder pressures were held relatively constant by decreasing the amount of boost pressure and

increasing engine effective compression ratio (CR). This trade provides the lowest turbocharger pressure ratio.

The ambient pressure at 90,000 ft is 0.25 psia. To provide the specific power of at least a naturally aspirated engine requires an inlet pressure of at least 1 atmosphere (14.696 psia) and this requires the turbocharger overall pressure ratio (OPR) to be at least 60:1. This level of OPR can be achieved only by using multistage compressors. To have a reasonable operating range for each compressor stage, its pressure ratio must not be excessive. For this reason, a three-stage compressor arrangement is required. With such a high OPR, there will be a significant difference in size and rotational speed between the three compressors. This dictates that each compressor should be on a separate spool. Also, such an arrangement gives the powerplant a high degree of self-matching capability when operating away from its design point.

Due to the high OPR, compressor and diesel inlet temperature limits require that there be intercooling between the compressors. The first intercooler effectiveness was selected to be 60% and the second intercooler effectiveness was chosen to be 65%. Setting the effectiveness of the first intercooler at 60% is a good trade between intercooler size required and compressor stage pressure ratio required to achieve a reasonably high level of air density from the low ambient inlet conditions. It was estimated at the beginning of this study that if the effectiveness of the second intercooler were increased 5%, then its resulting size would be close to the size of the first intercooler.

In the design point simulation of this powerplant, the airflow size of the turbomachinery was varied until the gas flow exiting the diesel equaled the sum of the airflow going into the pistons and the fuel flow added in the combustion part of the diesel cycle. Turbomachinery OPR was varied to get an initially assumed powerplant total output power of 300 shp.

3.1.1.1 Turbo-Compounded Two-Stroke Opposed-Piston Diesel - Advanced Technology

A configuration is referred to as turbo-compounded when the exit flow conditions from the low pressure (LP) turbine are expanded through a final power turbine to ambient conditions. This configuration enables maximum overall cycle efficiency since energy remaining in the gas stream is converted to shaft power. The penalty is the additional weight and complexity of adding the power turbine and gearboxes required to combine both the power turbine and diesel engine output shafts.

A parametric study at 90,000 ft, 0.4 Mach, 300 shp was performed to determine the optimum design for an advanced technology turbo-compounded diesel. Performance results for this study are shown in Figures 3 through 6. As noted previously, the baseline diesel had a bore of 3.101 in. and a compression ratio of 9.171. Different bore/stroke (2.75/2.607 and 3.6/3.412) sizes and higher compression ratios (12, 14, and 16) were evaluated. Notice that the baseline diesel bore/stroke ratio of 1.055 (3.101/2.94) was held when evaluating these new designs.

Smaller bore and stroke size diesels (<3.101 in.) were eliminated because the required OPR as shown in Figure 3 would increase the weight of the powerplant considerably. For this same reason, a larger bore of 3.6 in. was investigated since the OPR could be reduced down to around 70:1. Figure 3 also shows powerplant SFC to decrease as the diesel compression ratio (CR) is increased. A CR = 16 was chosen for this turbocharged diesel since the engine is showing diminishing returns and CR is approaching its upper limit.

Figure 4 shows how powerplant thermal efficiency and high pressure turbine, rotor inlet temperature (HPT RIT) varies with bore size and CR. This plot shows another benefit of selecting a higher CR diesel, which is that the RIT/exhaust gas temperature (EGT) is reduced to low enough levels that the HPT in this engine would be uncooled. Another benefit of increasing CR is that powerplant airflow size is reduced, as illustrated in Figure 5. Figure 6 shows how the diesel peak cylinder pressure and temperature vary with bore size and CR. The selected design (CR = 16 and bore = 3.6 in.) is low in peak pressure due to the low inlet manifold pressure (≈19 psia). However, the diesel brake mean effective pressure (BMEP) was allowed to run as high as 200 psi off-design, which will result in higher manifold pressures and results in a maximum peak cylinder pressure of approximately 3000 psi at sea level. The

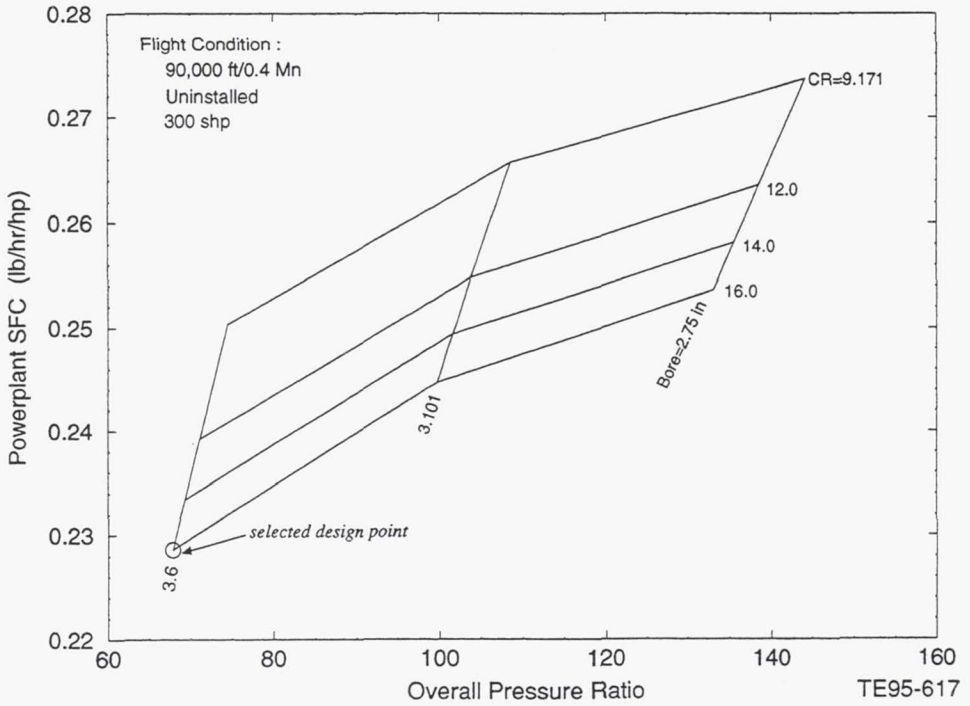

Figure 3. Two-stroke, turbo-compounded, diesel parametric: variation in SFC with compressor overall pressure ratio.

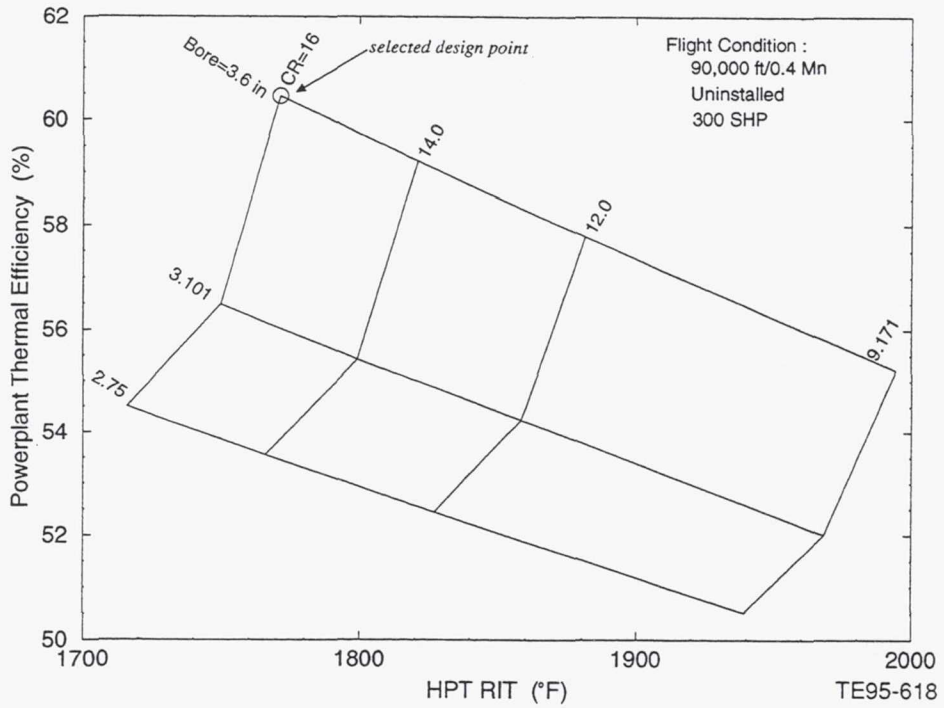

Figure 4. Two-stroke, turbo-compounded, diesel parametric: variation in thermal efficiency with rotor inlet temperature.

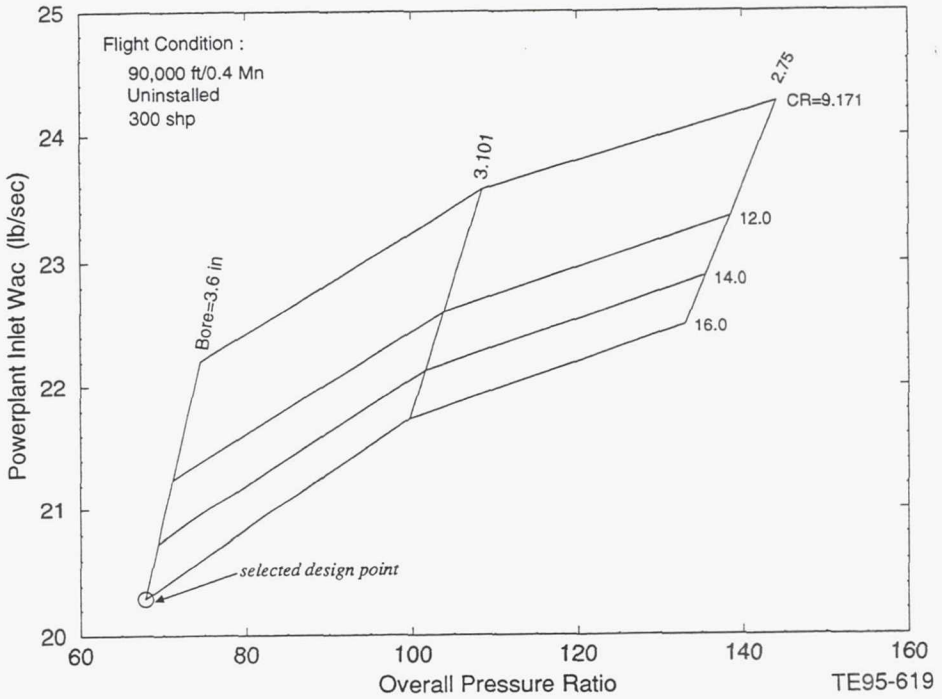

Figure 5. Two-stroke, turbo-compounded, diesel parametric: variation in inlet airflow with compressor overall pressure ratio.

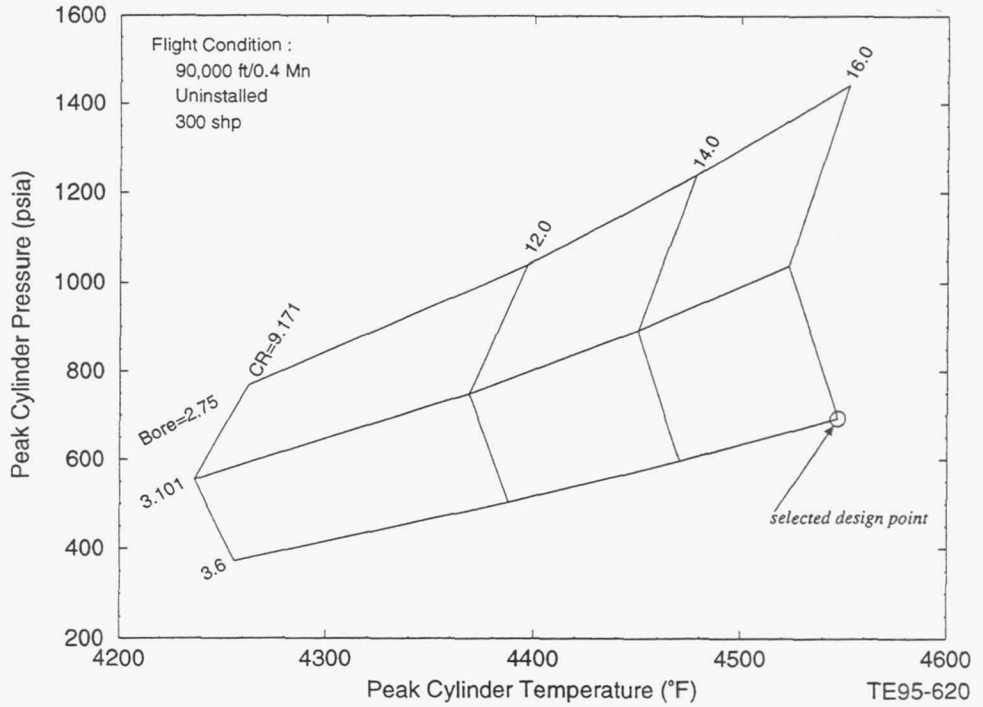

Figure 6. Two-stroke, turbo-compounded, diesel parametric: variation in peak cylinder pressure with peak cylinder temperature.

design is high in peak cylinder temperature because fuel-air ratio is high and an aftercooler was not used in this design, resulting in an inlet manifold temperature of approximately 450°F. The selected design point has been identified in all four parametric plots. The selected diesel engine design has a cubic inch displacement (CID) of 208.4 $in.^3$.

Aerodynamic designs of compressor and turbine turbomachinery components were created for this configuration at the 90,000 ft, 0.4 Mach, maximum power (300 shp, 100% corrected speed [$N/\sqrt{\theta}$]) design point. Both an axial and centrifugal compressor were interrogated for the first (LPC) compressor. After examining both an axial and centrifugal LPC, a centrifugal was chosen since both it and its drive turbine showed a higher efficiency potential. The inlet flow to the LPC is around 20 lbm/sec, which is low enough to justify a centrifugal compressor. Centrifugal compressors are desirable for their high pressure ratio per stage and reasonably compact overall dimensions. All four turbines are axial designs. The appreciable efficiency decrement due to the low Reynolds number at this design point condition was taken into account when evaluating the efficiency level of each component.

It is beneficial to have the first compressor Rc slightly higher than that of the other two compressors not only from a cycle performance standpoint but, for a given effectiveness, it results in a reduced size of the first intercooler. The reason for this is intercoolers require the density of the air coming in to be as high as possible. Another consideration taken into account in selecting the compressor Rc splits was the magnitude of the compressor discharge temperatures (CDT). If the CDT is less than 400°F, then a centrifugal compressor can be fabricated out of aluminum. Since the first compressor is the largest in diameter of the three, it should be fabricated of aluminum, which places an upper limit on the Rc of the LPC.

The second and third compressors were also chosen to be centrifugal in design. The pressure ratios for the second and third compressor were chosen to be 4.0 for the design point cycle at 90,000 ft, 0.4 Mach. This resulted in a low pressure Rc of 4.56:1 being required to produce 300 shp at 90,000 ft, 0.4 Mach.

A compressor pressure ratio (Rc) trade-off study was conducted at the 90,000 ft, 0.4 Mach, uninstalled flight condition to see if a more optimum arrangement of component pressure ratio distribution existed. The results of this study are shown in bar chart form in Figures 7 through 12. All of the configurations examined have their compressor Rc levels listed at the top of the bar in each figure. Configuration 1 is the baseline design point cycle. Configuration 5 has more of a preferred Rc split than the baseline configuration in terms of SFC (-0.2%), OPR (-3.6%), inlet corrected flow (-0.1%), and HPT RIT (-38°F), but is slightly higher in diesel BMEP and has higher compressor discharge temperatures. The results show that the 4.56/4.0/4.0 combination was near optimum such that the Rc levels were not changed.

The design point cycle was then updated to include a 5 hp extraction, which accounted for bearing losses, windage, fuel pump, oil pump, and PMG parasitic losses. An additional 11 hp extraction was added to the cycle for turbomachinery heat rejection (see section 3.3.4.1 for discussion). The gearbox loss was estimated at 2.2% (6.6 hp) for this turbo-compounded gearbox arrangement (see section 3.4.1). These power extractions resulted in a slightly larger flow size and higher OPR engine.

A schematic with aerothermodynamic details of the two-stroke, turbo-compounded diesel is presented in Figure 13. The 90,000 ft, 0.4 Mach design point has a OPR of 73.0:1, a powerplant inlet corrected flow of 21.5 lbm/sec, an HPT RIT equal to 1789°F, a diesel brake mean effective pressure (BMEP) of 72.7 psia, and a powerplant SFC of 0.2424 lb/hp-hr at the 300 shp maximum power point. The 300 shp output power consists of 234 shp from the two-stroke diesel, 72.6 shp from the power turbine, and a 6.6 shp loss through the gearboxes. Table 4 is a summary of performance and weights of all the candidate powerplants for this ERAST study. The two-stroke, turbo-compounded diesel engine powerplant is listed in the first column of this table for comparison.

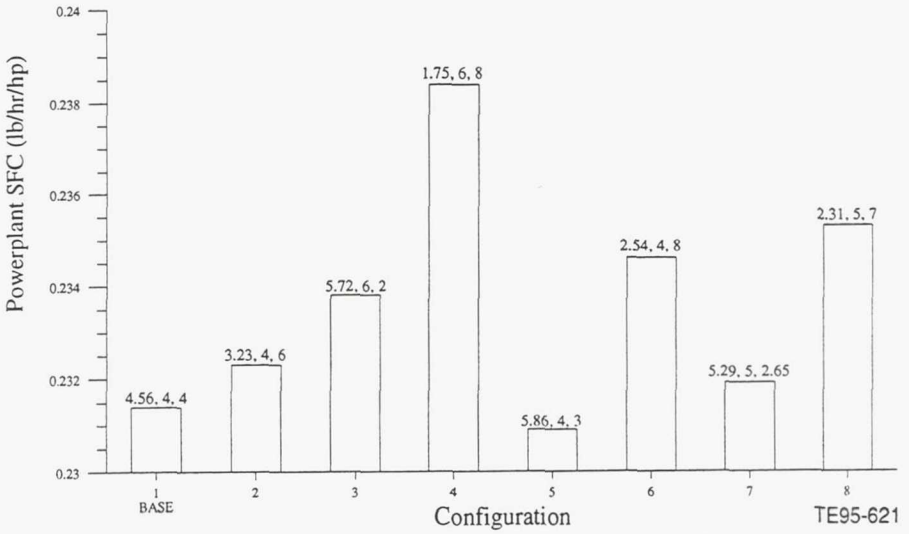

Figure 7. Two-stroke, turbo-compounded diesel Rc trade-off study: variation in SFC with compressor pressure ratio split.

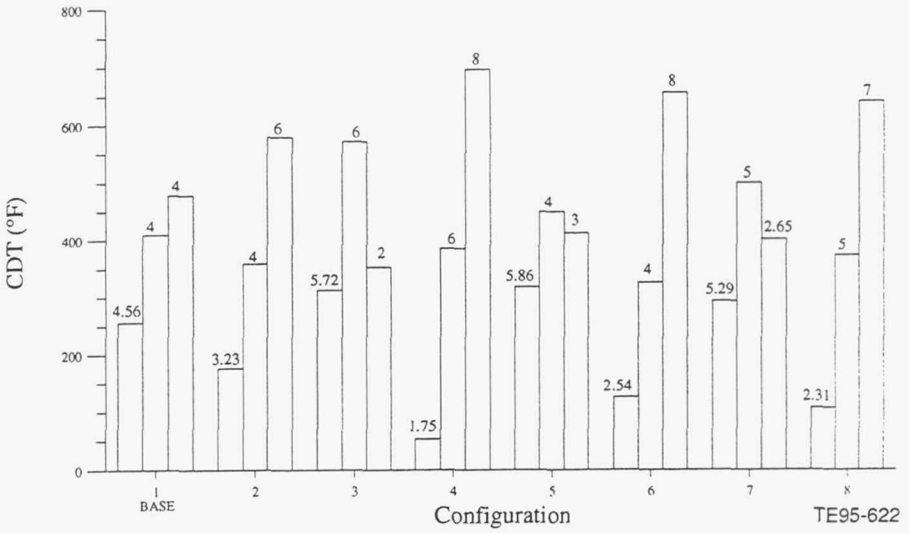

Figure 8. Two-stroke, turbo-compounded diesel Rc trade-off study: variation in compressor discharge temperature with compressor pressure ratio split.

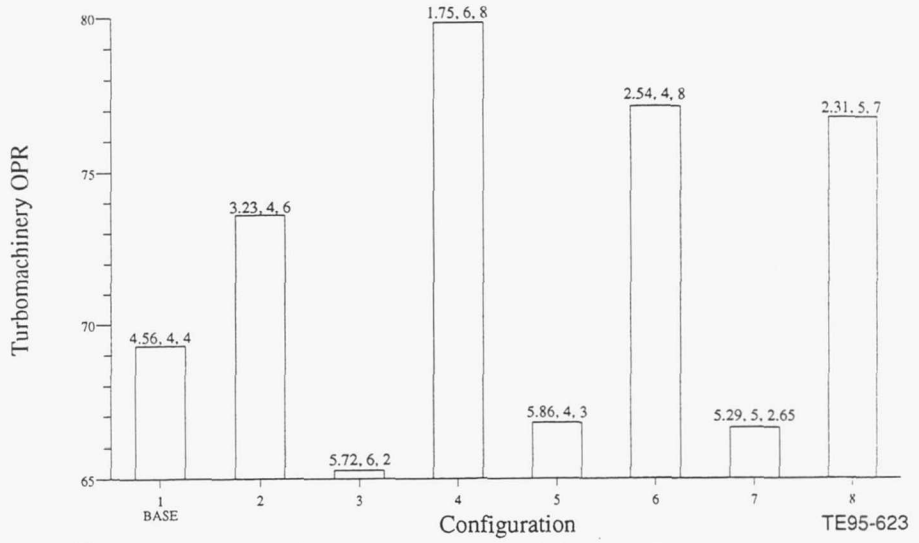

Figure 9. Two-stroke, turbo-compounded diesel Rc trade-off study: variation in overall pressure ratio with compressor pressure ratio split.

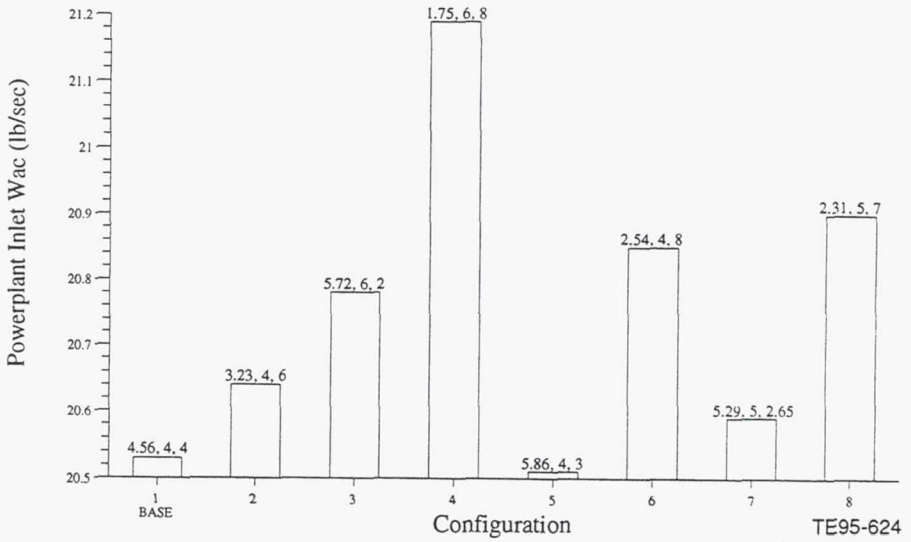

Figure 10. Two-stroke, turbo-compounded diesel Rc trade-off study: variation in inlet corrected airflow with compressor pressure ratio split.

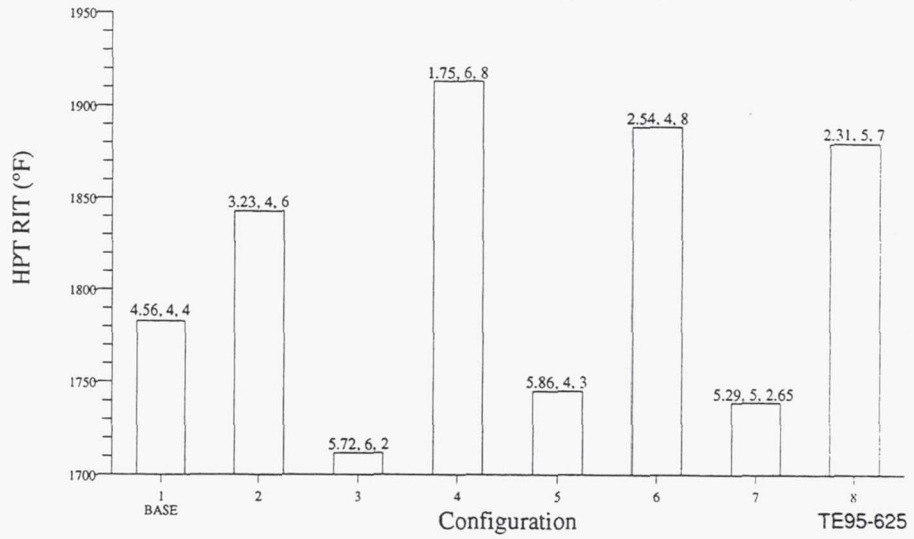

Figure 11. Two-stroke, turbo-compounded diesel Rc trade-off study: variation in HP turbine rotor inlet temperature with compressor pressure ratio split.

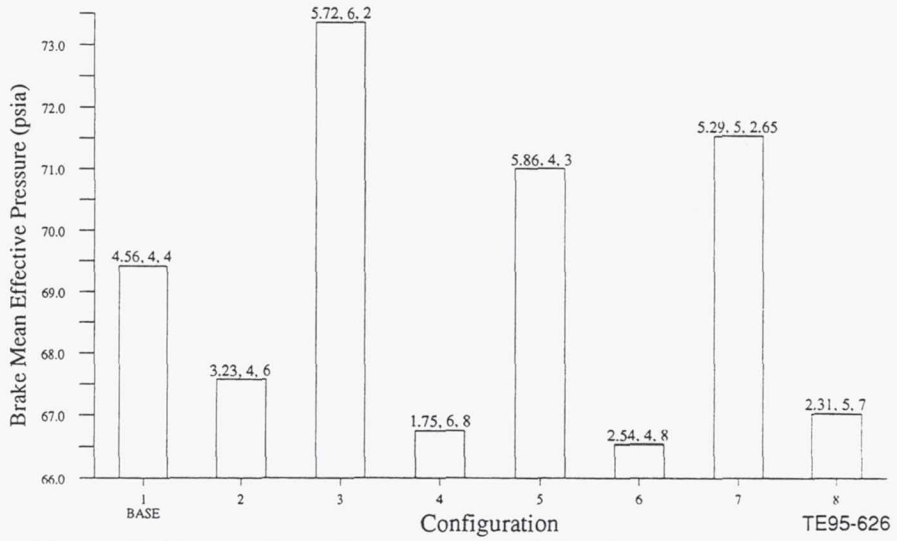

Figure 12. Two-stroke, turbo-compounded diesel Rc trade-off study: variation in brake mean effective pressure with compressor pressure ratio split.

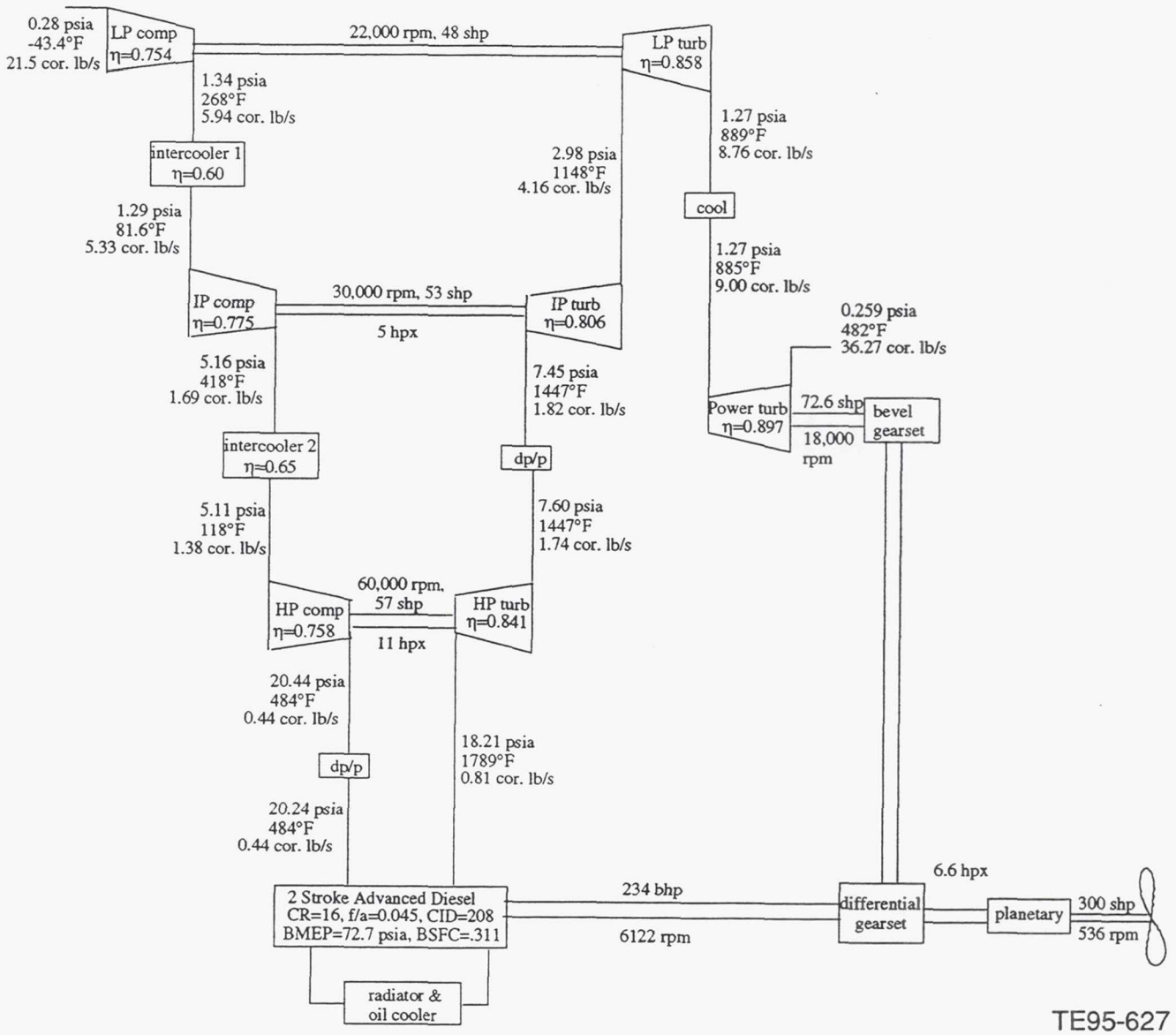

Figure 13. ERAST two-stroke, turbo-compounded diesel schematic: 90,000 ft, 0.4 Mach, 300 shp design point.

Table 4.

ERAST powerplant candidates —designed for 300 shp at 90,000 ft/0.4 Mach.

Technology Level	ADV	ADV	SOA	SOA	NT	NT	NT	NT	SOA	NT	ADV
ENGINE DESCRIPTION	2 STR DSL - TURBO	2 STR DSL - NON	4 STR DSL	4 STR SI	4 STR H2 SI	ROTARY	COLEMAN	RECUP TS	NON - RC=16	NON = RC=20	FUEL CELL
No. Cylinders/Rotors	6	6	6	6	6	3	-----	-----	-----	-----	-----
Bore (in)	3.6	3.6	5.118	5.25	5.25	-----	-----	-----	-----	-----	-----
Stroke (in)	3.412	3.412	5.472	4.25	4.25	-----	-----	-----	-----	-----	-----
CID (cu. in)	208.4	208.4	675.4	552.0	552.0	121.2	-----	-----	-----	-----	-----
Compression Ratio	16.0	18.0	16.0	8.5	8.5	8.5	-----	-----	-----	-----	-----
MAX POWER @ 90K											
Engine Speed (RPM)	6122.0	6122.0	1800.0	2600.0	2600.0	6000.0	-----	-----	-----	-----	-----
Manifold Press. (psia)	20.2	25.5	28.4	13.3	13.3	28.1	-----	-----	-----	-----	-----
Manifold Temp (°F)	483.9	500.6	132.3	88.9	88.9	129.0	-----	-----	-----	-----	-----
EGT / RIT (°F)	1789.2	1768.2	1161.4	1720.0	2008.0	1150.1	2500	2500	2500	2500	2442
Engine BHP (hp)	234	303	303	225	184	300	-----	-----	-----	-----	300
Engine BSFC (lb/hp-hr)	0.3105	0.3002	0.3385	0.4948	0.1576	0.3934	-----	-----	-----	-----	-----
Air Flow (lb/hr)	1615.4	2021.0	2561.8	1590.3	1587.4	3750.1	-----	-----	-----	-----	-----
BMEP (psi)	72.7	94.1	197.5	124.2	101.7	163.4	-----	-----	-----	-----	-----
TURBOMACHINERY											
Inlet Corrected Flow (lb/sec)	21.5	26.9	33.8	21.2	21.2	49.4	28.3	77.2	64.4	64.5	199.7
OPR	73.0	92.1	101.3	47.6	47.6	100.9	35	14.3	14.3	17.9	97.9
Comp 1st Stage Pr	4.79	6.09	5.32	4.13	4.13	5.37	6	14.3	14.3	17.9	6.24
Comp 2nd Stage Pr	4.00	4.00	4.50	3.50	3.50	4.50	6	-----	-----	-----	4
Comp 3rd Stage Pr	4.00	4.00	4.50	3.50	3.50	4.50	-----	-----	-----	-----	4
Powerplant SFC (lb/hp-hr)	0.2424	0.3032	0.3419	0.3708	0.0968	0.3936	0.4267	0.4221	0.4767	0.4573	0.3982
INTERCOOLER SIZE											
1st Volume (cu. ft) [# modules]	0.35 [4]	0.43 [4]	3.34 [2]	2.1 [2]	2.1[2]	1.23 [6]	0.92 [10]	-----	-----	-----	-----
2nd Volume (cu. ft) [# modules]	0.42 [4]	0.58 [4]	2.78 [2]	1.79[2]	1.79 [2]	0.47 [6]	-----	-----	-----	-----	-----
3rd Volume (cu. ft) [# modules]	-----	-----	4.1 [2]	2.51 [2]	2.51 [2]	0.32 [6]	-----	-----	-----	-----	-----
Oil Cooler Volume (cu. ft)	0.06	0.23	0.55	0.58	0.28	0.3	-----	-----	-----	-----	-----
Radiator Volume (cu. ft) [#]	0.65 [1]	0.83 [1]	1.68 [1]	1.46 [1]	0.24 [1]	0.33 [2]	-----	-----	-----	-----	-----
WEIGHTS (lb)											
Core Engine	230	230	610	486	486	420	-----	-----	-----	-----	2250
Gear Box	439	214.5	196.7	391	433	130.6	266.8	293.3	293.4	293.5	190
Turbomachinery (core)	319.9	238.1	371.7	359.6	366.5	584.3	874.6	2598.5	2200.8	2155.5	2883.6
(exter.)	85.6	77.3	90.9	89.7	90.4	112.6	197.4	306.4	276.9	275.4	597.1
Intercooler #1	21.4	26.5	58.6	36.9	36.9	77.9	154.1	-----	-----	-----	-----
#2	26.1	36.2	65.3	42.3	42.3	53.1	-----	-----	-----	-----	-----
#3	-----	-----	96.6	59.1	59.1	50.1	-----	-----	-----	-----	-----
Recuperator	-----	-----	-----	-----	-----	-----	245.8	1267.7	-----	-----	1000*
Radiator(s) + coolant	20.4	20.5	46.6	40.6	14	38.9	-----	-----	-----	-----	-----
Oil Cooler	21.5	26.1	33.4	28.4	26.5	37.6	23.6	38.9	35.3	35.3	62.6
Oil & Oil Tank	46.5	47.4	67.6	58.6	59.5	69	26.1	26.1	26.1	26.1	26.1
TOTAL WEIGHT (lb)	1210.4	916.6	1637.4	1592.2	1614.2	1574.1	1788.4	4530.9	2832.5	2785.8	7009.4
											*estimate

An energy balance was performed on the two-stroke diesel engine for this turbo-compounded configuration. The energy balance consists of determining the percentage of fuel heating value that is converted into brake horsepower, energy lost out the piston engine exhaust, energy lost to the engine coolant, and energy lost to the oil due to friction and piston lubrication. The sum of these four percentages plus energy lost from engine case heat rejection to ambient should total 100%. The engine case heat rejection estimate was derived by the difference remaining from the sum of the four calculated values such that the total equaled 100%. The energy balance for the two-stroke, turbo-compounded diesel is given in the first column of Table 5.

Table 5.
Piston and rotary engine energy balances—design point condition (300 shp).

Technology level	Advanced 2-stroke	Advanced 2-stroke	SOA 4-stroke	SOA 4-stroke gas	NT 4-stroke	NT
Engine description	diesel turbo	diesel non	diesel	SI	H_2 SI	Rotary
FHV, Btu/lb	18,410	18,410	18,410	18,006	51,593	18,410
% brake hp	44.5	46	40.8	28.6	31.3	35.1
% exhaust	45	43.7	37.4	53	54	46.1
% coolant (radiator)	7.9	7.5	14.9	11.7	8.8	12.8
% friction (oil)	0.6	1.2	3.1	3.2	3.9	3
% engine case heat rejection to ambient	2	1.6	3.8	3.5	2	3
Total, %	100	100	100	100	100	100

SOA = state of the art
FHV = fuel heating value
SI = spark ignition
NT = near term

3.1.1.2 Non-Turbo-Compounded Two-Stroke Opposed-Piston Diesel - Advanced Technology

A non-turbo-compounded two-stroke diesel cycle was created by removing the power turbine from the turbo-compounded cycle. This configuration was included in the ERAST study to determine whether the weight decrease achieved by removing the power turbine (and associated gearboxes) would offset the SFC increase incurred by losing significant energy out of the exhaust of the powerplant.

With the power turbine removed from the engine cycle, the two-stroke diesel must now generate all of the required power (300 shp). To achieve this the turbomachinery OPR increased approximately 43%, the flow size increased approximately 40%, and RIT/EGT increased 32°F. Increasing the diesel CR from 16 to 18 results in deltas of OPR (-4.3%), airflow (-4.2%), and RIT (-45°F). A CR of 18 is considered within limits for advanced technology diesel engines.

Compressor and turbine aerodynamic designs were completed for this configuration at the 90,000 ft, 0.4 Mach, maximum power (300 shp, 100% $N/\sqrt{\theta}$) design point. After examining both an axial and centrifugal LPC, a centrifugal was chosen since both it and its drive turbine showed a higher efficiency potential. Therefore, all three compressors were chosen as centrifugal and all three turbines were chosen as axial designs. The appreciable efficiency decrement due to the low Reynolds number at this design point condition was taken into account when evaluating the efficiency level of each component.

The second and third compressor pressure ratios were chosen to be 4.0:1 for the design point cycle at 90,000 ft, 0.4 Mach, so that they would be less than the LPC Rc. This resulted in a low pressure Rc of 6.22:1 being required to produce 300 shp at 90,000 ft, 0.4 Mach. A compressor pressure ratio (Rc) trade-off study was conducted to see if a more optimum arrangement of component pressure ratio distribution

existed. The results show that the 6.22/4.0/4.0 combination was near optimum such that the Rc levels were not changed.

The design point cycle was then updated to include a 5 hp extraction for parasitics, an 11 hp extraction for turbomachinery heat rejection (see section 3.3.4.1 for discussion), and 3 hp (1%) for a planetary gearbox loss (see section 3.4.2). Adding these power extractions to the engine cycle resulted in a decrease in the nozzle expansion ratio. Less energy is now being lost out of the powerplant exhaust.

A schematic with aerothermodynamic details of the two-stroke non-turbo-compounded diesel is presented in Figure 14. The 90,000 ft, 0.4 Mach design point has a OPR of 92.1:1, a powerplant inlet corrected flow of 26.9 lbm/sec, an HPT RIT equal to 1768°F, a diesel BMEP of 94.1 psia, and a powerplant SFC of 0.3032 lb/hp-hr at the 300 shp maximum power point. The non-turbo-compounded two-stroke diesel powerplant SFC is 25% higher than the turbo-compounded two-stroke diesel powerplant SFC. The two-stroke, non-turbo-compounded diesel engine powerplant is summarized in the second column of Table 4 for comparison purposes. The energy balance for the two-stroke, non-turbo-compounded diesel is given in the second column of Table 5.

3.1.2 Four Stroke Diesel Engine - SOA Technology

A four-stroke diesel was evaluated using the diesel modeling program (discussed in section 3.1.1) and TERMAP. The four-stroke diesel baseline engine used to calibrate the model was the Detroit Diesel Series 60 engine (Ref 2). This engine has a compression ratio (CR) of 16, a bore of 5.118 in., a stroke of 5.472 in., a fuel-air ratio of 0.03095, and a speed of 1800 rpm. A horizontal piston configuration was chosen as optimum for weight considerations. Also today's lightweight materials (aluminum for block, cylinder heads, titanium connecting rods, etc) were used in reducing engine weight, trading typical engine life from 20,000 to 2,000 hr.

As discussed in section 3.1.1, diesel engines require an inlet pressure of at least 1 atmosphere to provide the specific power of a naturally aspirated engine. This requires a turbocharger overall pressure ratio (OPR) to be at least 60:1 at the 90,000 ft design point condition. Just as with the two-stroke diesels, three compressors, each operating on a separate spool, will probably be required to achieve this OPR. Aftercooling will be required, in addition to intercooling between each compressor, to maximize the density of the airflow going into this four-stroke diesel.

The first intercooler effectiveness for this configuration was selected to be 60%, the second intercooler effectiveness was chosen to be 65%, and the aftercooler effectiveness was chosen to be 70%. Setting the effectiveness of the first intercooler at 60% is a good trade between intercooler size required and compressor stage pressure ratio required to achieve a reasonably high level of air density from the low ambient inlet conditions. It was estimated at the beginning of this study that if the effectiveness of the second intercooler was increased an additional 5% above the first intercooler effectiveness and the effectiveness of the aftercooler was increased 10% then their resulting size would be close to the size of the first intercooler.

In the design point simulation of this powerplant, the airflow size of the turbomachinery was varied until the gas flow exiting the diesel equaled the sum of the airflow going into the pistons and the fuel flow added in the combustion part of the diesel cycle. Turbomachinery OPR was varied to get a powerplant total output power of 300 shp.

One potential problem with the four-stroke diesel is at a fuel-air ratio (FAR) of 0.03095 and CR of 16 the exhaust temperature has difficulty in driving the turbines. Therefore, when a 6-cylinder, four-spool, turbo-compounded version is simulated, the power turbine (PT) expansion ratio is only 1.16 and the resulting diesel compression ratio CR is around 8. The goal is to have CR near 16.

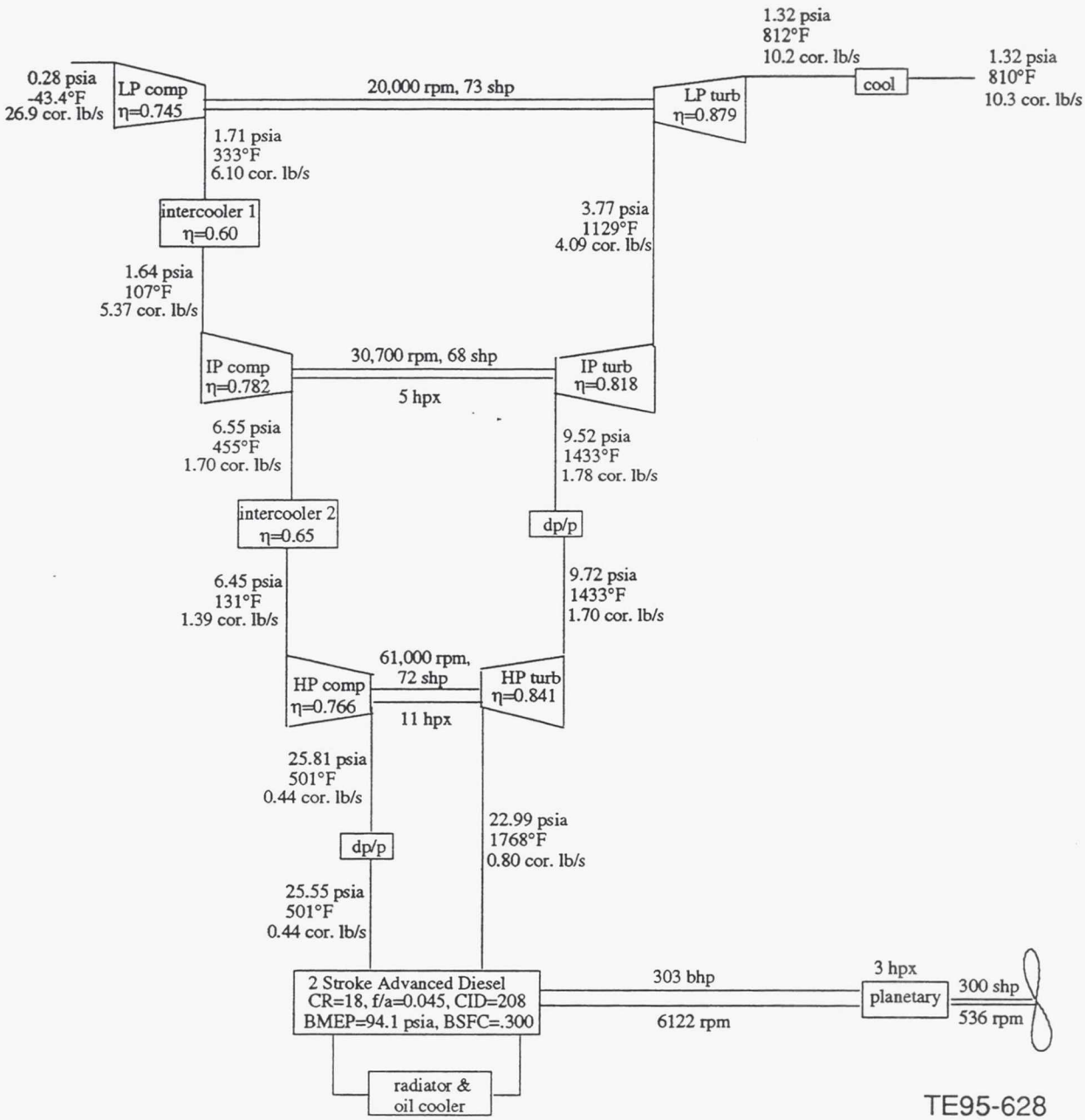

Figure 14. ERAST two-stroke, non-turbo-compounded diesel schematic: 90,000 ft, 0.4 Mach, 300 shp design point.

The power turbine was removed since there is little energy to make use of in the flow stream after exiting the LP turbine. The FAR was increased to 0.038, which is approaching the upper limit for a current day technology diesel engine. The compression ratio for this engine is 16. This non-turbo-compounded configuration has an OPR = 106, a corrected flow size of 35.4 lbm/sec, and an SFC = 0.340 lb/hr/hp. This configuration has the appearance of being a good first pass solution for a four-stroke, 6-cylinder, SOA technology, turbocharged diesel engine.

A parametric in number of pistons/cylinders (4,6,8,10, and 12) was conducted to determine if there was a better solution than an engine with 6-cylinders. The results are presented as SFC, FAR, Wac, OPR, manifold temperature, and manifold pressure versus number of pistons in Figures 15 through 17. Figure 15 shows how SFC improves only 1.75% when going from a 4-cylinder engine to a 12-cylinder engine. The FAR for 4 cylinders is approximately 0.042, while the FAR for 12 cylinders is approximately 0.032. Figure 16 shows that powerplant inlet corrected flow is 29% higher and OPR is 39.4% lower when

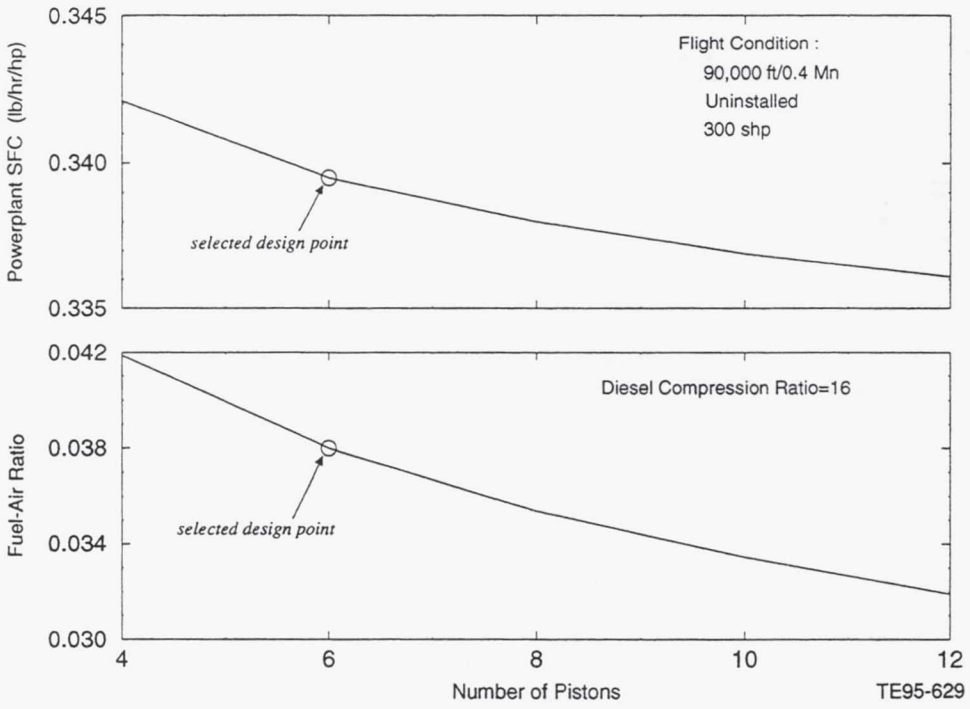

Figure 15. Four-stroke, non-turbo-compounded, diesel parametric: variation in SFC and fuel-air ratio with number of pistons.

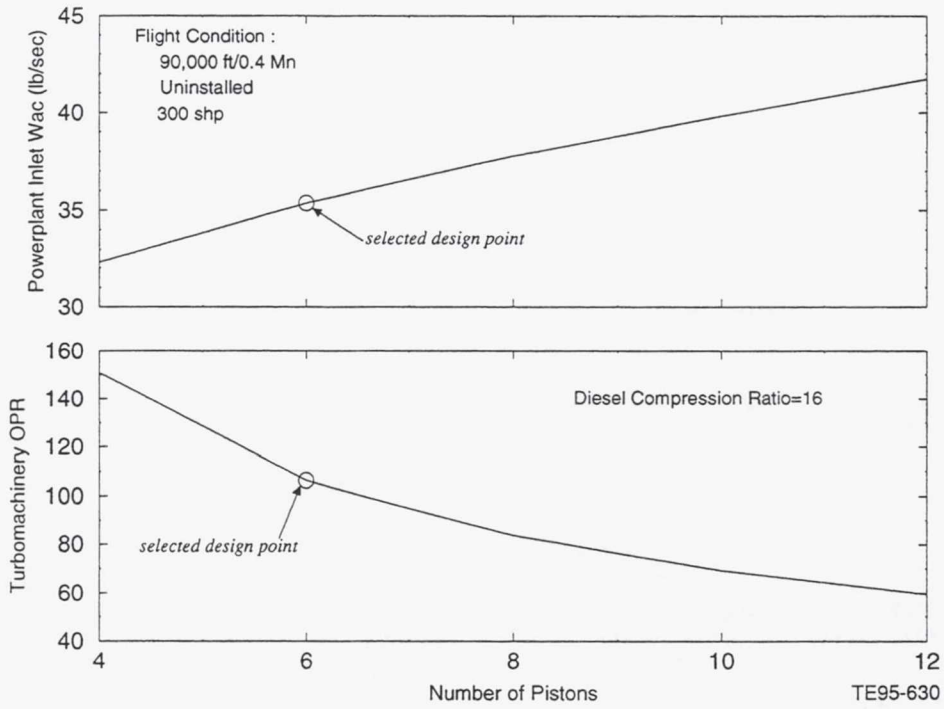

Figure 16. Four-stroke, non-turbo-compounded, diesel parametric: variation in inlet flow and compressor overall pressure ratio with number of pistons.

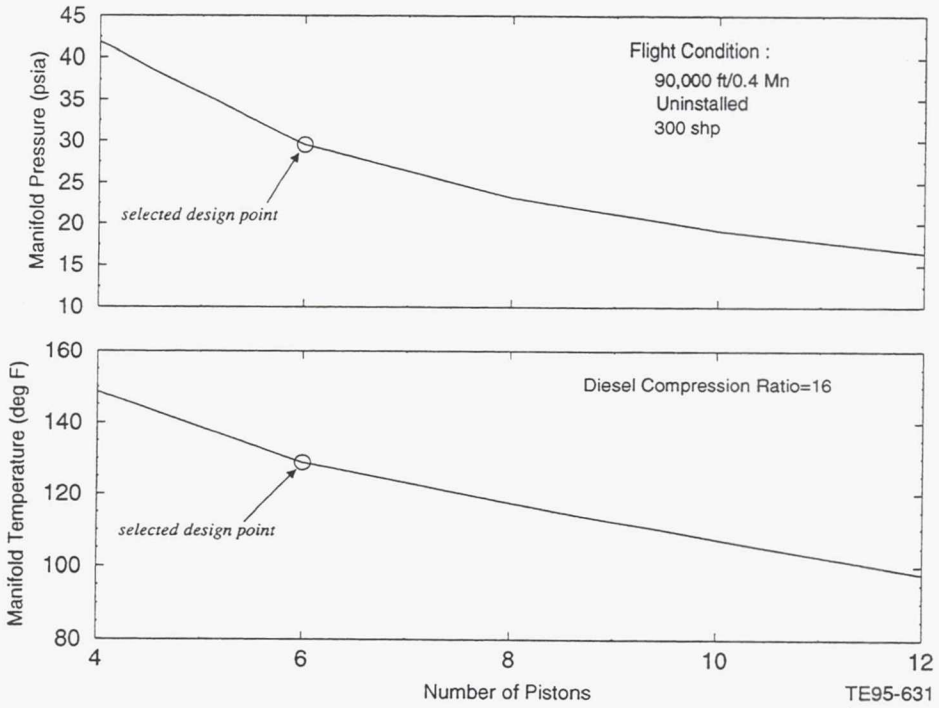

Figure 17. Four-stroke, non-turbo-compounded, diesel parametric: variation in manifold pressure and temperature with number of pistons.

comparing the 12-cylinder engine with the 4-cylinder version. The resulting level of manifold pressure and temperature for each cylinder number is shown in Figure 17. These levels are considered acceptable.

Since the powerplant weight increases and the SFC improvement is minimal with each increase in number of cylinders, it was concluded that the smaller the number of cylinders the better the solution. The 4-cylinder engine was not chosen, however, since its FAR of 0.042 was considered more appropriate for an advanced technology engine than for a SOA technology engine. Therefore, the 6-cylinder version was retained as the four-stroke diesel candidate. The selected design point has been highlighted in all six parametric plots. The cubic inch displacement (CID) of this four-stroke diesel is 675.4 $in.^3$.

Compressor and turbine component aerodynamic designs were completed for this configuration at the 90,000 ft, 0.4 Mach, maximum power (300 shp, 100% $N/\sqrt{\theta}$) design point. After examining both an axial and centrifugal LPC, a centrifugal was chosen since both it and its drive turbine showed a higher efficiency potential. Therefore, all three compressors were chosen as centrifugal and all three turbines were chosen as axial designs. The appreciable efficiency decrement due to the low Reynolds number at this design point condition was taken into account when evaluating the efficiency level of each component.

The second and third compressor pressure ratios were chosen to be 4.5:1 for the design point cycle at 90,000 ft, 0.4 Mach. This resulted in a low pressure Rc of 5.65:1 being required to produce 300 shp at 90,000 ft, 0.4 Mach. A compressor pressure ratio (Rc) trade-off study was conducted to see if a more optimum arrangement of component pressure ratio distribution existed. The results show that the 5.65/4.5/4.5 combination was near optimum such that the Rc levels were not changed.

The design point cycle was then updated to include a 5 hp extraction for parasitics, an 11 hp extraction for turbomachinery heat rejection (see section 3.3.4.1 for discussion), and 3 hp (1%) for a planetary gearbox loss (see section 3.4.2). Adding these power extractions to the engine cycle resulted in the nozzle expansion ratio decreasing to zero. The fuel-air ratio was then increased to 0.04 to get the nozzle expansion ratio into the 2.5% range, thus approaching the fuel-air limit for a SOA technology diesel engine.

A schematic with aerothermodynamic details of the four-stroke, non-turbo-compounded diesel is presented in Figure 18. The 90,000 ft, 0.4 Mach design point has a OPR of 101.3:1, a powerplant inlet corrected flow of 33.8 lbm/sec, an HPT RIT equal to 1161°F, a diesel BMEP of 197.5 psia, and a powerplant SFC of 0.3419 lb/hp-hr at the 300 shp maximum power point. The four-stroke, non-turbo-compounded diesel engine powerplant is summarized in the third column of Table 4 for comparison purposes. The energy balance for the four-stroke, non-turbo-compounded diesel is given in the third column of Table 5.

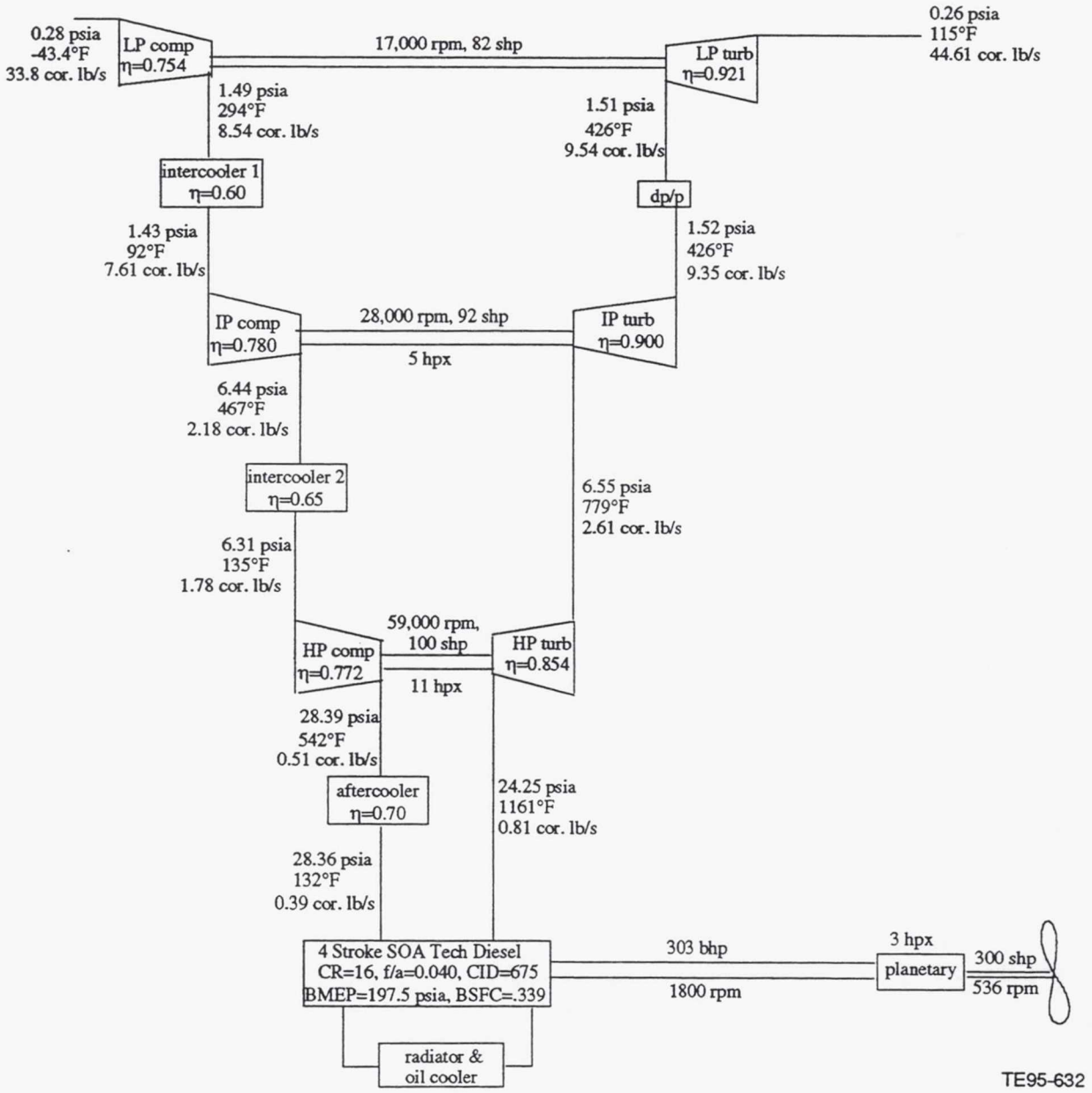

Figure 18. ERAST four-stroke, non-turbo-compounded diesel schematic: 90,000 ft, 0.4 Mach, 300 shp design point.

3.1.3 Four-Stroke Spark Ignition Engine - SOA and NT Technology

A computer program was developed to simulate spark ignition (SI) engine performance. The Benson ideal OTTO Cycle Program (presented in Reference 1) was updated to include engine block heat loss and piston friction loss modeling so that a more realistic spark ignition engine could be simulated. This program was then further calibrated with actual engine data.

Modeling of a turbocharged spark ignition engine was accomplished by replacing TERMAP's BURNER building block subroutine with the SPARK IGNITION program. These two programs were then run simultaneously to perform design point cycle analysis for turbocharged SI engines.

The baseline engine used in the spark ignition analysis was the Teledyne Continental TSIO-520 converted to liquid cooling as described in Reference 3. This engine is a turbocharged, 6-cylinder, four-stroke design with a compression ratio (CR) of 7.5. A slightly rich fuel-air ratio (FAR) of 0.07 was chosen for the 90,000 ft, 0.4 Mach maximum power design point. The stroke length was increased from 4.0 to 4.25 in. to better represent a current day SI engine CID of 552 $in.^3$ (as in the Voyager T-550). The engine bore size is 5.25 in., and the design speed is 2600 rpm.

Similar to diesel engines, the higher the SI engine inlet pressure the better the specific performance. To raise the ambient pressure at 90,000 ft to 14.696 psia requires a turbomachinery overall pressure ratio (OPR) of approximately 60:1. Just as with the diesels, three compressors, each operating on a separate spool, will probably be required to achieve this OPR. Aftercooling (in addition to intercooling) is required to assure preignition does not occur and to raise the air density as high as possible for this four-stroke application. This spark ignition configuration is turbo-compounded.

The first intercooler effectiveness for this configuration was selected to be 60%, the second intercooler effectiveness was 65%, and the aftercooler effectiveness was 70%. Setting the effectiveness of the first intercooler at 60% is a good trade between intercooler size required and compressor stage pressure ratio required to achieve a reasonably high level of air density from the low ambient inlet conditions. It was estimated at the beginning of this study that if the effectiveness of the second intercooler was increased an additional 5% above the first intercooler effectiveness and the effectiveness of the aftercooler was increased 10% then their resulting size would be close to the size of the first intercooler.

In the design point simulation of this powerplant, the airflow size of the turbomachinery was varied until the gas flow exiting the SI engine equaled the sum of the airflow going into the pistons and the fuel flow added in the combustion part of the SI cycle. Turbomachinery OPR was varied to get a powerplant total output power of 300 shp.

3.1.3.1 Gasoline Fuel - SOA Technology

A parametric study at 90,000 ft, 0.4 Mach, 300 shp was performed to determine the optimum design for a SOA technology, gasoline driven, turbo-compounded SI engine. The parametric was run for both 4 and 6 cylinders, and four compression ratios (CR = 7.5, 8.5, 9.5, and 11).

This parametric has been plotted in Figures 19 through 22 as SFC, OPR, Wac (inlet corrected flow), and HPT RIT versus SI engine brake mean effective pressure (BMEP). Peak cylinder pressure is plotted versus peak cylinder temperature in Figure 23. Specific fuel consumption, OPR, and Wac do not vary significantly with CR but do vary with number of cylinders. The 6-cylinder SFC is approximately 3.5% higher than the 4-cylinder SFC. The 6-cylinder OPR is approximately 50% lower, and the 6-cylinder Wac is approximately 3% higher than the 4-cylinder. The RIT levels are low enough that all the turbines would be uncooled. The 4-cylinder peak cylinder pressure is too high for SOA technology. This pressure should be less than 1200 psi. Also, the BMEPs for all of the 4-cylinder design points are at the high end of SOA technology levels, which would be considered to be about 195 psi.

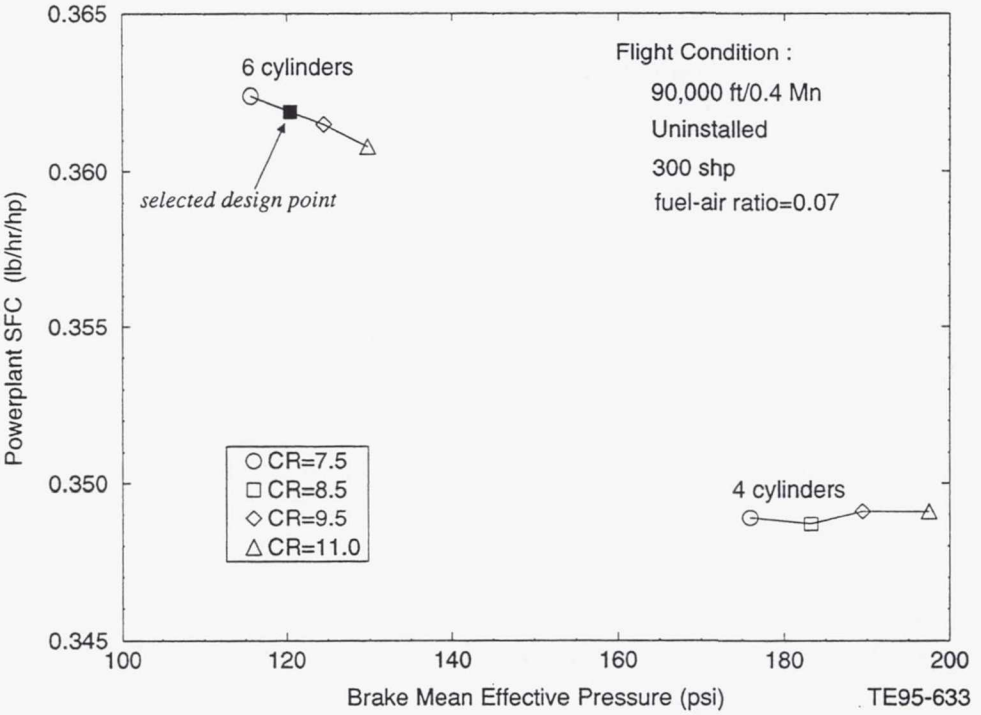

Figure 19. Four-stroke, turbo-compounded gas spark ignition parametric: variation in SFC with BMEP.

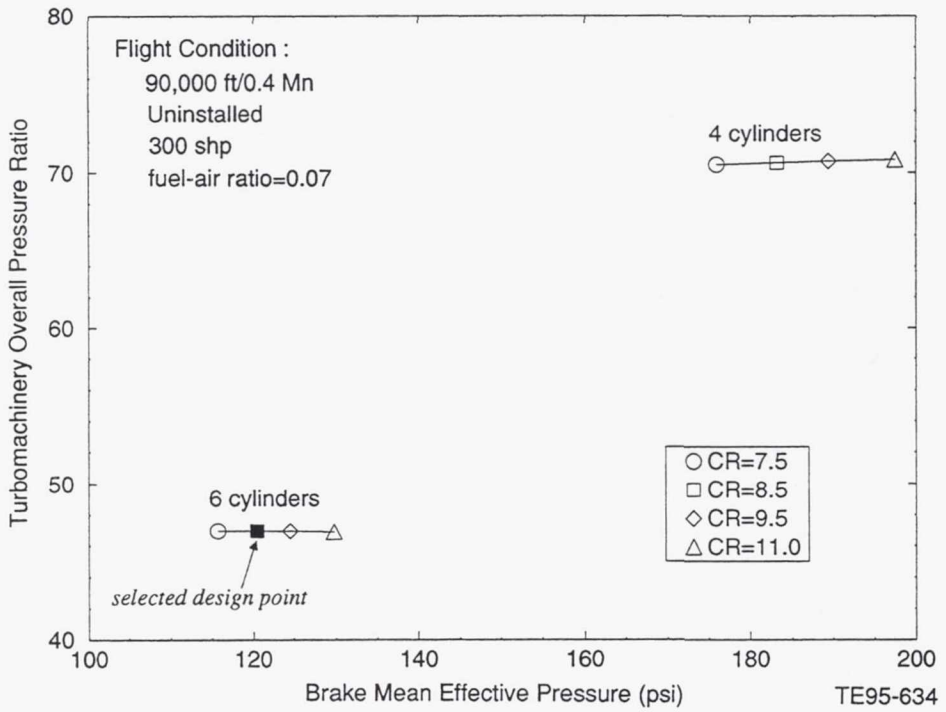

Figure 20. Four-stroke, turbo-compounded gas spark ignition parametric: variation in overall pressure ratio with BMEP.

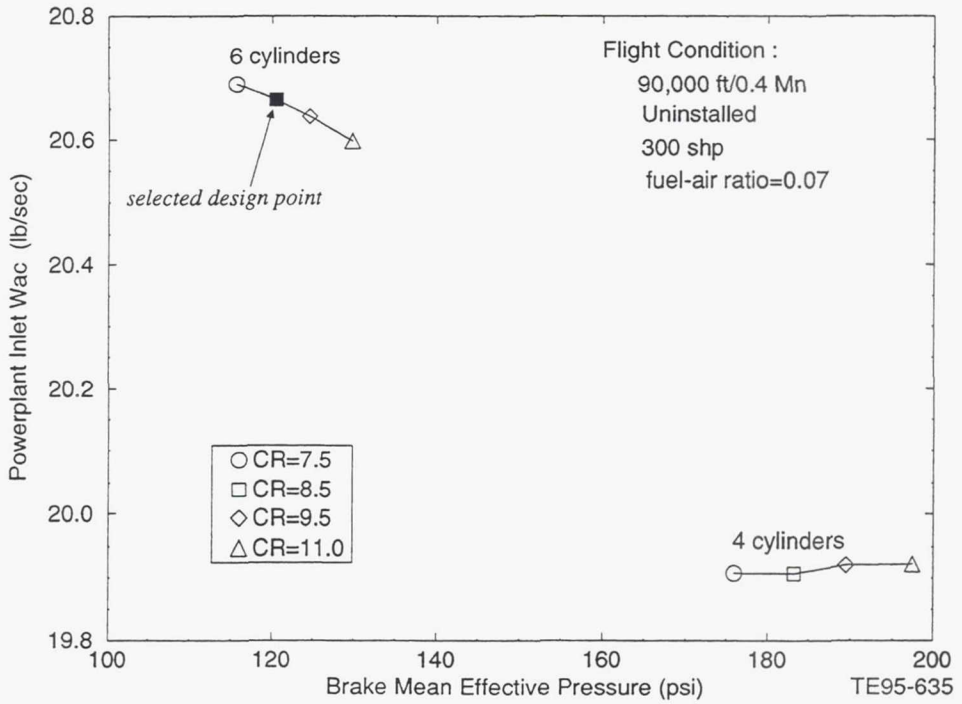

Figure 21. Four-stroke, turbo-compounded gas spark ignition parametric: variation in inlet corrected airflow with BMEP.

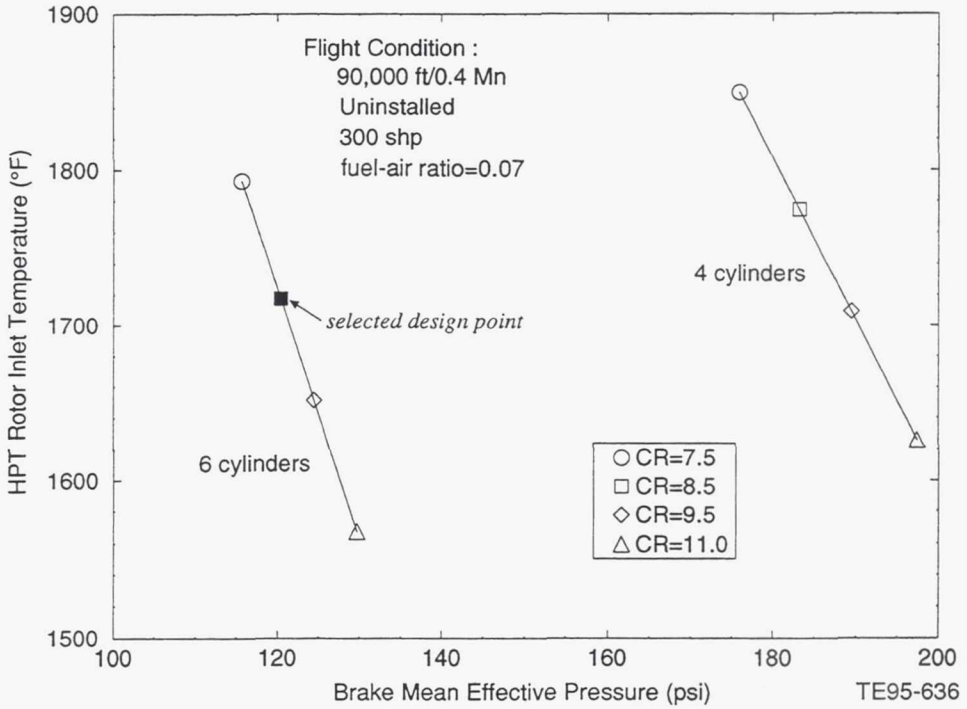

Figure 22. Four-stroke, turbo-compounded gas spark ignition parametric: variation in rotor inlet temperature with BMEP.

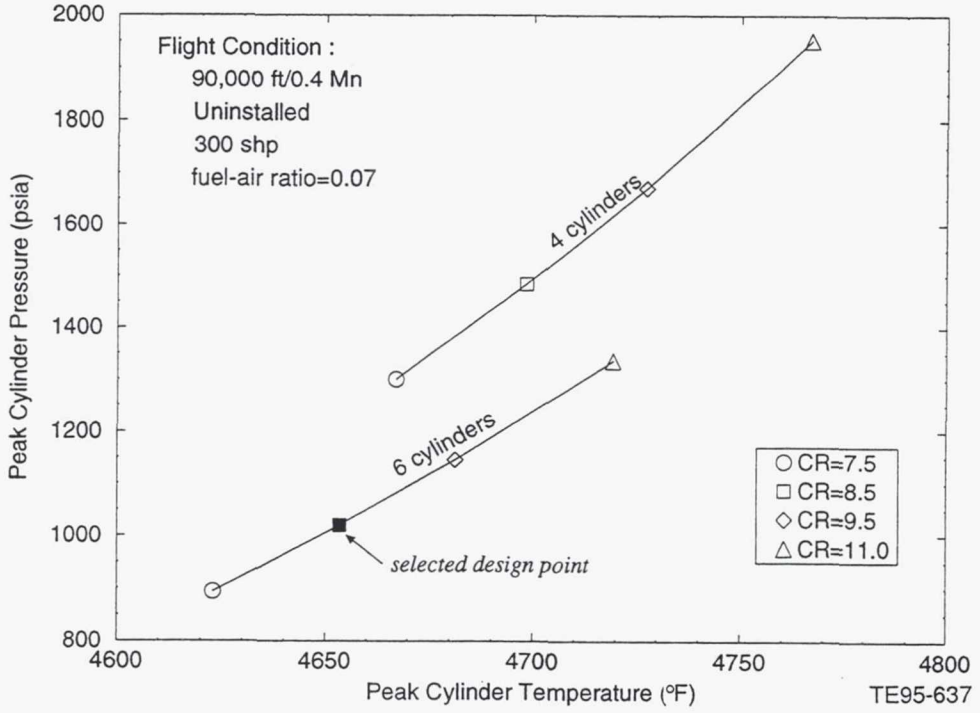

Figure 23. Four-stroke, turbo-compounded gas spark ignition parametric: variation in peak cylinder pressure with peak cylinder temperature.

The peak cylinder pressure and BMEP limits essentially eliminate any of the 4-cylinder possibilities. The drawback to having to go with a 6-cylinder engine is the 3.5% higher SFC and 3% higher Wac. A benefit in going with a 6-cylinder engine is the OPR is 50% lower, which tends to reduce the turbomachinery weight. Specific fuel consumption, OPR, and Wac are essentially unchanged for all of the CRs, and peak cylinder pressure can be kept below the 1200 psi limit if CR is 9.5 or less. The 8.5 CR point was chosen as the new design point because a peak cylinder pressure closer to 1000 psi is considered more representative of a current day design value. The selected design point has been highlighted (as a filled-in square) in all five parametric plots.

Compressor and turbine component aerodynamic designs were completed for this configuration at the 90,000 ft, 0.4 Mach, maximum power (300 shp, 100% $N/\sqrt{\theta}$) design point. After examining both an axial and centrifugal LPC, a centrifugal was chosen since both it and its drive turbine showed a higher efficiency potential. Therefore, all three compressors were chosen as centrifugal and all four turbines were chosen as axial designs. The appreciable efficiency decrement due to the low Reynolds number at this design point condition was taken into account when evaluating the efficiency level of each component.

The second and third compressor pressure ratios were chosen to be 3.5:1 for the design point cycle at 90,000 ft, 0.4 Mach. This resulted in a low pressure Rc of 4.03:1 being required to produce 300 shp at 90,000 ft, 0.4 Mach. A compressor pressure ratio (Rc) trade-off study was conducted to see if a more optimum arrangement of component pressure ratio distribution existed. The results show that the 4.03/3.5/3.5 combination was near optimum such that the Rc levels were not changed.

The design point cycle was then updated to include a 5 hp extraction for parasitics, an 11 hp extraction for turbomachinery heat rejection (see section 3.3.4.1 for discussion), and 6.6 hp (2.2%) for the turbo-compounded gearbox loss (see section 3.4.1). These power extractions resulted in a slightly larger flow size and higher OPR engine.

A schematic with aerothermodynamic details of the four-stroke, turbo-compounded gasoline SI engine is presented in Figure 24. The 90,000 ft, 0.4 Mach design point has an OPR of 47.7:1, a powerplant inlet corrected flow of 21.2 lbm/sec, an HPT RIT equal to 1720°F, an SI engine BMEP of 124.1 psia, and a powerplant SFC of 0.3707 lb/hp-hr at the 300 shp maximum power point. The 300 shp output power consists of 225 shp from the gas SI engine, 81.6 shp from the power turbine, and a 6.6 shp loss through

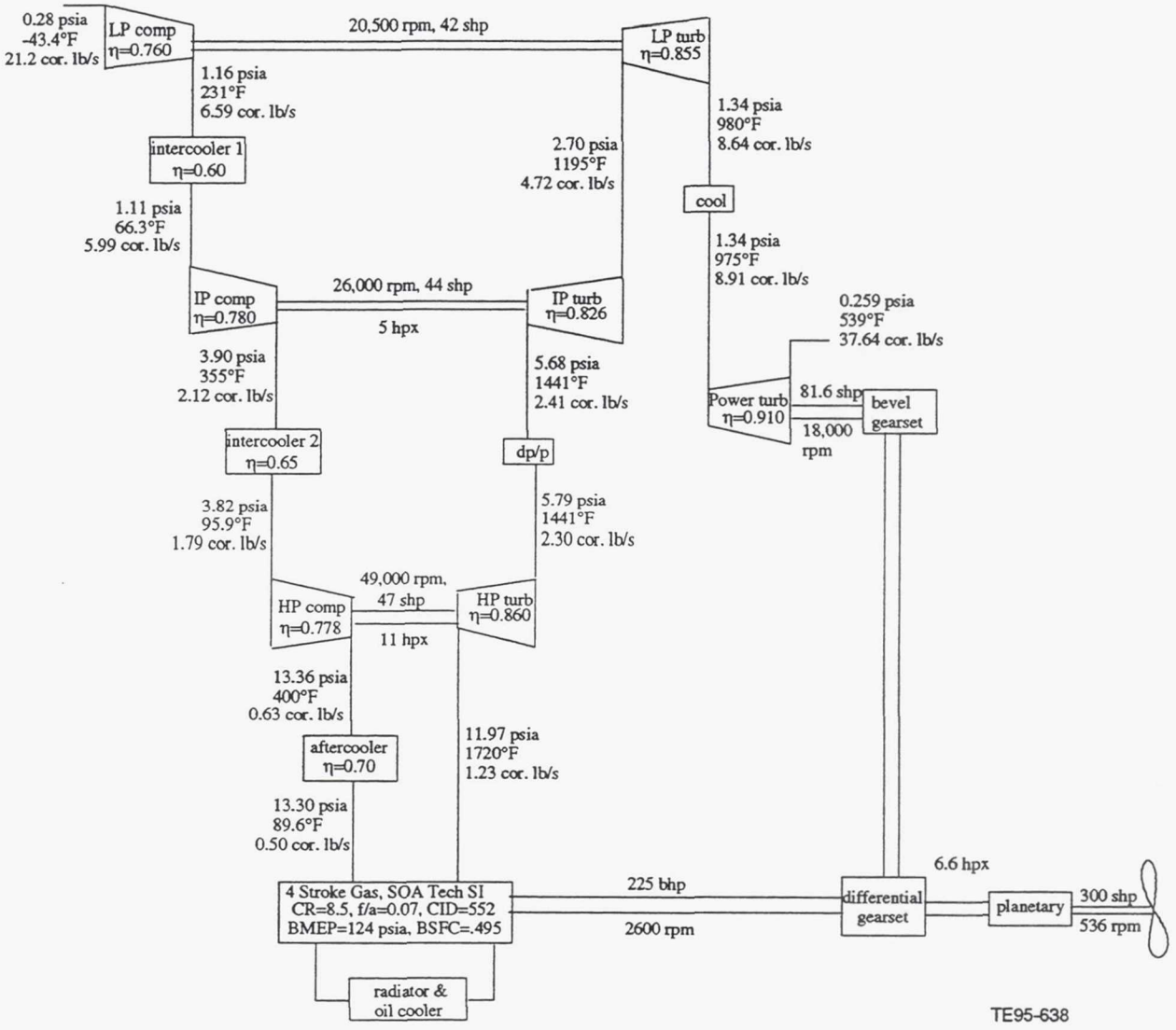

Figure 24. ERAST four-stroke, turbo-compounded gas spark ignition schematic: 90,000 ft, 0.4 Mach, 300 shp design point.

the gearboxes. The four-stroke, turbo-compounded gasoline SI engine powerplant is summarized in the fourth column of Table 4. The energy balance for the four-stroke, turbo-compounded spark ignition engine running on gasoline is given in the fourth column of Table 5.

3.1.3.2 Hydrogen Fuel - NT Technology

The SPARK IGNITION modeling program was modified so that a SI engine running on hydrogen (H_2) fuel could be simulated. The turbo-compounded, gasoline-powered SI engine described in section 3.1.3.1 was then run on H_2 fuel to get a comparison between an engine running on gasoline and one running on hydrogen fuel. Since gasoline has a fuel heating value (FHV) around 18,410 Btu/lbm and H_2 has a FHV = 51,593 Btu/lbm, SFC should roughly decrease by the ratio of these numbers (18,410/51,593 = 0.357). In reality, when the SI engine is run on H_2, the powerplant SFC decreases only 25.9%. One of the reasons for the higher than expected H_2 powerplant SFC is the exhaust temperature coming out of the H_2 SI engine is 280°F higher than the gasoline SI engine. This along with the fact that the H_2 SI engine is running at a lower BMEP contributes to the powerplant SFC improvement discrepancy for this turbo-compounded engine. The phi (FAR/FAR_{stoich}) for this H_2 version of the SI engine is 0.626.

As a check to see if there is a more optimum H_2 SI engine design than the above derived one, a parametric in number of cylinders (6 and 4), compression ratio (CR = 7.5, 8.5, 9.5, and 11), and phi (0.626, 0.7, and 0.8) was conducted. The results of this parametric are presented in Figures 25 through 29. This parametric shows that designing with a higher phi can be negated due to the SFC penalty, as shown in Figure 25. Also, the elevated level of RIT as presented in Figure 26 indicates that possibly cooled turbines would be required. A 4-cylinder design decreases SFC around 2.2% (for a CR = 8.5 and phi = 0.626) and decreases inlet corrected airflow as illustrated in Figure 27 approximately 2.5%; but Figure 28 shows an increase in OPR of 49%. Also, if a 4-cylinder, CR = 8.5, phi = 0.626 design were chosen, the peak cylinder pressure noted in Figure 29 is near the upper limit for NT technology (~1200 psi).

Since the payoffs in going to 4 cylinders (SFC and airflow) are small at the cost of a large OPR increase, it was decided that a 4-cylinder H_2 SI version would not be included as one of the engine candidates. Therefore, the 6-cylinder, CR = 8.5, phi = 0.626 design was chosen as the hydrogen SI engine candidate. This design point has been highlighted in all five parametric plots.

The compressors and intercoolers for this H_2 SI powerplant are the same as those in the gasoline SI powerplant, but the turbine designs are different. Turbine aerodynamic designs were completed for this configuration at the 90,000 ft, 0.4 Mach, maximum power (300 shp, 100% $N/\sqrt{\theta}$) design point. The appreciable efficiency decrement due to the low Reynolds number at this design point condition was taken into account when evaluating the efficiency level of each component.

The design point cycle was then updated to include a 5 hp extraction for parasitics, an 11 hp extraction for turbomachinery heat rejection (see section 3.3.4.1 for discussion), and 6.6 hp (2.2%) for the turbo-compounded gearbox loss (see section 3.4.1). An additional 1% in chargeable cooling flow was added to the cycle to account for the increase in RIT. These power extractions and cooling flow increases result in a slightly larger flow size and higher OPR engine.

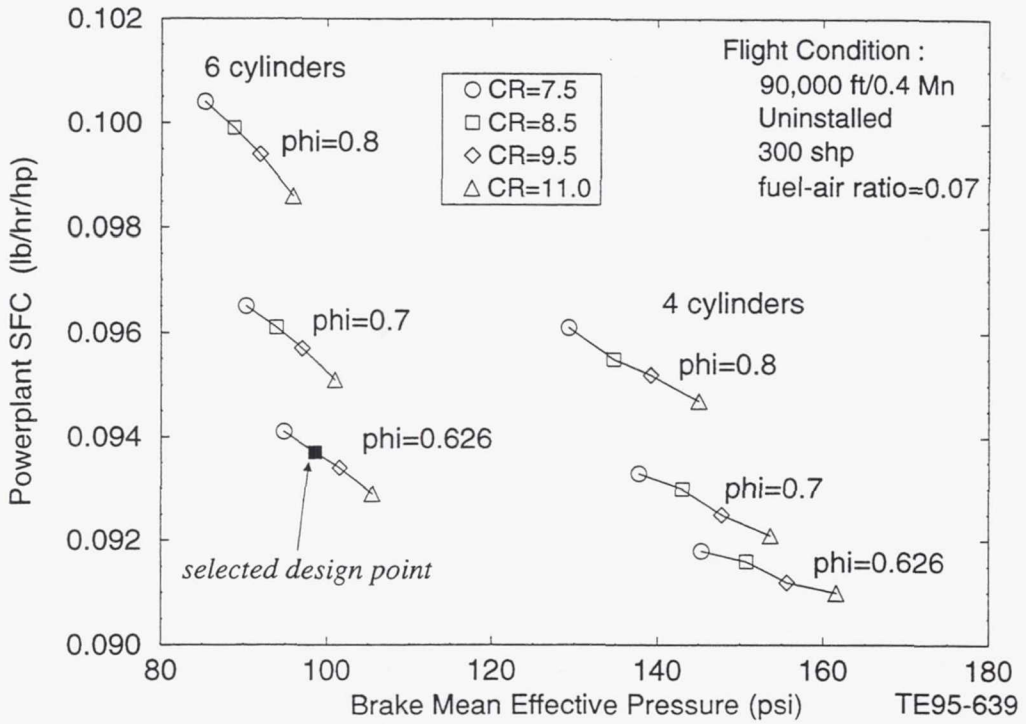

Figure 25. Four-stroke, turbo-compounded H_2 spark ignition parametric: variation in SFC with BMEP.

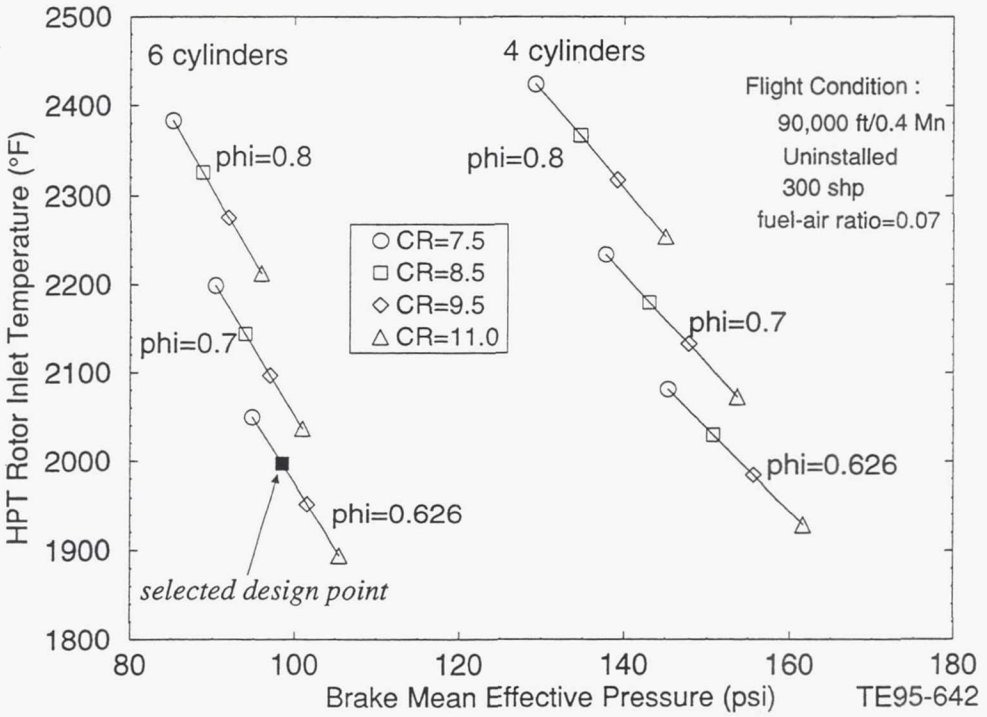

Figure 26. Four-stroke, turbo-compounded H_2 spark ignition parametric: variation in HP turbine rotor inlet temperature with BMEP.

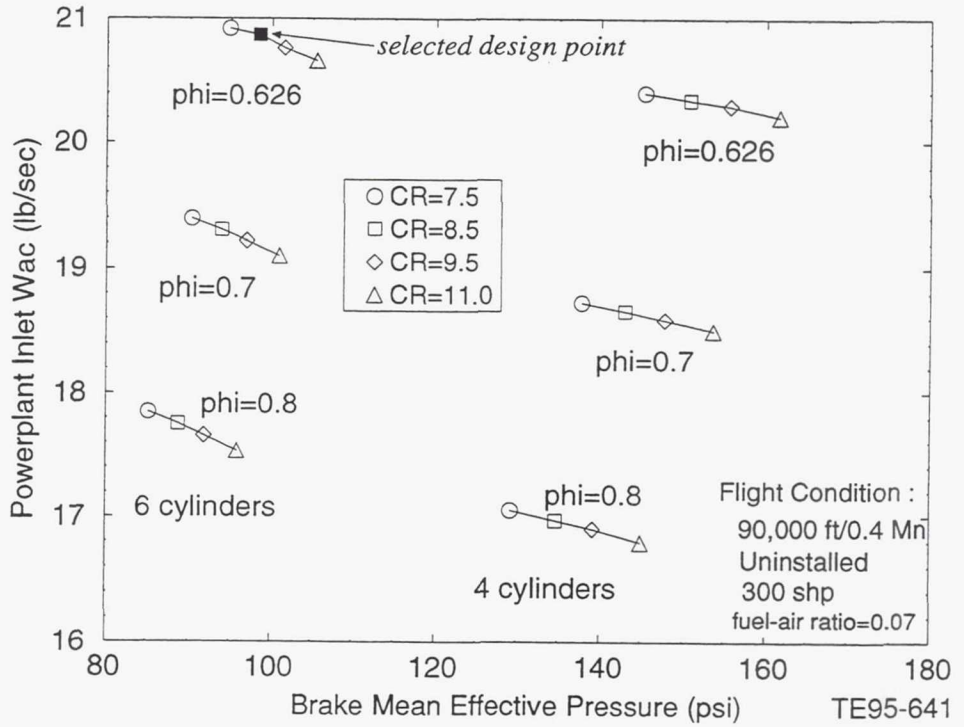

Figure 27. Four-stroke, turbo-compounded H_2 spark ignition parametric: variation in inlet corrected airflow with BMEP.

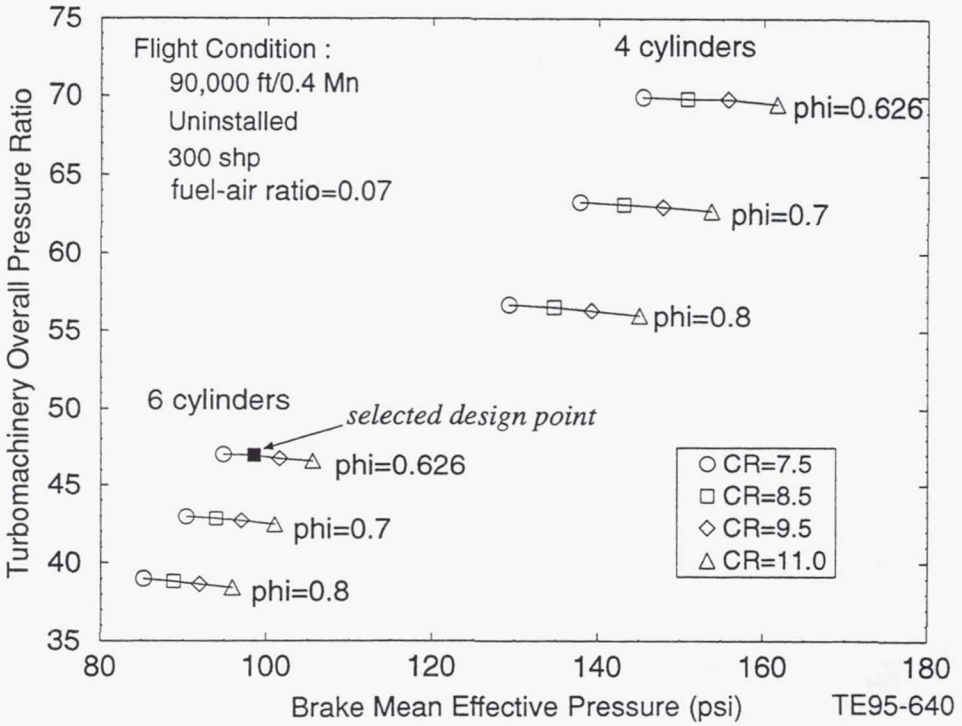

Figure 28. Four-stroke, turbo-compounded H_2 spark ignition parametric: variation in overall pressure ratio with BMEP.

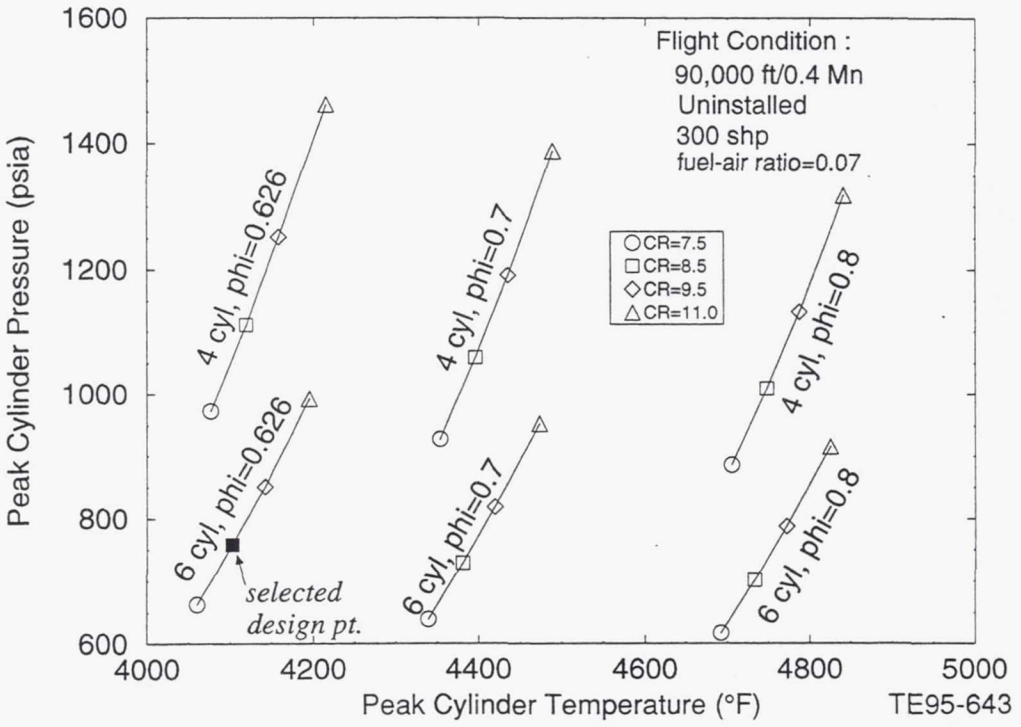

Figure 29. Four-stroke, turbo-compounded H_2 spark ignition parametric: variation in peak cylinder pressure with peak cylinder temperature.

A schematic with aerothermodynamic details of the four-stroke, turbo-compounded H_2 SI engine is presented in Figure 30. The 90,000 ft, 0.4 Mach design point has an OPR of 47.7:1, a powerplant inlet corrected flow of 21.2 lbm/sec, an HPT RIT equal to 2008°F, an SI engine BMEP of 101.7 psia, and a powerplant SFC of 0.0968 lb/hp-hr at the 300 shp maximum power point. The 300 shp output power consists of 184 shp from the H_2 SI engine, 122.6 shp from the power turbine, and a 6.6 shp loss through the gearboxes. The four-stroke, turbo-compounded H_2 SI engine powerplant is summarized in the fifth column of Table 4. The energy balance for the four-stroke, turbo-compounded spark ignition engine running on hydrogen is given in the fifth column of Table 5.

3.1.4 Rotary Engine - NT Technology

Rotary engine data for two different size engines were received from Rotary Power International (RPI) and are presented in this section. One data set (Figures 31 through 34) represents the RPI 70 series, model 3020R engine, which has three rotors with a total cubic inch displacement (CID) of 121.2 $in.^3$. Brake horsepower, airflow, BSFC, BMEP, EGT, volumetric efficiency, and engine speed have been correlated. The volumetric efficiency at each speed is an average of the number of points per speed line.

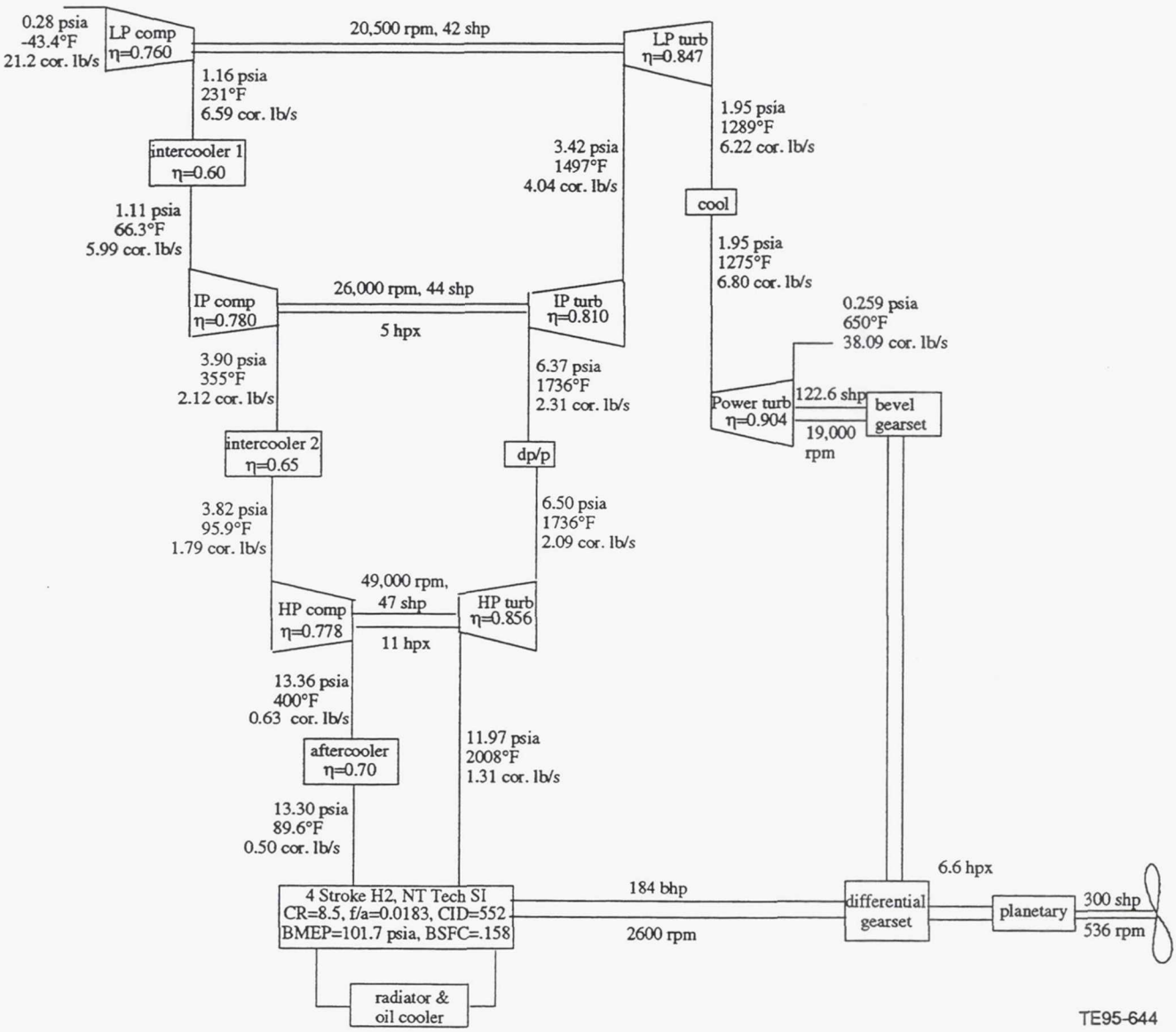

Figure 30. ERAST four-stroke, turbo-compounded H2 spark ignition schematic: 90,000 ft, 0.4 Mach, 300 shp design point.

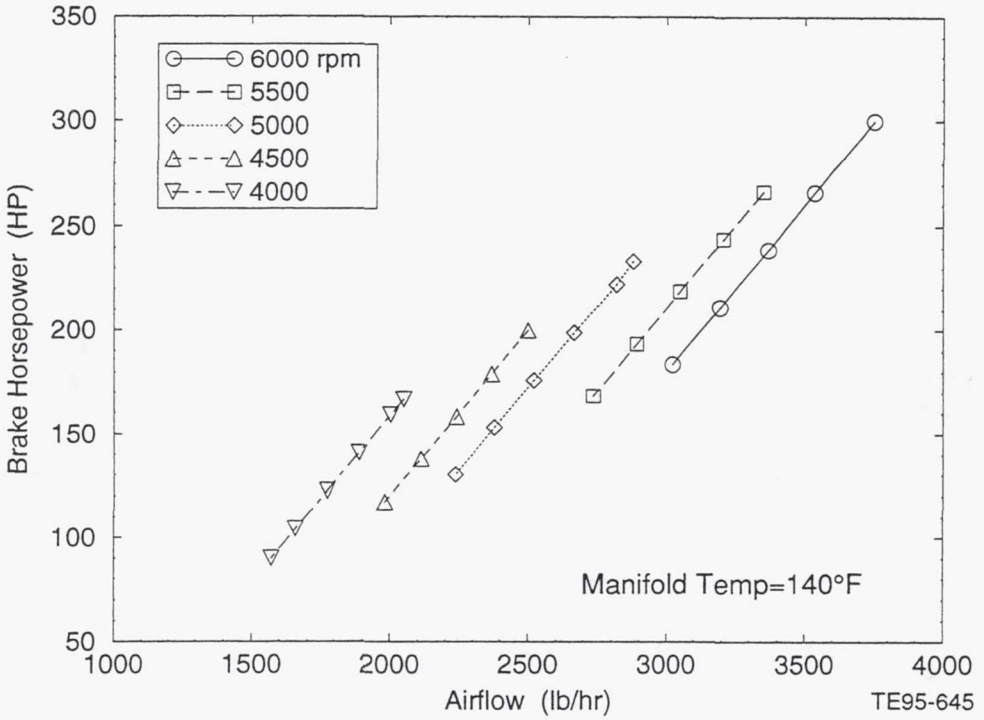

Figure 31. RPI stratified charge 70 series, Model 3020R rotary engine: variation in brake horsepower with physical airflow.

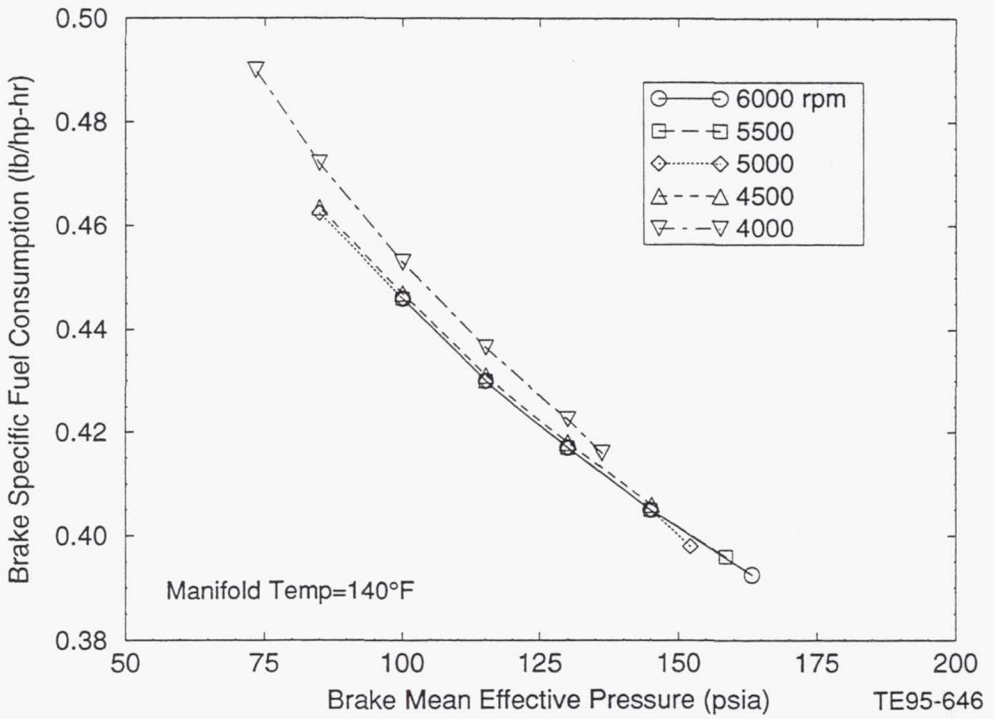

Figure 32. RPI stratified charge 70 series, Model 3020R rotary engine: variation in brake SFC with BMEP.

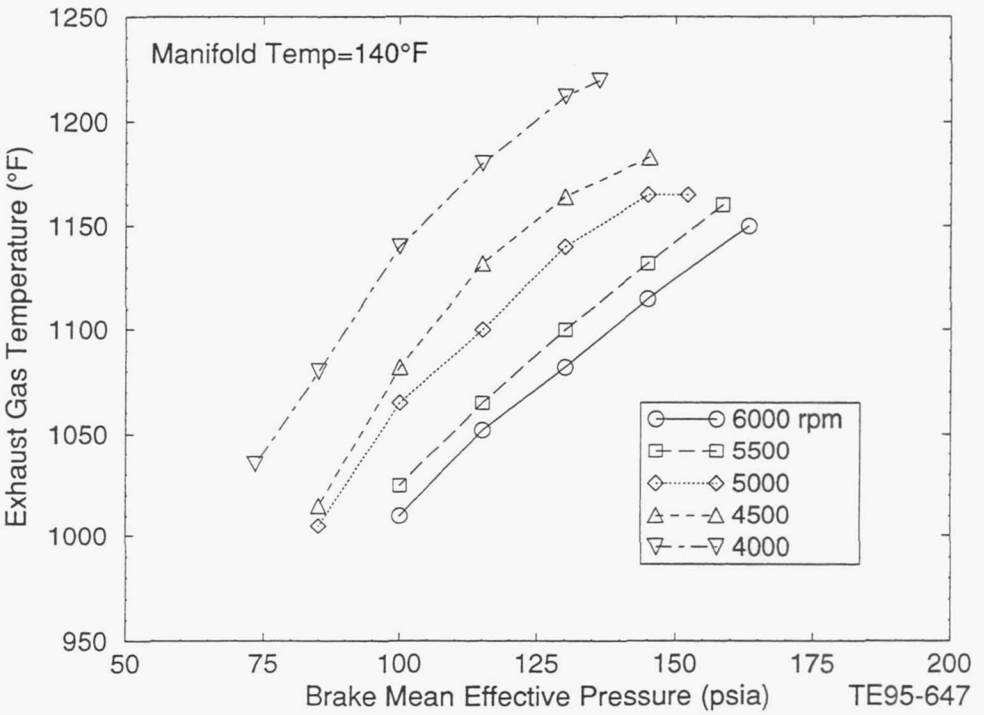

Figure 33. RPI stratified charge 70 series, Model 3020R rotary engine: variation in EGT with BMEP.

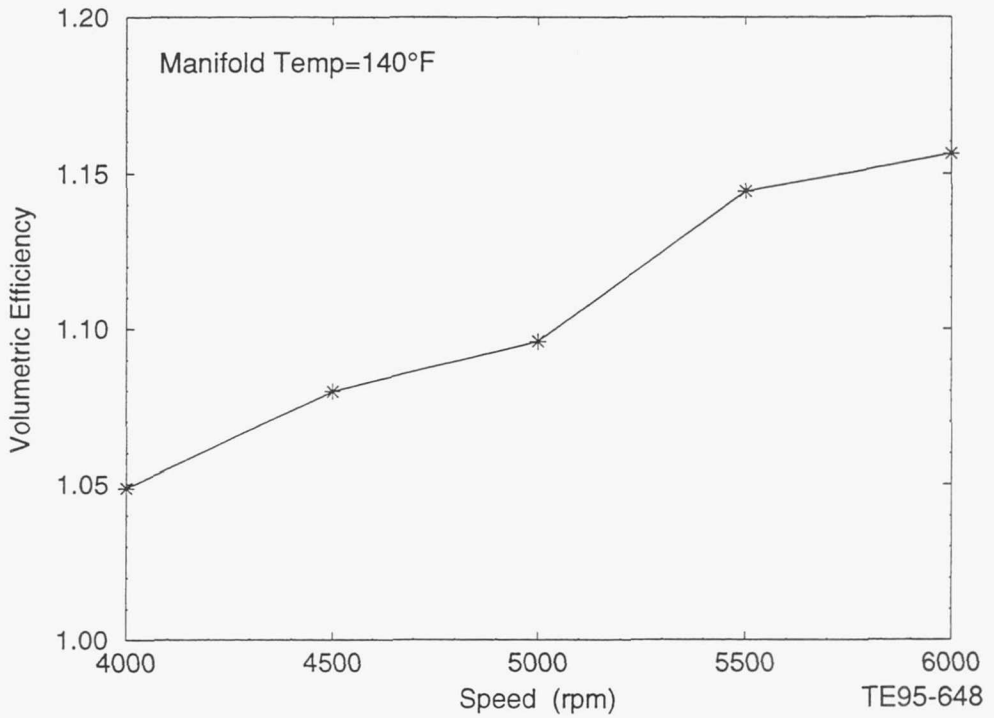

Figure 34. RPI stratified charge 70 series, Model 3020R rotary engine: variation in volumetric efficiency with engine speed.

The second data set (Figures 35 through 38) represents the RPI 170 series, Model 2034R engine, which has two rotors with a total CID of 210 in.^{3}. Again, brake horsepower, airflow, BSFC, BMEP, EGT, volumetric efficiency, and engine speed have been plotted. A modeling scheme was devised to enable this engine data to be used along with TERMAP so that a turbocharged rotary engine could be simulated.

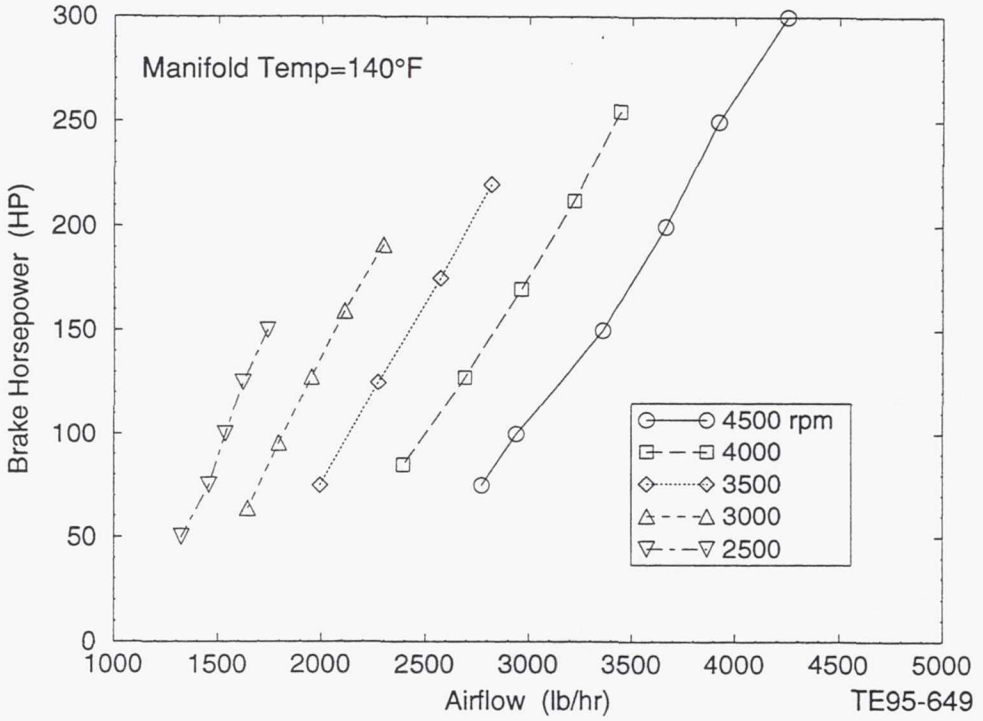

Figure 35. RPI stratified charge 170 series, Model 2034R rotary engine: variation in brake horsepower with physical airflow.

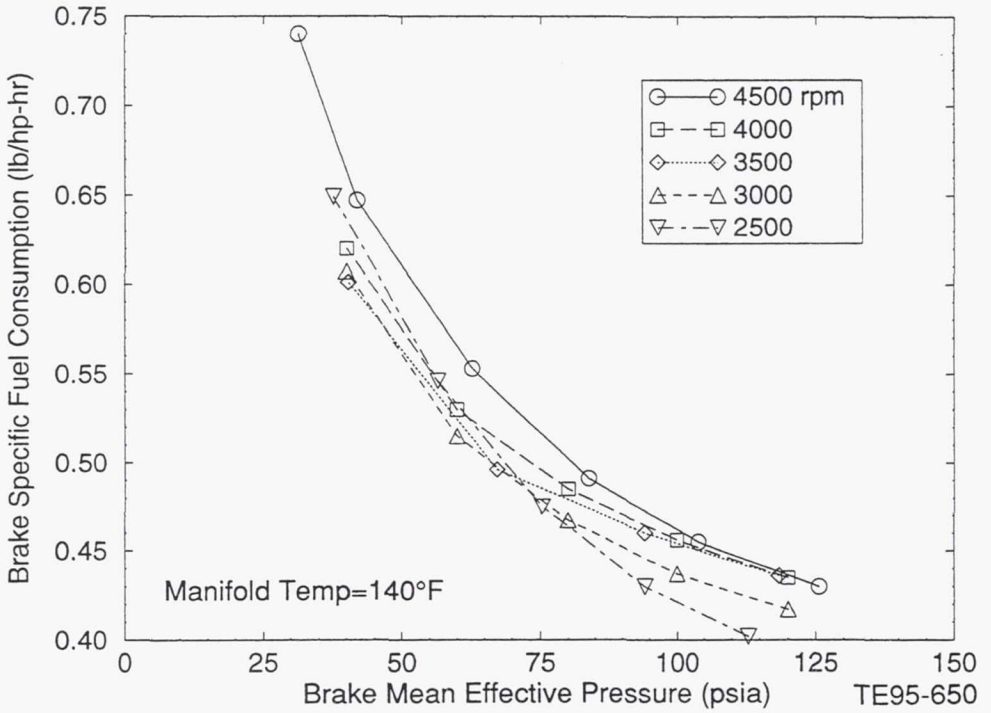

Figure 36. RPI stratified charge 170 series, Model 2034R rotary engine: variation in brake SFC with BMEP.

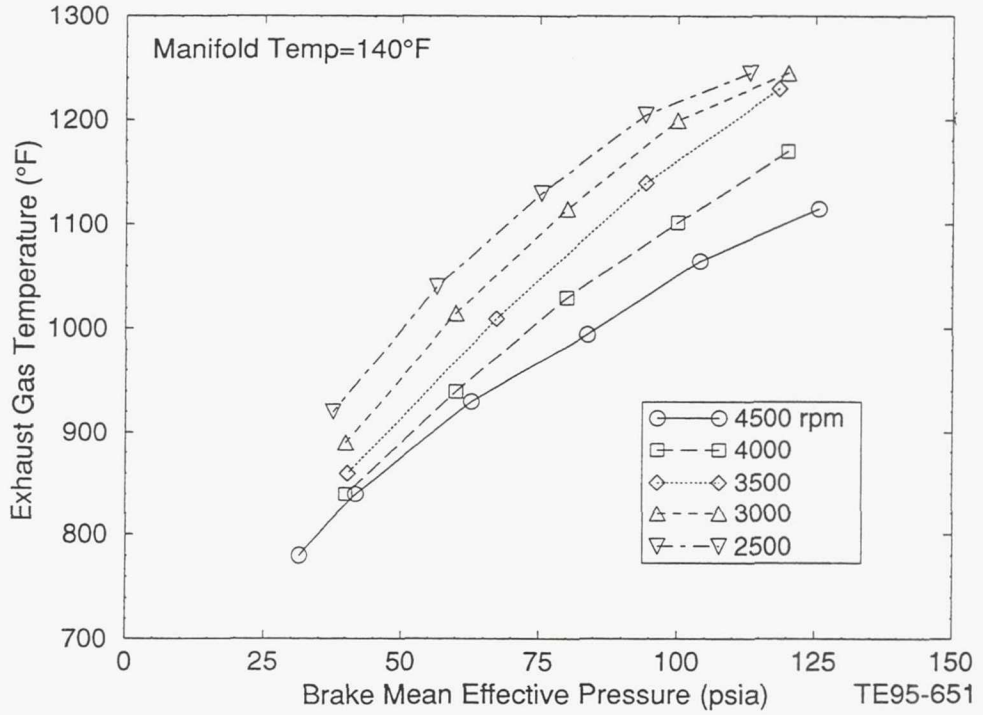

Figure 37. RPI stratified charge 170 series, Model 2034R rotary engine: variation in EGT with BMEP.

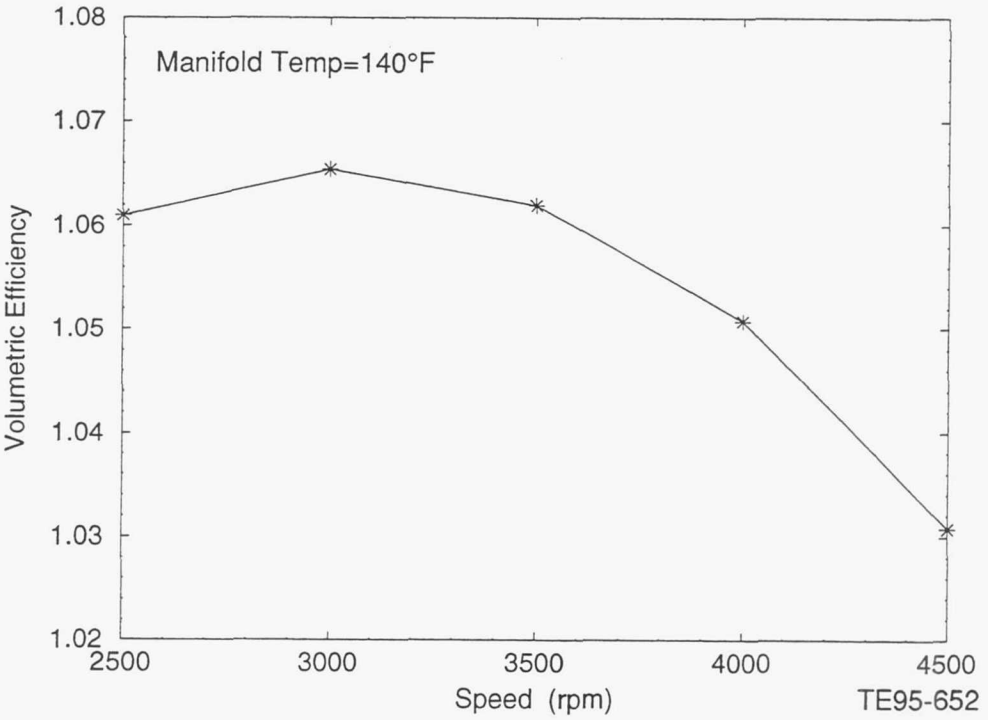

Figure 38. RPI stratified charge 170 series, Model 2034R rotary engine: variation in volumetric efficiency with engine speed.

The rotary engine is similar to the diesel and spark ignition engines in the fact that specific power increases with inlet boost pressure. This requires a turbocharger OPR to be at least 60:1 at the 90,000 ft design point condition. Just as with the turbocharged pistons, three compressors, each operating on a separate spool, will be required to achieve this OPR. Aftercooling will be required, in addition to intercooling between each compressor, to maximize the density of the airflow going into this rotary engine.

The first intercooler effectiveness for this configuration was selected to be 60%, the second intercooler effectiveness was chosen to be 65%, and the aftercooler effectiveness was chosen to be 70%. Setting the effectiveness of the first intercooler at 60% is a good trade between intercooler size required and compressor stage pressure ratio required to achieve a reasonably high level of air density from the low ambient inlet conditions. It was estimated at the beginning of this study that if the effectiveness of the second intercooler was increased an additional 5% above the first intercooler effectiveness and the effectiveness of the aftercooler was increased 10% then their resulting size would be close to the size of the first intercooler.

In the design point simulation of these powerplants, the airflow size of the turbomachinery was varied until the gas flow exiting the rotary equaled the sum of the airflow going into the rotary and the fuel flow added in the combustion part of the rotary cycle. Turbomachinery OPR was varied to get a powerplant total output power of 300 shp.

This turbocharged rotary engine is non-turbo-compounded. The reason for not having a power turbine is the small amount of energy remaining in the flow stream after exiting the LP turbine.

Three different versions of each engine were simulated by adding and subtracting one rotor from each baseline engine. Therefore, for the 70 series engine, 2, 3, and 4 rotors were evaluated, and for the 170 series engine 1, 2, and 3 rotors were evaluated. The results are shown in Figures 39 through 42.

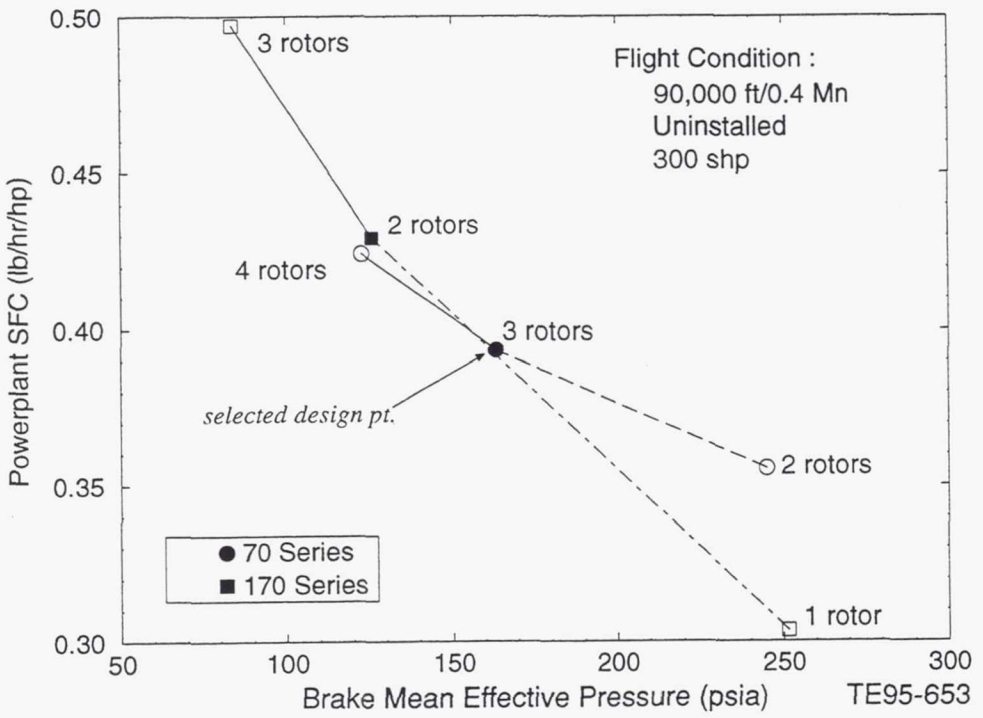

Figure 39. Rotary parametric: variation in SFC with BMEP and number of rotors for both engine candidates.

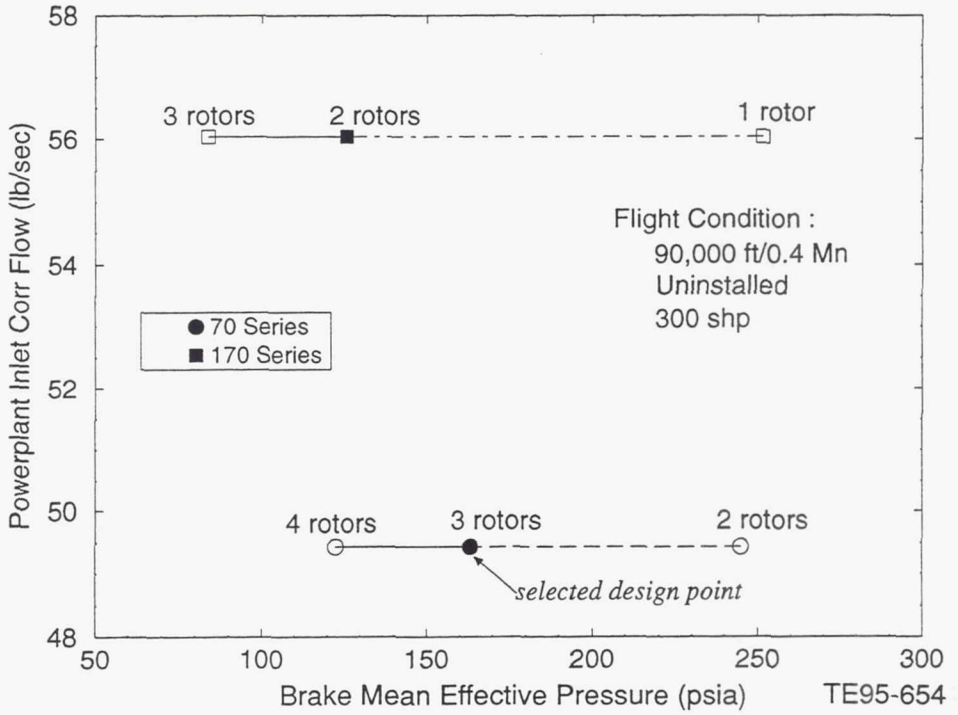

Figure 40. Rotary parametric: variation in airflow with BMEP and number of rotors for both engine candidates.

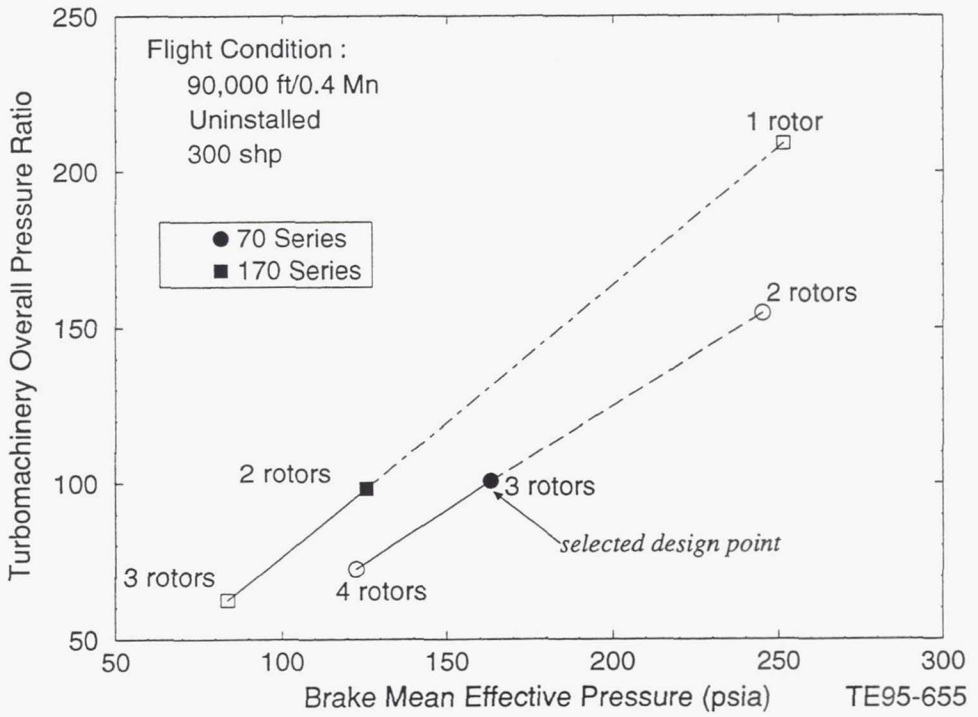

Figure 41. Rotary parametric: variation in OPR with BMEP and number of rotors for both engine candidates.

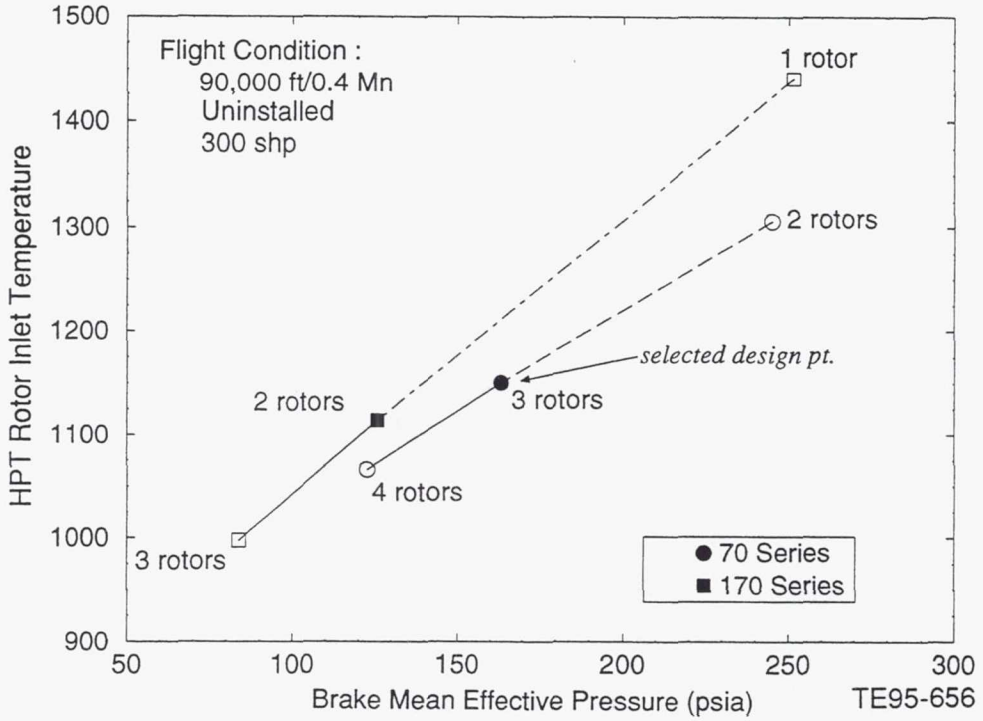

Figure 42. Rotary parametric: variation in HP turbine RIT with BMEP and number of rotors for both engine candidates.

For both of the engines, when one rotor was removed, the BMEP increased considerably and as a result the supplied engine data required excessive extrapolation to the point that its accuracy is questionable. That is why there are dotted lines extending from the baseline to these one rotor less points. In each case, when a rotor was added, the BMEP decreased. Since removing one rotor results in a BMEP that was considered too high, these points were eliminated from further consideration.

Adding a rotor results in an SFC increase, as shown in Figure 39, and a reduction in OPR, as illustrated in Figure 41. Though it would be beneficial from a turbomachinery weight standpoint to have the lower OPR, the SFC increase is too large to justify this trade-off. Therefore, with SFC being a key design parameter, the series 70 baseline engine (SFC = 0.394 lb/hr/hp) was chosen for further study.

Compressor and turbine component aerodynamic designs were completed for this configuration at the 90,000 ft, 0.4 Mach, maximum power (300 shp, 100% $N/\sqrt{\theta}$) design point. After examining both an axial and centrifugal LPC, an axial was chosen since its corrected flow of 49.4 lbm/sec is too large to justify a centrifugal compressor. The second and third compressors were chosen as centrifugal and all three turbines were chosen as axial designs. The appreciable efficiency decrement due to the low Reynolds number at this design point condition was taken into account when evaluating the efficiency level of each component.

The second and third compressor pressure ratios were chosen to be 4.5:1 for the design point cycle at 90,000 ft, 0.4 Mach. This resulted in a low pressure Rc of 5.24:1 being required to produce 300 shp at 90,000 ft, 0.4 Mach. A compressor pressure ratio (Rc) trade-off study was conducted to see if a more optimum arrangement of component pressure ratio distribution existed. The results show that the 5.24/4.5/4.5 combination was near optimum such that the Rc levels were not changed.

The design point cycle was then updated to include a 5 hp extraction for parasitics, an 11 hp extraction for turbomachinery heat rejection (see section 3.3.4.1 for discussion), and 3 hp (1%) for a planetary gearbox loss, as described in section 3.4.2. The result of adding these power extractions to the engine cycle was a decrease in the nozzle expansion ratio.

A schematic with aerothermodynamic details of the turbocharged RPI 70 Series Rotary engine is presented in Figure 43. The 90,000 ft, 0.4 Mach design point has an OPR of 100.9:1, a powerplant inlet corrected flow of 49.4 lbm/sec, an HPT RIT equal to 1150°F, a rotary BMEP of 163.3 psia, and a powerplant SFC of 0.3936 lb/hp-hr at the 300 shp maximum power point. The non-turbo-compounded rotary engine powerplant is summarized in the sixth column of Table 4 for comparison purposes. The energy balance for the rotary engine is given in the sixth column of Table 5.

3.1.5 Coleman Cycle Engine - NT Technology

3.1.5.1 Concept Description

The Coleman Engine is a regenerative feedback turbine engine (RFTE) concept proposed by the Coleman Engine Corporation, Nevada. The engine cycle incorporates two compressors and two turbines all connected to a common shaft. The unique feature of this cycle is that a portion of the gas stream exiting the high pressure turbine is used for recirculation. As shown in Figures 44 and 45, a portion of the gas stream exiting the high pressure turbine, T1, is used to preheat the air exiting the high pressure compressor (C2) through the use of a recuperator (REC). The recuperated T1 air is then mixed with all

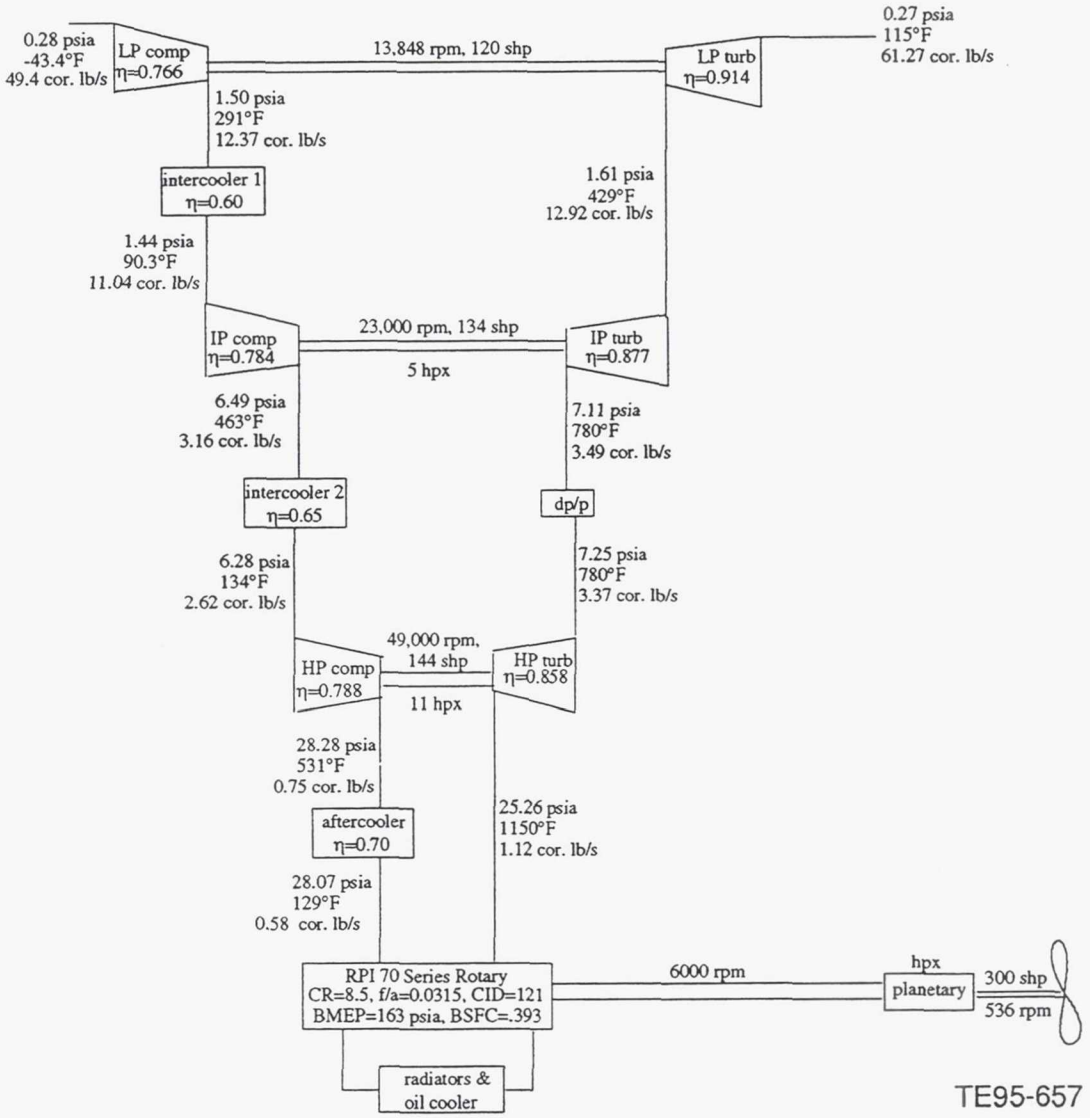

Figure 43. ERAST non-turbo-compounded rotary schematic: 90,000 ft, 0.4 Mach, 300 shp, design point.

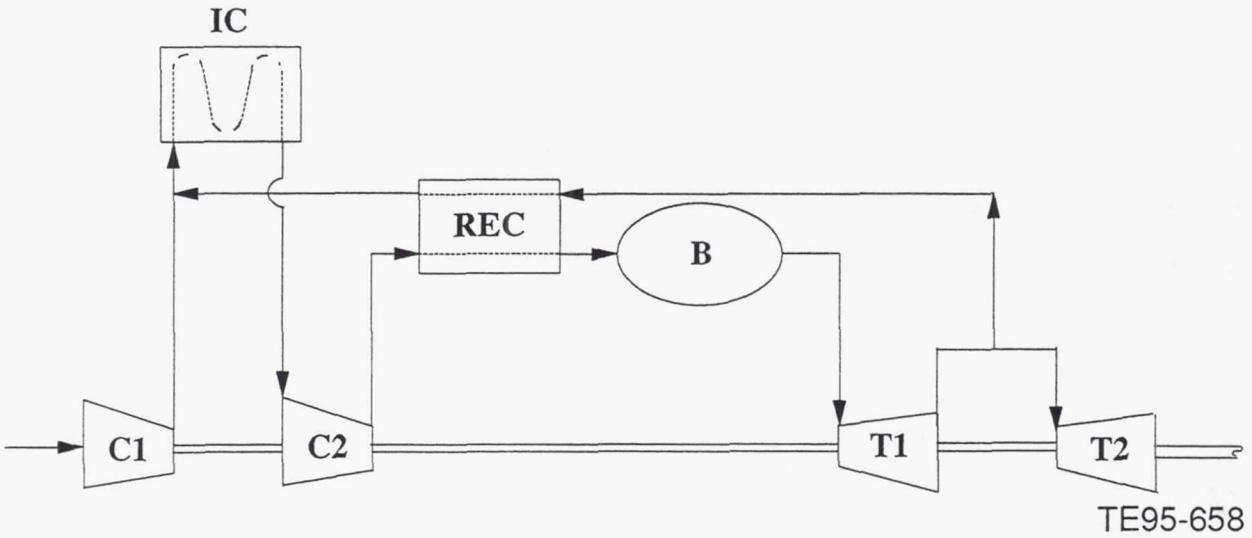

Figure 44. ERAST Coleman engine concept.

of the air exiting the low pressure compressor (C1). This mixture is then passed through an intercooler (IC) before being reintroduced at the inlet of C2.

The cycle's greatest advantage is much higher specific power because much of the work is accomplished by the "inner spool" combination of C2 and T1, which uses recirculated flow. Much less inlet flow is required. However, because C2 and T1 must be sized for the recirculated flow, they will be larger than a conventional gas turbine engine and thus the lower specific power may not equate to lower engine weight. Because the cycle uses an intercooler and a recuperator, the thermal efficiency will be higher than a conventional cycle. For aircraft applications, however, consideration must be given to the weight of the intercooler and the recuperator, as well as the ram drag associated with the intercooler, which may offset the decreased ram drag resulting from the decreased inlet flow.

3.1.5.2 Coleman Engine Model

The Coleman Engine model for the NASA ERAST contract uses the Turbine Engine Reverse Modeling Aid Program (TERMAP), a cycle-matching engine performance computer program developed under contract for the Wright-Patterson Air Force Base Foreign Technologies Division. The design point was selected to be 90,000 ft, Mach 0.4, ISA, 300 hp, and with a burner outlet temperature (BOT) of 2500°F.

Feedback flow ratio (FFR), defined as the ratio of feedback flow to engine inlet flow, was constrained to maintain combustion at 90% stoichiometric. The work split between the high and low pressure turbines was constrained to maintain a feedback flow pressure ratio of 1.05 (this would allow a 5% pressure loss through the plumbing, regenerator, and intercooler). Initially, both the intercooler and recuperator were modeled as 80% effective. Ram drag associated with the intercooler was not book-kept in the engine model so as to be consistent with the manner in which the piston engines, which used intercoolers, were modeled.

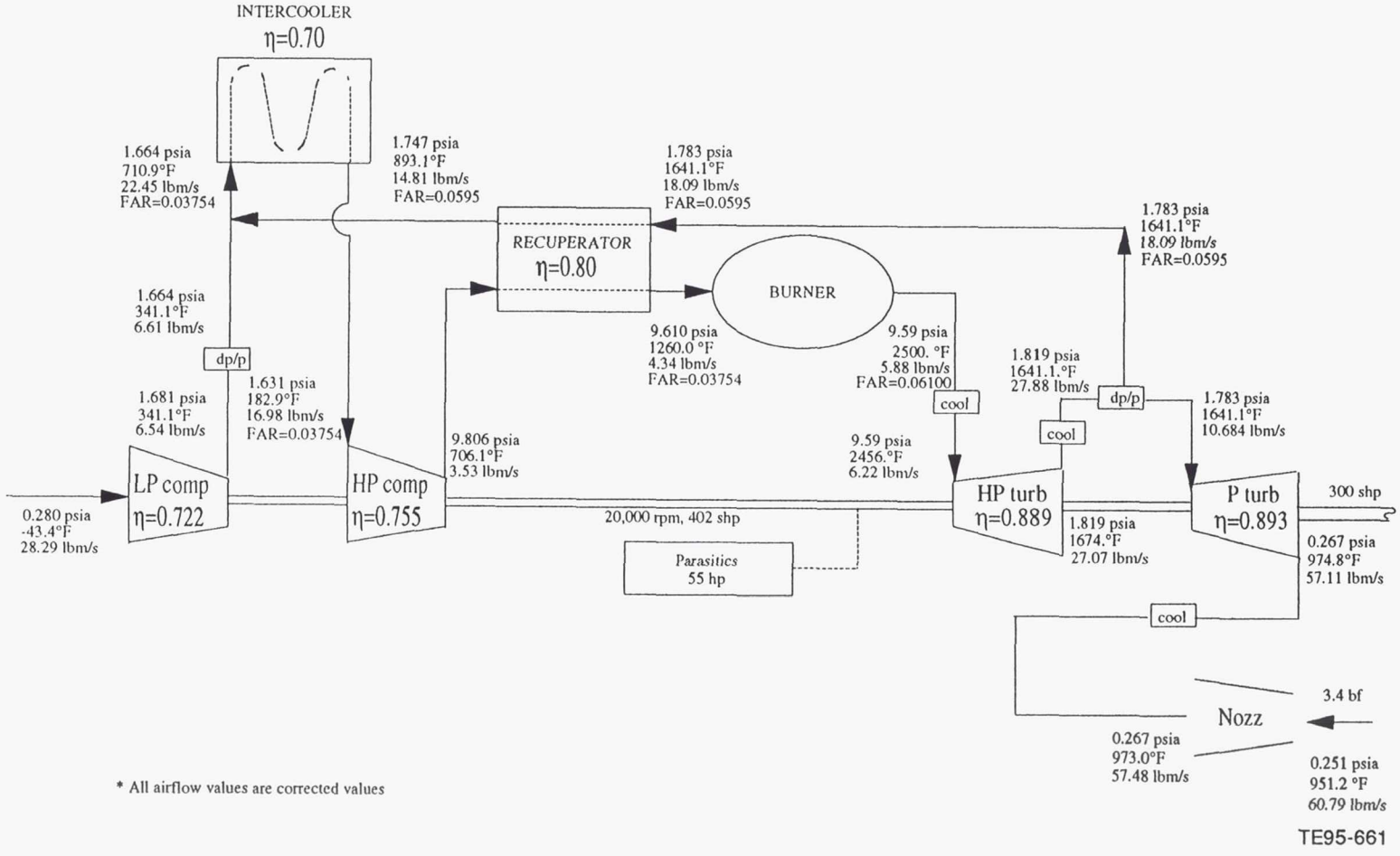

Figure 45. ERAST Coleman engine:
90,000 ft, 0.4 Mach, 300 shp design point.

A parametric study was conducted to determine the optimum pressure ratios of the low and high pressure ratio compressors. A polytropic efficiency estimate of 87% was used as the initial assumption for the compressor and turbine components based on exit corrected flow and pressure ratio. These polytropic efficiencies were corrected for Reynolds number effects at the 90,000 ft design point. Figures 46 and 47 show the results of this study.

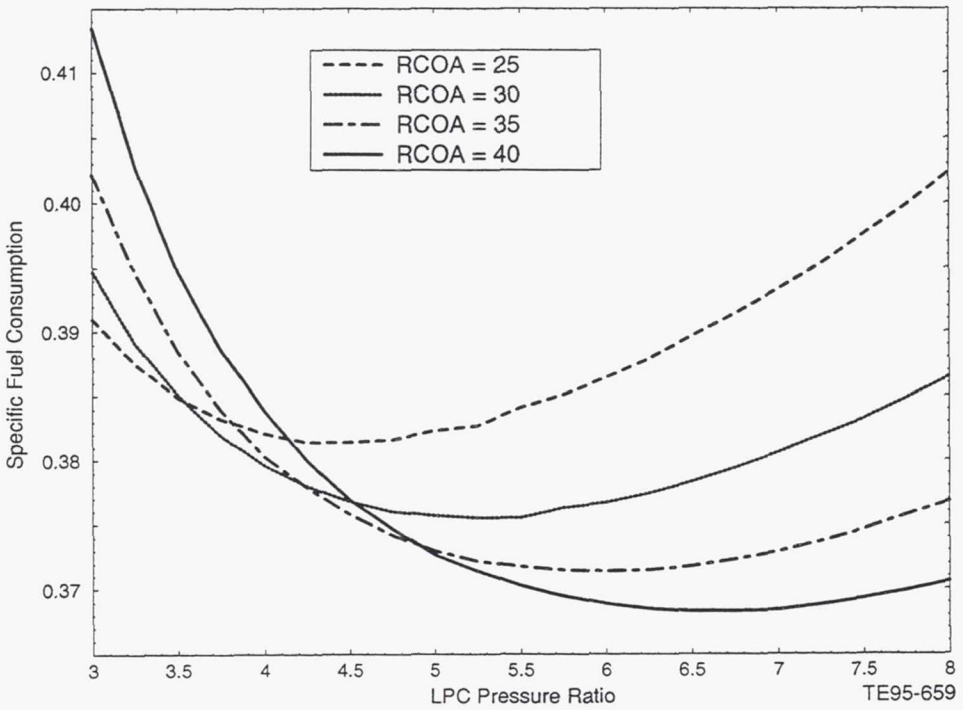

Figure 46. ERAST Coleman engine parametric study: design point, 90,000 ft/0.4 Mach/ISA 300 shp.

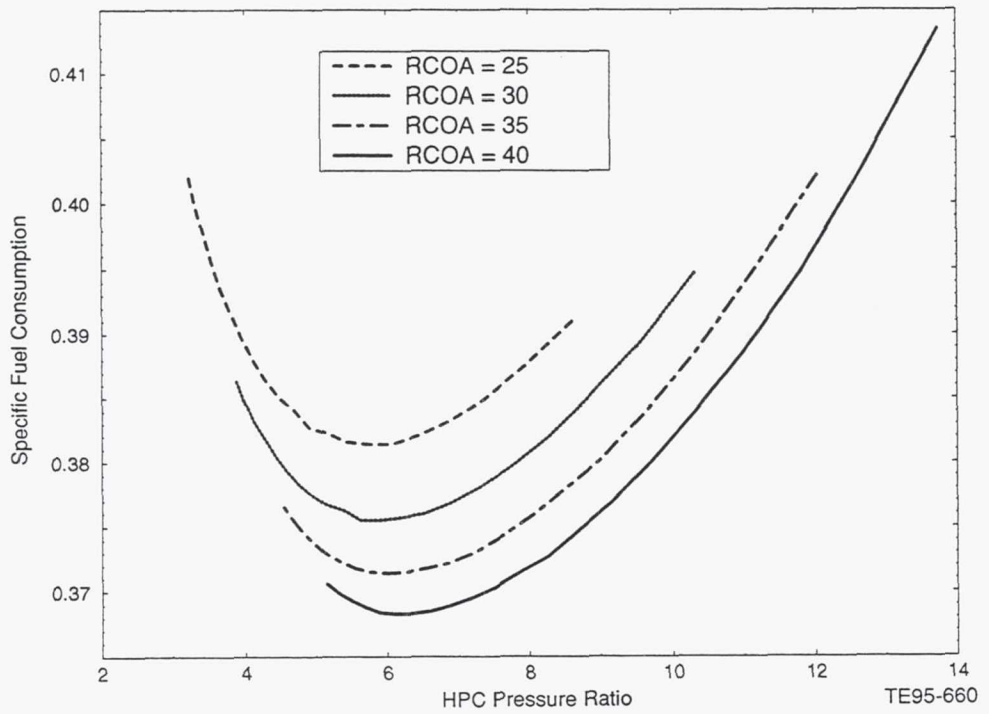

Figure 47. ERAST Coleman engine parametric study: design point, 90,000 ft/0.4 Mach/ISA 300 shp.

An overall pressure ratio of 35.0:1 was selected as a reasonable choice for the given magnitude of inlet corrected airflow. Allowing for 3% pressure drop between the compressors (which includes an intercooler) and evaluating the optimum pressure ratios indicated in Figures 46 and 47, compressor pressure ratios of 6.0 and 6.0125 were selected for the first and second compressors, respectively. Centrifugal compressors were selected because of higher pressure ratios at off-design conditions, and reasonably compact overall dimensions. A first pass assumption of 55 hp extraction was imposed to account for parasitics and waste heat rejection (the waste heat rejection estimates determined for the turboshaft engines in section 3.1.6 were used as the basis of this assumption).

Aerodynamic design of compressor and turbine turbomachinery components were created for this configuration at the 90,000 ft, 0.4 Mach, maximum power (100% $N/\sqrt{\theta}$) design point. The 100% design point mechanical speed was selected to be 20,000 rpm. The inlet corrected flow to the low pressure compressor (LPC) is 28.29 lbm/sec and 16.98 lbm/sec to the high pressure compressor (HPC). Because the Reynolds number indexes (RNI) of the first and second compressors are 0.0254 and 0.0848, respectively, severe penalties in efficiency as well as flow and pressure ratio associated with Reynolds number effects are expected at this high flight condition. The design point adiabatic efficiencies of the two compressors are 80.3%, which yield Reynolds number corrected efficiencies of 72% and 75.5%, respectively, at the 90,000 ft, Mach 0.4 flight condition. The compressor maps for the LPC and HPC were scaled versions of representative Allison high performance centrifugal compressors with ample surge margin.

The inlet corrected flow of the high pressure turbine (HPT) is 6.22 lbm/sec and 10.68 lbm/sec for the low pressure turbine (LPT). The expansion ratios are 5.27 and 6.67 for the high and low pressure turbines, respectively. The efficiencies corrected for Reynolds number effects are 88.9% for the HPT and 89.3% for the LPT. The HPC provided 7.45% unchargeable and 10.4% chargeable cooling flows. Both turbines are two-stage turbines that have provisions for feedback flow to be removed from the flow stream between them and rerouted to the second compressor via a recuperator and intercooler. Turbine maps were generated based on these design point flow conditions and RN scalars were tabulated based on RNI.

The heat exchangers were designed based on inlet and exit flow conditions with 80% effectiveness as described in section 3.3.1 and 3.3.2. The initial Coleman engine design consisted of an intercooler composed of 10 plates with a cold flow length of 5.798 in., hot flow length of 17.39 in., and a width of 35.909 in. The weight of each plate was 22 lb, making the total weight of the intercooler 220 lb, not including the plumbing. The recuperator consisted of six plates with a cold flow length of 2.12 in., plate length of 12.62 in., and a width of 12.302 in. The weight of each plate was 10.68 lb, making the total weight of the recuperator 64 lb, not including plumbing. A performance trade study was made in favor of a 70% effective intercooler, which significantly reduced engine weight while still retaining a competitive SFC. The 70% effective intercooler weighed only 96 lb.

The feedback flow ratio (FFR) is defined as the ratio of feedback flow exiting from between the turbines to the inlet flow. The FFR at the design point is 1.81 and was determined by forcing the combustion FAR to be 90% that of stoichiometric (FAR = 0.061). The work split was determined by forcing the feedback flow to be 5% higher in pressure than the re-entry point pressure. The work split is defined by the ratio of HPT work to total work (HPT and LPT) at the design point, which is 76.9% by horsepower, and by the ratio of HPT ΔH to total (HPT and LPT) ΔH, which is 54.38% by $\%\Delta H$. This $\%\Delta H$ ratio was employed in the off-design analysis.

A schematic with aerothermodynamic details of the Coleman engine is presented in Figure 45. The 90,000 ft, 0.4 Mach design point has an OPR of 35.0:1, a powerplant inlet corrected flow of 28.291 lbm/sec, an HPT RIT equal to 2456°F (burner outlet temperature BOT = 2500°F), and a powerplant SFC of 0.4267 lb/hp-hr (TSFC = 0.3781 lb/lbf-hr) at the design power point (300 shp resulting in 338 lbf total thrust).

3.1.6 Turboshaft Engine - SOA and NT Technology

The turboshaft engines for the NASA ERAST study were modeled using the Turbine Engine Reverse Modeling Aid Program (TERMAP). Because the Allison Engine Company had conducted an extensive preliminary design of a turboshaft engine for the High Altitude Long Endurance (HALE) engine program, the turboshaft engine designs for the ERAST contract were based on the HALE engine design. The HALE engine had a design point of 65,000 ft, Mach 0.4, ISA, with a power output of 600 hp. The HALE engine was a derivative T406 turboshaft derivative engine, which incorporated a modified combustor to account for lower combustion pressures and a recuperator to improve thermal efficiency. Figure 48 shows a drawing of the HALE engine. A HALE-based engine was selected due to the amount of design work that had been conducted to accommodate the high altitude, low Reynolds number environment, specifically with regard to waste heat rejection and parasitic losses. Both recuperated and nonrecuperated engines were examined for the HALE study.

A design point study for a recuperated and nonrecuperated turboshaft configuration was completed using the HALE engine as a basis. The design point power output was defined as 300 shp. A 2% pressure loss with 98.3% efficiency was initially modeled for the combustor at the design point. Design efficiencies for the HPT and LPT of 0.85 and 0.88, respectively, were assumed for the ERAST engines. An initial waste heat rejection/parasitic horsepower extraction of 47 hp was imposed as per the HALE engine. This consisted of 22 hp for waste heat rejection and 25 hp for parasitics including bearing windage, sumps, and fuel pump.

A parametric study was conducted to determine pressure ratio and size of the engine for the 90,000 ft, Mach = 0.4 design point based on optimum SFC. Reynolds number correction factors taken from the results of the HALE study and latest Allison experimental data were applied to airflow, pressure ratio, and efficiency to account for Reynolds number effects. Compressor design map pressure (Rc) ratio was varied as well as RIT and airflow to meet the 300 shp requirement. Engine size was determined by linear scale factor (LSF), which is equal to the square root of the ratio of ERAST compressor design airflow to the HALE T406 compressor design airflow. Thus an engine with an LSF of 1.5 is 1.5 times larger than the HALE T406 engine. Figures 49 and 50 show the results of this parametric study.

A compressor design map pressure ratio of 16.0 was selected for the recuperated turboshaft, taking into account the Reynolds number effect results in an OPR of 14.34:1 at the design point. A similar parametric study was conducted for the nonrecuperated engine that indicated an optimum Rc of 20.0:1 and an OPR of 17.93:1. An RIT of 2500°F was selected as a technologically feasible limit while keeping engine size down. To compare the recuperated and nonrecuperated turboshaft engine configurations on equal terms, two nonrecuperated turboshaft configurations were analyzed: one with an Rc of 16.0:1 and one with an Rc of 20.0:1.

A design study was conducted to determine the combustion system size required for the low combustion pressure inherent in the ERAST engine. The following design limits were used, based on AE 3007 (a turbofan derivative of the T406 engine in the 7000 lb thrust range) combustor design: reference velocity < 75 ft/sec, residence time > 10 ms, burner loading parameter < 0.5. A parametric study for all three configurations was made on the effect of liner diameter and length on combustion efficiency. Combustor efficiency was determined empirically for various size combustion systems using a model based on AE 3007 performance data. Figure 51 shows the results of this study. The liner's inner diameter is assumed to be 12.5 in. for all calculations. Although these predictions lie in a regime far from the operating envelope of the AE 3007 engine and are a significant extrapolation of the current data base, they are sufficient for preliminary design of the combustor. All configurations assumed a propeller efficiency of 80% at the design point.

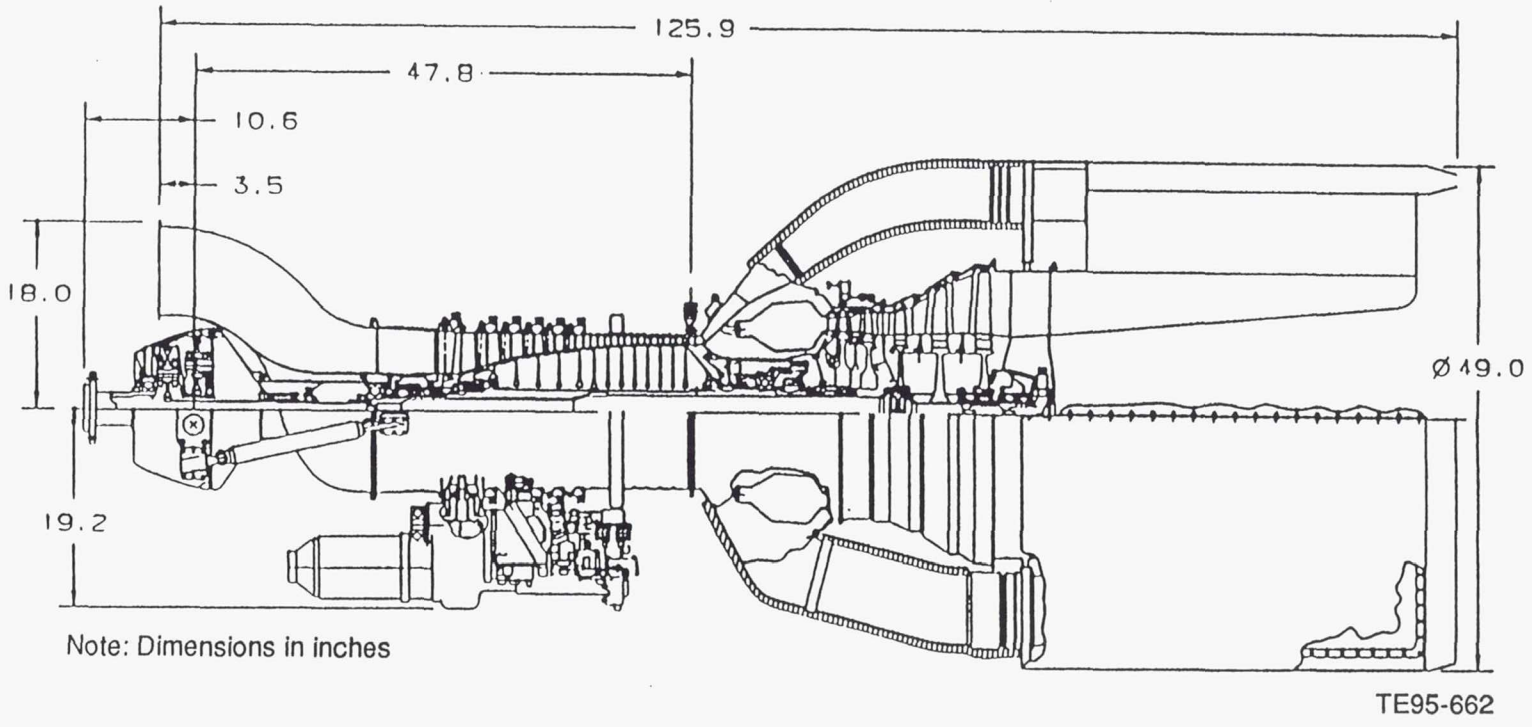

Figure 48. HALE engine.

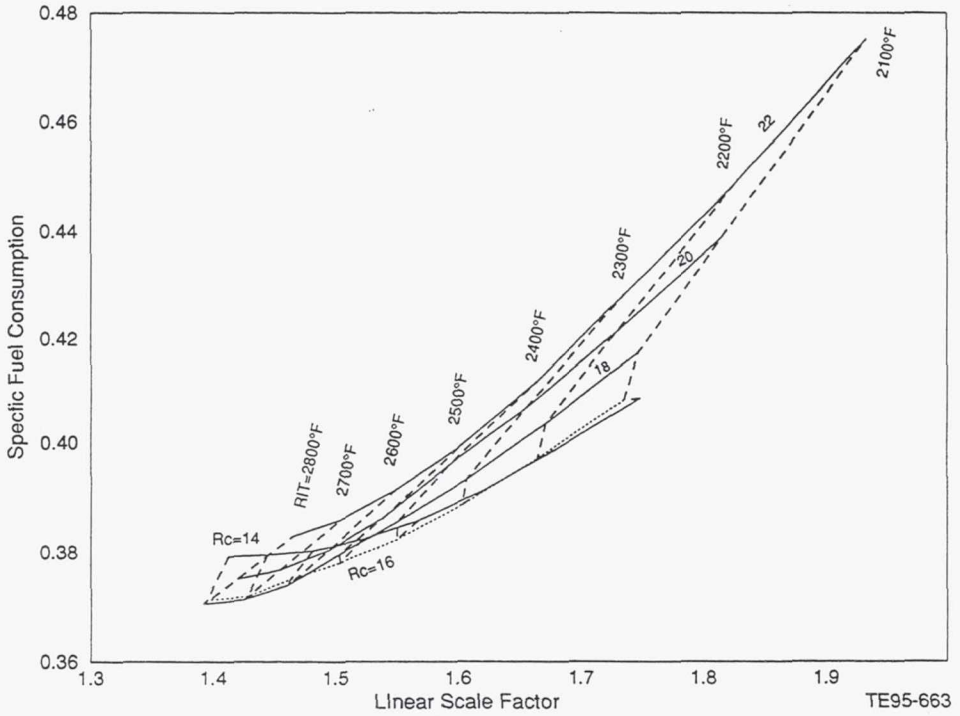

Figure 49. ERAST recuperated turboshaft parametric study: design point, 90,000 ft/0.4 Mach/ISA 300 shp.

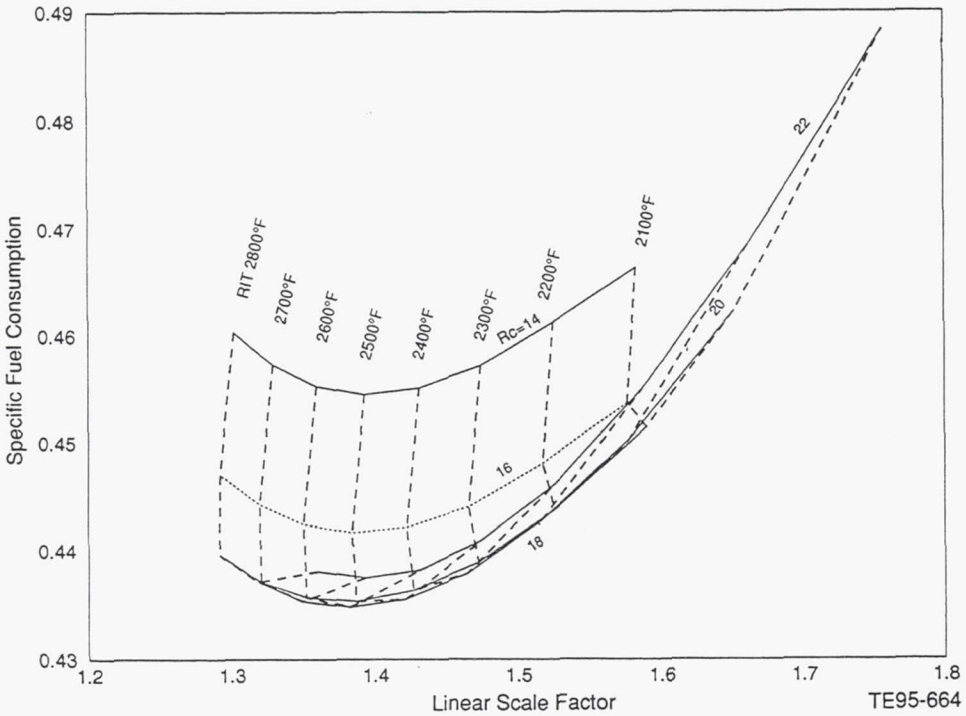

Figure 50. ERAST nonrecuperated turboshaft parametric study: design point, 90,000 ft/0.4 Mach/ISA 300 shp.

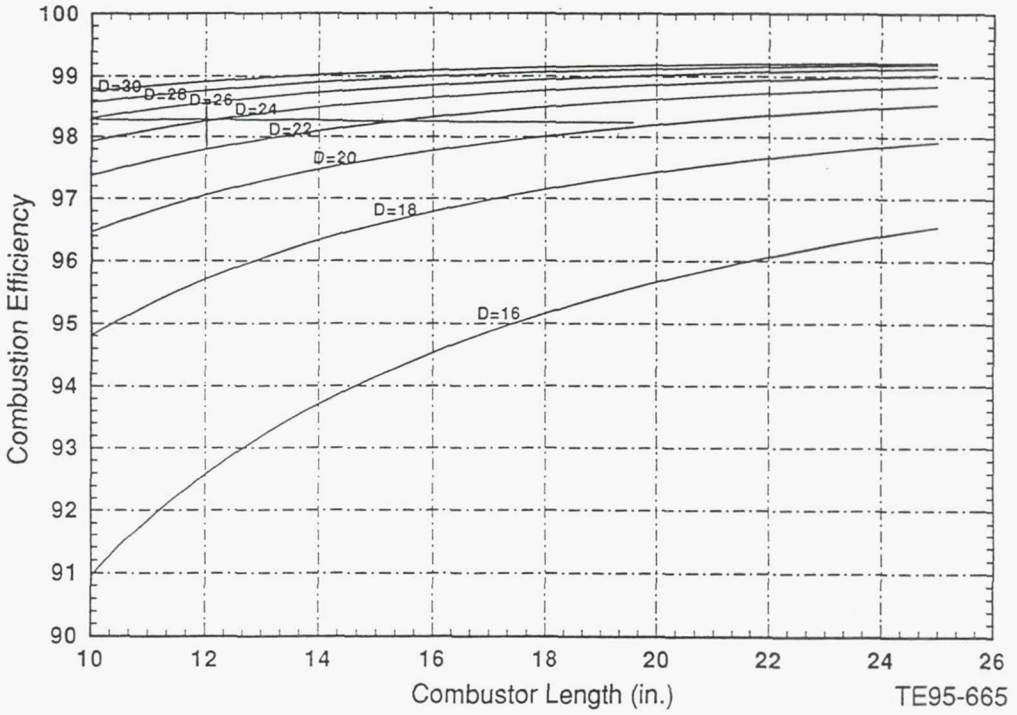

Figure 51. ERAST turboshaft combustor parametric study: design point, 90,000 ft/0.4 Mach/ISA 300 shp.

3.1.6.1 Recuperated Turboshaft Engine Rc = 16:1 - NT Technology

The compressor for the recuperated turboshaft engine is derived from the HALE engine. It is a 14-stage axial compressor with a design pressure ratio of 16.0:1 and design corrected airflow of 87.1 lbm/sec. Reynolds number (RN) effect scalars for corrected airflow, pressure ratio, and efficiency have been tabulated based on Reynolds Number Index (RNI) and are based on T406 rig data and other size compressors from the open literature. The RNI is defined as the RN at the operating point divided by the RN at the compressor design point. The RN at the compressor design point is based on sea level ambient air conditions and the first rotor midspan chord relative velocity. The RNI at the design point is 0.0251. The scalars for corrected flow, efficiency, and pressure ratio at the design point are 0.895, 0.900, and 0.896, respectively. This results in an OPR of 14.34:1, an adiabatic efficiency of 76%, and a corrected inlet flow of 77.2 lbm/sec. The design point map speed is 102.0 % with a mechanical speed of 13,949 rpm.

The HP turbine is a two-stage axial flow design utilizing advanced cooling techniques to accommodate the 2500°F RIT. First-stage vane total cooling is 5.33% (unchargeable) and 9.01% for the two rotors and number 2 vane (chargeable). The RN scalars for corrected flow and efficiency are 0.975 and 0.958, respectively. The design point map speed is 103.0% with a mechanical speed of 13,949 rpm. The LP turbine (power turbine) is a three-stage axial design that is close coupled and corotates with the gas generator (HP) turbine. It was designed for the HALE study to operate in the high altitude, low RN environment. The third-stage vane (first stage of power turbine) is variable to provide high efficiency over a broad range of low power operating conditions. Total cooling for the LP turbine is 2.07% (chargeable). The RN scalars for the LP turbine are 0.969 and 0.935 for corrected flow and efficiency, respectively. The adiabatic efficiencies of the HPT and LPT are 85% and 88%, respectively. The design mechanical speed is 15,000 rpm and the design corrected map speed is 90%.

The design constraints for the recuperator were drawn from the HALE engine study. An effectiveness of 80% was selected with a 2% pressure loss in the cold side and 10% pressure loss in the hot side. A 6% hot side pressure loss and 1.15% cold side pressure loss associated with plumbing was added to the model. Refer to section 3.3.2 for details on the recuperator. Based on the parametric study described in section 3.1.6 and shown in Figure 51, the combustor length was selected to be 12 in. and outer diameter chosen to be 25 in. This yielded an L/D ratio of about 1.85, similar to the HALE engine design.

The initial estimate of horsepower extraction used to model waste heat rejection was revised to 48 hp as described in section 3.3.4.2, and parasitic losses to 19.5 hp, make the total horsepower extraction of 67.5 hp imposed on this cycle.

A schematic with aerothermodynamic details of the recuperated turboprop engine is presented in Figure 52. The 90,000 ft, 0.4 Mach design point has an OPR of 14.34:1, powerplant inlet corrected flow of 77.2 lbm/sec, HPT RIT equal to 2500°F, and powerplant SFC of 0.422 lb/hp-hr (TSFC = 0.368 lb/lbf-hr) at the design point power (300 shp resulting in 344 lbf total thrust). The linear scale factor (LSF) is 1.487. This LSF is used by the mechanical designers to scale up the HALE engine for designing the ERAST engine.

3.1.6.2 Nonrecuperated Turboshaft Engine Rc = 16 - SOA Technology

To compare the usefulness of using a recuperator for the ERAST application, an engine using the same design pressure ratio (Rc) was evaluated without a recuperator. The same design approach was used to design the nonrecuperated turboshaft engine with an Rc of 16.0:1. The same compressor is used for the nonrecuperated turboshaft engine that is used for the recuperated turboshaft. The 2500°F RIT and 300 shp were also retained. The compressor inlet corrected flow is 65.1 lbm/sec, resulting in an LSF of 1.358. The HPT and LPT components remain the same (except for scaling per LSF). The combustor geometry also remains the same with reduced efficiency due to lower burner inlet temperatures.

Because the engine is smaller and there is no recuperator, less power is lost to waste heat rejection. Only 33.8 hp is penalized due to waste heat rejection (see section 3.3.4.2 for discussion). Thus, the entire power extraction at the design point is 53.29 hp. A schematic with aerothermodynamic details of the nonrecuperated turboshaft engine (Rc = 16:1) is presented in Figure 53. The 90,000 ft, 0.4 Mach design point has an OPR of 14.34:1, a powerplant inlet corrected flow of 64.40 lbm/sec, an HPT RIT equal to 2500°F, and a powerplant SFC of 0.4767 lb/hp-hr (TSFC = 0.4132 lb/lbf-hr) at the design point power (300 shp resulting in 346 lbf total thrust). The LSF is 1.358. This LSF is used by the mechanical designers to scale up the HALE engine for designing the ERAST engine.

3.1.6.3 Nonrecuperated Turboshaft Engine Rc = 20 - NT Technology

The parametric study described in section 3.1.6 and presented in Figure 50 indicated that the optimum design pressure ratio (for minimum SFC) for a nonrecuperated turboprop is Rc = 20:1. The same design approach of using the HALE engine as a basis was used to design the nonrecuperated turboshaft engine with an Rc of 20.0:1. The same compressor is used for the nonrecuperated turboshaft engine that is used for the recuperated turboshaft. The 2500°F RIT and 300 shp remain the same. The compressor inlet corrected flow is 64.2 lbm/sec resulting in an LSF of 1.359. The HPT and LPT components remain the same (except for scaling per LSF). The combustor geometry also remains the same with reduced efficiency due to lower burner inlet temperatures.

As with the nonrecuperated turboshaft with Rc = 16:1, the entire power extraction at the design point is 53.29 hp. A schematic with aerothermodynamic details of the nonrecuperated turboshaft engine (Rc = 20:1) is presented in Figure 54. The 90,000 ft, 0.4 Mach design point has an OPR of 17.93:1, a powerplant inlet corrected flow of 64.50 lbm/sec, an HPT RIT equal to 2500°F, and a powerplant SFC of 0.4573 lb/hp-hr at the design point power (300 shp resulting in 345 lbf total thrust). The linear scale factor (LSF) is 1.359. This LSF is used by the mechanical designers to scale up the HALE engine for designing the ERAST engine.

3.1.7 Fuel Cell Engine - Advanced Technology

A fuel cell is an energy conversion device that produces electrical power directly from electrochemical reactions. Like a battery, a fuel cell has electrodes, an electrolyte, and positive and negative terminals. Unlike a battery, however, a fuel cell can operate continuously as long as it is supplied with a stream of fuel and oxidant. In a proton exchange membrane (PEM) fuel cell, the planar polymer electrolytic transports protons and water between a catalyzed oxidation reaction on its fuel (anode) side and a corresponding catalyzed reduction reaction on its air (cathode) side, producing DC power, plus

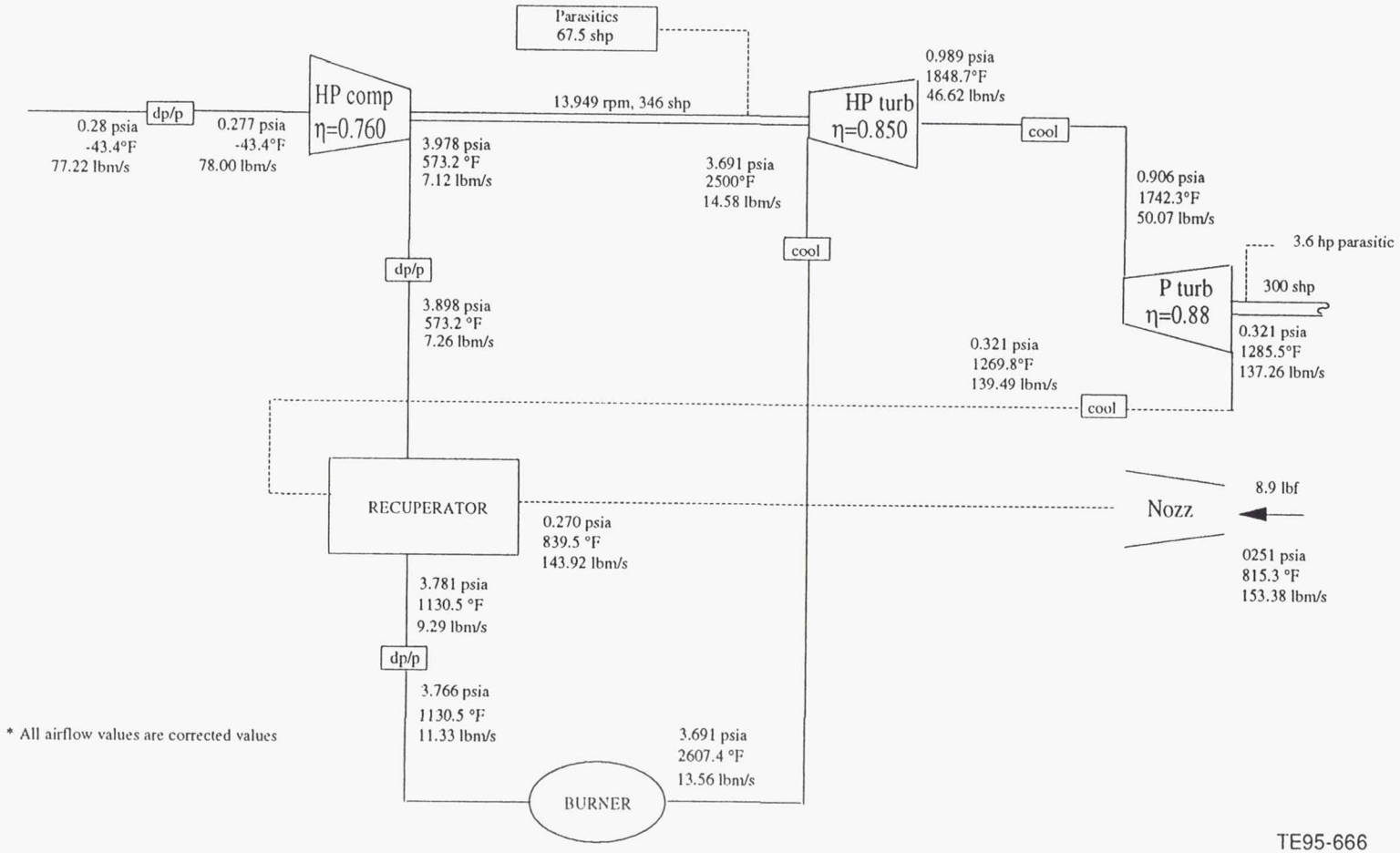

Figure 52. ERAST recuperated turboshaft Rc = 16:
90,000 ft, 0.4 Mach, 335 lbf design point.

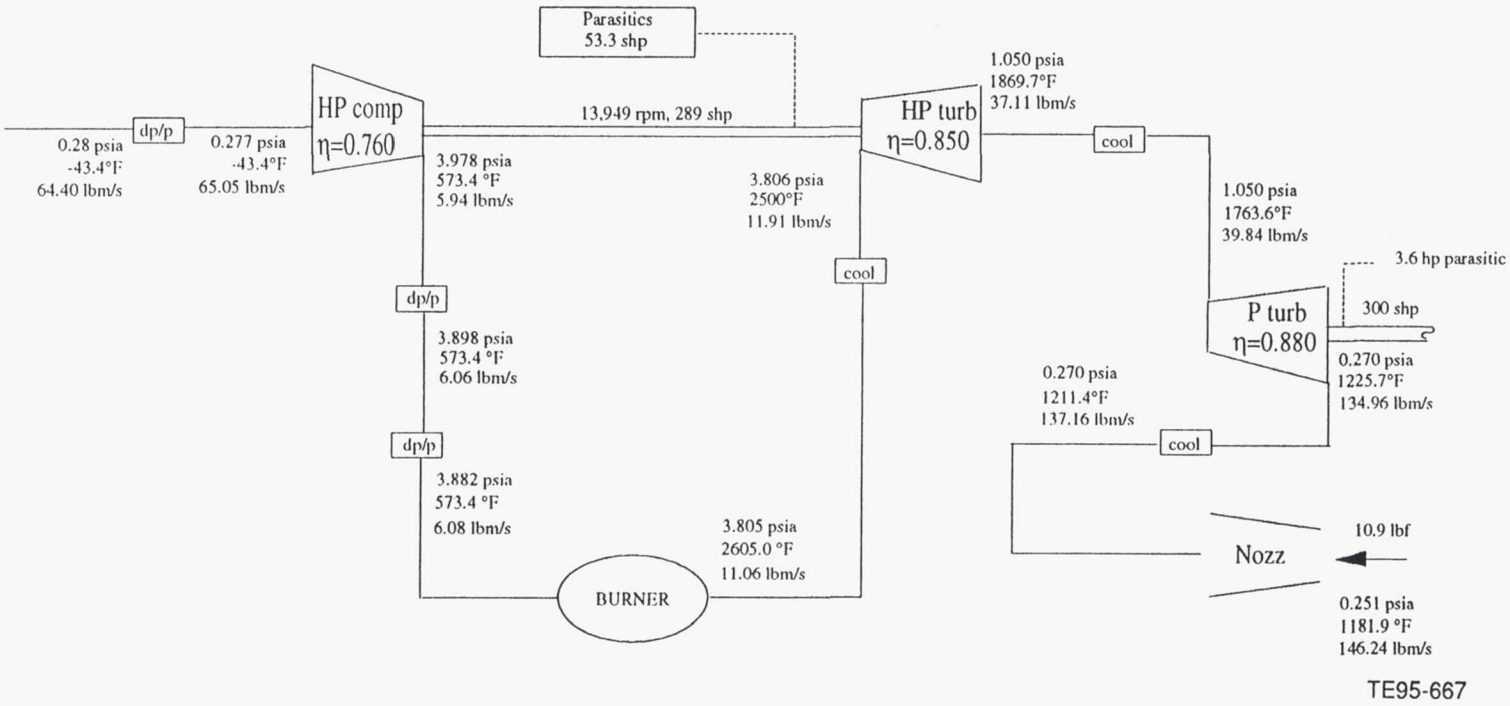

* All airflow values are corrected values

Figure 53. ERAST nonrecuperated turboshaft Rc = 16:
90,000 ft, 0.4 Mach, 335 lbf design point.

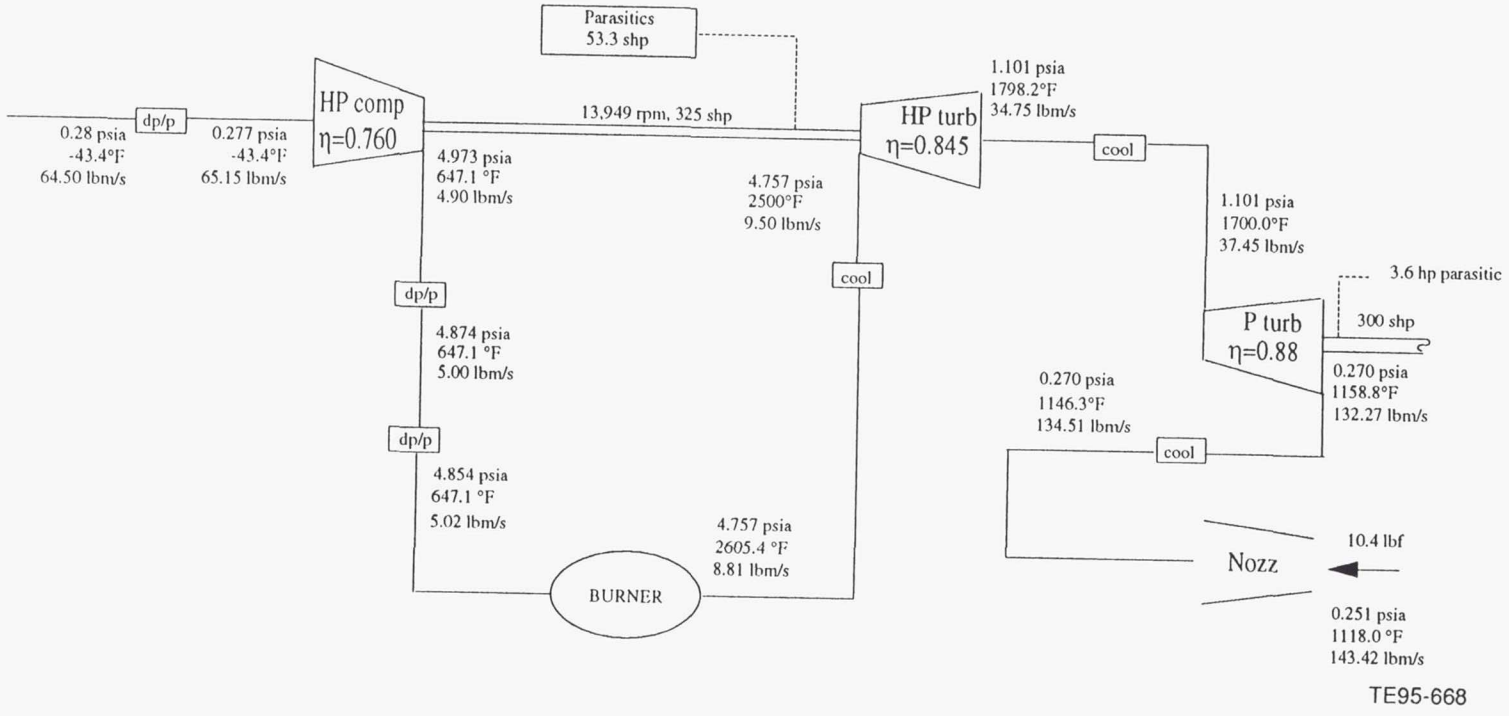

* All airflow values are corrected values

Figure 54. ERAST nonrecuperated turboshaft Rc = 20:
90,000 ft, 0.4 Mach, 335 lbf design point.

water and heat as by-products. While a single fuel cell such as that shown in Figure 55, provides an output of less than a single volt, a series of cells can be "stacked" together in series to produce an appropriate amount of energy. A typical stacking arrangement is illustrated in Figures 56 and 57.

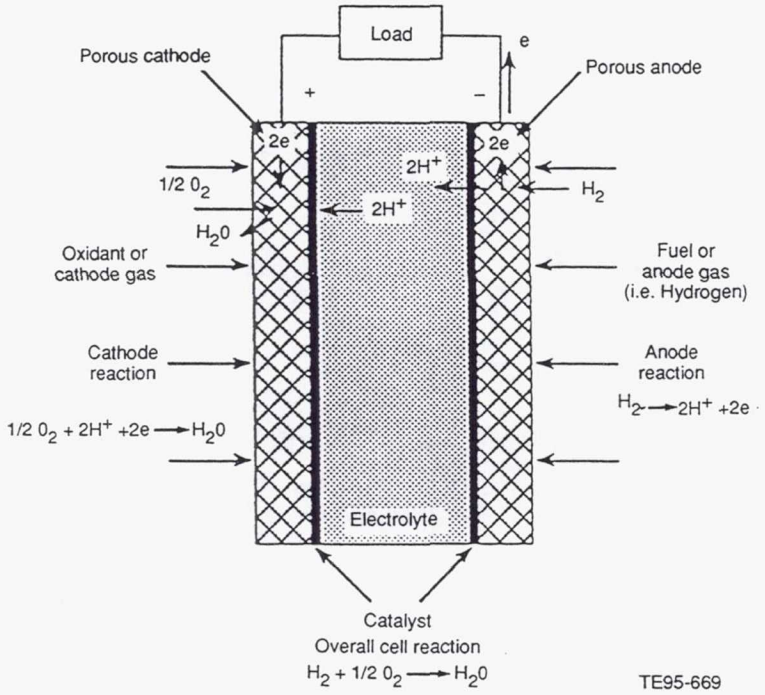

Figure 55. Single PEM fuel cell with principle of operation.

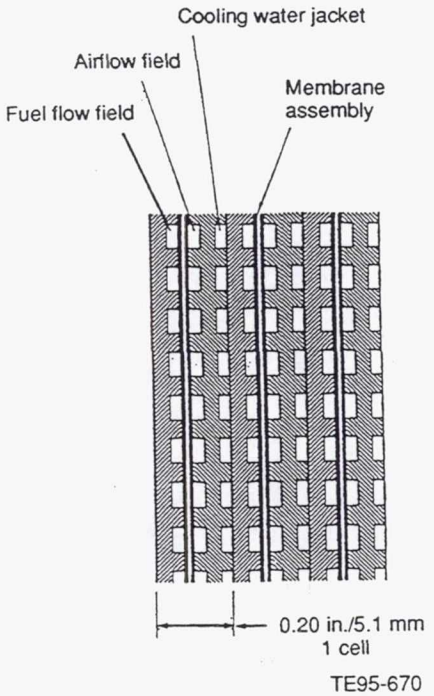

Figure 56. Section view of typical PEM fuel cell stack assembly.

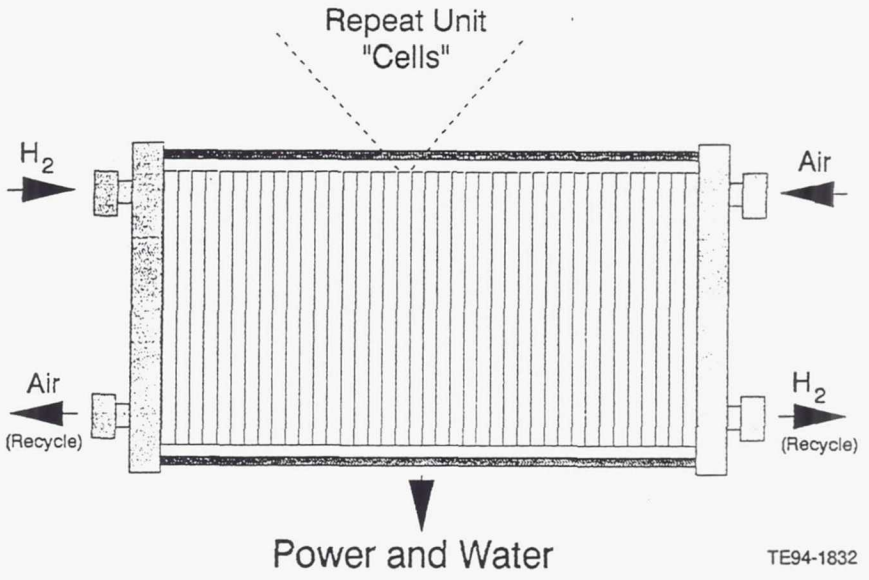

Figure 57. Typical PEM fuel cell stack arrangement.

The Advanced Engineering Technology Group, at Los Alamos National Laboratory in Los Alamos, New Mexico, has developed a computer simulation of a fuel cell power system called the Fuel Cell System model (FCSYS). This model characterizes the performance of a proton exchange membrane (PEM) fuel cell that is being fed hydrogen from a methanol-to-hydrogen processor as fuel, and air compressed by turbomachinery as an oxidant.

The FCSYS code was originally developed to study electrochemical engine characteristics at sea level conditions, primarily for automotive applications; some modifications to this program were necessary for high altitude flight operations. The ERAST aircraft can carry hydrogen itself as a fuel, so the original FCSYS methanol-to-hydrogen fuel processor is not required. In addition, the FCSYS turbomachinery code was not designed to accurately reflect compressor and turbine performance at the extremely high pressure ratio and corrected flow conditions required for operation at 90,000 ft. For these reasons, the FCSYS methanol-to-hydrogen fuel processor code was removed, and the turbomachinery modeling was conducted with TERMAP, Allison's primary thermodynamic performance analysis tool.

The baseline fuel cell used in this study was based on a PEM stack designed as part of the joint General Motors/Los Alamos National Laboratory "Electrochemical Engine Project" with sponsorship from the U.S. Department of Energy's Office of Transportation Technologies (Ref 4). That fuel cell stack was designed to produce 60 kW of gross electrical power output at 56.9% fuel cell stack efficiency at its design operating condition. These operating conditions included a fuel cell temperature of 194°F, a cathode (oxidant side) pressure of 44 psia, and an anode (fuel side) pressure of 22 psia. This reference cycle, and other "off-design condition" cycles provided by the FCSYS programming team, were used as verification points during the installation of the fuel cell subroutine in TERMAP.

Although the cathode and anode pressures may be allowed to vary somewhat, the 0.25 psia ambient pressure at 90,000 ft far exceeds the expected range of efficient operation for a PEM fuel cell stack. Even at 0.4 Mach, the turbomachinery operating at this altitude must achieve a 98:1 compression ratio to provide nearly ideal pressures for this device. However, this pressure ratio drives the gas path temperature up toward 1500°F, which far exceeds the very narrow comfort band around 194°F required by the conductivity characteristics of the proton exchange membrane. Thus, the anode and cathode streams fed by the turbomachinery must be significantly cooled prior to introduction into the fuel cell itself. Also, this airstream requires filtration to remove any traces of oil, which would contaminate the membrane in the fuel cell.

Three fuel-cell powerplant configurations were considered for this study. These diagrams are presented in Figures 58 through 60. Two of these were briefly studied and discarded. The first, using a three-stage 98:1 intercooled compressor, attempted to bring the fuel cell exhaust stream back into the turbomachinery cycle aft of the primary burner to recover useful energy from the 98:1 pressurization. However, because the fuel cell exhaust is at such a low temperature, the net effect was a very damaging dilution of the thermal energy created by the primary burner. In the end, this variant was unable to obtain enough turbine horsepower to drive the compression system.

The second variant, also using a three-stage 98:1 intercooled compressor, experimented with exhausting the fuel cell stream to ambient through a free power turbine to absorb the 98:1 expansion and contribute, through a gearbox, to the power generated by the electric motor. However, the power turbine size and weight (combined with the added gearbox) required to expand a 98:1 stream were prohibitive. If the

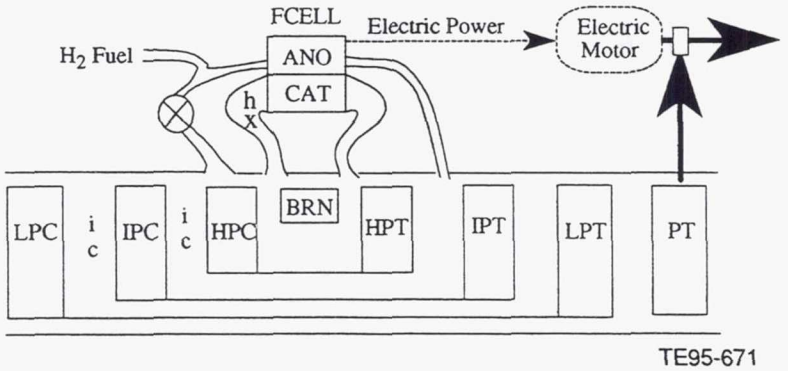

Figure 58. ERAST proton exchange membrane fuel cell cycle candidate 1.

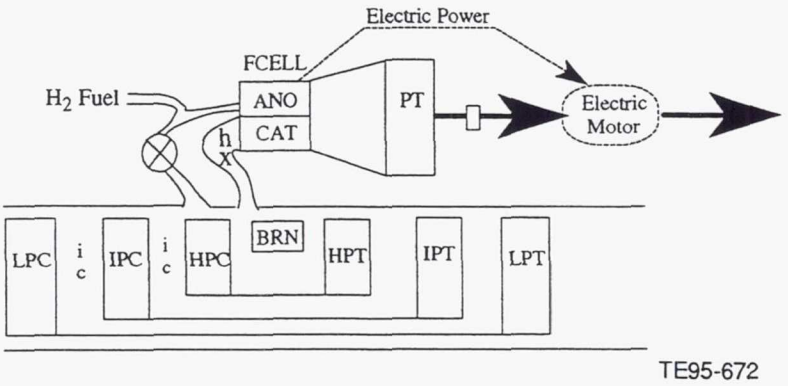

Figure 59. ERAST proton exchange membrane fuel cell cycle candidate 2.

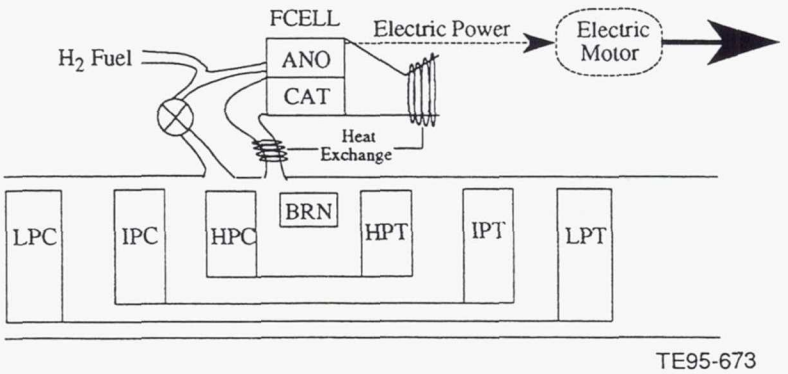

Figure 60. ERAST proton exchange membrane fuel cell cycle candidate 3 (selected for study).

expansion ratio across the turbine was reduced to achieve a more reasonable looking piece of hardware, the amount of horsepower recovered by it was too small to be a useful supplement.

The third configuration selected for this study uses a three-stage 98:1 Rc compressor without intercoolers. While this configuration also exhausts the fuel cell stream to ambient, it discards the free power turbine and associated gearbox in exchange for a slightly larger fuel cell. Expansion of the 98:1 fuel cell exhaust is used, along with vaporization of the liquid hydrogen fuel for the fuel cell stacks and turbomachinery, to cool the cathode inlet stream to the correct operating temperature.

Due to the high pressure ratio required for operation of this fuel cell, a series of three compressors has been modeled, achieving a combined overall Rc of 98:1. Aerothermodynamic conditions for these three components are noted in Figure 61. Given the substantial difference in size and rotational speeds required for each stage, each is driven by a turbine on a dedicated shaft. Just prior to reaching the primary burner, 19% of the compressed airstream is diverted to feed the three fuel cell stacks. This diverted flow is first passed through heat exchangers, cooling the airstream to the fuel cell's operating temperature by exchanging energy with the vaporizing hydrogen and with the 98:1 expansion process taking place at the fuel cell stacks' exhaust-to-ambient.

Now pressurized, cooled, and filtered, the diverted flow enters the fuel cell cathode at 194°F and 26 psia. The fuel cell anode is fed by the on-board store of pressurized/humidified hydrogen fuel. In the fuel cell stacks, the catalyzed reactions take place, producing electric power, heat, and water. The heat produced by the reaction is compensated for by an integrated fuel cell cooling system, and the water is partially recirculated for anode humidification, with the remainder expelled as a by-product with the rest of the gas stream. The power produced is fed to a power conditioner and then to an electric motor that, in turn, converts this energy to 300 shp to drive the aircraft propeller.

Back in the turbomachinery, the 81% of "undiverted" compressor discharge air continues into the system's primary burner. Here, vaporized hydrogen is burned to achieve a turbine rotor inlet temperature of 2442°F. This gas stream is then expanded through the three turbines, providing each enough horsepower to drive its respective compressor.

Parasitic losses in this cycle have been accounted for in two horsepower extractions from the turbomachinery spools. Bearing losses, windage, fuel pump, oil pump, and PMG are modeled as a 5 hp extraction from the IP spool. Heat rejection for this cycle is modeled as a 35 hp extraction from the HP spool.

The final fuel cell cycle design point configuration at 90,000 ft, 0.4 Mach, is a 199.7 lbm/sec corrected flow engine, with an OPR of 97.9:1, an HPT RIT of 2442°F, with a PEM fuel cell operating at 44% efficiency, generating 263 kW (352.9 hp), feeding an 85% efficient electric motor to produce 300 shp total output power. The system BSFC at this condition is 0.398 lbm/hp-hr, using hydrogen as its fuel. Table 4 is a summary of performance and weights of all the candidate powerplants for this ERAST study. The fuel cell is listed among these for comparison purposes.

3.2 HIGH ALTITUDE PROPELLER ANALYSIS

Propeller performance information was provided by the Hamilton Standard Division of United Technology Corporation.

3.2.1 Propeller Terminology

The following terms and definitions are key propeller design variables:

Activity factor (AF): $100000/16 \int b/D * (r/R)^{**}3 * d(r/R)$

where b is the local chord, D is the propeller diameter, r is the local radius, and R is the tip radius. The integral is performed over the radius of the blade. Thus, AF is a tip weighted blade area. Typical values of AF range from 75 to 250. Regional propeller blade AFs are around 100, while propfan AFs have been as high as 250. The larger the AF value, the larger the blade chord:

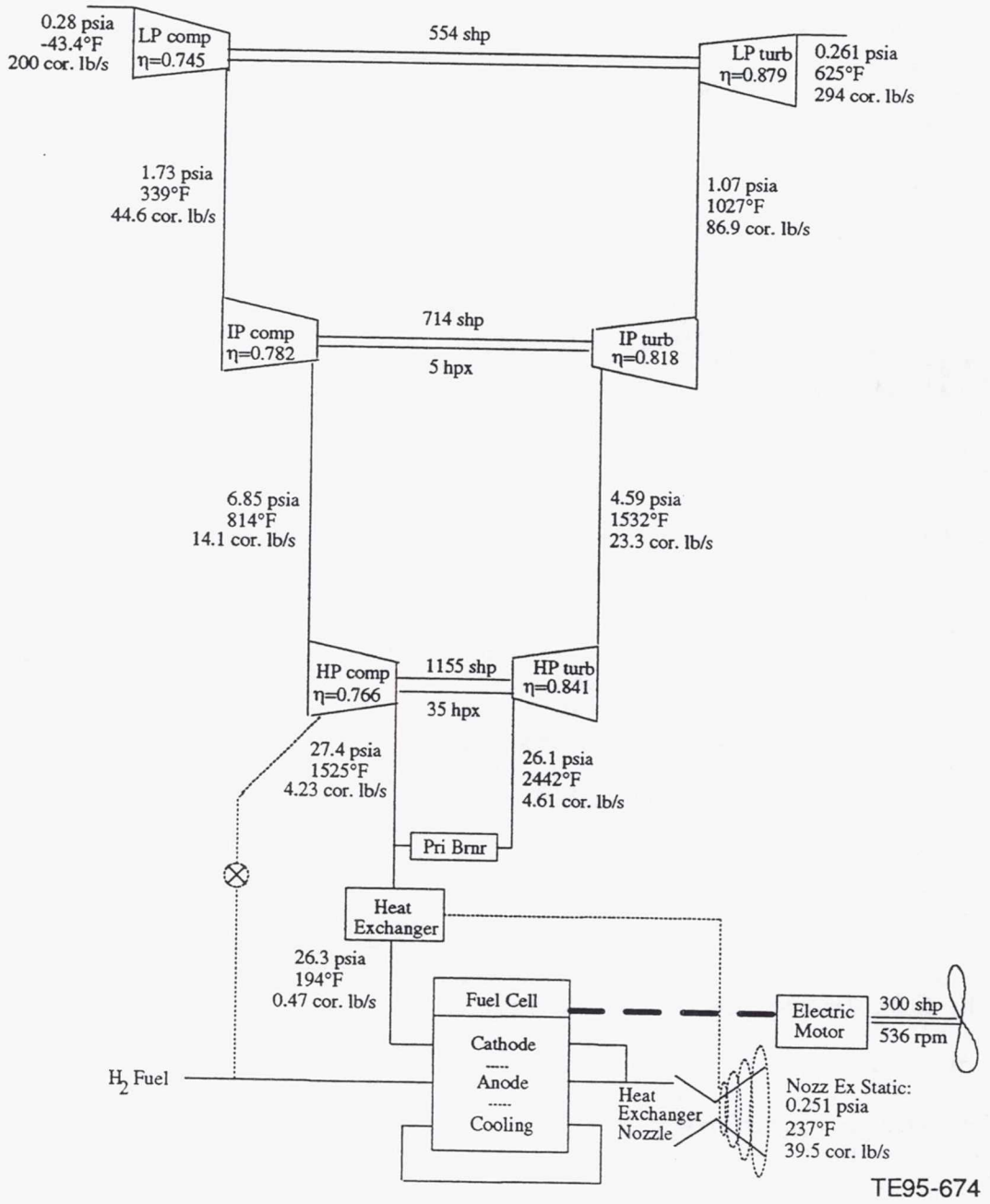

Figure 61. ERAST proton exchange membrane fuel cell cycle schematic: 90,000 ft, 0.4 Mach, 300 shp design point.

Integrated design lift coefficient (Cli): $\int$ Cld * (r/R)**3 * d(r/R)

where Cld is the airfoil design lift coefficient. Cli is a tip weighted measure of the camber in the blade.

Tip speed: π*rpm/60* diameter

where speed of the propeller tip is in the rotational direction only.

3.2.2 Methodology Used for Performance Prediction

A versatile computational propeller performance method was required to be able to provide the vast range of data required for a preliminary propeller and aircraft sizing study being performed herein. Because of these requirements, the Goldstein-Locke (Ref 5) propeller "strip analysis" method was used to provide all of the propeller performance data. The Goldstein-Locke analysis is based on a lifting line vortex theory and uses two-dimensional airfoil data. Simplistically, the vortex theory calculates the downwash at the propeller at 10 stations along the blade radius due to a trailing vortex system. The strength of the vortex system is dependent on the local blade lift, which is related to the angle of attack and 2-D airfoil data. This method has been used successfully for many years on both high speed and low speed propellers. The success of the method in accurately predicting the propeller efficiency is tied directly to the 2-D airfoil data. CFD methods provide insight into the spanwise and chordwise propeller loading at high speeds and are routinely used for detailed design of propellers. However, they are not suitable, nor needed, for preliminary design.

As noted, the "strip analysis" method was used for performance prediction for the ERAST propeller using 2-D airfoil data. A Reynolds number correction to the airfoil data was used to account for the severely reduced Reynolds numbers at 90,000 ft. Reynolds numbers at the 75% blade radius based on the relative velocity and local chord ranged between 200,000 and 700,000, depending on the propeller diameter and activity factor (AF) and the aircraft flight speed. The Reynolds number correction used raised the drag level of the airfoil according to the local Reynolds number, whereas no correction was applied to the lift. Reynolds number effects to lift generally result in a loss of maximum lift coefficient at low Reynolds numbers, whereas a properly designed propeller operates well below maximum lift to maximize the lift-to-drag ratio. Thus it was rationalized that no correction was necessary.

3.2.3 Propeller Performance Data

3.2.3.1 Scaling

The performance charts were obtained using the methodology noted previously by independent scaling of the diameter and AF of an existing commercial unswept propeller geometry. Thus, the width of a 20 ft 100 AF propeller would be twice that of a 10 ft 100 AF propeller, and it would be twice as thick. And the width of the 20 ft 200 AF propeller would also be twice that of a 20 ft 100 AF propeller, and it would be twice as thick. To land and launch a large diameter propeller, it was thought that the propeller should have only two blades. All studies herein were for a two bladed propeller. For operation in which Reynolds number is not of concern, a three-bladed propeller of the same AF (number of blades times AF/blade) as a two-bladed propeller might be expected to provide a 2-3% increase in efficiency. However, at the low ERAST Reynolds numbers the reduced chord of the three-bladed propeller would increase the Reynolds number loss, and mitigate the benefit of the increased number of blades.

3.2.3.2 Tip Speed

Initial discussions regarding propeller performance focused on a 25 ft/600 rpm propeller, which resulted in a propeller tip speed of 785 ft/sec (fps). At Mach = 0.40/90,000 ft and a tip speed of 785 fps, the tip relative Mach number is approximately 0.90. Since the aircraft flight spectrum was beginning to settle out around Mach = 0.40, the tip speed of 785 fps seemed to be appropriate, and it was retained for the entire study. For the 18.5 ft diameter design, the corresponding speed is 800 rpm. Decreasing the tip

speed would reduce performance by decreasing the Reynolds number, and increasing the swirl losses of the propeller, resulting in lower efficiency. Raising the tip speed would improve the performance slightly until compressibility losses overcame the benefit of reduced swirl losses. Thus, the selected tip speed is reasonable for this preliminary design study. Once flight spectrums are defined more precisely, a more detailed examination of tip speed would be warranted.

3.2.3.3 *Twist*

The propeller twist was selected to provide an acceptable loading distribution at the 90,000 ft/0.4 Mach flight condition at 785 fps tip speed.

3.2.3.4 *Integrated Design Lift Coefficient and Airfoils*

An integrated design lift coefficient (Cli) of 0.58 provides low drag airfoil performance at the design tip relative Mach number of 0.90. This particular value resulted from using the airfoils on an existing commercial propeller. These airfoils were designed for a tip relative Mach number around 0.9. A Cli value of 0.3 was used because the range of cruise speeds was assumed to be from 0.4 to 0.7 Mach number. With the cruise speed settling out at 0.4 Mach, it was possible to increase the Cli to 0.58, which will also improve the low speed, low altitude performance of the propeller. No investigation was made into the possibility of improving performance through use of airfoils designed specifically for low Reynolds number. However, it should be noted that an 80% efficient propeller loses about 13% in efficiency from unavoidable axial and swirl momentum changes and tip losses. The airfoil drag accounts for the other 7% in efficiency loss. Thus, use of an airfoil which reduces the drag by 25% will improve the performance by only ~2%, indicating that a different airfoil will not improve the ERAST propeller performance dramatically.

3.2.3.5 *Propeller Performance*

Initial studies focused on an available power of 300 shp at 90,000 ft, and a Mach number range of 0.4 to 0.7. Because 0.7 Mach number was being considered as part of the aircraft flight envelope, it was decided to use a Cli of 0.30 to minimize the compressibility losses and reduce the number of parameters used in the sizing study. These studies led to the selection of propeller diameters ranging from 25 to 30 ft.

Subsequent mission analysis studies of both the aircraft and engine performance reduced the shaft horsepower requirements to 135 shp at 90,000 ft, and limited the Mach number range from 0.4 to 0.5. The reduction of shaft horsepower allowed the diameter to be reduced to 18.75 ft. And the reduction in maximum speed of the aircraft allowed the Cli to be increased to 0.58.

3.2.3.6 *Planform*

The planform used for study was based on the scaling of a current commercial unswept propeller. Detailed planform changes will have some effect on performance, but the gross performance is controlled by the AF. The Cli and tip speed chosen for the propeller studies preclude the need for blade sweep to improve performance. The planform for the 18.75 ft and 30 ft diameter blades with a 123 AF blade are shown in Figure 62.

3.2.3.7 *Performance Maps*

Several sets of performance maps were generated during the study, however, only the set used for the final evaluation is presented herein as Figures 63 through 70. As noted earlier, the cruise condition power level has been reduced since the initial set of performance maps was calculated. These maps show the performance of the scaled propeller at three speed/altitude combinations, and at three different power levels. Each figure presents propeller efficiency against AF for different diameters for two-bladed propellers. Only one diameter shows in Figure 63 because the propeller performance is very poor at the larger diameters with low power. As the power is increased in Figure 64, the propeller becomes more "on size" and the efficiency improves.

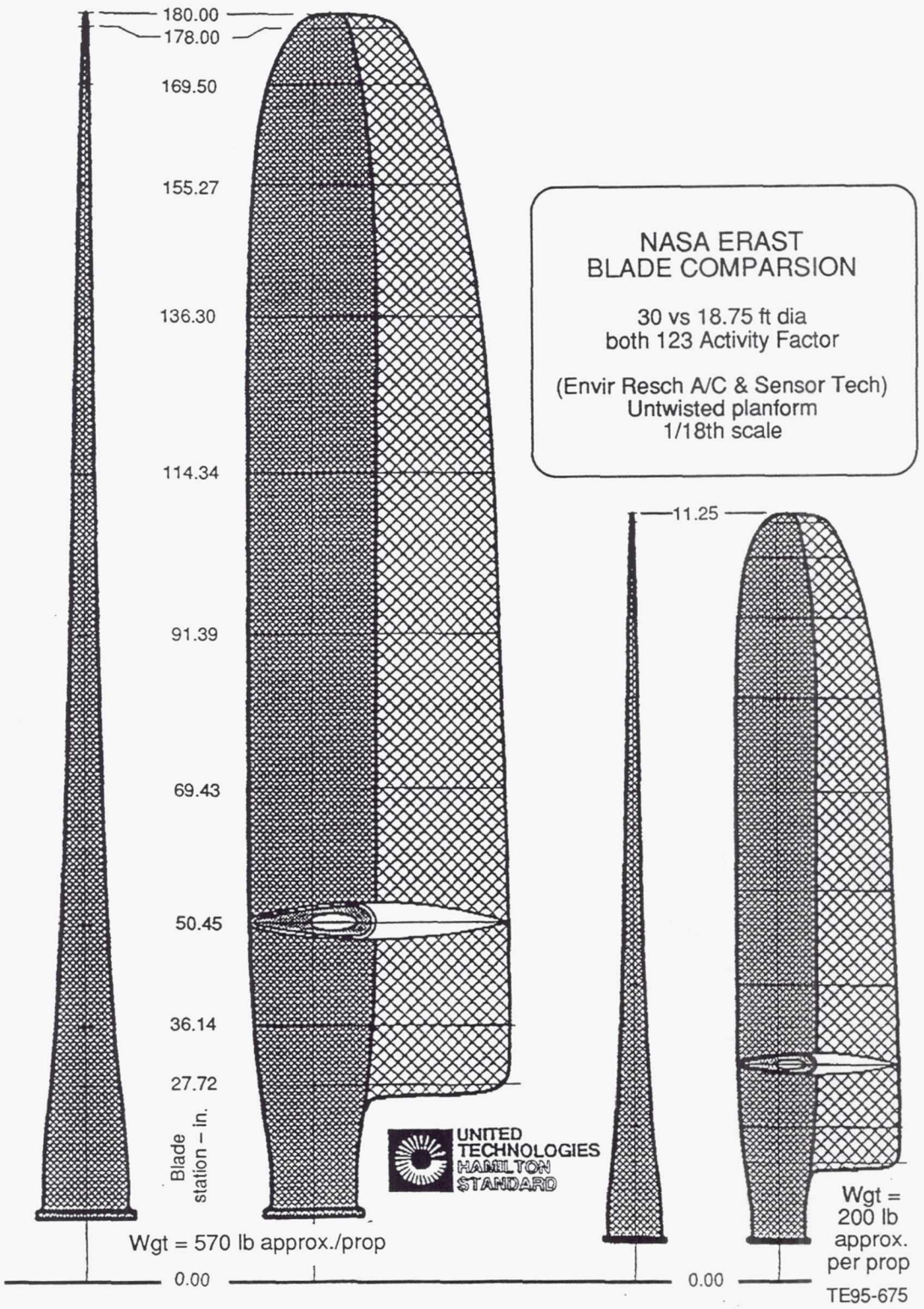

Figure 62. NASA ERAST propeller blade comparison.

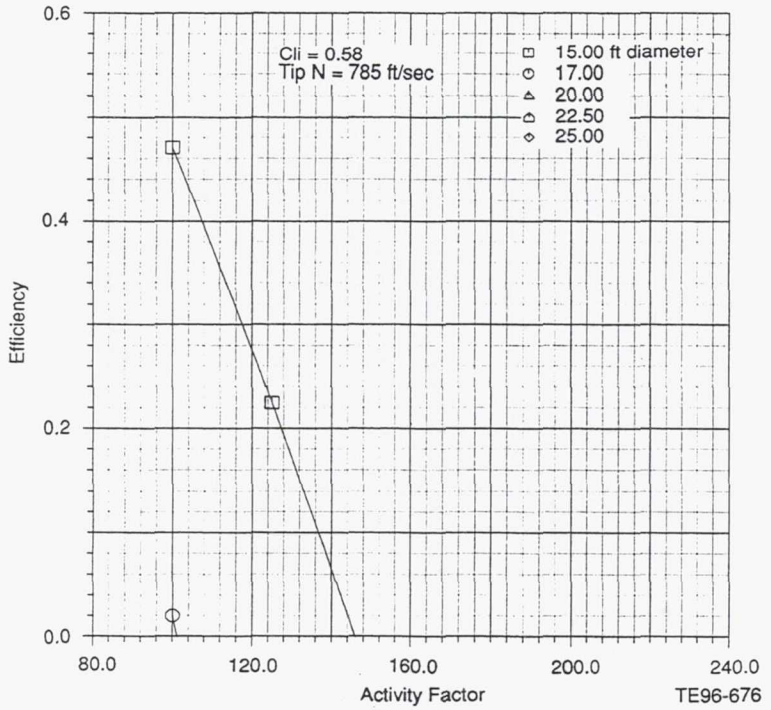

Figure 63. ERAST two-bladed performance:
100 hp, 30,000 ft, 118 ktas.

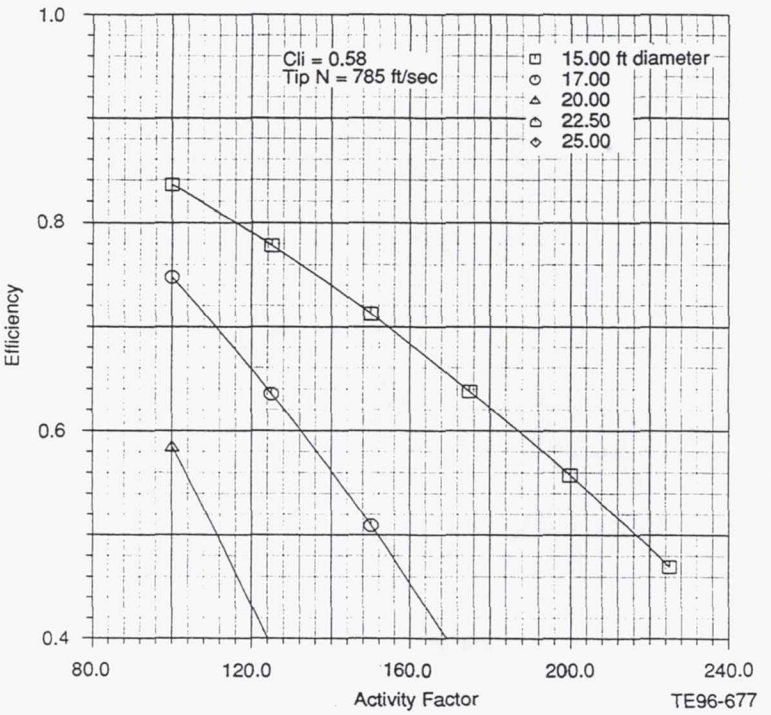

Figure 64. ERAST two-bladed performance:
200 hp, 30,000 ft, 118 ktas.

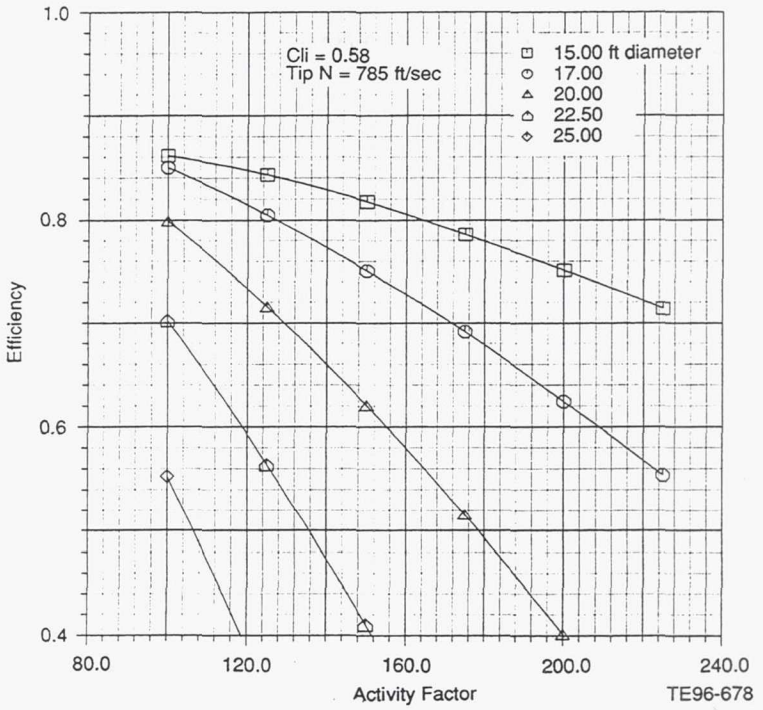

Figure 65. ERAST two-bladed performance:
300 hp, 30,000 ft, 118 ktas.

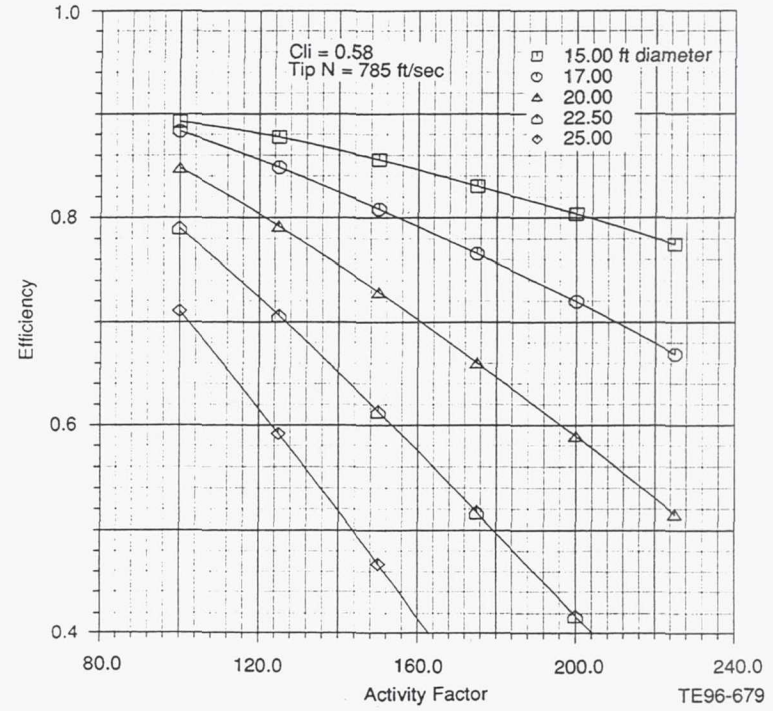

Figure 66. ERAST two-bladed performance:
100 hp, 60,000 ft, 172 ktas.

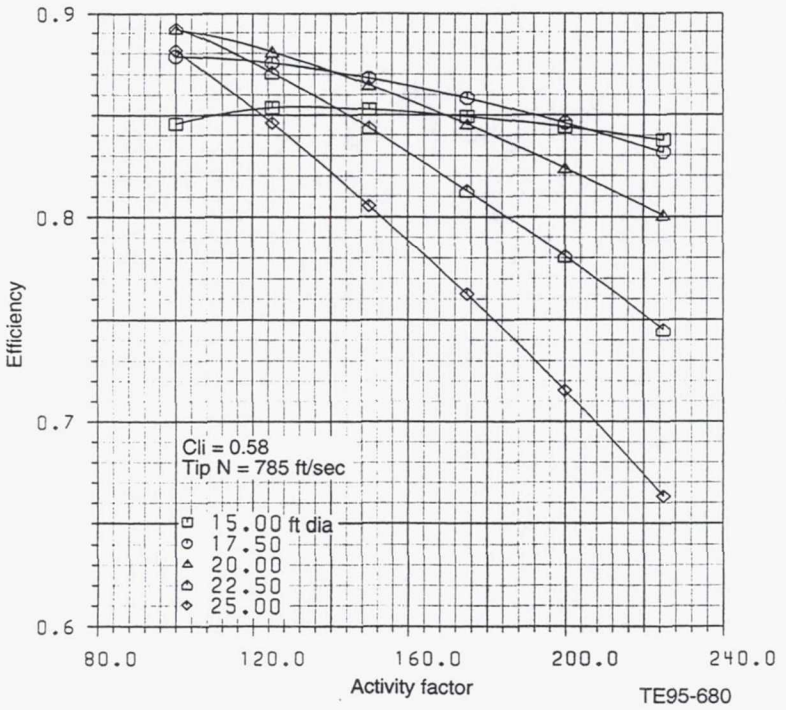

Figure 67. ERAST two-bladed performance:
200 hp, 60,000 ft, 172 ktas.

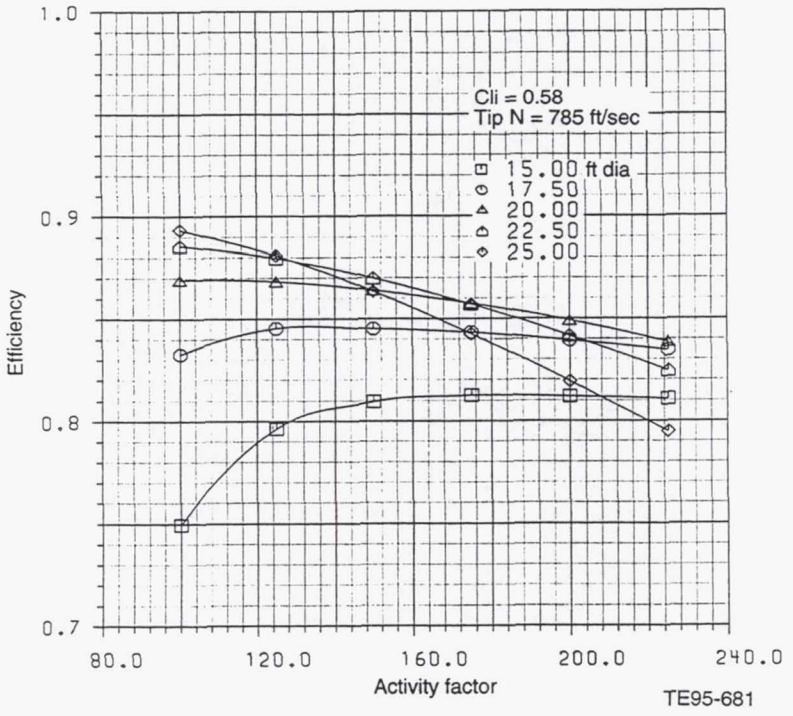

Figure 68. ERAST two-bladed performance:
300 hp, 60,000 ft, 172 ktas.

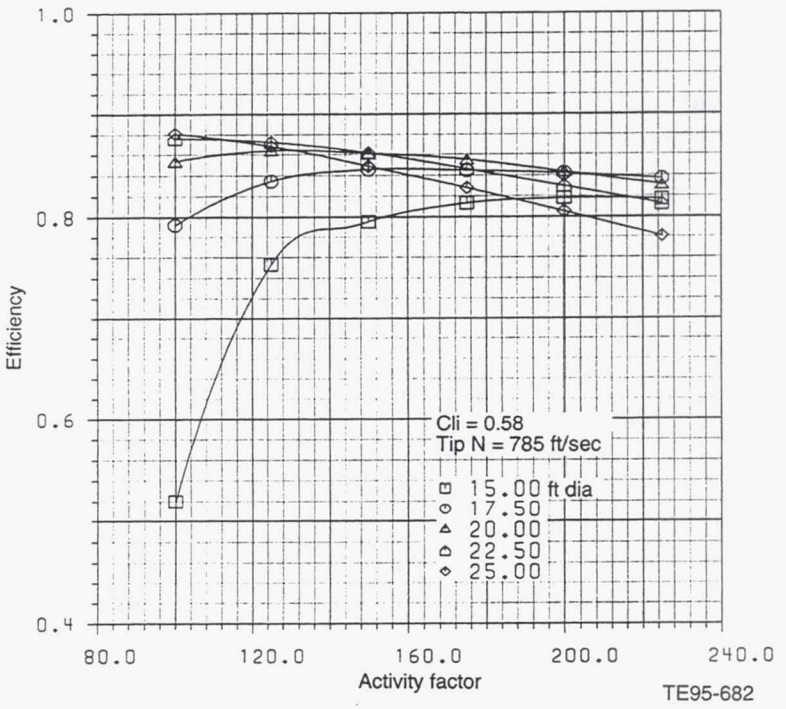

Figure 69. ERAST two-bladed performance:
135 hp, 90,000 ft, 292 ktas.

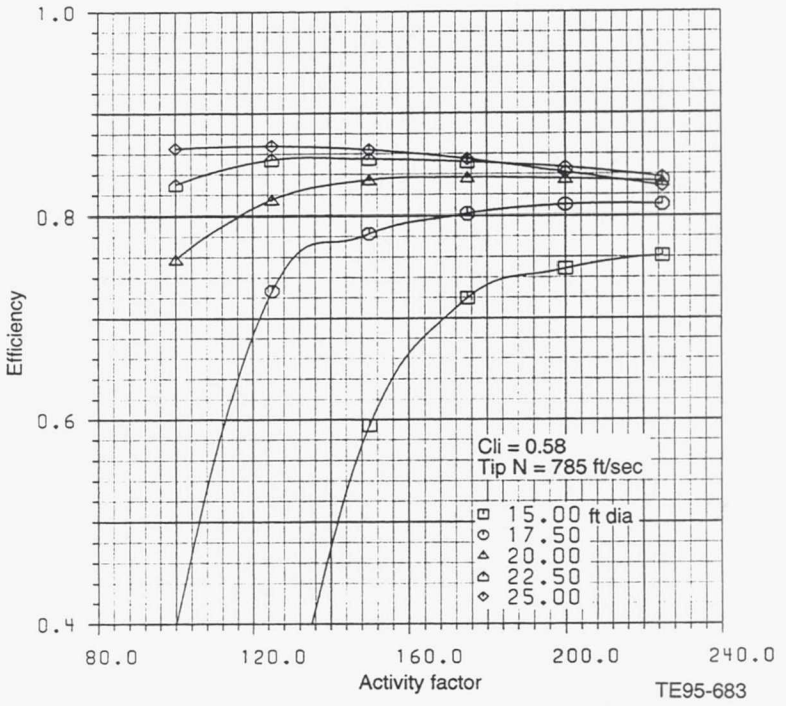

Figure 70. ERAST two-bladed performance:
200 hp, 90,000 ft, 292 ktas.

3.3 THERMAL ANALYSIS

3.3.1 Intercooler Design

Intercooler design begins with TERMAP, a computer program that predicts engine performance characteristics. Engine temperatures, pressures, and mass flows obtained from TERMAP are considered in the design of the intercoolers.

The heat exchanger design program uses TERMAP performance data to calculate an effectiveness and allowable pressure drop for the intercooler to be designed. Before running the intercooler design program, several assumptions must be made concerning the internal geometry of the intercoolers and the properties of the airflow. Assumed geometric characteristics include internal plate-fin spacings and thicknesses based on previous heat exchangers and their requirements. Figure 71 is a sketch of a plate-fin cross flow heat exchanger.

Assumptions on airflow begin with the air and gas mass flows being distributed evenly throughout the heat exchanging unit(s). For example, if two heat exchanging modules are used, then each module sees exactly half of the total flow, or, in the case of four modules, one fourth the flow. Second, if no air inlet size is specified, a cooling flow (ambient air) slightly larger than the amount of hot flow (compressor discharge air) is chosen for better heat transfer capability.

Selection of the number of modules is another determination that must be made before running the sizing program and depends on considerations such as the amount of flow to be handled, the amount of reasonable ducting required, and the size envelope devoted to the intercoolers. The operating temperatures for the ERAST project allow the intercoolers and/or aftercoolers to be made of aluminum rather than steel, thereby reducing the weight. The reduction in weight allows a design to be more accepting to a larger number of modules.

Two options are available when running the intercooler design program. Either a weight optimization sequence or a strict evaluation of a particular design concept can be initiated. Use of the optimization option requires a target pressure drop and intercooler effectiveness along with the standard geometric data. Heat transfer relations published by Kays and London (Ref 6) are used by the program to determine the prospective heat exchanger performance and physical dimensions such as length, width, and height. In addition to producing intercooler weight and dimensions, the program also returns numerous flow properties such as the heat capacity rates of the fluids.

The design process applied to the heat exchangers used in the rotary engine configuration summarizes typical intercooler design procedure. Beginning with TERMAP data sheets, inlet and exit pressures, temperatures, mass flows, and desired pressure drops through the heat exchangers are established. Each separate heat exchanger requires a separate input file. The individual files contain the desired performance characteristics of a particular heat exchanger along with a proposed internal geometry. The effectiveness of the first, second, and third sets of intercoolers in series was 60, 65, and 70%, respectively. Their allowable pressure drops decreased from the first set of intercoolers to the last, going from 4 to 1% and then finally to 0.5%.

Using the optimization option of the design program, the desired heat exchanger effectiveness and pressure drop stated in the input file were iterated upon until a suitably sized heat exchanger satisfying all constraints is determined. If the program was unable to produce a suitable design, then either the performance conditions or proposed internal geometry must be amended until a configuration can be found. Review of the program output can reveal gains in performance of the heat exchanger.

Performance can sometimes be traded for increases in other areas. For example, gains in pressure drop may allow a flow passage area to be decreased to make a given heat exchanger smaller. The new passage area may produce a higher pressure drop, which remains within the desired limits in exchange for a smaller design. Performing these types of trade-off techniques can provide the best heat exchanger for an application.

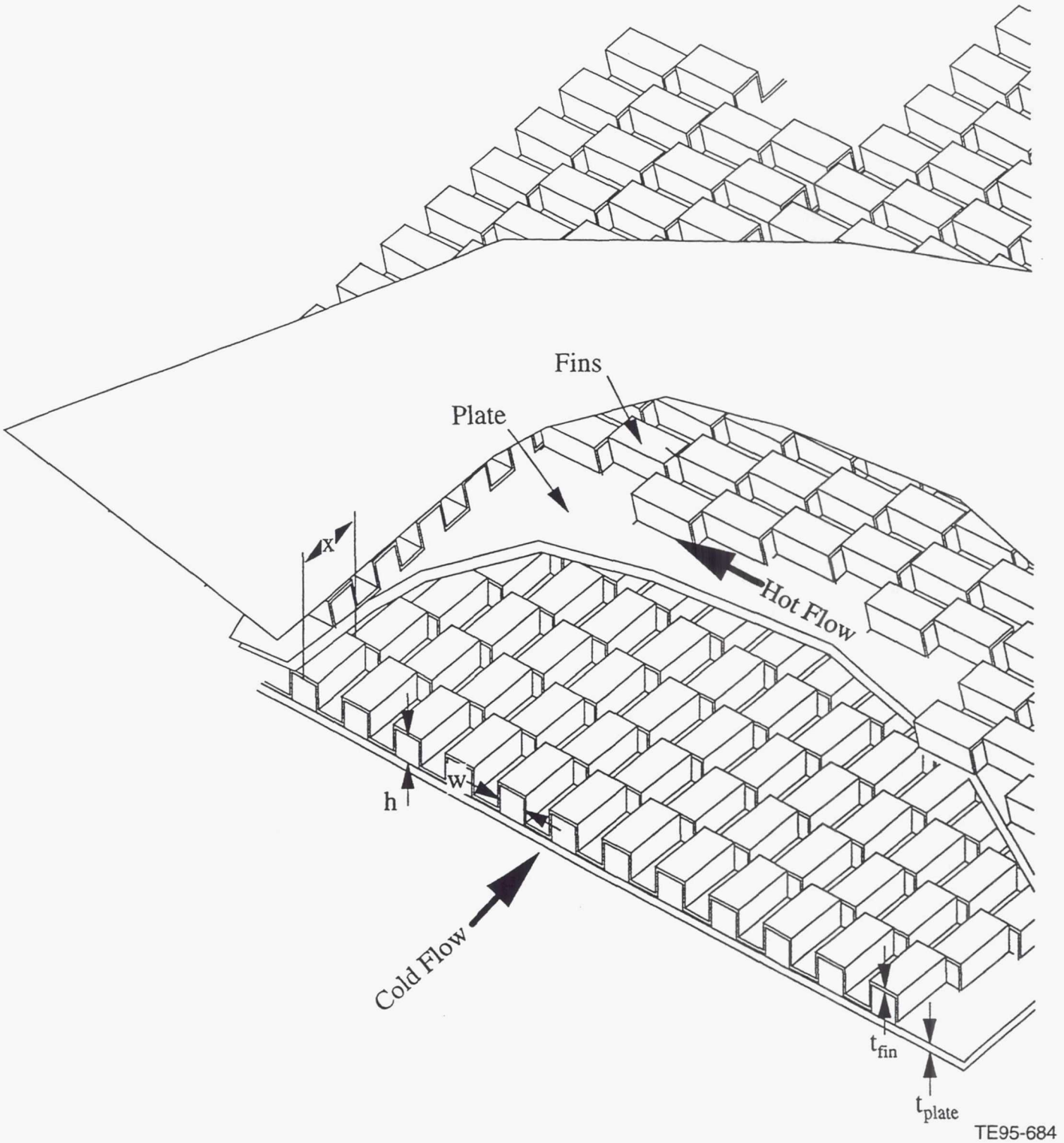

Figure 71. Plate-fin geometry for a cross flow heat exchanger.

All heat exchangers utilize an offset-fin plate-fin type surface for the core. A summary of intercooler internal dimensions are given in Table 6 for each powerplant configuration and each intercooler module.

Table 6.
Intercoolers' internal design variables (spacings, thicknesses, and lengths).

2-stroke diesels	Intercooler 1	Intercooler 2	Intercooler 3
Cold fin spacing, in.	0.1	0.1	NA
Hot fin spacing, in.	0.1	0.1	NA
Cold plate spacing, in.	0.5	0.5	NA
Hot plate spacing, in.	0.5	0.5	NA
Cold fin thickness, in.	0.004	0.004	NA
Hot fin thickness, in.	0.004	0.004	NA
Plate thickness, in.	0.006	0.006	NA
Cold fin length, in.	0.5	0.5	NA
Hot fin length, in.	0.5	0.5	NA
4-stroke diesel & 4-stroke spark ignition			
Cold fin spacing, in.	0.2	0.25	0.25
Hot fin spacing, in.	0.25	0.15	0.15
Cold plate spacing, in.	0.8	0.55	0.55
Hot plate spacing, in.	0.55	0.23	0.23
Colf fin thickness, in.	0.004	0.004	0.004
Hot fin thickness, in.	0.004	0.004	0.004
Plate thickness, in.	0.006	0.006	0.006
Cold fin length, in.	0.8	0.53	0.55
Hot fin length, in.	0.7	0.23	0.26
Rotary			
Cold fin spacing, in.	0.2	0.09	0.06
Hot fin spacing, in.	0.2	0.09	0.06
Cold plate spacing, in.	0.5	0.35	0.35
Hot plate spacing, in.	0.5	0.35	0.2
Cold fin thickness, in.	0.004	0.004	0.004
Hot fin thickness, in.	0.004	0.004	0.004
Plate thickness, in.	0.006	0.006	0.006
Cold fin length, in.	0.5	0.3	0.3
Hot fin length, in.	0.5	0.3	0.2
Coleman			
Cold fin spacing, in.	0.08	NA	NA
Hot fin spacing, in.	0.1	NA	NA
Cold plate spacing, in.	0.5	NA	NA
Hot plate spacing, in.	0.5	NA	NA
Cold fin thickness, in.	0.004	NA	NA
Hot fin thickness, in.	0.004	NA	NA
Plate thickness, in.	0.006	NA	NA
Cold fin length, in.	0.5	NA	NA
Hot fin length, in.	0.5	NA	NA

NA = not applicable

A summary of intercooler external dimensions and weights is given in Table 7. It should be noted that the weights listed in the table contain what is called a wrap-up factor. The wrap-up factor is a coefficient used to account for the weight of the manifolds and ducting required to supply flow to a given heat exchanger. This coefficient is based on empirical data compiled here at Allison. The wrap-up factor for use with intercoolers is 1.6. This number is nondimensional.

Table 7.
Intercooler and recuperator component weights.

	Intercooler 1			Intercooler 2			Intercooler 3		
	No. of modules	Weight, lb	Dimensions, in.	No. of modules	Weight, lb	Dimensions, in.	No. of modules	Weight	Dimensions
Opp 2-stoke diesel turbo	4	21.4	3.27 x 7.40 x 24.67	4	26.1	3.42 x 13.81 x 15.34	—	—	—
Opp 2-stroke diesel	4	26.5	3.01 x 8.95 x 27.34	4	36.2	3.45 x 10.32 x 28.30	—	—	—
4-stroke diesel	2	58.6	10.39 x 22.92 x 24.21	2	65.3	9.37 x 26.15 x 19.58	2	96.6	11.65 x 30.21 x 20.15
4-stroke SI turbo	2	36.9	11.12 x 18.22 x 17.87	2	42.3	10.4 x 16.91 x 17.68	2	59.1	12.46 x 24.11 x 14.45
4-stroke H2 fuel turbo	2	36.9	11.12 x 18.22 x 17.87	2	42.3	10.4 x 16.91 x 17.68	2	59.1	12.46 x 24.11 x 14.45
Strat chg rotary	6	77.9	7.17 x 18.88 x 15.7	6	53.1	2.31 x 19.28 x 18.2	6	50.1	1.68 x 18.05 x 18.4
Coleman IC	10	154	3.31 x 8.88 x 54.11	—	—	—	—	—	—
Coleman recup	6	152	2.12 x 12.62 x 12.3	—	—	—	—	—	—
2100 growth recup	6	234	1.83 x 22.62 x 29.11	—	—	—	—	—	—

Arrangement of the intercoolers is relatively arbitrary and is usually subject to installation constraints beyond the scope of this study. In placing the intercoolers within a system, it was therefore only required that the ducting and manifolds accompanying the intercooler provide the necessary flows in a manner that provides each module with an equal amount of flow and promotes an even flow distribution.

During the design of the two-stroke, non-turbo-compounded diesel engine's intercoolers, a trade study evaluating intercooler weight versus increases in cooling inlet pressure was performed. The intercoolers' expected installment location and inlet characteristics were determined assuming that it would be placed within a nacelle. Pressure increases were to be achieved through the use of a fan placed at the inlet. The load measurements were a summation of the weights of the intercooler and fan and of the weight of the fuel needed for fan operation. Weight of the fan was based on a factor equivalent to 1 lb of fan weight per horsepower.

Results showed negligible weight savings with small increases in inlet pressure (Figure 72). As the pressure was increased, the sum of the heat exchanger and fan weight increased exponentially. The concluding assertion from this study was that it would not be favorable to use a fan-intercooler system to increase efficiency. Using a version of the original heat exchanger design program, various intercooler characteristics can be evaluated regarding their effect on things such as size, weight, and effectiveness.

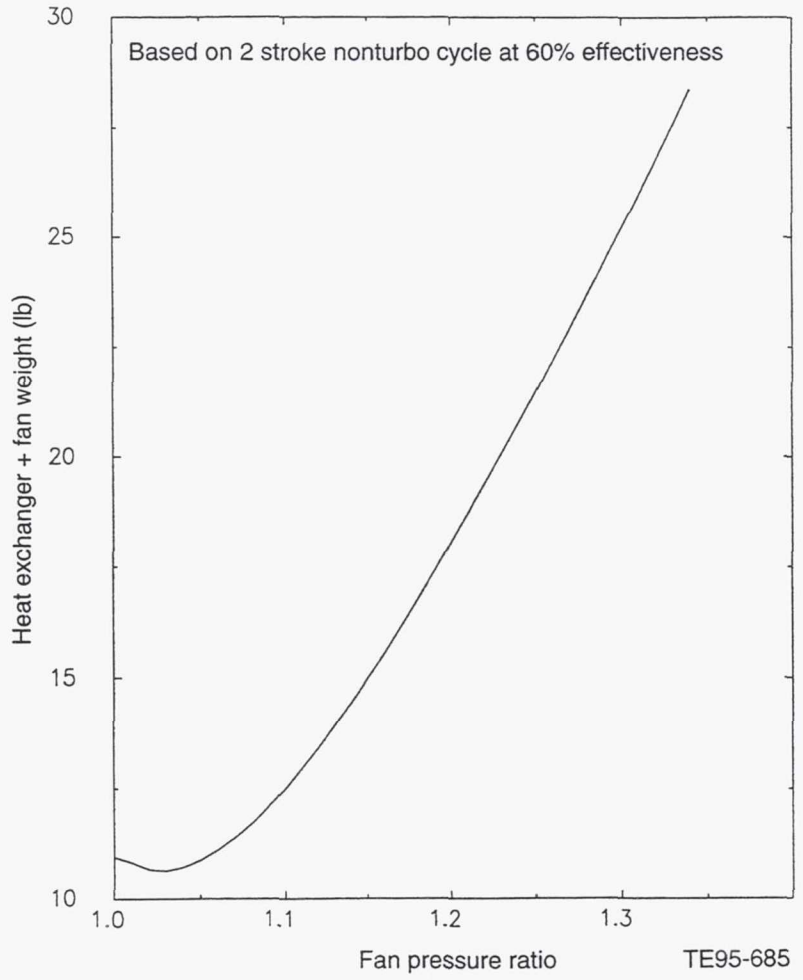

Figure 72. Weight versus inlet pressure trade-off results.

A plot of effectiveness versus the hot side physical flow was produced for evaluating off-design performance. Representative plots of effectiveness versus the hot side physical flow for the two-stroke, turbo-compounded diesel engine are given in Figure 73 for both intercoolers. It was assumed that these curves would represent the performance of the heat exchangers sized for the other turbocharged piston and rotary engine configurations. By shifting the curves to the other configuration design point hot flows, the same downward trend was assumed. Was this a justifiable assumption?

The basic heat exchanger performance concern is how the effectiveness of the different heat exchanger designs change with increasing hot flow. This relationship can be understood by examining the basic cross flow heat exchanger effectiveness equation. Since the exact equations used in the computer program cannot be expressed in closed form, a widely accepted approximation is shown:

$$\varepsilon \equiv 1 - \exp[(1/C_r)NTU^{0.22}\{\exp(-C_r NTU^{0.78}) - 1\}]$$

C_r is the heat capacity ratio C_{min}/C_{max}, where the heat capacity $C = m\,c_p$ (m is the mass flow and c_p is the specific heat of the flow). *NTU* is the dimensionless number of transfer units, $NTU = [A(U_m)]/C_{min}$. *A* is the heat transfer surface area and U_m is the overall mean heat transfer coefficient, which includes the convection coefficients (*h*) and the conduction coefficient (*k*). During the heat exchanger design, the cooling flow was set to always be slightly greater than the hot flow, and therefore the capacity ratio C_r remained roughly constant at 0.95. Since the cold side c_p is approximately equal to the hot side c_p, the C_{min} will be for the hot side and the C_{max} will be for the cold side since the cold side flow is slightly higher than the hot side flow. Therefore, as the hot flow is increased, the effectiveness is only changed by a change in *NTU*. The denominator of *NTU* contains m_h because C_{min} contains m_h.

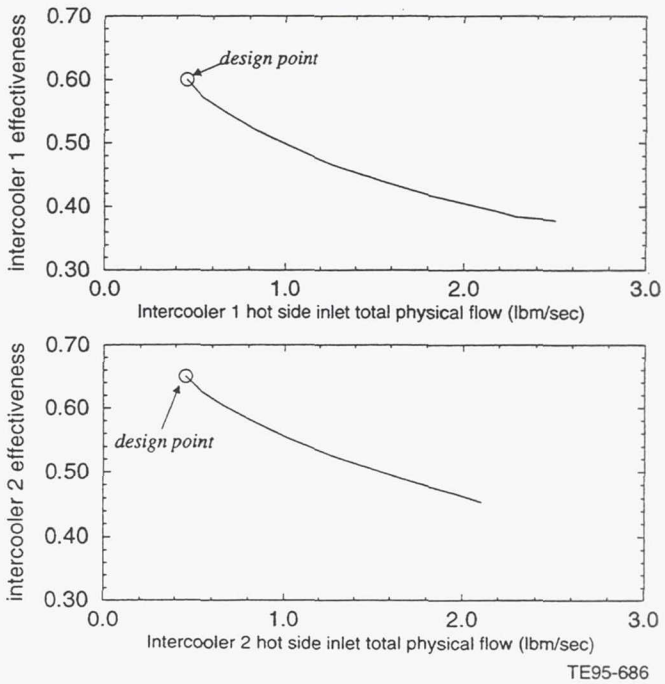

Figure 73. Two-stroke, turbo-compounded diesel intercooler effectiveness versus hot mass flow.

The intercoolers used in the study for all of the engine configurations were selected to have either 60, 65, or 70% effectiveness. For each configuration with a set effectiveness, the design point NTU was fixed, because of a fixed ε and C_r. Each configuration has a different flow rate, and therefore the numerator of the *NTU* ($A U_m$) was adjusted to give a specific value. This can be expressed mathematically by:

$$NTU = a_1/m_{h1} = a_2/m_{h2} = a_3/m_{h3} = \ldots$$

where subscripts 1,2,3,... refer to the different engine configurations. The coefficient a_n includes the terms A, U_m, and c_{ph}, which are assumed to remain roughly constant as the flow rate is varied. If the hot flow rates change with altitude for the other configurations in the same proportion to the two-stroke, turbo-compounded diesel, then the assumption for the change in effectiveness is valid. For example, if the mass flow of the two-stroke, turbo-compounded diesel changes by a factor of 5 between the design point altitude and the sea level, the *NTU* value will decrease by approximately a factor of 5. If the other configurations also change in flow rate by a factor of 5 from design point to sea level, then the proper NTU, and then ε, will be calculated. The amount they differ from the two-stroke, turbo-compounded diesel is the error. After evaluating all the piston and rotary engine configurations off-design, it was discovered that their hot side flow does increase by a factor of 5. Therefore, the curves presented in Figure 73 can be used for all the configurations.

3.3.2 Recuperator Design

The method for recuperator design at Allison is identical to that for intercoolers and is subject to similar considerations. Goal temperatures and pressure drops are again obtained from TERMAP output data provided by the performance group.

All preparatory inputs for running the recuperator design program are the same as those used for the intercooler design program. A proven internal geometry from a previous HALE (High Altitude Long Endurance) vehicle report was used to begin a new recuperator design for the ERAST project. Recuperator design after this phase was performed using the optimization option of the program and evaluating recuperators with varying effectiveness and performance.

The standard recuperator arrangement used by Allison is a six-module polygon configuration shown in Figure 74. The recuperator designs for both the Coleman and turboshaft engines are given in Table 7. The recuperator weight numbers in Table 7 include a 2.37 wrap-up factor. A summary of recuperator internal dimensions are given in Table 8 for both the Coleman and turboshaft engines.

Table 8.
Recuperators' internal design variables (spacings, thicknesses, and lengths).

	Coleman recuperator	Recuperated turboshaft recuperator
Cold fin spacing, in.	0.23	0.23
Hot fin spacing, in.	0.08	0.08
Cold plate spacing, in.	0.07	0.07
Hot plate spacing, in.	0.3	0.3
Cold fin thickness, in.	0.004	0.004
Hot fin thickness, in.	0.004	0.004
Plate thickness, in.	0.006	0.006
Cold fin length, in.	0.3	0.5
Hot fin length, in.	0.4	0.5

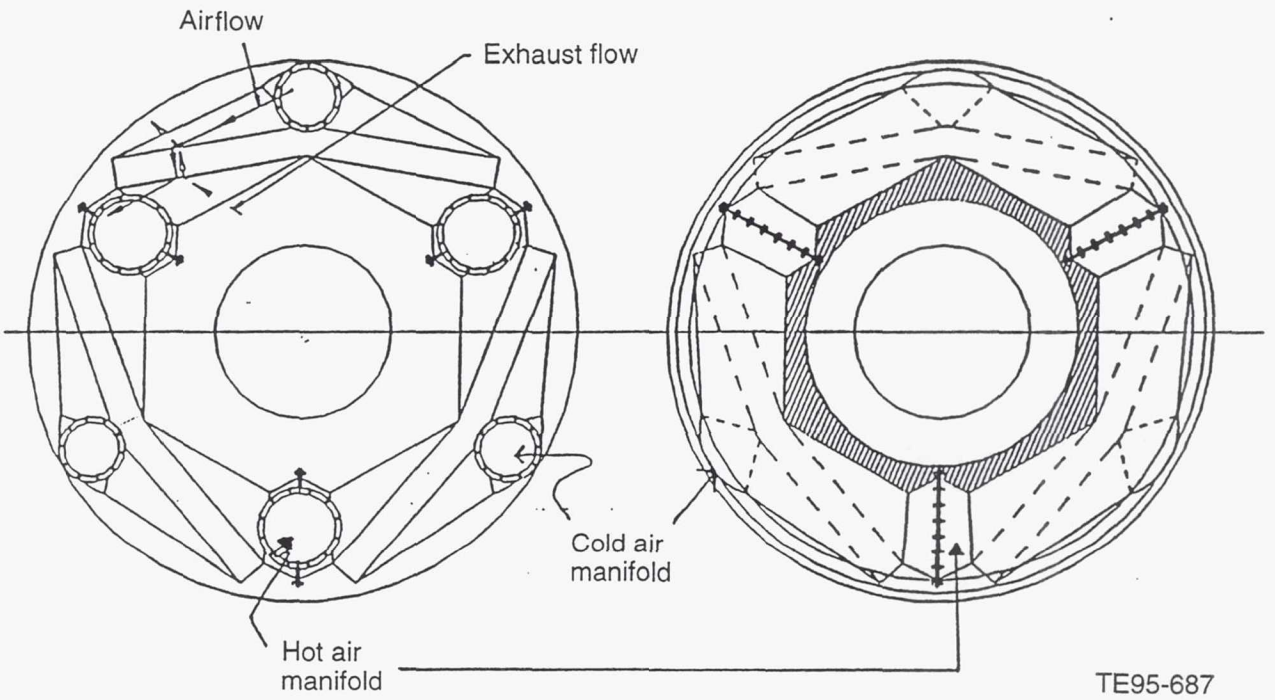

Figure 74. HALE recuperator showing modular design of heat exchanger.

The recuperator design process can be illustrated in a description of the procedure used for designing the turboshaft engine configuration's recuperator. First, a TERMAP data sheet is furnished by the performance group. The fuel-air ratio, hot and cold flows, inlet and exit temperatures and pressures, and pressure drops are all obtained from the TERMAP cycle sheets. The allowable pressure drops for the hot and cold flows can also be determined by the performance engineer. In the case of the turboshaft engine, the allowable pressure drop was approximately 2% for the cold flow and 10% for the hot flow. The desired recuperator effectiveness can either be calculated using the given inlet and exit conditions or given by the performance engineer. The recuperator was designed to 80% effectiveness for the ERAST study.

After setting these parameters within the design program's input data set and defining an internal geometry, the program is then compiled and run. The internal geometry is determined based on experience or through the use of dimensions obtained from existing recuperators with similar requirements. The optimization process of the program then iterates on the input boundary conditions until a suitable design satisfying the boundary conditions is produced. The resulting recuperator characteristics are given in an output file.

Throughout the ERAST project, several trade studies relating to recuperator effectiveness were performed. The main focus was to perform sensitivity studies of heat exchanger geometry versus effectiveness. Recuperator non-flow length, volume, and weight were examined relative to effectiveness to establish a baseline set of plots (Figures 75 to 77). Recuperator effectiveness appears to be most sensitive to increases in volume and weight. Figure 75 shows the variation of the non-flow length with effectiveness. Non-flow length is the dimension contained within a plane that is perpendicular to either of the flow directions. This dimension contains the height of the hot and cold layers of the heat exchanger core, also known as the stacks. It does not appear, from the plot of non-flow length versus the effectiveness, that the best means of raising effectiveness is through increasing the number of recuperator stacks. It would be more advantageous to increase either the hot or cold flow length if possible without exceeding predetermined constraints.

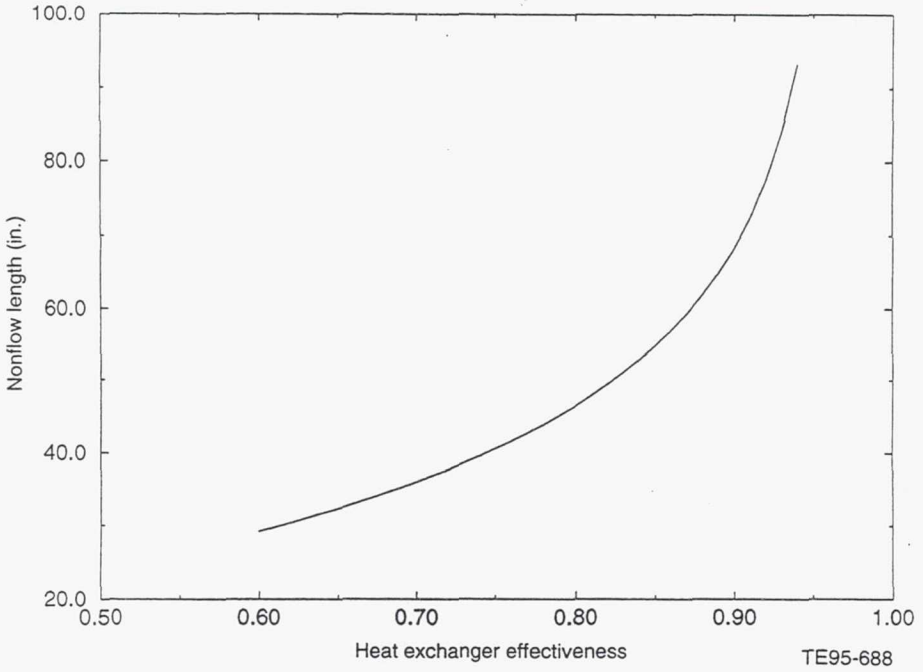

Figure 75. Heat exchanger nonflow length versus effectiveness: valid for ERAST counterflow heat exchanger.

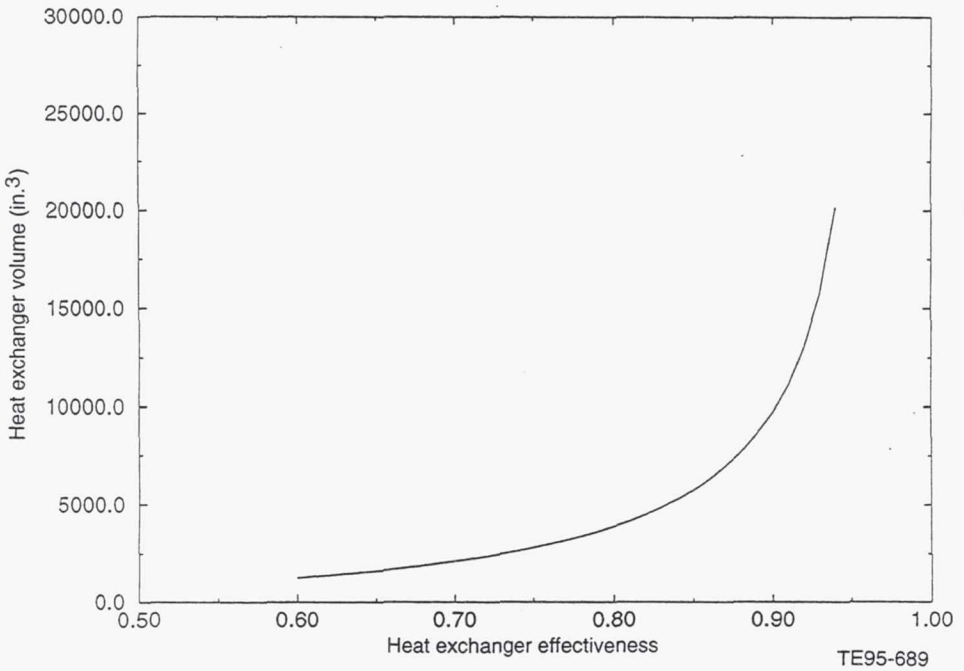

Figure 76. Heat exchanger volume versus effectiveness: valid for ERAST counterflow heat exchanger.

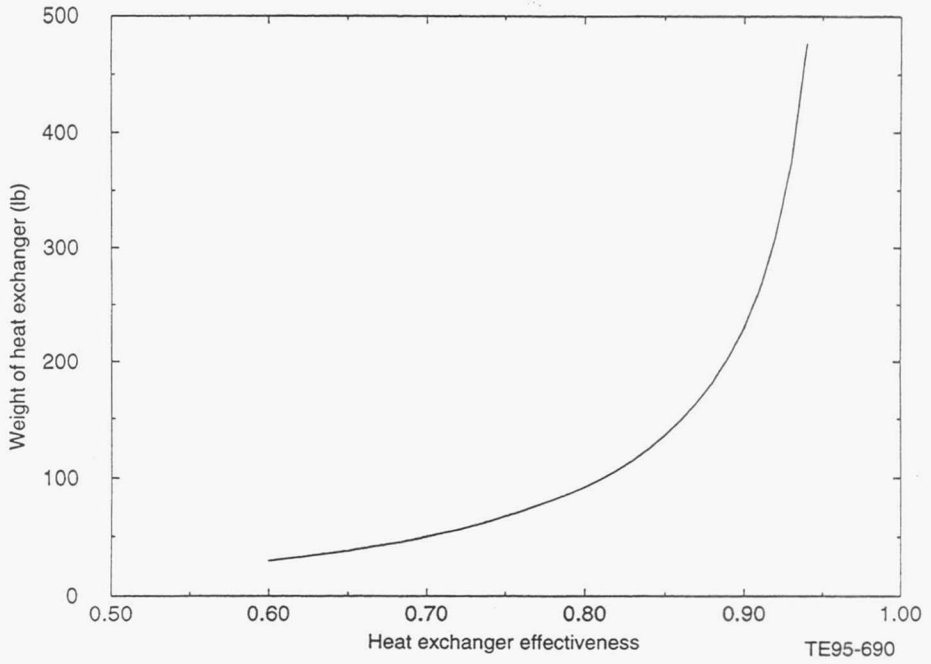

Figure 77. Heat exchanger weight versus effectiveness: valid for ERAST counterflow heat exchanger.

3.3.3 Radiator and Oil Cooler Sizing

The radiators and oil coolers are essentially intercoolers that utilize liquids as the heated medium. The design process of these components is very similar to the method used for the previous intercoolers. The method of assuming the inlet conditions of the flow mediums provides the major difference between the design process of radiators and oil coolers and regular intercoolers.

3.3.3.1 Radiator

The purpose of the radiators is to keep the engine block temperature down for both the piston and rotary engine configurations. The hot inlet temperature of the water/glycol was assumed to be 230°F. This temperature was chosen because the required pressure to prevent the water/glycol from boiling at a higher temperature would add unnecessary complication to containment considerations. The cool outlet temperature of the water/glycol mixture was given as 200°F in the TERMAP cycle sheets. Using the following relations, hot and cold mass flow rates were determined and applied within the heat exchangers optimization program:

Relations:

1. Energy rate = mass flow rate * specific heat * ΔT
2. ε = (heat capacity rate$_{hot}$ * ΔT_{hot})/(heat capacity rate$_{cold}$ * ΔT_{cold})
3. Heat capacity rate = mass flow rate * specific heat

The hot mass flow rate was determined using the rate of energy transfer obtained by converting furnished horsepower loss data into its energy equivalent and applying it within relation one. The effectiveness was assumed according to a typical radiator performance of 50%. The hot flow heat capacity rate taken from the heat exchanger sizing program at the desired effectiveness was used to calculate the corresponding cooling flow heat capacity rate using relation two. Upon calculation of the cooling flow heat capacity rate, relation three could then be used to determine the required cooling mass flow rate. An additional running of the optimizer at the determined mass flow rates would then yield a final design.

A summary of radiator internal dimensions is given in Table 9 for all the powerplant candidates. Radiator weights with the wrap up factor taken into account are given in Table 10.

Table 9.
Radiators' internal design variables (spacings, thicknesses, and lengths).

	2-stroke diesels	4-stroke diesel & 4-stroke gas spark ignition	4-stroke H2 spark ignition & rotary
Cold fin spacing, in.	0.15	0.15	0.06
Hot fin spacing, in.	0.06	0.05	0.08
Cold plate spacing, in.	0.8	0.8	0.5
Hot plate spacing, in.	0.1	0.1	0.2
Cold fin thickness, in.	0.004	0.004	0.004
Hot fin thickness, in.	0.004	0.004	0.004
Plate thickness, in.	0.006	0.006	0.006
Cold fin length, in.	0.8	0.8	0.2
Hot fin length, in.	0.4	0.4	0.4

Table 10.
Radiator and piston oil cooler weights.

	Oil coolers (piston cooling only)			Radiators		
	No. of modules	Weight, lb	Dimensions, in.	No. of modules	Weight, lb	Dimensions, in.
Opp 2-stroke diesel turbo	1	0.9	3.65 x 13.7 x 2.23	1	9.04	2.35 x 21.84 x 22.03
Opp 2-stroke diesel	1	3.13	3.65 x 13.86 x 7.75	1	11.47	2.35 x 21.99 x 27.72
4-stroke diesel	1	7.63	2.91 x 28.35 x 11.55	1	23.78	2.34 x 35.41 x 35.06
4-stroke SI turbo	1	8.02	2.91 x 28.36 x 12.1	1	20.72	2.33 x 32.59 x 33.27
4-stroke H2 fuel turbo	1	6	0.484 x 17.145 x 19.20	2	5.41	0.56 x 32.63 x 22.31
Strat chg rotary	1	6.37	1.48 x 17.16 x 20.3	1	2 x 7.49	0.56 x 32.60 x 30.9
Coleman IC	—	—	—	—	—	—
Coleman recup	—	—	—	—	—	—
2100 growth recup	—	—	—	—	—	—

3.3.3.2 Piston and Rotary Oil Coolers

Oil coolers were designed for piston and rotary engine cooling only. Oil cooler sizing required an assumption method similar to that used for radiator sizing. Again a determination of hot flow (MIL-L-7808 oil) inlet and outlet temperatures was necessary. The hot inlet temperature of the oil was assumed to be 220°F. This temperature was chosen knowing that the temperature of the oil could not be greater than that of the engine block itself, which was 230°F. The cool outlet temperature of the oil was assumed to be 180°F. Using relations and procedures identical to those for the radiators, the oil and air mass flow rates were determined and applied within the heat exchanger optimization program. Design effectiveness was set for 70%.

A summary of oil cooler internal dimensions is given in Table 11 for all the powerplant candidates. The weights of the oil coolers (Table 10) and turbomachinery (bearing cooling, etc) have also been added together to get the total oil cooler weight tabulated in Table 4. All weights given in Table 10 contain a 1.6 wrap-up factor.

Table 11.
Oil coolers' internal design variables (spacings, thicknesses, and lengths).

	2-stroke diesels	4-stroke diesel & 4-stroke gas spark ignition	4-stroke H2 spark ignition & rotary
Cold fin spacing, in.	0.15	0.15	0.08
Hot fin spacing, in.	0.06	0.06	0.06
Cold plate spacing, in.	0.8	0.8	0.5
Hot plate spacing, in.	0.1	0.1	0.2
Cold fin thickness, in.	0.004	0.004	0.004
Hot fin thickness, in.	0.004	0.004	0.004
Plate thickness, in.	0.006	0.006	0.006
Cold fin length, in.	0.8	0.3	0.5
Hot fin length, in.	0.4	0.4	0.4

3.3.4 Heat Loss Analysis

3.3.4.1 Turbocharged Engines

Heat rejection from the turbomachinery component of the turbo-compounded two-stroke diesel was calculated by determining the sum of the heat rejected by convection and radiation for engine operation consistent with various flight conditions. The approach consisted of dividing the subject configuration (see Figure 78) into 20 zones representing the various components (e.g., compressor, combustor, and turbine), assigning metal temperatures to the casing, and calculating the heat rejected by both radiation and convection. Table 12 shows a summary of the calculations performed for the 90,000 ft, 0.4 Mach, standard day flight condition.

The metal temperature (T wall in Table 12) estimates for use in the heat rejection calculations were made using TERMAP cycle information on gas path gas temperatures. Metal temperatures were assumed to be equal to gas path temperatures except in the turbine where a metal temperature limit of 1200°F for contemporary turbine case materials was assumed. Zonal surface areas (Area in Table 12) were determined from the configuration sketch. Estimates of the surface area for and the heat rejected from accessories such as pipes, oil pump, permanent magnet alternator, etc, were also included.

Casing-to-nacelle air convection heat transfer coefficients (Hc in Table 12) were set to be typical of those achievable at the different flight conditions. The temperature difference used to determine the convective heat loss component (Q conv) was taken to be the difference between casing metal temperatures and the prevailing ambient air stagnation temperature (Tc in Table 12). This temperature was assumed to be invariant across the configuration. This assumption makes the heat rejected conservative in that any nacelle cooling air temperature rise would reduce the convective component temperature difference.

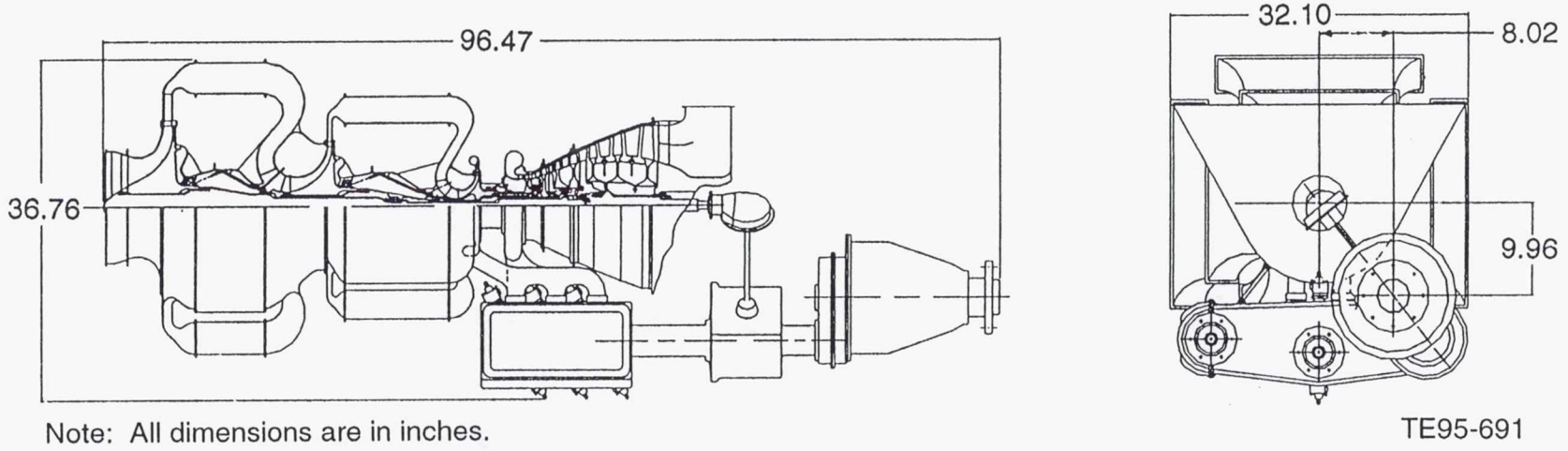

Figure 78. General arrangement—turbo-compounded two-stroke diesel engine.

Table 12.
Two-stroke, turbo-compounded diesel—heat rejection estimate.

90,000 ft, 0.4 Mach, standard, design point								
Zone identification	Area, $in.^2$	Hc, Btu/hr-ft^2-°F	Rad fac	Twall, °F	Cooling temp, °F	Q conv, Btu/hr	Q rad, Btu/hr	Q total, Btu/hr
LPC case segment 1	55.3	0.25	0.60	7.0	-43.4	4.8	6.9	11.7
LPC case segment 2	54.4	0.25	0.60	107.4	-43.4	14.2	28.6	42.8
LPC case segment 3	90.8	0.25	0.60	207.8	-43.4	39.6	109.4	149.0
Accessories	700.0	0.25	0.60	233.0	-43.4	335.9	1002.4	1338.3
LPC case segment 4	216.9	0.25	0.60	233.0	-43.4	104.1	310.6	414.7
LPC-IPC inlet manifold	420.2	0.25	0.60	233.0	-43.4	201.6	601.7	803.4
LPC-IPC exit manifold	761.6	0.25	0.60	78.0	-43.4	160.5	291.8	452.4
IPC case	193.4	0.25	0.60	245.1	-43.4	96.9	299.8	396.7
IPC-HPC inlet manifold	348.8	0.25	0.60	400.0	-43.4	268.5	1287.6	1556.1
IPC-HPC exit manifold	492.0	0.25	0.60	110.0	-43.4	131.0	265.1	396.1
HPC case	68.6	0.25	0.60	275.0	-43.4	37.9	128.2	166.1
HPC scroll	109.5	0.25	0.60	457.0	-43.4	95.1	529.4	624.5
HPC impeller rear	42.7	0.25	0.60	457.0	-43.4	37.1	206.4	243.5
HPC to HPT transition	30.1	0.25	0.60	457.0	-43.4	26.1	145.5	171.7
HPT inlet scroll	189.3	0.25	0.10	1786.0	-43.4	601.2	5727.0	6328.2
HPT case	30.1	0.25	0.60	1200.0	-43.4	65.1	1628.0	1693.0
IPT case	51.7	0.25	0.60	1200.0	-43.4	111.6	2792.5	2904.1
LPT case	123.9	0.25	0.60	1078.0	-43.4	241.2	4924.4	5165.6
PT case	351.3	0.25	0.60	669.0	-43.4	434.5	4000.6	4435.1
Exhaust	161.8	0.25	0.60	435.0	-43.4	134.4	706.6	841.0

A surf total	4,492.4 $in.^2$
Q conv total	3,141.5 Btu/hr
Q rad total	24,992.6 Btu/hr
Q rejected	28,134.1 Btu/hr
Q rejected	11.05 hp

LPC = low pressure compressor
IPC = intermediate pressure compressor
HPC = high pressure compressor
HPT = high pressure turbine
IPT = intermediate pressure turbine
LPT = lower pressure turbine
PT = power turbine

The radiation component of the heat loss (Q rad in Table 12) is the major contributor to heat rejection at the very high altitude conditions of this study. The radiation heat loss component was calculated assuming that radiation exchange was between the configuration casing and the nacelle at a temperature invariant in the axial direction and equal to the ambient air stagnation temperature. This assumption leads to a conservative radiation heat loss estimate since any heating of the nacelle by heat exchange from the engine would increase the nacelle skin temperature and lower the source to sink temperature difference. Metal surface emissivities were taken to be that of typical materials used for turbomachinery components with the exception of selected areas. The prevalent metal surface emissivity used was 0.7. Radiation exchange from each engine zone was assumed to be with a like zone of the nacelle as a first approximation. The radiation configuration factor was, therefore, calculated from the configuration factor equation for two-component gray enclosures. Taking a mean radius of the engine and the maximum engine envelop radius as indicative of the nacelle along with surface emissivity values of 0.7 yields a shape factor of 0.6 (Rad fac in Table 12). The turbine inlet scroll was assumed to be plated with a low emissivity material (e.g., gold or platinum) or surrounded by a series of shields to reduce the heat loss from this major contributor.

The estimated total turbomachinery heat loss for the two-stroke, turbo-compounded diesel configuration at the design point condition is 28,134 Btu/hr or 11 hp. For the other turbocharged piston and rotary engine powerplants, the assumption was made that they would have approximately the same heat loss of 11 hp.

3.3.4.2 Turboshaft Engines

Heat rejection from both the 16:1 Rc recuperated (Figure 79) and 16:1 Rc nonrecuperated turboshaft (Figure 80) was calculated by dividing the propulsion system package at the major split lines into 12 cylindrical sections (Figure 81). A set of simultaneous nonlinear equations representing a one-dimensional energy balance at the surface of the engine and nacelle was solved at each axial station to calculate the following:

- engine and nacelle surface temperatures
- nacelle cooling air temperature rise
- enthalpy addition due to split line leakage
- heat addition from engine accessories

The calculations account for conduction through the engine and nacelle skin and convection and radiation from the surfaces of the control volume formed by the engine exterior and nacelle interior walls. Tables 13 and 14 show summaries of the calculations for the 16:1 Rc turboshaft engines at the 90,000 ft, 0.4 Mach, standard day conditions.

Table 13.
16:1 Rc recuperated turboshaft—heat rejection estimate.

90,000 ft, 0.4 Mach, standard, design point									
Zone ID	Area, $in.^2$	Hc, Btu/hr-ft^2-°F	Hrad, Btu/hr-ft^2-°F	Twall, °F	Tc, °F	Q conv, Btu/hr	Q rad, Btu/hr	Q leak, Btu/hr	Q tot, Btu/hr
Station 1	1463.2	0.42	0.33	-31.2	-43.2	51.6	40.3	—	91.9
Station 2	1682.5	0.40	0.57	134.9	-38.0	816.0	1152.1	400.8	2368.8
Station 3	1353.8	0.46	0.85	260.2	-25.9	1237.0	2283.1	889.3	4409.3
Station 4	1112.0	0.47	1.28	391.1	-10.8	1469.8	3974.3	922.5	6366.7
Aft end of compressor case									
Station 5	564.1	0.68	1.02	803.7	11.4	2128.2	3151.8	1699.0	6978.9
Station 6	920.6	0.68	1.06	832.3	30.8	3497.3	5458.4	—	8955.7
Station 7	560.6	0.64	0.94	736.7	48.3	1734.1	2523.5	—	4257.7
Station 8	496.5	0.69	1.04	784.5	59.3	1736.4	2611.8	—	4348.2
Aft end of combustor case									
Station 9	564.6	0.69	2.48	1296.6	83.5	3350.2	11,792.8	1199.0	16342.0
Station 10	517.8	0.79	2.76	1367.2	108.8	3612.1	12,475.5	—	16087.6
Station 11	1182.6	0.52	3.10	1438.5	143.4	5645.2	32,974.8	—	38620.0
Aft end of turbine case									
Station 12	918.4	0.58	2.40	421.1	166.4	935.9	3897.6	—	4833.6

A surf total	11,336.7 $in.^2$
Q conv total	26,213.8 Btu/hr
Q rad total	82,336.1 Btu/hr
Q leak total	5,110.4 Btu/hr
Q compr air delivery tubes	1,933.5 Btu/hr
Q compr air return tubes	6,708.6 Btu/hr
Q rejected	122,302.5 Btu/hr
	48.02 hp

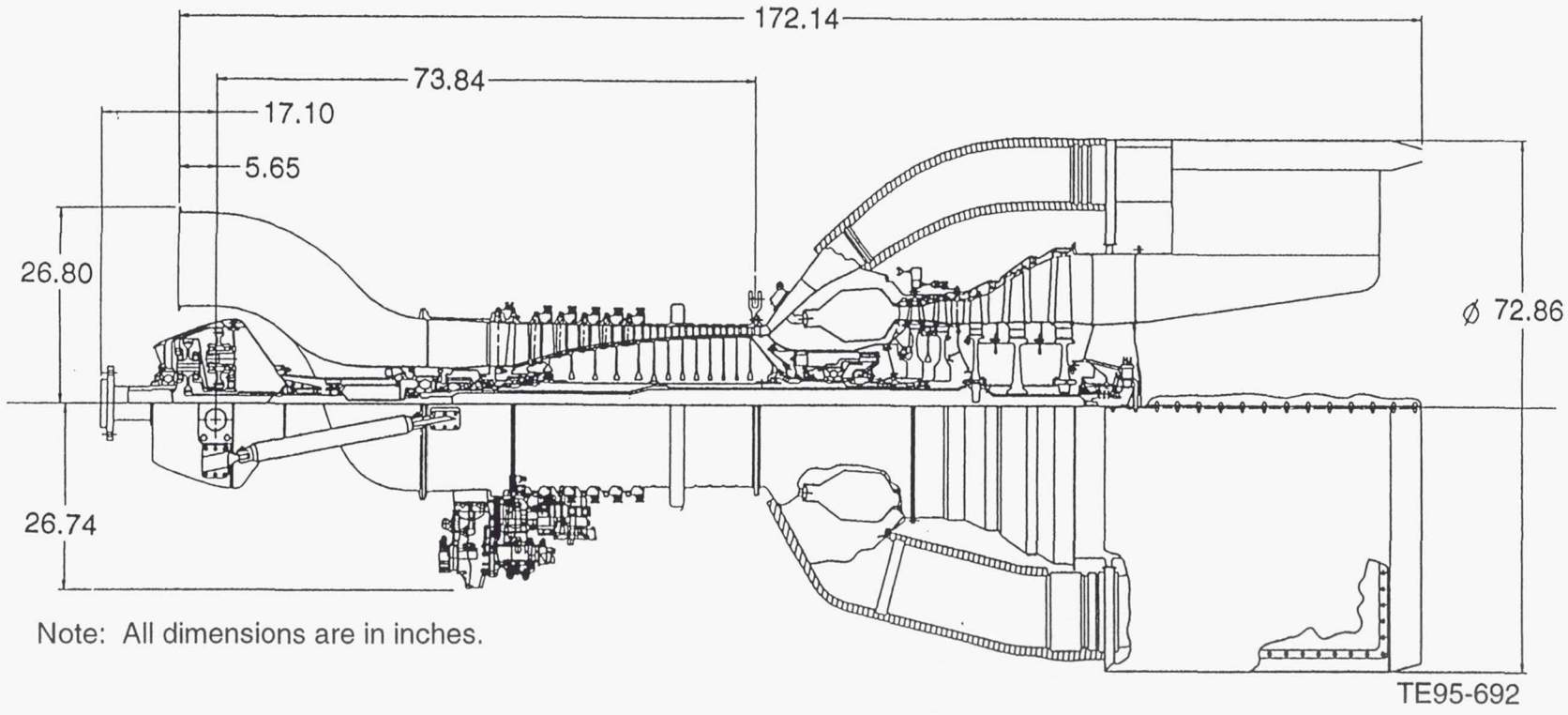

Figure 79. General arrangement—16:1 Rc recuperated turboshaft.

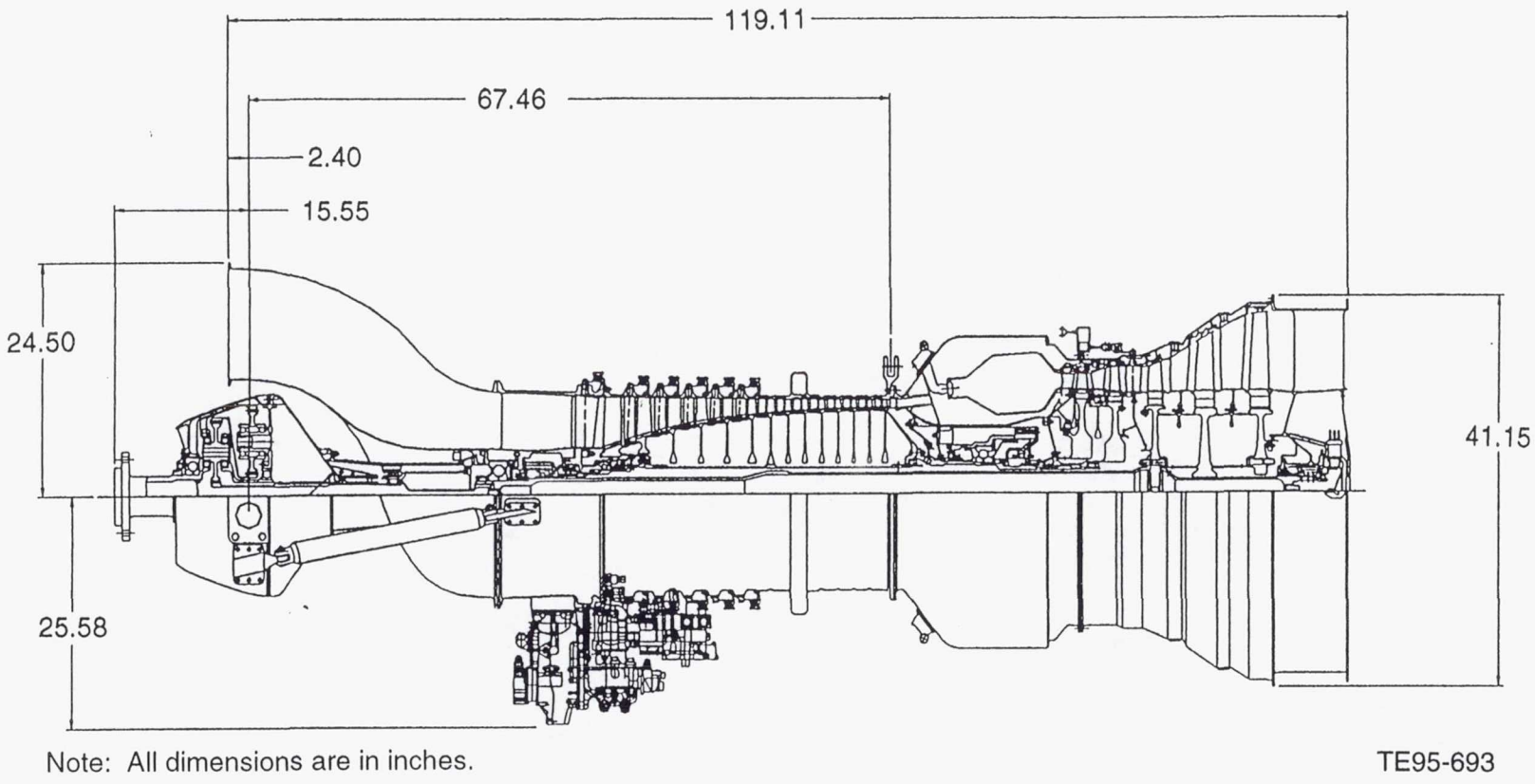

Figure 80. General arrangement—16:1 Rc nonrecuperated turboshaft.

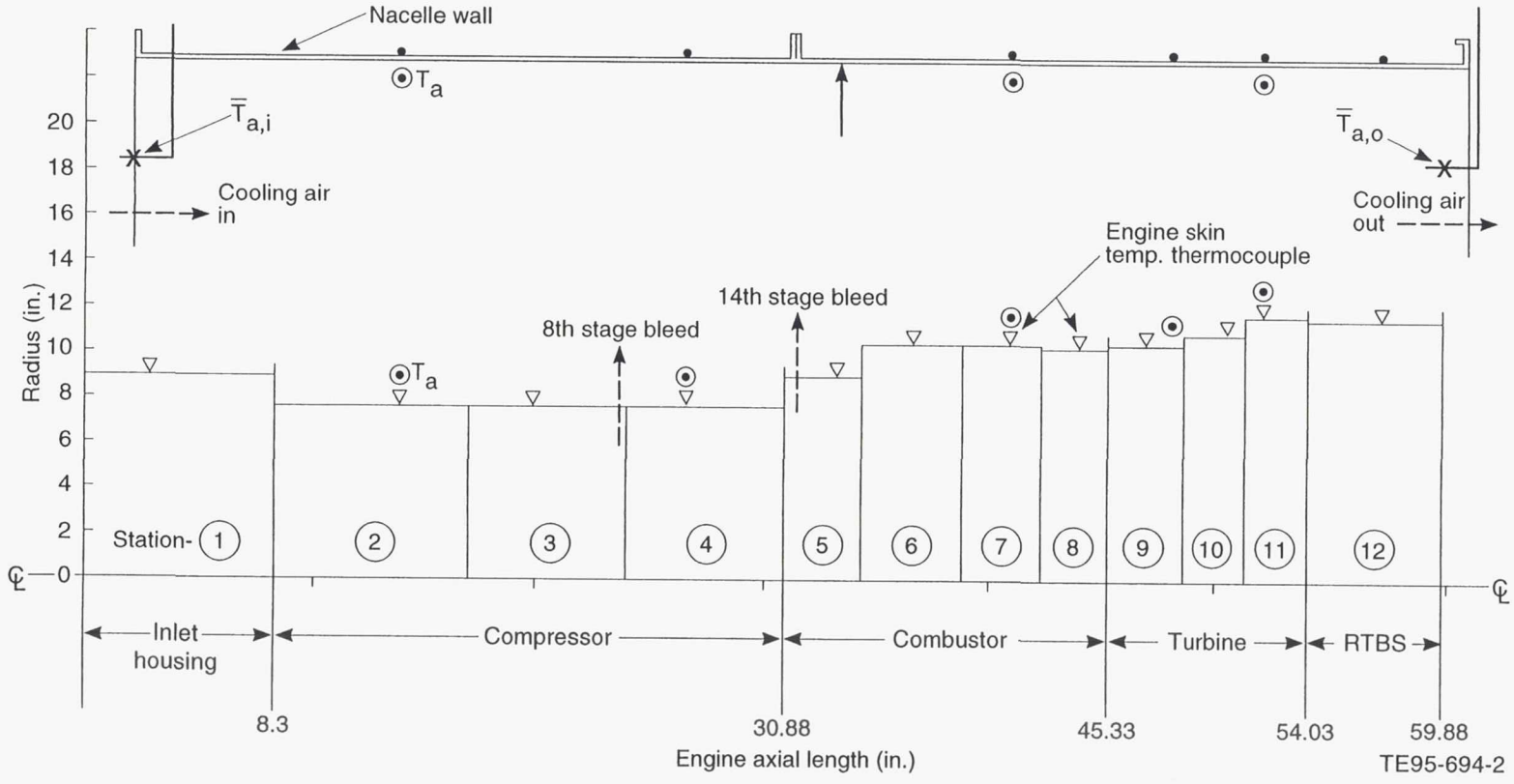

Figure 81. Turboshaft engine heat transfer model sector schematic.

Table 14.
16:1 Rc nonrecuperated turboshaft—heat rejection estimate.

90,000 ft, 0.4 Mach, standard									
Zone ID	Area, $in.^2$	Hc, Btu/hr-ft^2-°F	Hrad, Btu/hr-ft^2-°F	Twall, °F	Tc, °F	Q conv, Btu/hr	Q rad, Btu/hr	Q leak, Btu/hr	Q tot, Btu/hr
Station 1	1243.1	0.73	0.10	-32.0	-43.2	70.5	9.4	—	79.9
Station 2	1432.5	0.61	0.54	133.2	-37.2	1037.5	921.2	400.5	2359.2
Station 3	1152.8	0.69	0.81	257.7	-23.4	1571.1	1819.4	885.1	4275.6
Station 4	946.9	0.65	1.25	389.7	-6.6	1714.5	3245.2	915.0	5874.7
Aft end of compressor case									
Station 5	479.9	1.05	0.94	762.6	17.8	2650.8	2321.4	1691.7	6663.9
Station 6	781.5	1.29	0.95	765.4	43.2	5126.8	3726.6	—	8853.4
Station 7	486.1	1.02	0.87	688.5	66.2	2161.8	1828.0	—	3989.8
Station 8	422.5	1.07	0.97	736.8	79.0	2078.0	1876.3	—	3954.2
Aft end of combustor case									
Station 9	480.7	1.02	2.42	1276.4	106.1	4049.3	9,473.0	1185.8	13522.3
Station 10	441.5	1.20	2.73	1353.3	136.3	4508.4	10,170.6	—	14679.0
Station 11	418.5	1.42	3.04	1416.0	171.1	5189.8	10,982.6	—	16172.4
Aft end of turbine case									
Station 12	781.6	0.92	2.54	423.2	191.8	1154.1	3187.0		4341.1

A surf total	9,067.6 $in.^2$
Q conv total	31,312.6 Btu/hr
Q rad total	49,560.7 Btu/hr
Q leak total	5,078.1 Btu/hr
Q rejected	
	85,951.3 Btu/hr
	33.75 hp

The metal temperature (T wall in Tables 13 and 14) estimates for use in the heat rejection calculations were determined using engine internal gas-to-wall heat transfer coefficients established from test data obtained on a T406 engine. These coefficients were scaled to the subject turboshaft configurations. Engine (Area in Tables 13 and 14) and nacelle surface areas were also scaled from the T406 configuration. TERMAP cycle information was used to establish gas path temperatures.

Casing-to-nacelle air convection heat transfer coefficients (Hc in Tables 13 and 14 were calculated from turbulent flat plate correlations assuming a nacelle cooling flow equal to 12% of the engine inlet flow. The radiation heat loss component was calculated assuming the radiation exchange was between concurrent engine and nacelle zones. The prevalent metal surface emissivity used was 0.8. The combustor and turbine cases were assumed to be plated with a low emissivity material (e.g., gold or platinum) to reduce the heat loss from these major contributors. The radiation configuration factors were calculated from the configuration factor equation for two-component gray enclosures. Equivalent radiation heat transfer coefficients are shown as H rad in Tables 13 and 14.

The estimated total turbomachinery heat loss for the 16:1 Rc recuperated turboshaft configuration at the design point condition is 122,303 Btu/hr or 48 hp. The estimated total turbomachinery heat loss for the 16:1 Rc nonrecuperated turboshaft configuration at the design point is 85,951 Btu/hr or 34 hp. An assumption was made that the 20:1 Rc nonrecuperated heat loss would be the same as the 16:1 version, 34 hp. The heat loss estimate for the Coleman engine was factored in with parasitic losses as discussed in section 3.1.5.

3.4 GEAR SYSTEM ANALYSIS

All gearbox designs employed Allison's gearbox preliminary design system. This system sizes all components for conservative stress levels and life. For example, bearings and gears were sized for 30,000 hr and infinite life, respectively.

3.4.1 Turbo-Compounded

For the turbo-compounded designs, two inputs must be combined with one output. This is typically achieved using a differential system. Either a planetary differential or a bevel differential may be used. A bevel differential provides more compact packaging for this application. It is the same mechanism used in the rear axle of rear-wheel-drive cars and trucks. The fundamental speed relationship for a bevel differential is w1+w2 = 2*wa, where w1 is rotational speed of input or output 1, w2 is rotational speed of input or output 2, and wa is rotational speed of the arm, or carrier. If w1 = wa, then w1 = w2 = wa. This is the relationship proposed for this application. The output shafts of the diesel and turbine must have opposite direction of rotation for this relationship to be correct for the schematic as shown. The bevel pinion that is attached to the output of the turbine would be flipped to mesh with the opposite side if its mating gear if both turbine and diesel have the same direction of rotation. Gearbox weight and efficiency are the same for either design.

The turbo-compounded two-stroke diesel gearbox schematic is shown in Figure 82. A right angle gear set with a reduction ratio 2.94 is needed to transfer power from the turbine to the output of the diesel engine. The two output shafts are then combined in a bevel differential. The output speed from the differential is now 6122 rpm. Two stages of reduction are used to achieve the final output of 600 rpm. A simple offset gear mesh connects to an output planetary gear set. The low final output speed gives low bearing speeds in the planetary gear set. This causes low oil film thickness and therefore a low bearing lube film life factor. This in turn requires large bearings, which result in a large planetary gear set. It may be worthwhile to investigate the use of fluid film bearings to reduce the size of the planetary gear set. Total losses through the gear drive are 2.2%. Current technology cannot reduce these losses appreciably.

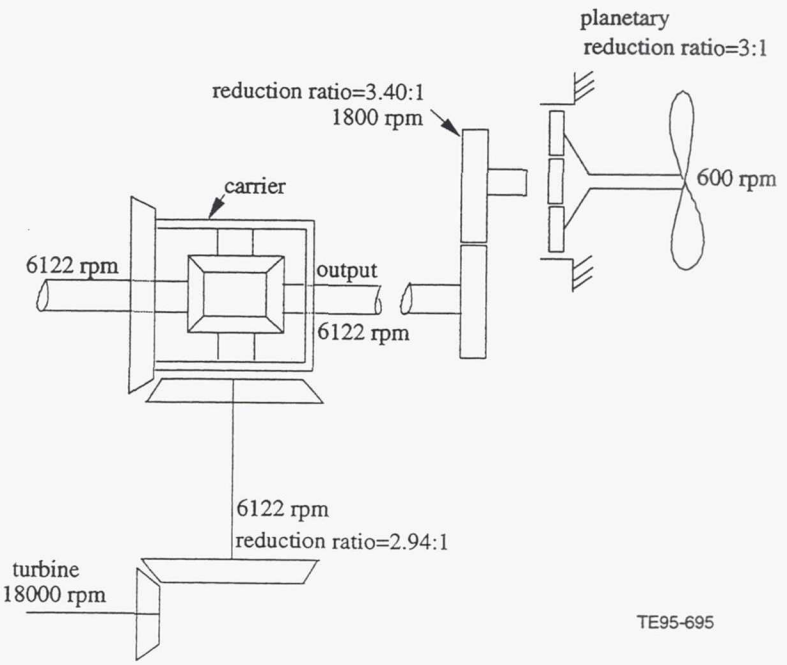

Figure 82. Two-stroke, turbo-compounded diesel gearbox schematic.

The spark ignition engine turbo-compounded gearbox schematic is shown in Figure 83. It is similar to the diesel turbo-compounded design. It is heavier than the comparable diesel design, because the spark ignition engine output is only 1800 rpm, instead of 6122 rpm for the two-stroke diesel. This gives a lower torque, requiring a heavier bevel differential. The increase in weight of the bevel differential more than offsets the weight of the offset reduction gears that are no longer needed.

3.4.2 Non-Turbo-Compounded Gearbox

An example of a non-turbo-compounded gearbox arrangement is shown as a schematic in Figure 84 for the four-stroke diesel. It is a very simple geartrain. It is the same geartrain used for the turbo-compounded design, but without the right angle gearbox and without the bevel differential. Also, the remaining gearing may be reduced in size. Total loss for this geartrain is 1% of transmitted horsepower.

3.5 CONFIGURATION ANALYSIS

3.5.1 Two-Stroke Diesel Engine - Advanced Technology

The two-stroke diesel configurations analyzed (turbo-compounded and non-turbo-compounded) are based on the same core engine. This engine is a 3-cylinder, 6-piston, horizontally opposed design. Each pair of pistons operates in a common horizontal cylinder, forming the combustion chamber as they come together at the end of their compression strokes. The action of the pistons is controlled by two outboard crankshafts that are connected through gearing. This two-stroke opposed piston design eliminates the need for cylinder heads, intake and exhaust valves, rockers, pushrods, camshafts, etc. Figure 85 shows cross sections of this core engine. The following sections describe the turbomachinery that is mated with this two-stroke diesel.

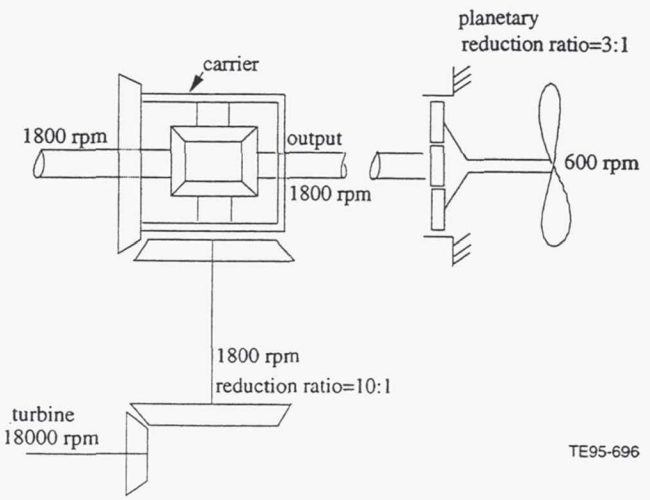

Figure 83. Turbo-compounded spark ignition gearbox schematic.

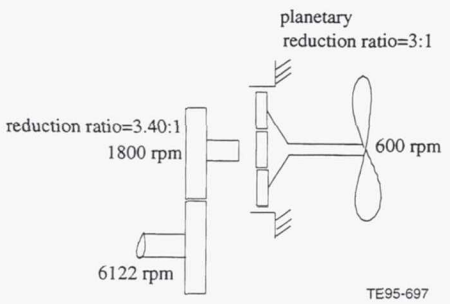

Figure 84. Non-turbo-compounded diesel gearbox schematic.

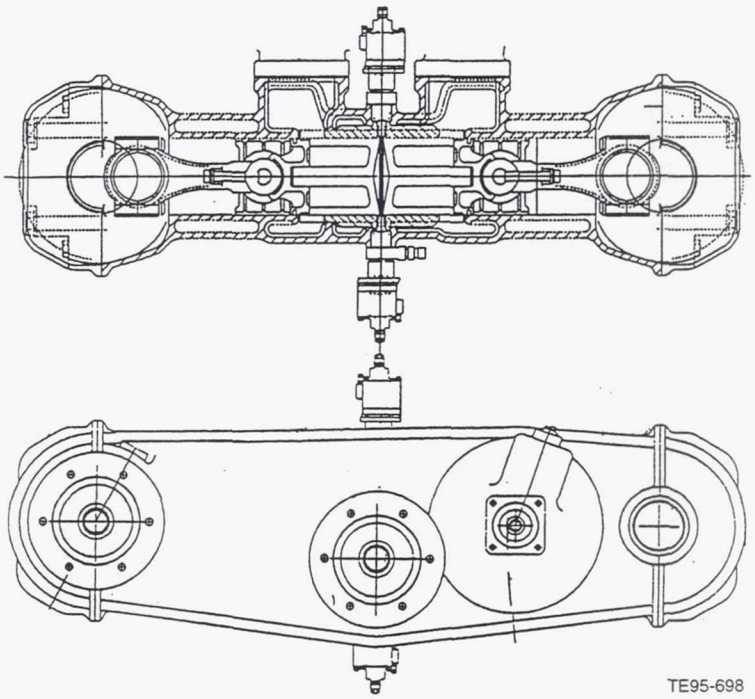

Figure 85. Two-stroke opposed piston diesel core engine.

3.5.1.1 Turbo-Compounded Two-Stroke Diesel - Advanced Technology

Because of the large amount of air compression required for engine operation at ultra-high altitudes, the resulting configurations demand a complex array of size and arrangement of turbomachinery. This is evident in the general arrangement of the turbo-compounded two-stroke diesel (Figure 86), as the turbocharger is the dominant feature.

The turbocharger consists of three concentric spools, plus a power turbine that routes power back into the core engine geartrain. Intercoolers are located between each stage of compression. The high pressure (HP) spool is comprised of a single-stage centrifugal compressor driven by a single-stage HP turbine. A single-stage intermediate pressure (IP) centrifugal compressor is driven by a single-stage IP turbine. The low pressure (LP) spool consists of a single-stage centrifugal compressor being driven by a two-stage LP turbine. The power turbine has three stages. The HP, IP, and LP spools, along with the power turbine, are positioned concentrically on a common centerline.

The LP turbine drives the LP compressor through a splined shaft. The LP turbine is supported by a small roller bearing forward of the LP first-stage wheel and a larger ball bearing aft of the LP second-stage wheel. The shaft connecting the turbine and compressor is supported intermediately by an intershaft bearing (in contact with the IP compressor shaft) and a roller bearing. The overhung LP compressor wheel is supported by a large ball bearing.

The IP spool is supported by a ball bearing aft of the IP turbine wheel (in a common sump with the LP turbine roller bearing), an intermediate roller bearing, an intershaft bearing (shared with the LP shaft), and a larger ball bearing. The overhung IP compressor wheel is forward of the ball bearing. The HP spool is supported by two bearings: a roller bearing aft the HP turbine wheel and a ball bearing aft of the overhung HP compressor.

The power turbine is supported at the forward end by a roller bearing (which shares a sump with the LP turbine ball bearing) and at the aft end by a ball bearing. The power turbine connects to a shaft that exits the rear of the turbocharger. This shaft feeds power back to the core engine drivetrain.

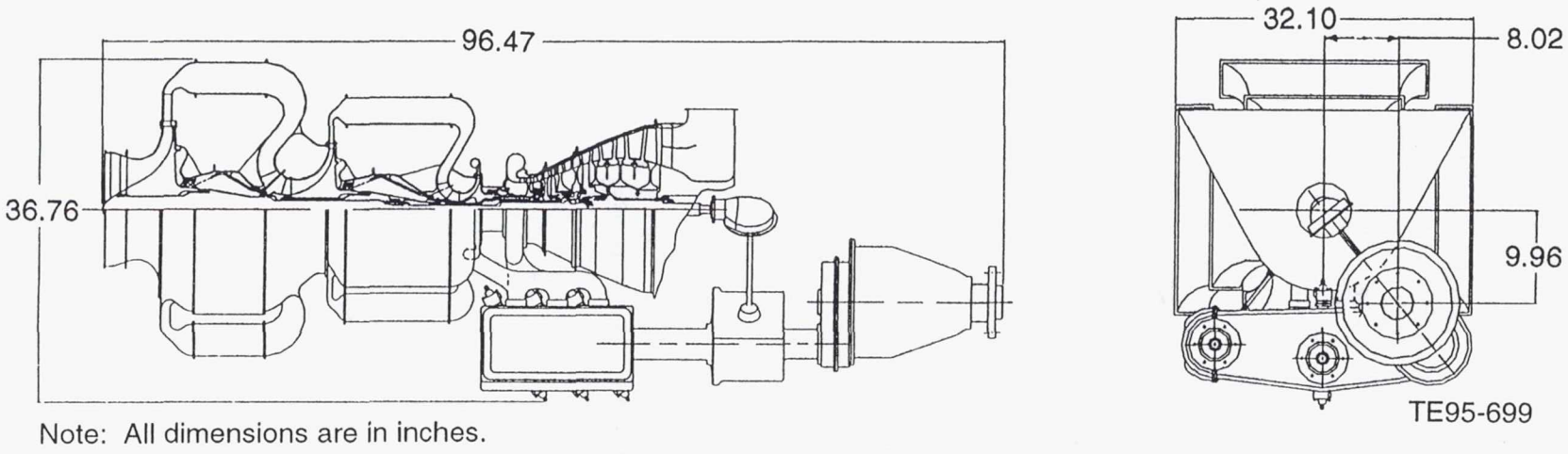

Figure 86. General arrangement—turbocompounded two-stroke diesel engine.

The basic turbocharger materials are as follows:

- LP compressor - aluminum alloy
- IP compressor - titanium alloy
- HP compressor - titanium alloy
- turbine wheels - Udimet 720 (Ni base alloy)
- turbine blades - Mar-M247 (cobalt base)
- intercoolers - aluminum alloy
- shafts - AMS 64500
- LP compressor scroll and case - aluminum alloy
- IP and HP compressor scrolls and cases - titanium alloy
- turbine cases - Inco 718

After the air exits the LP compressor, it is ducted into four intercoolers. The intercoolers then duct the air into the IP compressor. The air once again is ducted into four additional intercoolers. The intercoolers then direct the air to the HP compressor. Upon exiting the HP compressor, the air is scrolled into the core engine intake manifold. After combustion, the exhaust gases are directed to the turbine scroll. The gases then expand through the turbine and exit the exhaust stack.

The power captured by the power turbine is transmitted through a set of bevel gears, a tower shaft, and into another bevel gearset mounted to a differential gearset. This power is combined with that of the core engine, which is taken from one of the outboard crankshafts. The resultant power then goes through a spur gear that drives a planetary gearset, which is connected to the propeller flange.

To control core engine temperature, heat is rejected through a coolant radiator and a lube oil cooler, both remotely mounted.

3.5.1.2 Non-Turbo-Compounded Two-Stroke Diesel - Advanced Technology

The non-turbo-compounded version of the two-stroke diesel is very similar to that of the turbo-compounded version. The core engines are identical, and other similarities can be noted in the general arrangement shown in Figure 87.

The turbocharger consists of three concentric spools that are supported in the same fashion as those of the turbo-compounded diesel. The major differences between the turbomachinery are the three-stage LP turbine (turbo-compounded has two stages), the lack of a power turbine and the associated geartrain (bevel gears, tower shaft, differential gearset), a nozzled turbine exhaust, and larger intercooler sizes. The compressor and turbine flow paths are unique for this configuration. The turbocharger materials are the same as the turbo-compounded version. The propeller gearbox is now mounted directly to the core engine. The core engine still utilizes a remotely mounted radiator and oil cooler.

3.5.2 Four-Stroke Diesel Engine - SOA Technology

The four-stroke diesel core engine is a 6-cylinder horizontally opposed configuration. The engine is liquid cooled and utilizes a wet sump oil system. The coolant radiator and oil cooler are remotely mounted. The turbocharger has the same basic configuration as the aforementioned two-stroke diesel turbochargers. See the general arrangement in Figure 88. Its three concentric spools are supported in the same manner as they are in the non-turbo-compounded two-stroke diesel. The centrifugal LP compressor is driven by a two-stage LP turbine. The two-stage IP turbine is mated to a centrifugal IP compressor. The single-stage HP turbine drives a centrifugal HP compressor. There are two intercoolers between each compression stage as well as the addition of two aftercoolers between the HP compressor and the core engine. The general airflow path is the same as the two-stroke turbochargers, with the exception of flow through the two post-HP stage aftercoolers. The aftercooler exit air is ducted directly into the diesel engine. The exhaust gases are manifolded into the turbine scroll, where they are expanded through the turbines.

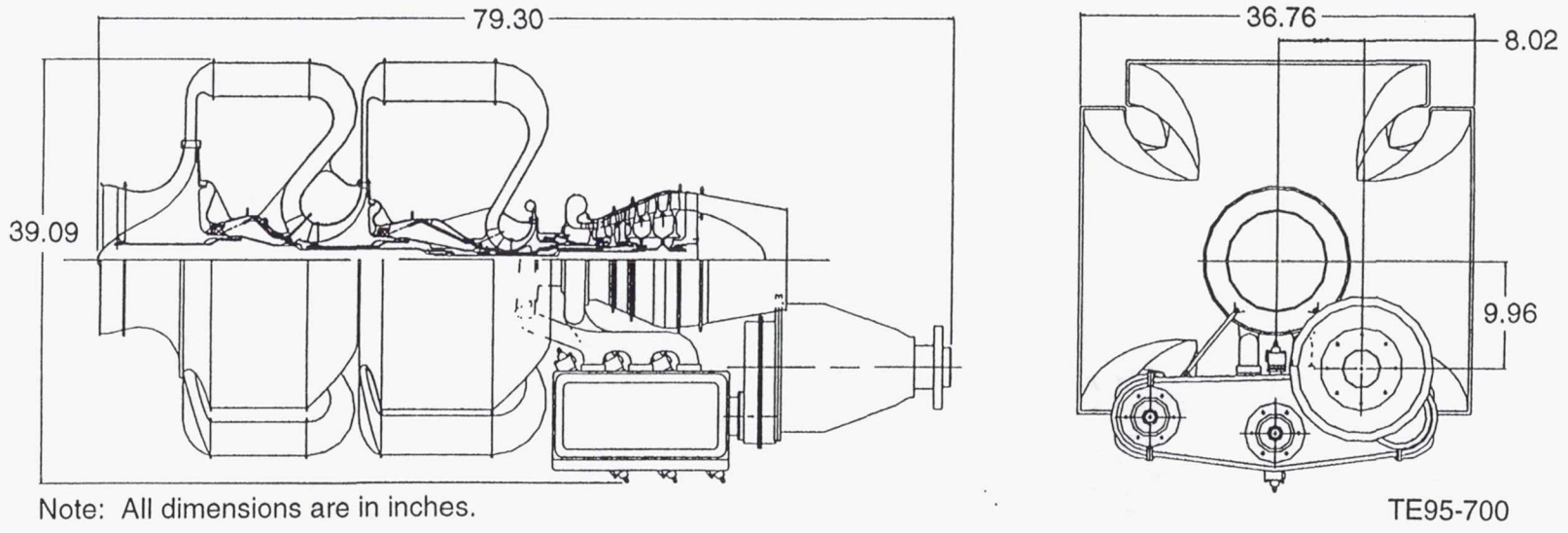

Figure 87. General arrangement—non-turbo-compounded two-stroke diesel engine.

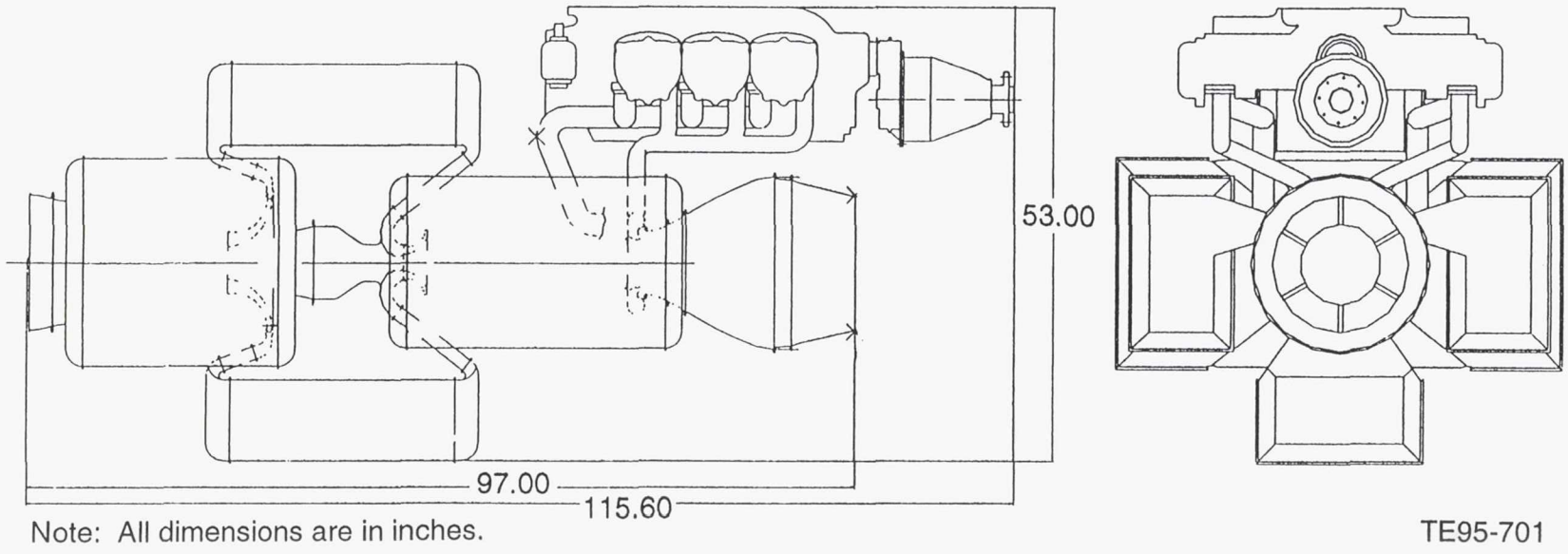

Figure 88. General arrangement—non-turbo-compounded four-stroke diesel engine.

The engine crankshaft directly drives the propeller gearbox, which is of the same configuration as the non-turbo-compounded two-stroke diesel gearbox.

3.5.3 Four-Stroke Spark Ignition Engine - SOA and NT Technology

The four-stroke spark ignition powerplants are analyzed both as gasoline fueled and hydrogen fueled. Both spark ignition engines are based on the Teledyne Continental Voyager 550 engine. The coolant radiators and oil coolers are remotely mounted. The turbomachinery for both the gasoline and hydrogen fueled engines is identical except for differences in the turbines. The power turbine geartrain and propeller gearboxes are similar.

3.5.3.1 Gasoline Fuel - SOA Technology

The turbomachinery for the gasoline fueled four-stroke spark ignition engine has similar materials and layout to each turbocharger configuration previously addressed. The general arrangement is shown in Figure 89. As in the four-stroke diesel, there are two intercoolers between each compressor stage and also two aftercoolers at the exit of the HP compressor. The HP, IP, LP, and power turbines are identical in stage number and flow path as those of the turbo-compounded two-stroke diesel. The turbo-compounding hardware (power turbine shaft, bevel gearset, and differential gearset) is the same in design and layout as the turbo-compounded two-stroke diesel.

3.5.3.2 Hydrogen Fuel - NT Technology

The general arrangement of the hydrogen fuel four-stroke spark ignition engine is shown in Figure 90. The core engine, radiator, oil cooler, and gearing are identical to those of the gasoline fueled engine. The turbomachinery is also identical, including the intercooler and aftercooler sizes, except for a different turbine flow path. The power turbine has an added stage, resulting in four stages total.

3.5.4 Rotary Engine - NT Technology

The rotary engine powerplant configuration is based on a three rotor, 120 $in.^3$ displacement rotary engine and a three spool, concentric shaft turbocharger. The general arrangement is shown in Figure 91. The turbomachinery is similar in concept to the previous two- and four-stroke engines' turbochargers, but there are some obvious differences. The LP compressor is a five-stage axial unit that is driven by a two-stage LP turbine. The compressor wheels are clamped together by a hollow shaft acting as a tie bolt. The LP compressor rotor is connected to the LP shaft by a cone shaft. The LP spool is supported by a ball bearing at the front of the compressor rotor, an intershaft roller bearing aft of the IP compressor wheel, a ball bearing forward of the LP turbine first-stage wheel, and a roller bearing aft of the LP turbine. The IP spool consists of a two-stage turbine driving a single-stage centrifugal compressor. It is supported by a ball bearing aft of the LP compressor wheel, the intershaft bearing shared with the LP shaft, and a ball bearing aft of the IP turbine in a common sump with the LP turbine forward bearing. The HP centrifugal compressor is driven by the single-stage HP turbine. The HP spool is supported by a ball bearing aft of the compressor wheel, and a roller bearing aft of the turbine wheel.

The materials of the turbocharger are as follows:

- LP compressor wheels - titanium alloy
- LP compressor blades - 17-4PH stainless steel
- IP compressor - titanium alloy
- HP compressor - titanium alloy
- turbine wheels - Udimet 720 (Ni base alloy)
- turbine blades - Mar-M247 (cobalt base)
- intercoolers and aftercoolers - aluminum alloy
- shafts - AMS 64500
- LP compressor case and ducting - aluminum alloy
- IP and HP compressor scrolls and cases - titanium alloy
- turbine cases - Inco 718

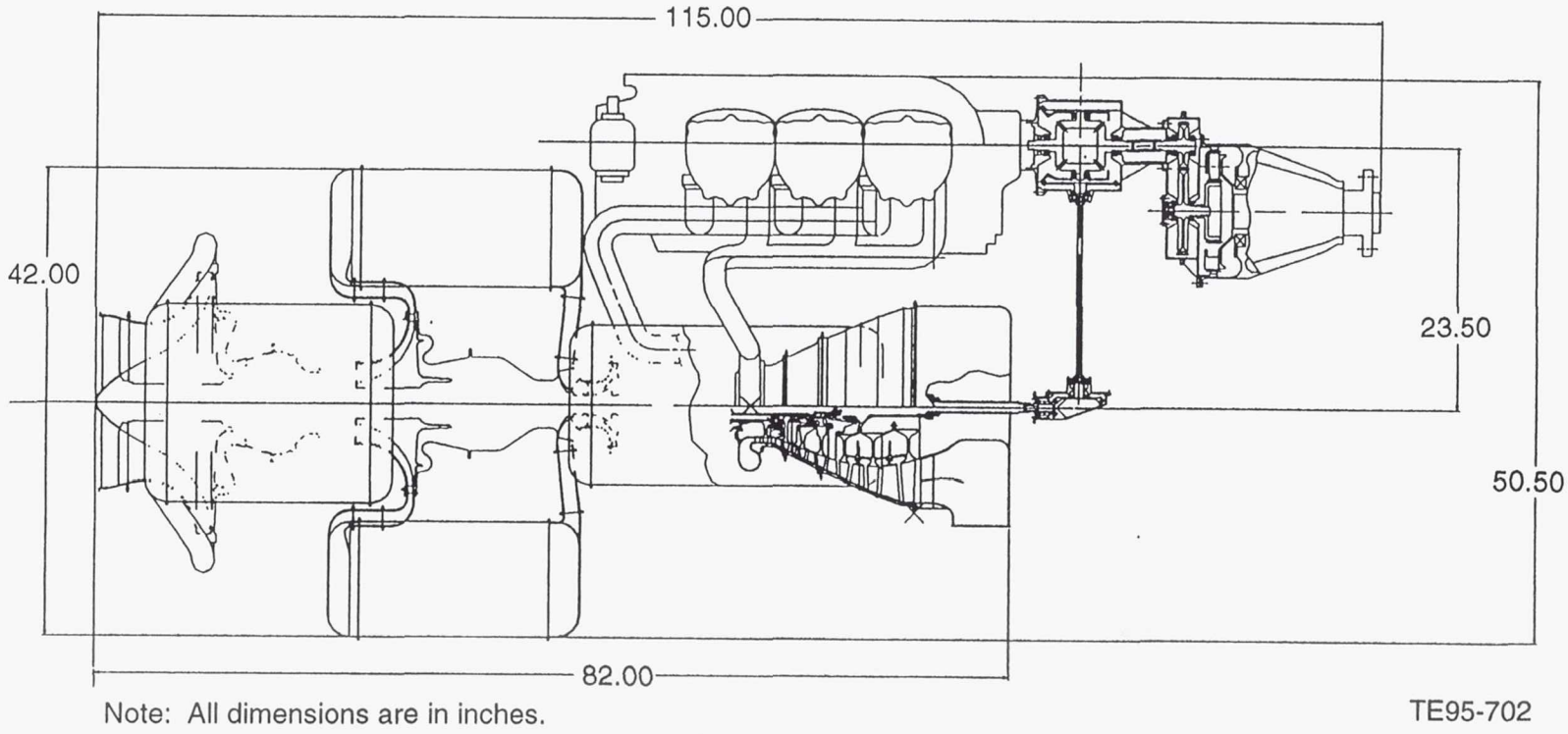

Figure 89. General arrangement—gasoline fuel four-stroke spark ignition engine.

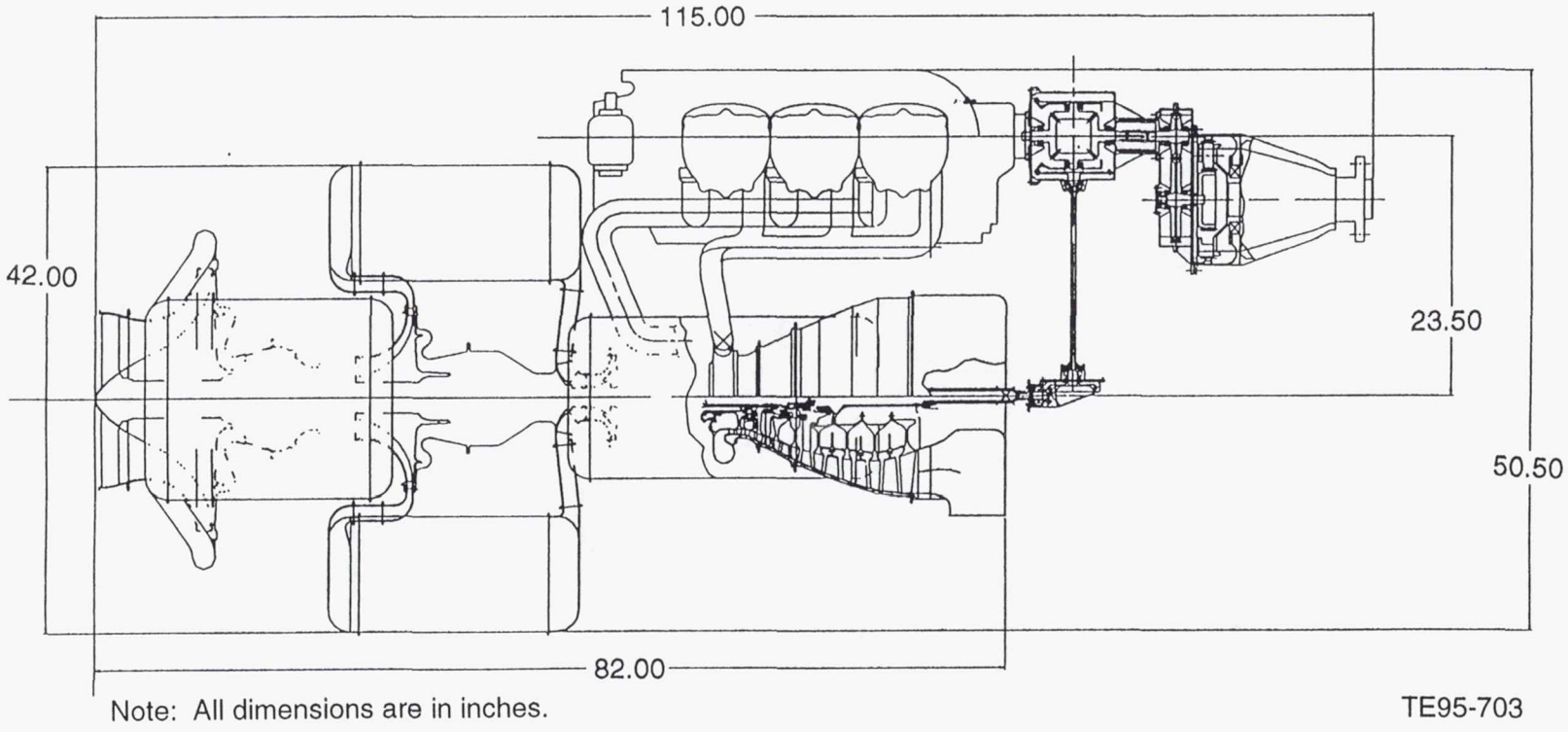

Figure 90. General arrangement—hydrogen fuel four-stroke spark ignition engine.

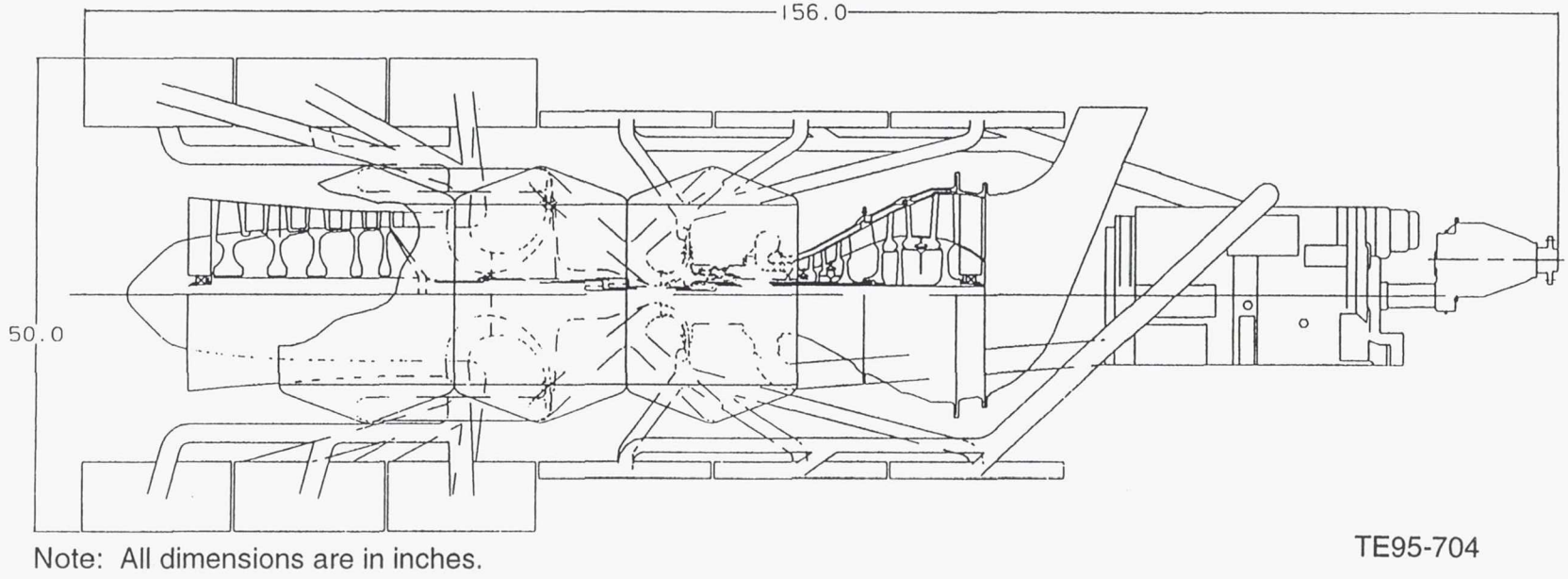

Figure 91. General arrangement—rotary engine.

There are six intercoolers each between the LP and IP compressor stages and IP and HP stages. HP compressor discharge air is routed through six aftercoolers before being ducted into the engine. The LP-IP intercoolers are mounted on the top and bottom of the turbocharger, near the forward end. LP compressor discharge air is ducted into these intercoolers, flowing in a transverse direction (in and out of the page). The ambient cooling air flows in around the turbocharger and up through the intercoolers. The intercooler discharge air is ducted into the IP compressor flow path. After exiting the IP compressor, the air is ducted into the six IP-HP intercoolers. These intercoolers are mounted on the right and left side of the turbocharger (the outlines as shown in Figure 91). The compressed air flows up or down through the intercoolers (depending on whether it's in the right or left bank) and is ducted into the HP compressor. The HP compressor discharge is then manifolded into the six aftercoolers that are situated in the same fashion as the LP-IP intercoolers. The compressed air travels in a transverse direction through the aftercoolers, like the LP-IP intercoolers, and is ducted into the intake tract of the rotary engine. The exhaust gases of the rotary are piped back into the turbine scroll and are expanded through the turbine. The gases exit out the upward-turned exhaust nozzle.

The propeller gearbox is similar to those used in the non-turbo-compounded two- and four-stroke diesel engines.

3.5.5 Coleman Cycle Engine - NT Technology

The Coleman cycle engine general arrangement is shown Figure 92. This engine uses a single shaft to couple the four stage turbine to the centrifugal LP and HP compressors. The single spool is supported by a roller bearing at the front of the rotor, a ball bearing between the HP compressor and the turbine section, and a ball bearing aft of the turbine. The propeller gearbox, at the front of the engine, is driven directly by this spool.

The intake air flows in through the inlet duct and is compressed by the LP compressor. The air is then scrolled off and combined with the recuperator exit flow, which is then routed to the intercoolers. These intercoolers are mounted on the top and bottom of the engine. Figure 92 shows the end views of each intercooler, the length of which is 54 in. The cooling air is ducted in from the front of the engine and flows up or down through each intercooler. The cooled mixture is collected and ducted directly into the flow path between the LP and HP compressors.

After being compressed, the air is scrolled off into three ducts that lead to the recuperator, located at the rear of the engine. It is a modular unit made up of six heat exchangers. After being heated by exhaust gases, the compressed air is ducted back to the diffuser, located aft of the HP compressor. Fuel is introduced into the combustion liner and combustion occurs. The gases are expanded through the turbine where a portion is routed to the recuperator (note the split in the turbine between the second and third stages). The remainder of the gases exit the exhaust nozzle. The exhaust gases that are routed to the recuperator flow through the heat exchangers and are then combined with the LP compressor exit flow and ducted to two banks of five intercoolers each.

The materials of the Coleman cycle engine are as follows:

- LP compressor wheels - titanium alloy
- HP compressor - titanium alloy
- turbine wheels - Udimet 720 (Ni base alloy)
- turbine blades - Mar-M247 (cobalt base)
- intercoolers - aluminum alloy
- recuperator modules - stainless steel
- shafts - AMS 64500
- LP compressor scroll and case - aluminum alloy
- HP compressor scrolls and cases - titanium alloy
- turbine cases - Inco 718

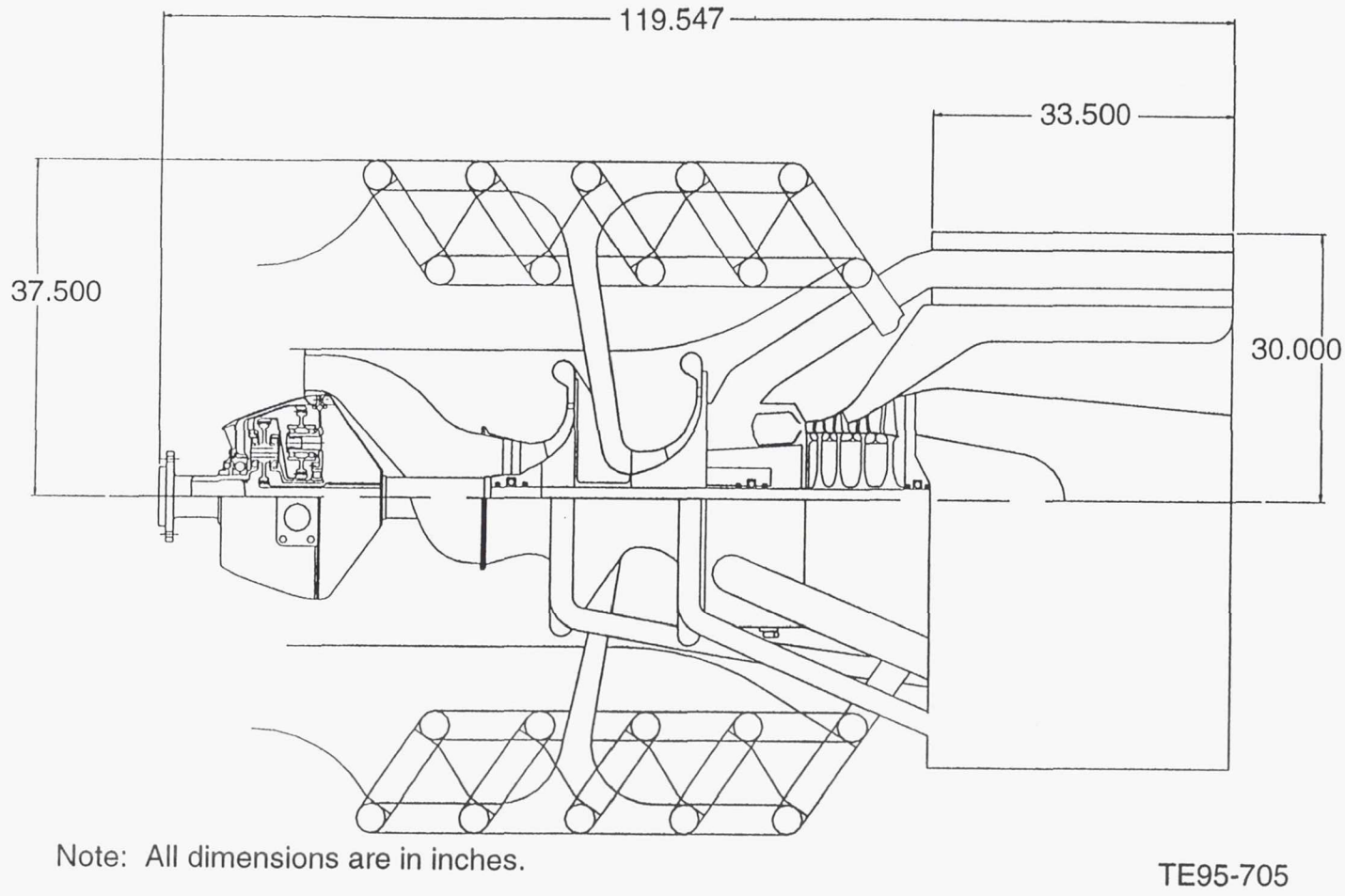

Figure 92. General arrangement—Coleman cycle engine.

3.5.6 Turboshaft Engine - SOA and NT Technology

Each of the following turboshaft arrangements is based on the Allison AE2100 turboprop configuration. The engines contain two main rotor systems: a gas generator rotor system and a power turbine rotor system. The gas generator rotor (GG rotor) system consists of a multistage axial compressor driven by a two-stage HP turbine. The GG rotor is supported by a roller bearing forward of the compressor and a ball bearing aft of the compressor. The HP turbine is overhung. The three-stage power turbine, or LP turbine, is supported by an aft roller bearing and a ball bearing located on the front of the long power turbine shaft. A diffuser and combustor are located between the compressor and turbine sections. The diffuser contains a sump area for the GG rotor ball bearing.

The compressor rotor consists of bladed wheels that are clamped together by a hollow shaft acting as a tie bolt. The compressor inlet guide vanes and the stage 1-5 compressor vanes are geometrically variable (i.e., can be turned to different setting angles while the engine is running). The power turbine first-stage vanes are also variable. The remainder of the compressor and turbine vanes are fixed.

The basic material of the turboshaft engines are as follows:

- air inlet housing - aluminum alloy
- compressor wheels - titanium alloy
- compressor blades - Inco 718
- compressor case - titanium alloy
- diffuser - titanium alloy
- turbine wheels - Udimet 720 (Ni base alloy)
- turbine blades - Mar-M247 (cobalt base)
- turbine cases - Inco 718
- shafts - AMS 64500

The accessory gearbox is located below the compressor section and is driven by the compressor rotor through a bevel gearset and a tower shaft. The propeller gearbox is mounted forward of the compressor and is driven directly by the power turbine through the power turbine shaft.

3.5.6.1 16:1 R_c Recuperated - NT Technology

The general arrangement is shown in Figure 93. The basic engine configuration is described in the preceding section. The compressor is a 14 -stage axial unit with a compression ratio of 16:1. The compressor discharge air is ducted into a modular recuperator consisting of six stainless steel heat exchangers. The compressed air is heated and ducted back into the diffuser, ready for combustion. The hot gases are expanded through the turbine and are routed through the recuperator. After passing through the heat exchangers, the gases exit out the rear of the recuperator.

3.5.6.2 16:1 R_c Nonrecuperated - SOA Technology

Figure 94 shows the general arrangement of the 16:1 R_c nonrecuperated turboshaft. This engine has the same 14-stage, 16:1 compression ratio compressor as the recuperated turboshaft. Since this engine does not have a recuperator, the combustion gases exit the engine after expanding through the turbine.

3.5.6.3 20:1 R_c Nonrecuperated - NT Technology

The general arrangement is shown in Figure 95. This engine is identical in layout and configuration as the 16:1 R_c nonrecuperated turboshaft except for a 15-stage, 20:1 R_c compressor.

3.5.7 Fuel Cell Engine - Advanced Technology

A conceptual general arrangement of the fuel cell engine was developed and is shown in Figure 96. At the 90,000 ft, 0.4 Mach design point, this concept engine requires a 98:1 turbocharger to provide the correct inlet conditions to the fuel cell component. This level of turbocharging was accomplished with the three spool turbocharger.

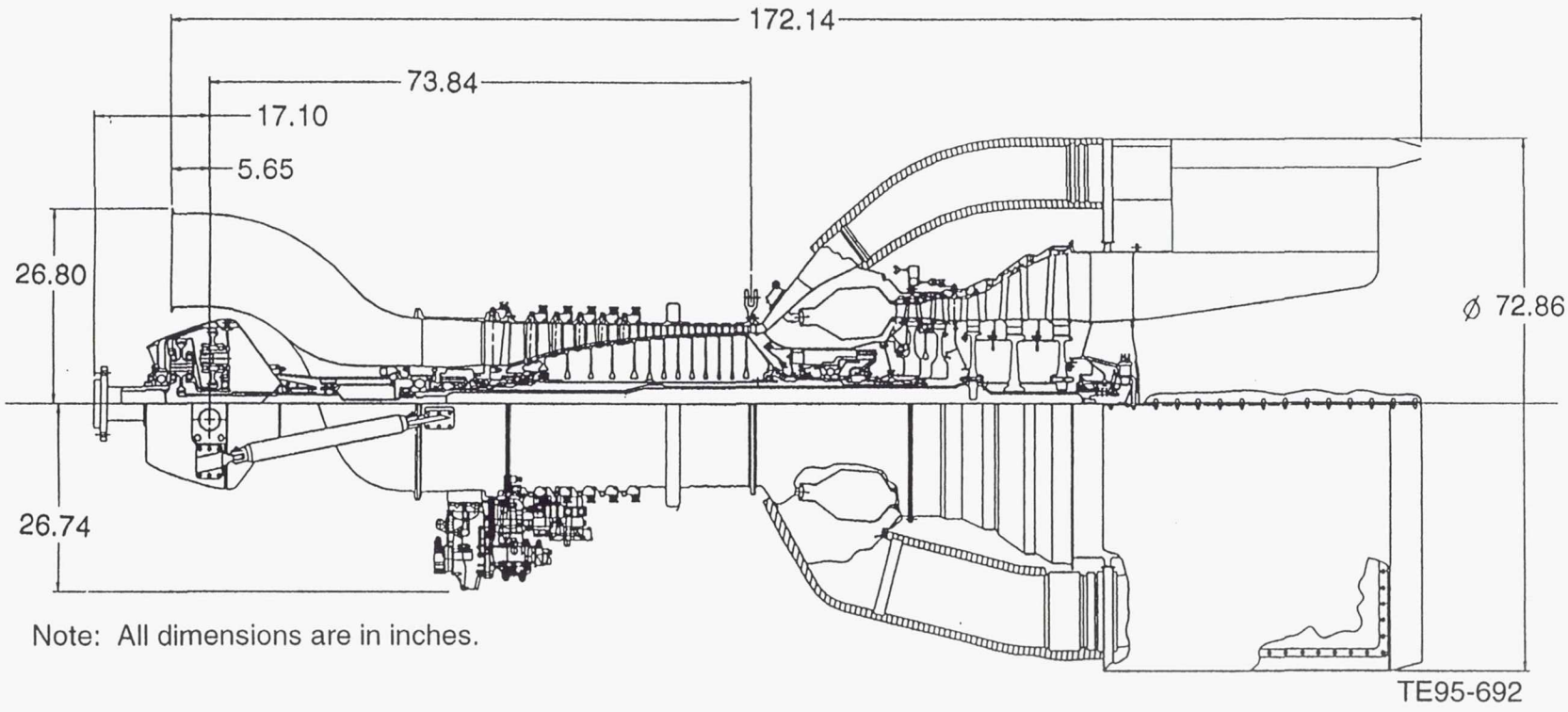

Figure 93. General arrangement—16:1 Rc recuperated turboshaft.

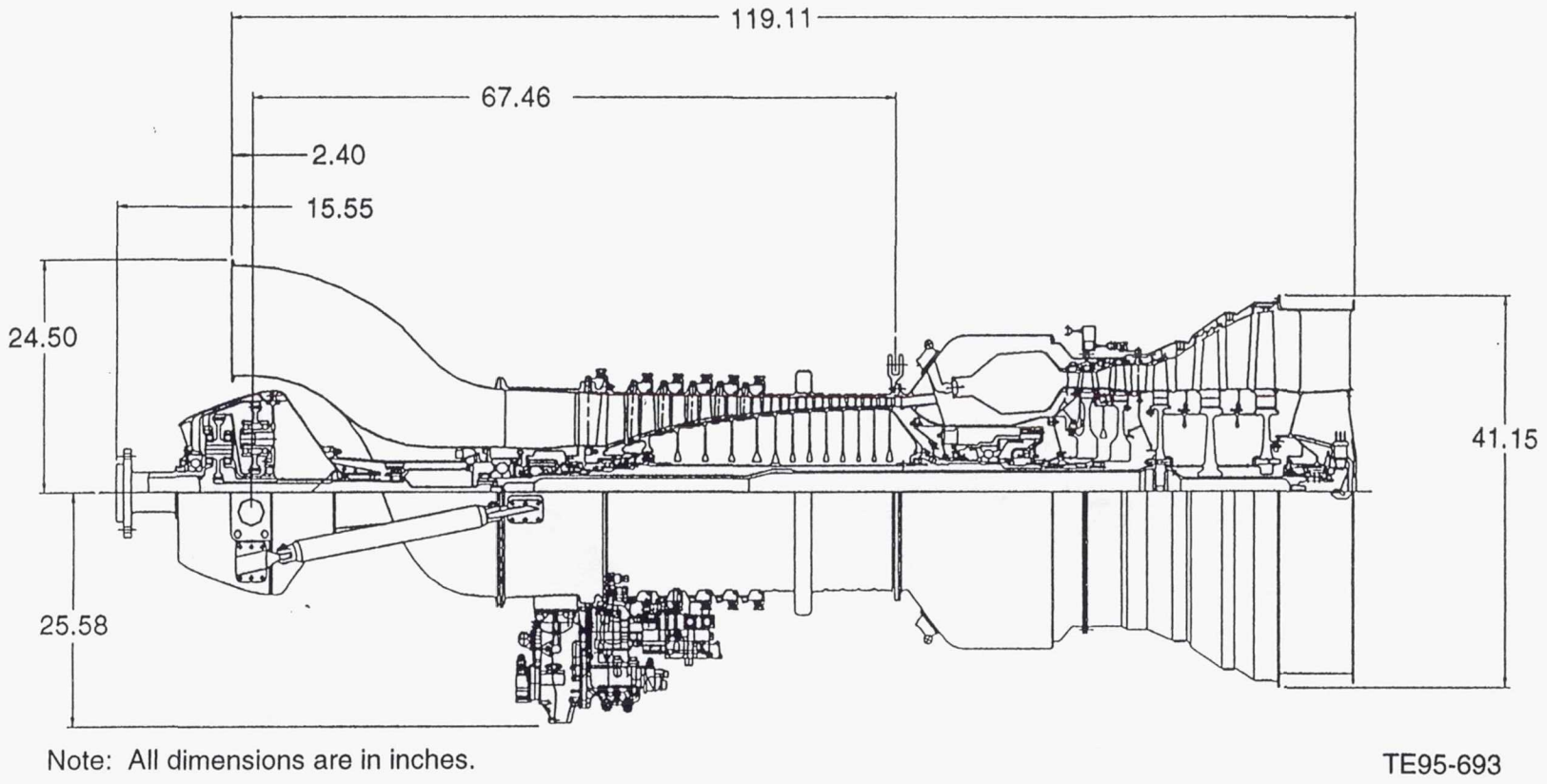

Figure 94. General arrangement—16:1 Rc nonrecuperated turboshaft.

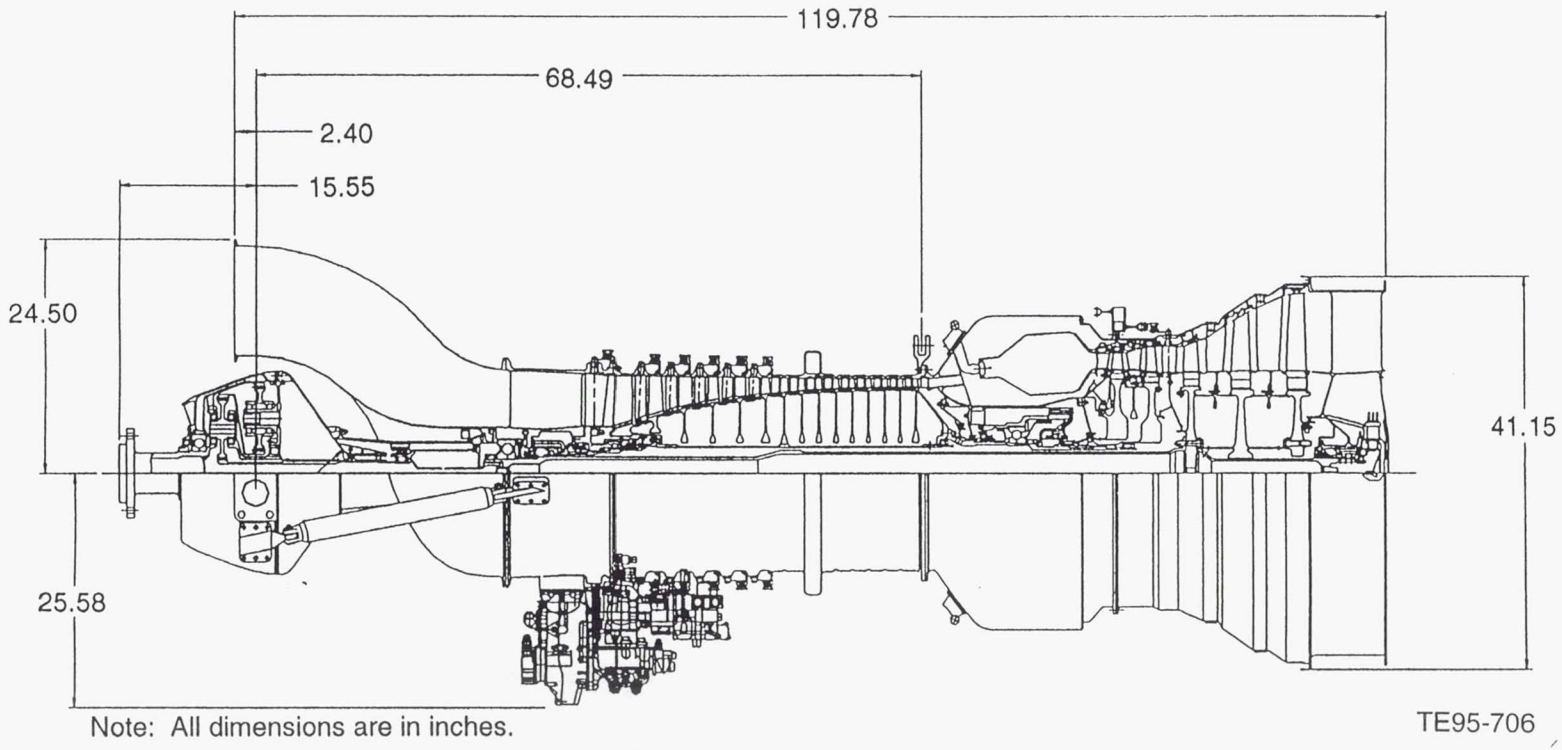

Figure 95. General arrangement—20:1 Rc nonrecuperated turboshaft.

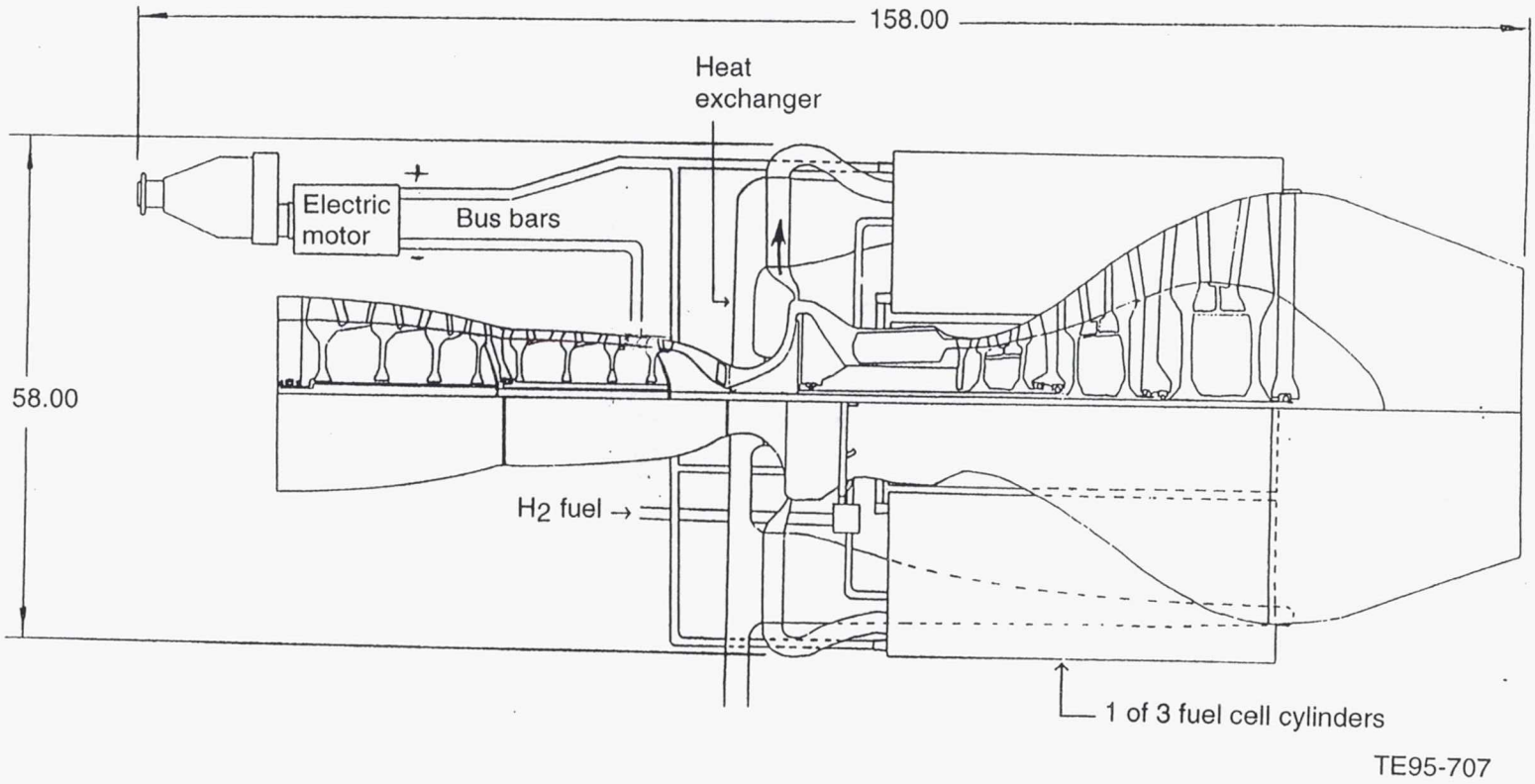

Figure 96. Fuel cell engine sketch.

The LP and IP compressors of the turbocharger feature four stages of axial compression each, while the HP compressor is a centrifugal design. The HP compressor is driven by a two-stage axial HP turbine; the IP compressor is driven by a two-stage axial IP turbine; and the LP compressor is powered by a two-stage axial LP turbine.

A portion of the compressor discharge air is bleed off to be heated by the fuel cell while the remainder passes through the hydrogen fueled burner to provide the energy source for the turbocharger turbine spools. Electrical output from the fuel cell is directed to an electric motor that powers a fan propulsor through a gear reduction system.

3.6 OFF-DESIGN ANALYSIS

3.6.1 Two-Stroke Diesel Engine - Advanced Technology

Off-design point performance maps for all of the turbomachinery components for both of the two-stroke diesels were created so the powerplants could be operated off-design. In addition to the component maps, correlations were developed to predict how flow and efficiency change with Reynolds number when the turbomachinery is operated from sea level to 90,000 ft.

Intercooler maps of effectiveness versus intercooler inlet hot side physical flow were generated to simulate how the intercooler performance varies with flight condition. These maps were created by operating the cross flow heat exchanger performance model to the simulated powerplant intercooler inlet and exit conditions. In this manner the effectiveness was evaluated. Figure 73 shows how effectiveness decreases with airflow for the two-stroke turbo-compounded diesel design. These curves were used as is in the off-design mode for the turbo-compounded configuration. For the non-turbo-compounded version, the curves were shifted on the x-axis (hot side flow) to get 60% and 65% effectiveness at the design point condition as discussed in Section 3.3.1.

Based on predictions obtained from Hamilton Standard, the propeller efficiency was assumed to be a constant 80% at all flight conditions. These propeller performance discussions are presented in section 3.2.

Both the parasitic and heat loss power extractions were input as a function of IPC and HPC spool speeds. Therefore, whenever the engine is spooled back in speed at the lower altitudes, these two losses have been decreased accordingly.

3.6.1.1 Turbo-Compounded Two-Stroke Diesel - Advanced Technology

Reynolds number effects on the centrifugal compressor efficiencies were applied per Figure 97. Lines of constant sea level efficiency (EFFsl) have been plotted as scale factor versus Reynolds number index (RNI). The scale factor is defined as altitude efficiency (EFFalt) divided by EFFsl. To determine which EFFsl line a given centrifugal compressor should operate on in the off-design mode, EFFsl was iterated on until the SF on the y-axis of Figure 97 matched the SF calculated at a given RNI (at the compressor inlet temperature and pressure).

As an example, the RNI at the inlet to the first LP compressor is 0.0254 at the 90,000 ft, 0.4 Mach design point condition. If a sea level efficiency of 84.5% is guessed, then the scale factor is 0.892 (0.754/0.845) which is close to the scale factor estimated by Figure 97. The IPC and HPC will be on different EFFsl curves because their RNI and design point efficiencies are different from the LPC. Airflow scale factors due to Reynolds number effects were not applied to the compressors.

Both airflow and efficiency scale factors due to Reynolds effects were applied to each turbine for all of the candidate powerplants. The Reynolds corrections for all of the two-stroke, turbo-compounded diesel turbines are presented in Figures 98 through 101. The x-axis parameter (RNI/RNIdes) is calculated by dividing RNI at a given flight condition by the design point RNI (RNIdes).

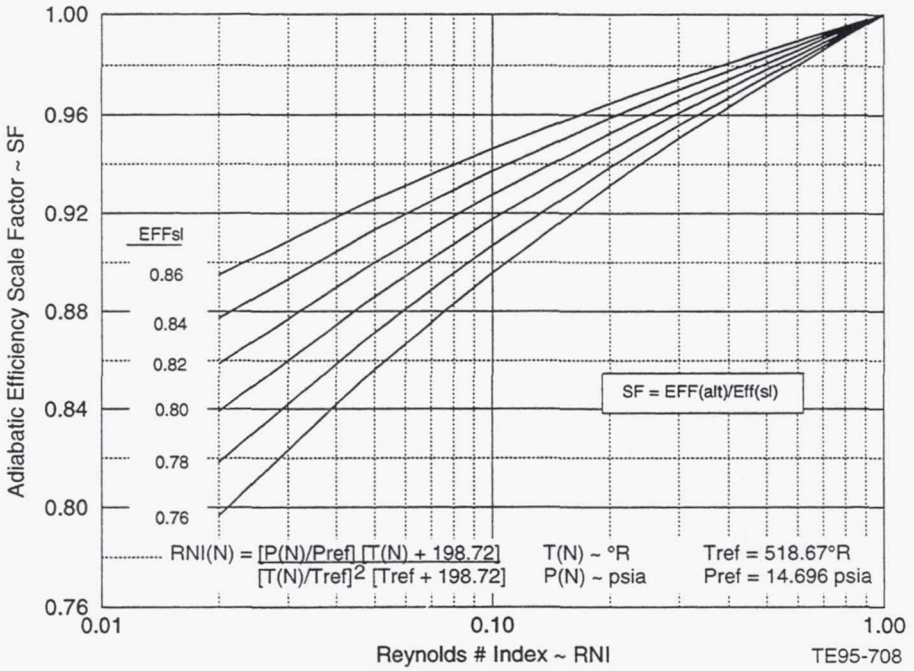

Figure 97. Centrifugal compressor Reynolds number effects.

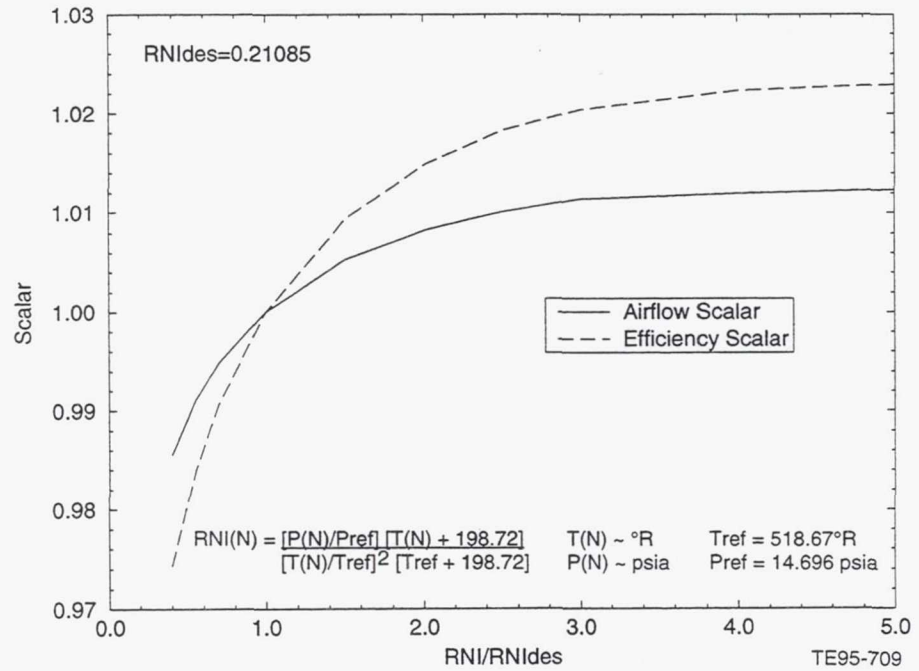

Figure 98. Two-stroke, turbo-compounded diesel:
Reynolds effects on HP turbine airflow and efficiency.

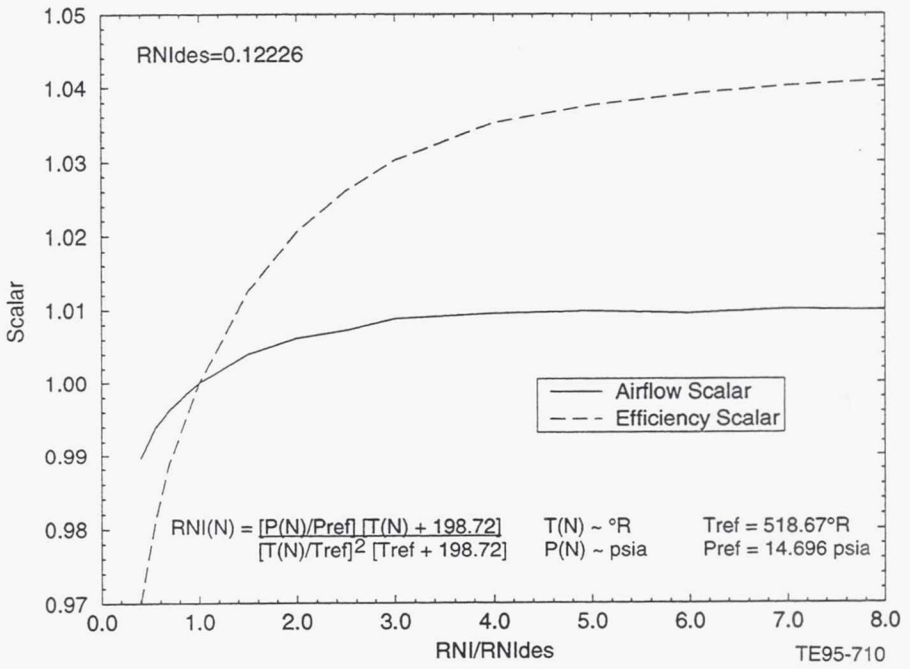

Figure 99. Two-stroke, turbo-compounded diesel:
Reynolds effects on IP turbine airflow and efficiency.

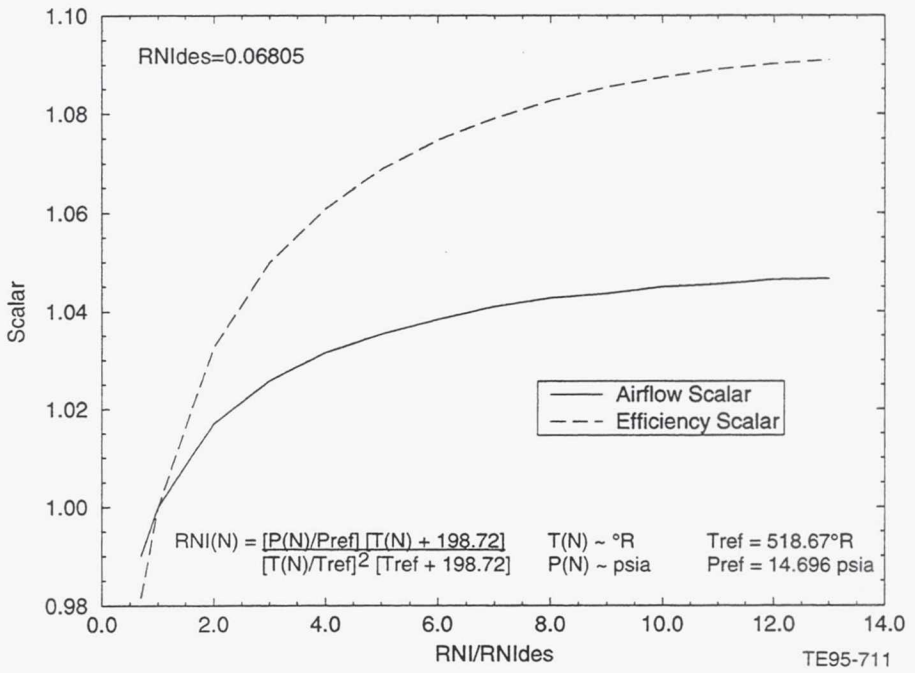

Figure 100. Two-stroke, turbo-compounded diesel:
Reynolds effects on LP turbine airflow and efficiency.

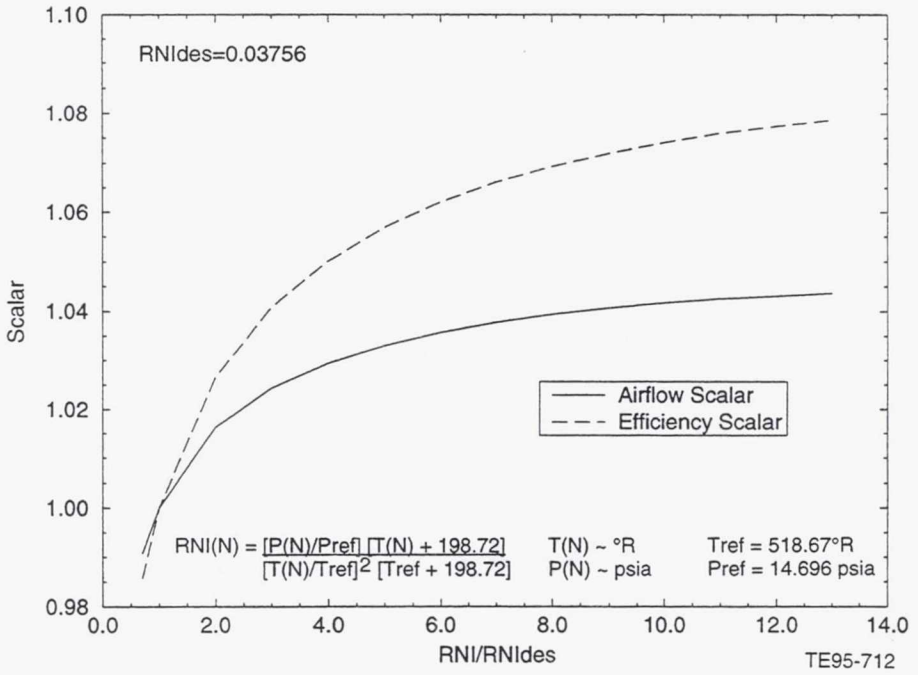

Figure 101. Two-stroke, turbo-compounded diesel:
Reynolds effects on power turbine airflow and efficiency.

Figure 102 presents powerplant specific fuel consumption (SFC) versus shaft horsepower for the turbo-compounded two-stroke diesel. Three different Mach numbers (0.4, 0.55, and 0.7) are illustrated for the 90,000 ft, standard day flight condition part power lines. Figure 103 is a presentation of complete powerplant thrust specific fuel consumption (TSFC) versus net thrust (Fn) for the same 90,000 ft, ISA condition.

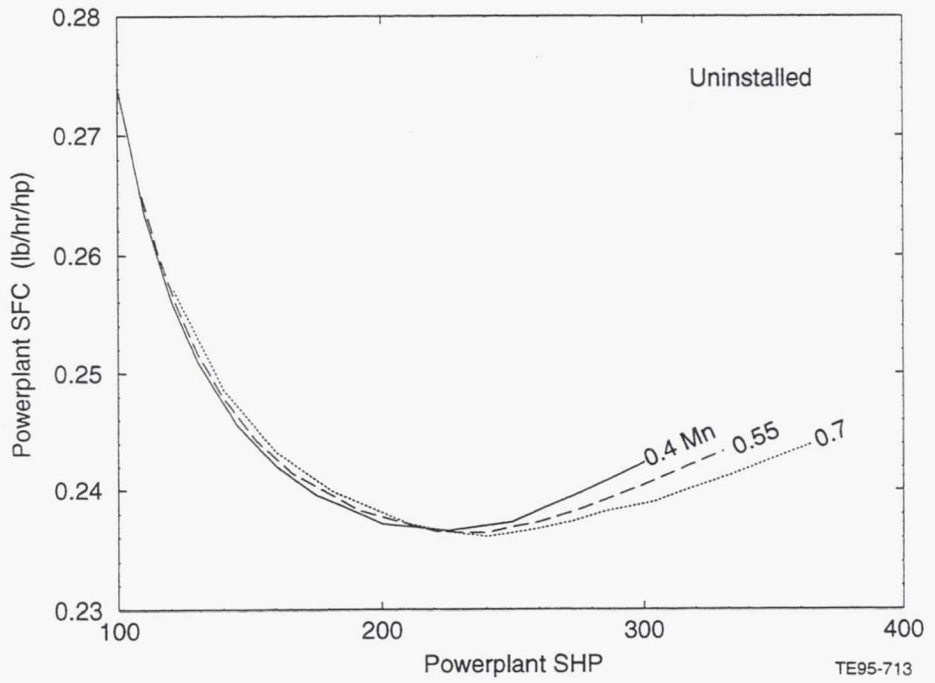

Figure 102. Two-stroke, turbo-compounded diesel off-design:
powerplant SFC versus shaft horsepower at 90,000 ft, ISA.

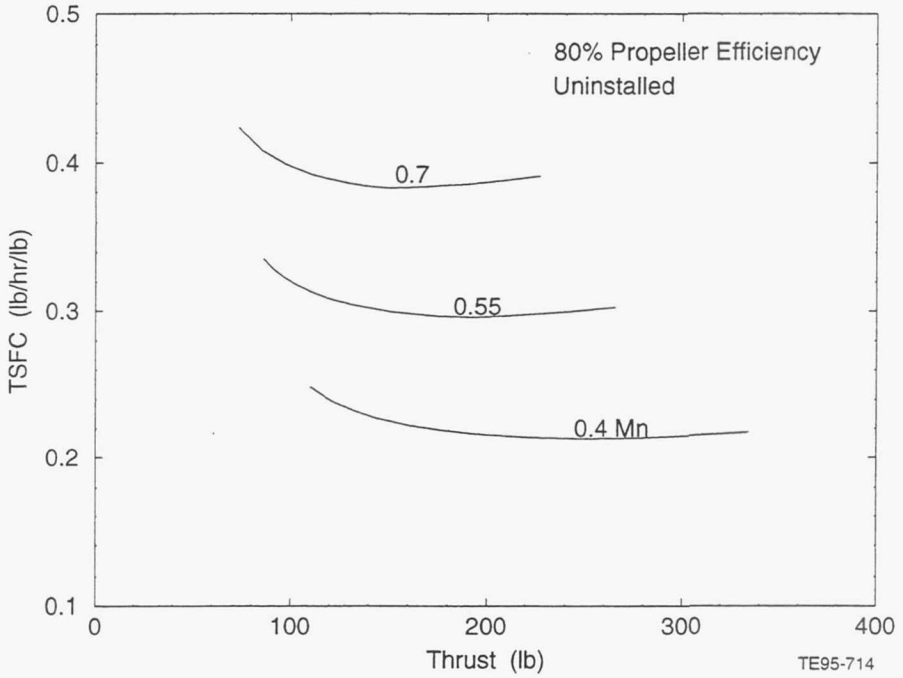

Figure 103. Two-stroke, turbo-compounded diesel off-design: powerplant TSFC versus thrust at 90,000 ft, ISA.

It was decided to require all of the turbocharged piston engines to operate up to a maximum BMEP of 200 psi in the off-design mode. Introduction of this requirement allows a more fair comparison of all piston engine propulsion systems. As the powerplant is operated from sea level to 90,000 ft, there is an altitude reached where one of the compressors 100% corrected speed limit is encountered. The powerplant then remains on this limit up to 90,000 ft. Figure 104 shows powerplant shaft horsepower, powerplant SFC, and diesel BMEP for a typical climb mission at maximum power. At sea level takeoff conditions this diesel is operating at a BMEP of 200 psi and then around 58,500 ft one of the compressors encounters its 100% $N/\sqrt{\theta}$ limit, with BMEP then falling to its design point level at 90,000 ft.

At sea level, the turbomachinery is spooled down in speed a significant amount due to the BMEP limit. This low speed results in poor component efficiencies and hence a lower than optimum shaft horsepower and higher than optimum SFC. As the aircraft/powerplant climbs in altitude the powerplant turbomachinery increases in speed, with the attendant improvement in efficiency. Since the diesel output brake horsepower remains constant while on its 200 psi BMEP limit and the turbomachinery is becoming more efficient, the power turbine has more energy to convert to shaft power. This results in more powerplant shaft horsepower and a lower powerplant SFC for this turbo-compounded configuration.

This trend continues until the turbomachinery encounters a compressor corrected speed limit, which is around 58,500 ft in this case. This point where the diesel is operating at a BMEP of 200 psi and the compressor is 100% corrected speed limited is the point of maximum powerplant output power. The powerplant shaft horsepower at this point is approximately 845 hp and the powerplant SFC is approximately 0.228 lb/hr/hp.

From this 58,500 ft altitude up to 90,000 ft the turbomachinery is operating on its 100% $N/\sqrt{\theta}$ limit which results in the reduction of manifold pressure. This decrease in manifold pressure results in a decrease in diesel power and BMEP. The diesel output power drops at a faster rate than the increase in power turbine output power. This results in the total powerplant shaft horsepower decreasing from 58,500 to 90,000 ft as depicted in Figure 104. Powerplant SFC is merely a reflection of the direction the powerplant shaft horsepower is moving.

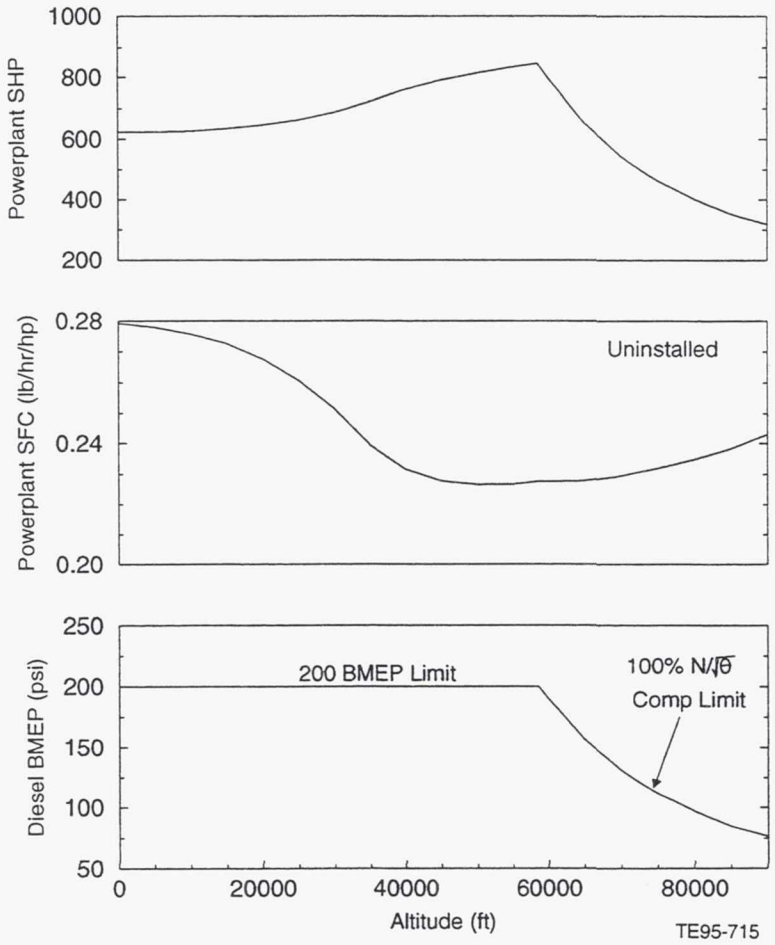

Figure 104. Two-stroke, turbo-compounded diesel off-design shaft horsepower, SFC, and BMEP during a typical climb at maximum power.

Table 15 contains a summary of the two-stroke, turbo-compounded diesel powerplant performance for both 90,000 ft, 0.48 Mach part power and a typical climb at maximum power. The typical climb maximum power shaft horsepower, SFC, and BMEP values agree with the results presented in Figure 104.

Table 15.
Fuel consumption and airflow requirements for two-stroke, turbo-compounded diesel, 90,000 ft, 0.48 Mach load line and typical climb at maximum power standard day, uninstalled.

Altitude, ft	Mach	Power setting, %	% corrected N LPC	BMEP, psi	Shp, hp	SFC, lb/hr/hp	Weng inlet, lb/sec	Wcool[1], lb/sec	Wcool[2], lb/sec
90,000	0.48	100	100	75.7	314.5	0.243	0.476	0.498	0.496
90,000	0.48	75	93.8	58.6	235.9	0.236	0.395	0.409	0.407
90,000	0.48	50	82.0	40.5	157.3	0.243	0.293	0.280	0.267
90,000	0.48	25	58.9	22.3	78.6	0.380	0.151	0.119	0.082
90,000	0.5	100	99.9	76.5	318.8	0.243	0.481	0.503	0.501
75,000	0.33	100	98.7	111.5	463.1	0.232	0.874	0.914	0.911
60,000	0.27	100	98.4	200	796.5	0.228	1.725	1.804	1.778
45,000	0.22	100	84.4	200	790.1	0.228	2.436	2.41	2.283
30,000	0.2	100	69.6	200	687.2	0.251	3.163	2.989	2.699
15,000	0.17	100	57.1	200	631.9	0.273	3.932	3.52	3.034
0	0.125	100	48.1	200	622.2	0.279	5.042	4.189	3.524

The typical climb Mach numbers in Table 15 agree with Mach numbers derived from the mission analysis part of this study. LPC % $N/\sqrt{\theta}$ and BMEP have also been included in the table to indicate which limit the powerplant is operating on. The reason the LPC % $N/\sqrt{\theta}$ is not 100% at the 75,000 ft maximum power condition is the IPC was the first compressor to hit the 100% corrected speed limit at this flight condition.

The Weng inlet term in Table 15 is the powerplant (LPC) inlet physical airflow. The $Wcool^1$ term is the physical ambient airflow going into the cold side of the first intercooler and $Wcool^2$ is the physical ambient airflow going into the cold side of the second intercooler.

All three compressors were set up with 17.5% surge margin at the 90,000 ft design point condition. At the lower altitudes it was necessary to use compressor bleed on both the LPC and IPC to maintain at least 10% surge margin. This is necessary due to the amount that the compressors are spooled back in speed at the lower altitudes. For example, the LPC and IPC are running around 48% and 75% corrected speed at sea level static conditions. The compressor exit bleed required to maintain 10% surge margin on these two compressors at sea level conditions is approximately 20% and 15%, respectively. It was discovered that a more optimum cycle resulted if this bleed was inserted back into the cycle in front of the power turbine. Since it was known at the start of the study that compressor bleed would be required to maintain at least 10% surge margin, more surge margin (17.5% versus typical 15%) was designed into the compressor at the design point.

3.6.1.2 Non-Turbo-Compounded Two-Stroke Diesel - Advanced Technology

Figure 105 is a plot of powerplant SFC versus shaft horsepower for the non-turbo-compounded two-stroke diesel. Three different Mach numbers (0.4, 0.55, and 0.7) are presented for the 90,000 ft, standard day flight condition part power lines. Figure 106 is a presentation of complete powerplant TSFC versus net thrust for the same 90,000 ft, ISA condition.

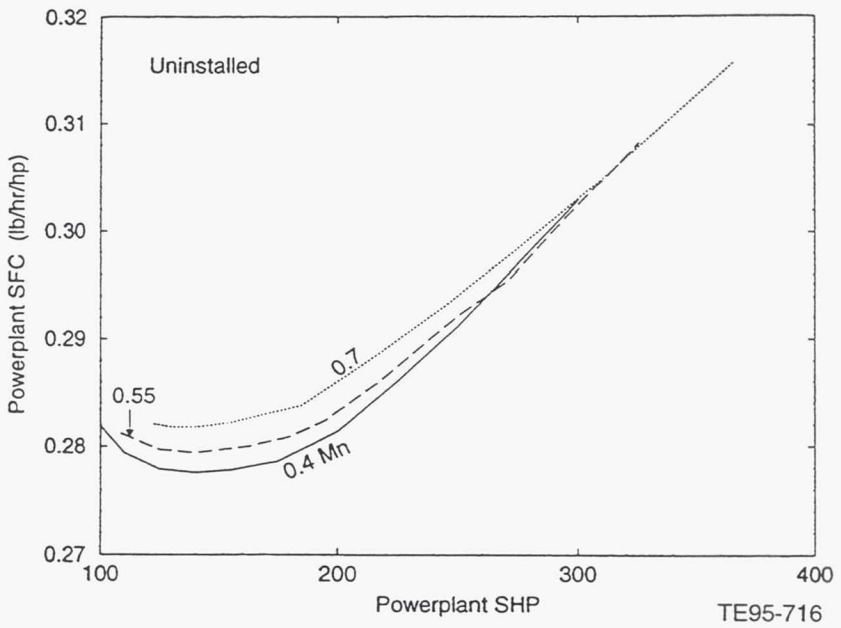

Figure 105. Two-stroke, non-turbo-compounded diesel off-design: powerplant SFC versus shaft horsepower at 90,000 ft, ISA.

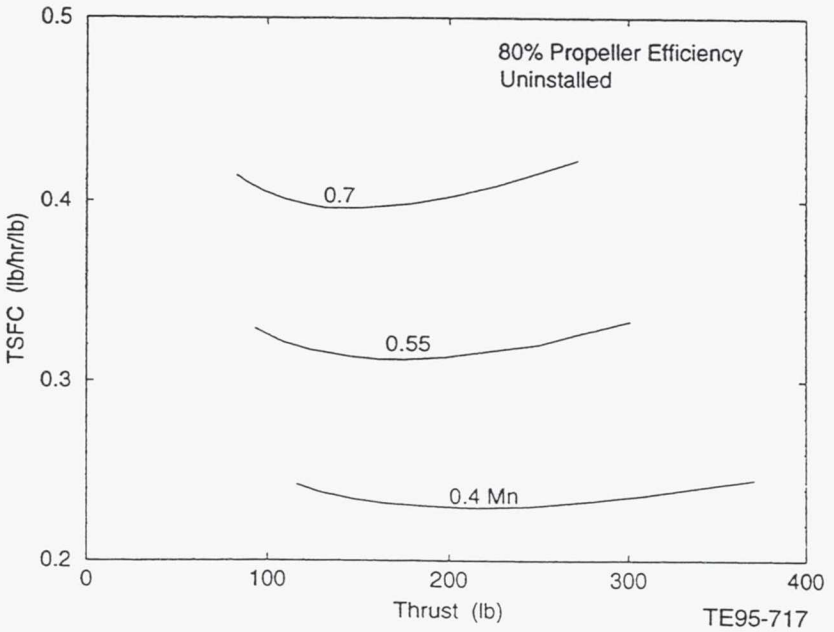

Figure 106. Two-stroke, non-turbo-compounded diesel off-design: powerplant TSFC versus thrust at 90,000 ft, ISA.

Figure 107 shows the powerplant shaft horsepower, powerplant SFC, and diesel BMEP for a typical climb mission at maximum power. At sea level takeoff conditions this diesel is operating at a BMEP of 200 psi whereas near 68,000 ft one of the compressors encounters its 100% $N/\sqrt{\theta}$ limit, with BMEP then falling to its design point level at 90,000 ft.

This configuration is not turbo-compounded, therefore the two-stroke diesel generates all of the powerplant output power. Since diesel power is directly related to BMEP, if BMEP is constant at 200 psi, then powerplant shaft horsepower remains constant (638 shp, in this case). The turbomachinery encounters a compressor corrected speed limit around 68,000 ft and from there to 90,000 ft remains on that speed limit which reduces BMEP and shaft horsepower to their design point levels.

SFC is a function of both the diesel performance (BMEP) and the amount of energy being lost out the back end of the turbomachinery. It is well established that as turbocharged pistons are operated from sea level to altitude they gain nozzle pressure ratio. Increasing nozzle pressure ratio results in an increase in SFC.

At sea level conditions, the LPC, IPC, and LPT are operating at approximately 36%, 71%, and 47% corrected speed. This results in poor component efficiencies that tend to offset the SFC improvement due to a lower nozzle pressure ratio. The result is a relatively flat SFC from sea level to around 35,000 ft. It should be noted that both the LPC and LPT are so low in speed that their component maps are being extrapolated in this region of flight.

From 35,000 to 68,000 ft the SFC is increasing due to the increasing spool speeds that result in more efficient turbomachinery and therefore more energy lost out the back end. Specific fuel consumption continues to increase from 68,000 to 90,000 ft due to both decreasing shaft horsepower (BMEP) and increasing nozzle pressure ratio.

Table 16 contains a summary of the two-stroke, non-turbo-compounded diesel powerplant performance for both 90,000 ft, 0.48 Mach part power and a typical climb at maximum power. The typical climb maximum power shaft horsepower, SFC, and BMEP values agree with the results presented in Figure 107. Section 3.6.1.1 has a more detailed discussion of the contents of Table 16.

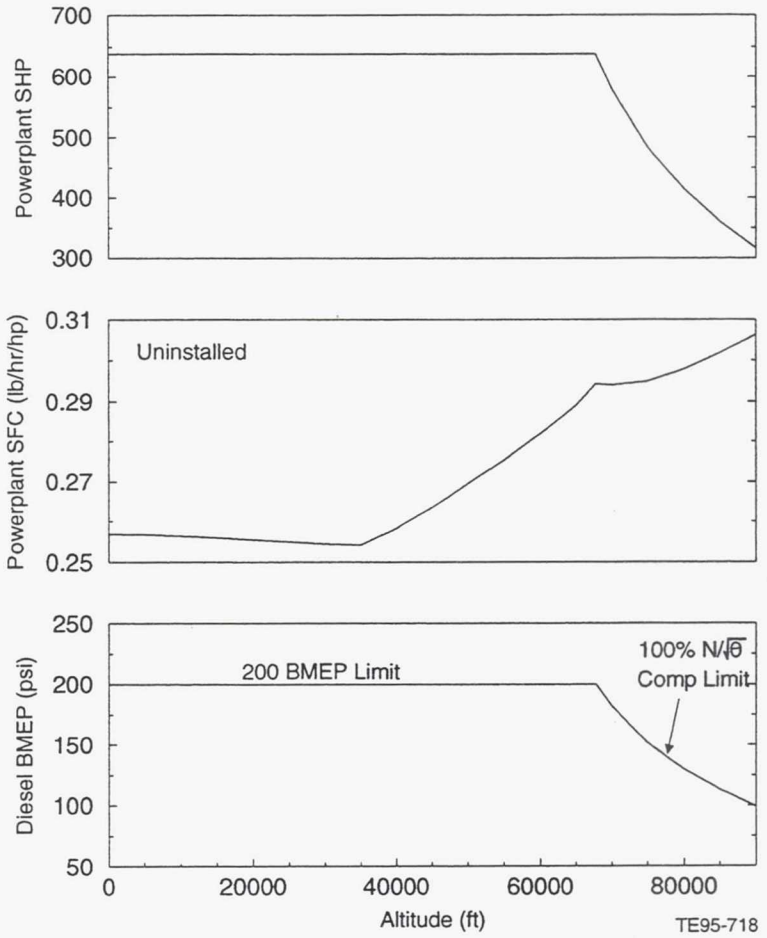

Figure 107. Two-stroke, non-turbo-compounded diesel off-design: powerplant shaft horsepower, SFC, and BMEP during a typical climb at maximum power.

Table 16.
Fuel consumption and airflow requirements for two-stroke, non-turbo-compounded diesel, 90,000 ft, 0.48 Mach load line and typical climb at maximum power standard day, uninstalled.

Altitude, ft	Mach	Power setting, %	% corrected N LPC	BMEP, psi	Shp, hp	SFC, lb/hr/hp	Weng inlet, lb/sec	Wcool[1], lb/sec	Wcool[2], lb/sec
90,000	0.48	100	100.0	98.0	312.5	0.305	0.596	0.626	0.622
90,000	0.48	75	93.3	73.6	234.6	0.289	0.488	0.504	0.501
90,000	0.48	50	82.8	49.0	156.4	0.279	0.375	0.345	0.327
90,000	0.48	25	63.2	24.5	78.2	0.300	0.214	0.166	0.122
90,000	0.5	100	99.9	99.2	316.5	0.306	0.602	0.632	0.629
75,000	0.33	100	99.2	151.6	483.6	0.295	1.107	1.162	1.157
60,000	0.27	100	93.0	200	638	0.282	1.861	1.893	1.864
45,000	0.22	100	79.6	200	638	0.264	2.680	2.465	2.310
30,000	0.2	100	64.4	200	638	0.254	3.408	3.016	2.684
15,000	0.17	100	47.2	200	638	0.256	3.687	3.129	2.778
0	0.125	100	36.0	200	638	0.257	4.410	3.052	2.844

All three compressors were set up with 17.5% surge margin at the 90,000 ft design point condition. At the lower altitudes compressor exit bleed was used on both the LPC and IPC to maintain at least 10% surge margin. This is necessary due to the degree that the compressors are spooled back in speed at the lower altitudes. The compressor exit bleed required at sea level to maintain 10% surge margin on the LPC and IPC is approximately 34% and 6%, respectively. It was discovered that a more optimum cycle resulted if this bleed was dumped overboard.

3.6.2 Four-Stroke Diesel Engine - SOA Technology

Off-design point performance maps for all of the turbomachinery components were created so the four-stroke diesel could be operated off-design. In addition to the component maps, correlations were developed to predict how flow and efficiency change with Reynolds number when the turbomachinery is operated from sea level to 90,000 ft. A more detailed explanation of where the Reynolds number corrections came from is given in section 3.6.1.1.

The intercooler maps of effectiveness versus inlet (turbomachinery) hot side physical flow presented in Figure 73 were modified by shifting them on the x-axis so that 60% and 65% effectiveness would be achieved at the design point condition. The justification for this assumption is discussed in Section 3.3.1. A curve to simulate how the aftercooler effectiveness varies off-design was created by modifying the second intercooler map such that a 70% effectiveness was achieved at the design point inlet hot side flow. These maps were then used to simulate how the intercooler and aftercooler performance varies with flight condition in the off-design mode. The propeller efficiency was assumed to be a constant 80% at all flight conditions. These propeller performance discussions are presented in Section 3.2.

Figure 108 is a presentation of powerplant specific fuel consumption (SFC) versus shaft horsepower for the non-turbo-compounded four-stroke diesel. Three different Mach numbers (0.4, 0.55, and 0.7) are illustrated for the 90,000 ft, standard day flight condition. Figure 109 is a presentation of complete powerplant thrust specific fuel consumption (TSFC) versus net thrust (Fn) for the same 90,000 ft, ISA condition.

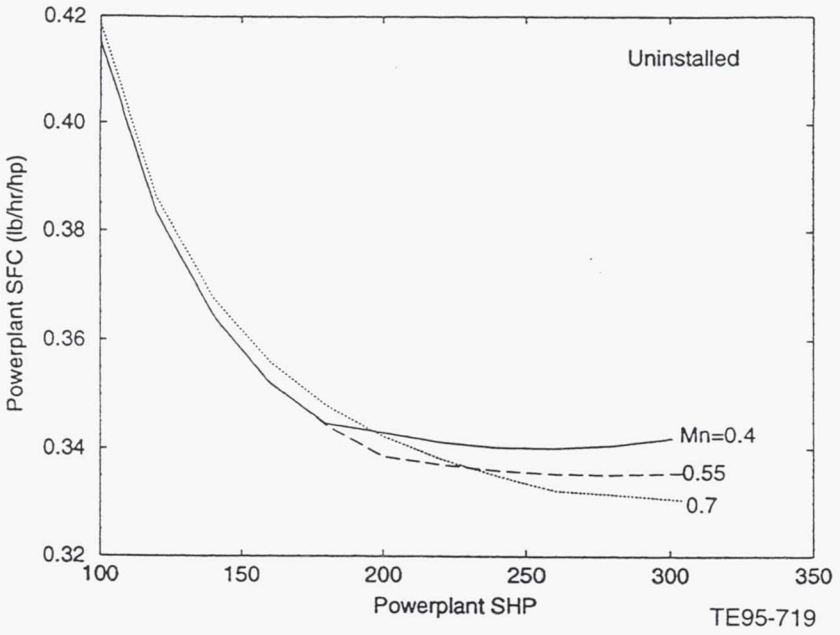

Figure 108. Four-stroke, non-turbo-compounded diesel off-design: powerplant SFC versus shaft horsepower at 90,000 ft, ISA.

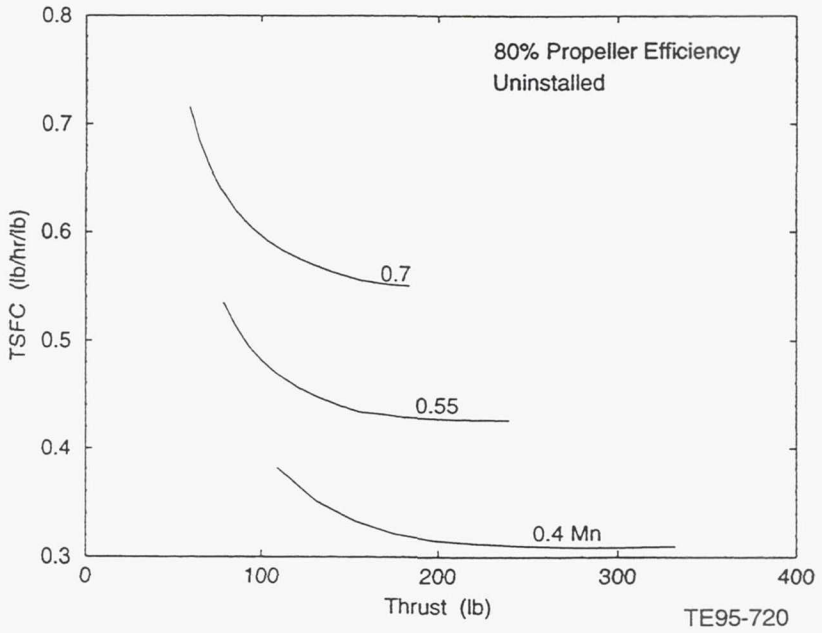

Figure 109. Four-stroke, non-turbo-compounded diesel off-design: powerplant TSFC versus thrust at 90,000 ft, ISA.

The four-stroke diesel design point BMEP of 197.5 psi is only slightly lower than the 200 psi limit. Therefore, the maximum output power this powerplant will generate (304 hp) is only slightly above the design shaft horsepower (300 hp). This is depicted in Figure 110 as shaft horsepower versus altitude. The powerplant SFC at sea level conditions is around 0.236 lb/hr/hp and then improves as the engine spools up, which results in better component efficiencies. This improvement in SFC continues to about 20,000 ft where the SFC is approximately 0.222 lb/hr/hp. From 20,000 to 90,000 ft the SFC increases due to increasing losses out the turbomachinery nozzle.

Table 17 contains a summary of the four-stroke, non-turbo-compounded diesel powerplant performance for both 90,000 ft, 0.48 Mach part power and a typical climb at maximum power. The typical climb

Table 17.
Fuel consumption and airflow requirements for four-stroke, non-turbo-compounded diesel 90,000 ft, 0.48 Mach load line and typical climb at maximum power standard day, uninstalled.

Altitude, ft	Mach	Power setting, %	% corrected N LPC	BMEP, psi	Shp, hp	SFC, lb/hr/hp	Weng inlet, lb/sec	Wcool[1], lb/sec	Wcool[2], lb/sec	Wcool[3], lb/sec
90,000	0.48	100	99.4	200	303.8	0.339	0.734	0.754	0.767	0.762
90,000	0.48	75	90.5	150	228.1	0.339	0.585	0.601	0.611	0.608
90,000	0.48	50	77.9	100	151.9	0.356	0.415	0.426	0.427	0.425
90,000	0.48	25	58.1	50	76	0.500	0.231	0.237	0.218	0.217
90,000	0.5	100	99.1	200	304	0.338	0.736	0.756	0.769	0.764
75,000	0.33	100	78.9	200	304	0.293	0.868	0.891	0.906	0.903
60,000	0.27	100	56.6	200	304	0.261	1.016	1.043	1.046	1.041
45,000	0.22	100	42.0	200	304	0.239	1.181	1.223	1.221	1.220
30,000	0.2	100	32.8	200	304	0.226	1.329	1.341	1.339	1.332
15,000	0.17	100	28.9	200	304	0.224	1.476	1.441	1.430	1.397
0	0.125	100	30.9	200	304	0.236	1.63	1.465	1.438	1.400

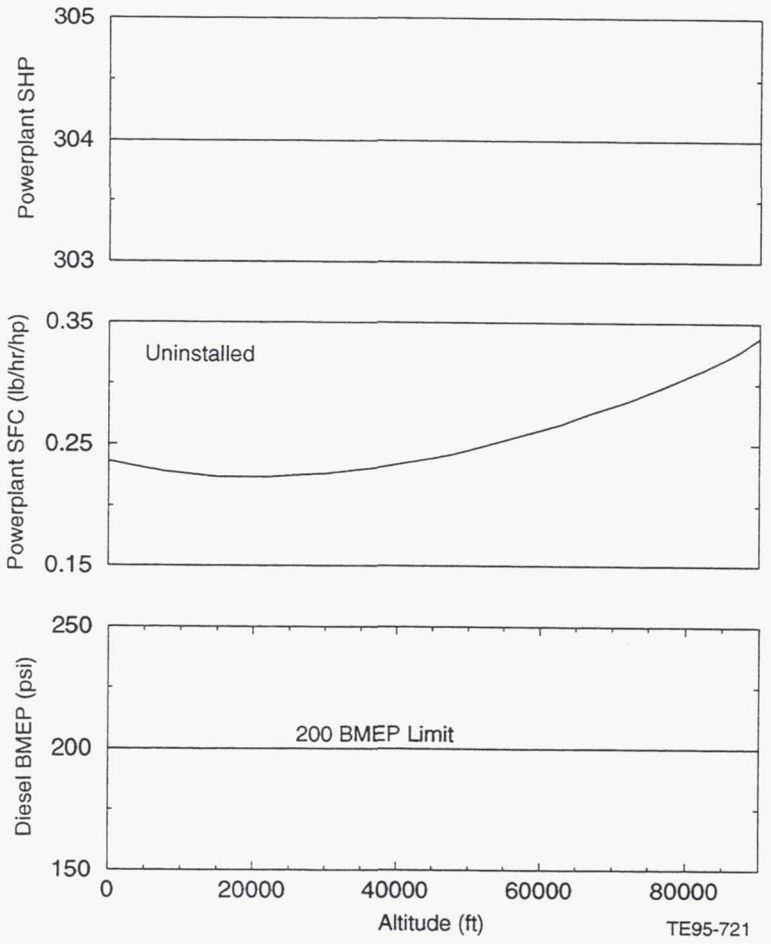

Figure 110. Four-stroke, non-turbo-compounded diesel off-design: shaft horsepower, SFC, and BMEP during a typical climb at maximum power.

maximum power shaft horsepower, SFC, and BMEP values agree with the results presented in Figure 110. Section 3.6.1.1 has a more detailed discussion of the contents of Table 17.

All three compressors were set up with 17.5% surge margin at the 90,000 ft design point condition. At the lower altitudes it was necessary to use compressor bleed on both the LPC and IPC to maintain at least 10% surge margin. This is necessary due to the degree that the compressors are spooled back in speed at the lower altitudes. It was discovered that a more optimum cycle resulted if this bleed was dumped overboard.

Both the parasitic and heat loss power extractions were input as a function of IPC and HPC spool speeds. Therefore, whenever the engine is spooled back in speed at the lower altitudes, these two losses have been decreased accordingly.

3.6.3 Four-Stroke Spark Ignition Engine - SOA and NT Technology

Off-design point performance maps for all of the turbomachinery components for both of the four-stroke spark ignition engines were created so they could be operated off-design. In addition to the component maps, correlations were developed to predict how flow and efficiency change with Reynolds number when the turbomachinery is operated from sea level to 90,000 ft. A more detailed explanation of where the Reynolds number corrections came from is given in section 3.6.1.1.

The intercooler maps of effectiveness versus inlet (turbomachinery) hot side physical flow presented in Figure 73 were modified by shifting them on the x-axis so that 60% and 65% effectiveness would be achieved at the design point condition. The justification for this assumption is discussed in section 3.3.1. A curve to simulate how the aftercooler effectiveness varies off-design was created by modifying the second intercooler map such that a 70% effectiveness was achieved at the design point inlet hot side flow. These maps were then used to simulate how the intercooler and aftercooler performance varies with flight condition in the off-design mode. The propeller efficiency was assumed to be a constant 80% at all flight conditions. These propeller performance discussions are presented in section 3.2.

All three compressors were set up with 17.5% surge margin at the 90,000 ft design point condition. At the lower altitudes it was necessary to use compressor bleed on both the LPC and IPC to maintain at least 10% surge margin. This is necessary due to the degree that the compressors are spooled back in speed at the lower altitudes. It was discovered that a more optimum cycle resulted if this bleed was dumped back into the cycle in front of the power turbine.

Both the parasitic and heat loss power extractions were input as a function of IPC and HPC spool speeds. Therefore, whenever the engine is spooled back in speed at the lower altitudes, these two losses have been decreased accordingly.

3.6.3.1 Gasoline Fuel - SOA Technology

Figure 111 is a plot of powerplant SFC versus shaft horsepower for the turbo-compounded four-stroke gas spark ignition engine. Three different Mach numbers (0.4, 0.55, and 0.7) are plotted for the 90,000 ft, standard day flight condition. Figure 112 is a presentation of complete powerplant TSFC versus net thrust for the same three Mach numbers and at the same 90,000 ft, ISA condition.

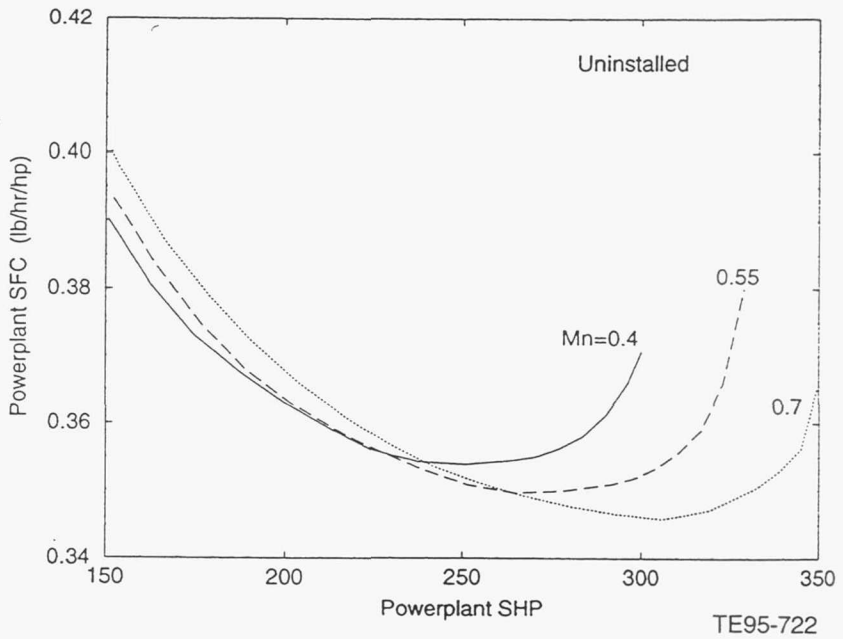

Figure 111. Four-stroke, turbo-compounded, gas spark ignition off-design: powerplant SFC versus shaft horsepower at 90,000 ft, ISA.

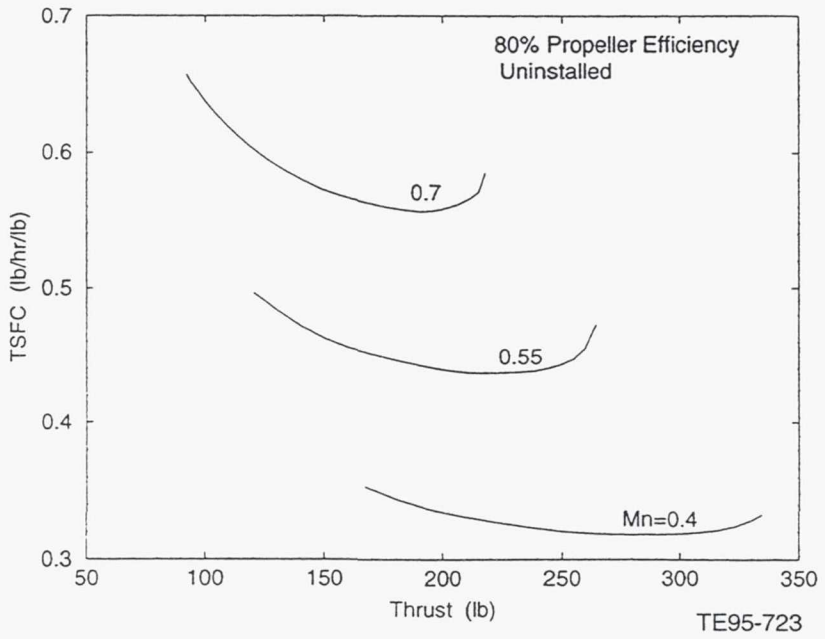

Figure 112. Four-stroke, turbo-compounded, gas spark ignition off-design: powerplant TSFC versus thrust at 90,000 ft, ISA.

The decision to run the gas SI engine to a BMEP of 200 psi in the off-design mode results in the powerplant shaft horsepower varying from 300 shp (BMEP = 131 psi) at 90,000 ft to a maximum of 472 shp at 76,700 ft as depicted in Figure 113. From sea level to 76,700 ft the SI engine is on its 200 psi BMEP limit and then from 76,700 to 90,000 ft the turbomachinery is limited to 100% corrected speed.

Figure 113 shows SFC to be around 0.38 lb/hr/hp at sea level, then improving to approximately 0.29 lb/hr/hp at 60,000 ft, then increasing to 0.38 lb/hr/hp at 90,000 ft. At sea level the turbomachinery is spooled down in speed resulting in poor component efficiencies and corresponding less than optimum SFC. As the powerplant is operated up in altitude during the climb segment of the mission, the spool speeds (and component efficiencies) are increasing. The increase in efficiency of the components more than offsets the increasing nozzle pressure ratio loss from sea level to 60,000 ft. From 60,000 to 90,000 ft the nozzle pressure ratio loss is increasing at a faster rate than the component efficiencies resulting in a increasing SFC.

Table 18 contains a summary of the four-stroke, turbo-compounded gasoline fueled spark ignition powerplant performance for both 90,000 ft, 0.48 Mach part power and a typical climb at maximum power. The typical climb maximum power shaft horsepower, SFC, and BMEP values agree with the results presented in Figure 113. Section 3.6.1.1 has a more detailed discussion of the contents of Table 18.

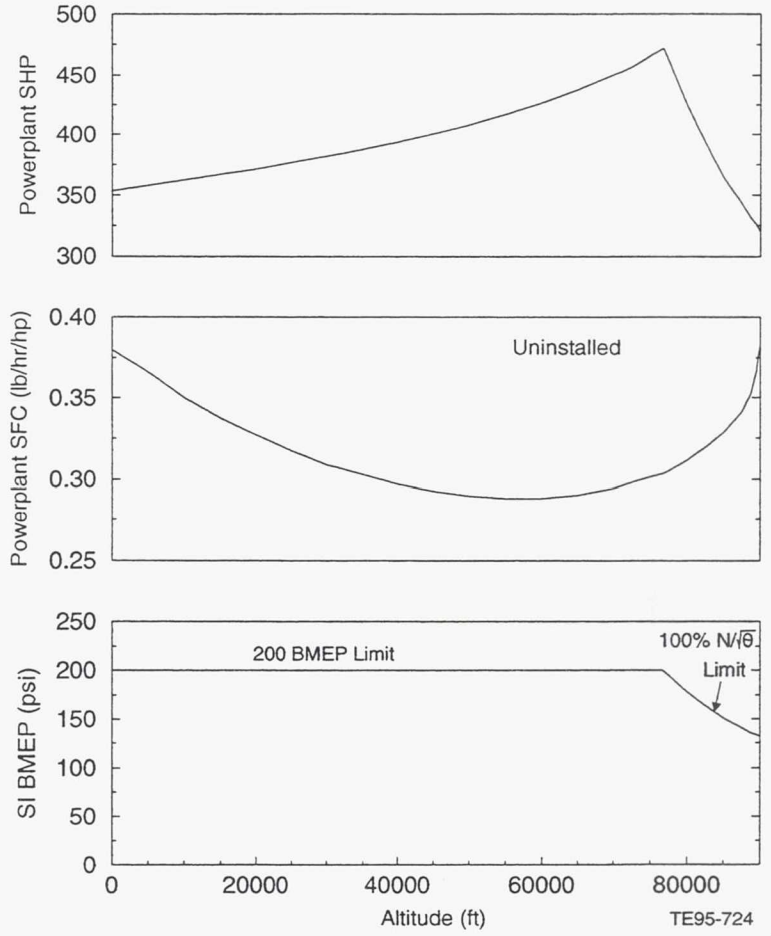

Figure 113. Four-stroke, turbo-compounded, gas spark ignition off-design: shaft horsepower, SFC, and BMEP during a typical climb at maximum power.

Table 18.
Fuel consumption and airflow requirements for four-stroke, turbo-compounded spark ignition, gasoline fuel, 90,000 ft, 0.48 Mach load line and typical climb at maximum power standard day, uninstalled.

Altitude, ft	Mach	Power setting, %	% corrected N LPC	BMEP, psi	Shp, hp	SFC, lb/hr/hp	Weng inlet, lb/sec	Wcool[1], lb/sec	Wcool[2], lb/sec	Wcool[3], lb/sec
90,000	0.48	100	99.8	129.8	314.3	0.384	0.464	0.487	0.485	0.478
90,000	0.48	75	94.6	99.1	235.8	0.354	0.396	0.415	0.413	0.406
90,000	0.48	50	84.9	67.3	157.2	0.387	0.312	0.303	0.297	0.293
90,000	0.48	25	71.9	37.1	78.6	0.540	0.214	0.192	0.170	0.164
90,000	0.5	100	99.8	131.8	319.9	0.382	0.471	0.495	0.491	0.484
75,000	0.33	100	97.0	200	465.9	0.300	0.818	0.859	0.855	0.842
60,000	0.27	100	81.1	200	426.5	0.288	1.022	1.042	1.040	1.011
45,000	0.22	100	66.8	200	400.5	0.293	1.277	1.223	1.176	1.163
30,000	0.2	100	55.1	200	382.0	0.309	1.513	1.385	1.349	1.314
15,000	0.17	100	47.2	200	367.0	0.338	1.741	1.561	1.537	1.468
0	0.125	100	42.4	200	353.5	0.38	1.902	1.74	1.670	1.636

3.6.3.2 *Hydrogen Fuel - NT Technology*

Figure 114 depicts powerplant SFC versus shaft horsepower for the turbo-compounded four-stroke H_2 spark ignition engine. Three different Mach numbers (0.4, 0.55, and 0.7) are shown for the 90,000 ft, standard day flight condition. Figure 115 is a presentation of complete powerplant TSFC versus net thrust for the same three Mach numbers and at the same 90,000 ft, ISA condition.

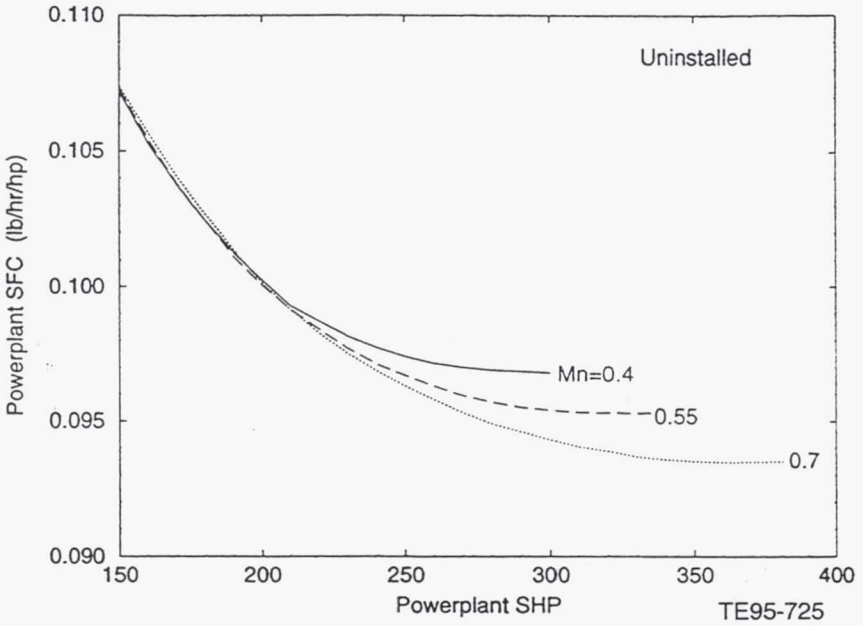

Figure 114. Four-stroke, turbo-compounded, H2 spark ignition off-design: powerplant SFC versus shaft horsepower at 90,000 ft, ISA.

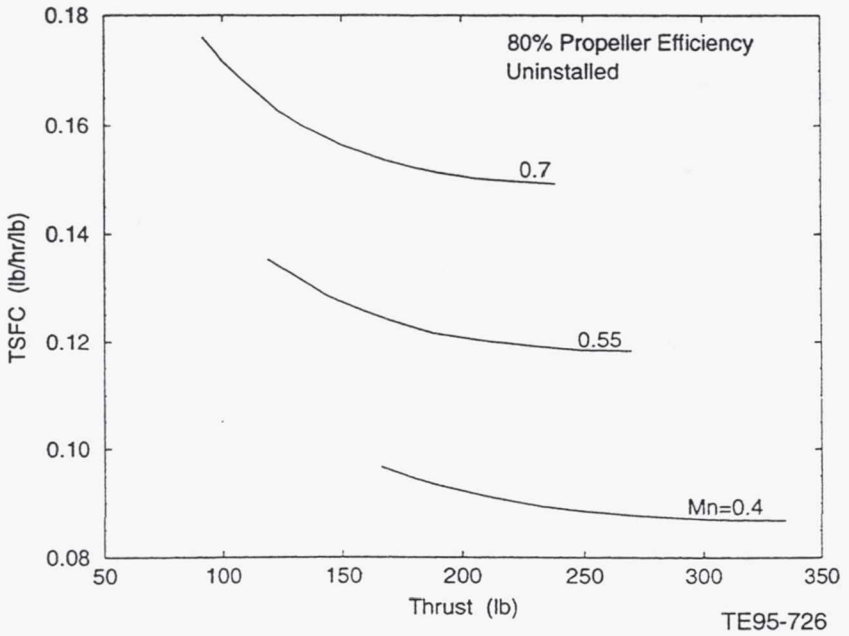

Figure 115. Four-stroke, turbo-compounded, H2 spark ignition off-design: powerplant TSFC versus thrust at 90,000 ft, ISA.

The decision to run the H_2 SI engine to a BMEP of 200 psi in the off-design mode results in the powerplant shaft horsepower varying from 300 shp (BMEP = 107 psi) at 90,000 ft to a maximum of 556 shp at 73,400 ft as depicted in Figure 116. From sea level to 73,400 ft the H_2 SI engine is on its 200 psi BMEP limit and then from 73,400 to 90,000 ft the turbomachinery is limited to 100% corrected speed.

Figure 116 shows SFC to be around 0.102 lb/hr/hp at sea level, then improving to approximately 0.084 lb/hr/hp at 65,000 ft, then increasing to 0.096 lb/hr/hp at 90,000 ft. At sea level the turbomachinery is spooled down in speed resulting in poor component efficiencies and corresponding less than optimum SFC. As the powerplant is operated up in altitude during the climb segment of the mission, the spool speeds (and component efficiencies) are increasing. The increase in efficiency of the components more than offsets the increasing nozzle pressure ratio loss from sea level to 65,000 ft. From 65,000 to 90,000 ft the nozzle pressure ratio loss is increasing at a faster rate than the component efficiencies resulting in an increasing SFC.

Table 19 contains a summary of the four-stroke, turbo-compounded hydrogen fueled spark ignition powerplant performance for both 90,000 ft, 0.48 Mach part power and a typical climb at maximum power. The typical climb maximum power shaft horsepower, SFC, and BMEP values agree with the results presented in Figure 116. Section 3.6.1.1 has a more detailed discussion of the contents of Table 19.

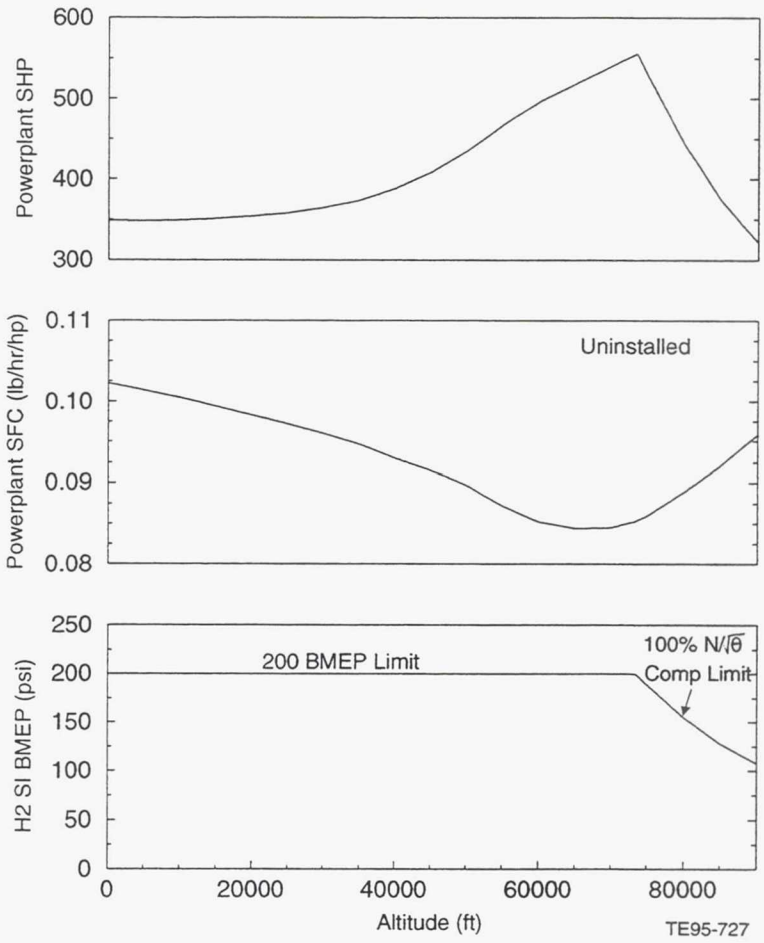

Figure 116. Four-stroke, turbo-compounded, H2 spark ignition off-design: shaft horsepower, SFC, and BMEP during a typical climb at maximum power.

Table 19.

Fuel consumption and airflow requirements for four-stroke, turbo-compounded spark ignition, hydrogen fuel, 90,000 ft, 0.48 Mach load line and typical climb at maximum power standard day, uninstalled.

Altitude, ft	Mach	Power setting, %	% corrected N LPC	BMEP, psi	Shp, hp	SFC, lb/hr/hp	Weng inlet, lb/sec	Wcool[1], lb/sec	Wcool[2], lb/sec	Wcool[3], lb/sec
90,000	0.48	100	99.9	106.2	316	0.096	0.472	0.496	0.494	0.481
90,000	0.48	75	94.2	83.1	237	0.097	0.396	0.407	0.405	0.402
90,000	0.48	50	84.3	56.2	158	0.106	0.310	0.297	0.291	0.284
90,000	0.48	25	70.2	28.1	79	0.138	0.208	0.179	0.161	0.158
90,000	0.5	100	100	107.9	322	0.096	0.478	0.502	0.500	0.487
75,000	0.33	100	99.4	188.8	526.9	0.086	0.874	0.918	0.914	0.903
60,000	0.27	100	83.8	200	495.9	0.085	1.176	1.105	1.077	1.050
45,000	0.22	100	68.3	200	408.5	0.092	1.531	1.359	1.262	1.231
30,000	0.2	100	54.6	200	364.5	0.096	2.044	1.66	1.481	1.444
15,000	0.17	100	44.6	200	351	0.099	2.605	2.105	1.843	1.785
0	0.125	100	39.9	200	349	0.102	3.053	2.554	2.207	2.142

3.6.4 Rotary Engine - NT Technology

Off-design point performance maps for all of the turbomachinery components were created so a more representative off-design analysis could be performed for the rotary engine powerplant. In addition to the component maps, correlations were developed to predict how flow and efficiency change with Reynolds number when the turbomachinery is operated from sea level to 90,000 ft. A more detailed explanation of where the Reynolds number corrections came from is given in section 3.6.1.1.

The intercooler maps of effectiveness versus inlet (turbomachinery) hot side physical flow presented in Figure 73 were modified by shifting them on the x-axis so that 60% and 65% effectiveness would be achieved at the design point condition. The justification for this assumption is discussed in section 3.3.1. A curve to simulate how the aftercooler effectiveness varies off-design was created by modifying the second intercooler map such that a 70% effectiveness was achieved at the design point inlet hot side flow. These maps were then used to simulate how the intercooler and aftercooler performance varies with flight condition in the off-design mode. The propeller efficiency was assumed to be a constant 80% at all flight conditions. These propeller performance discussions are presented in section 3.2.

The design BMEP of 163 psi for the rotary engine also corresponds to the maximum allowable off-design BMEP. Therefore, the maximum power output at any altitude or flight condition will be 300 shp at maximum rotary engine speed. Rotary brake horsepower versus airflow and speed is plotted in Figure 31. The powerplant SFC will also remain constant at 0.3936 lb/hr/hp for the climb portion of the mission as long as the maximum rotary speed of 6000 rpm is maintained. Figure 32 shows rotary SFC versus BMEP and engine speed.

Table 20 contains a summary of the rotary powerplant performance for both 90,000 ft, 0.48 Mach part power and a typical climb at maximum power. The typical climb at maximum power shaft horsepower, SFC, and BMEP values remains constant when operating at a maximum rotary speed of 6000 rpm and agrees with Figures 31 and 32. Section 3.6.1.1 has a more detailed discussion of the contents of Table 20.

Table 20.
Fuel consumption and airflow requirements for rotary engine, 90,000 ft, 0.48 Mach load line and typical climb at maximum power standard day, uninstalled.

Altitude, ft	Mach	Power setting, %	% corrected N LPC	BMEP, psi	Shp, hp	SFC, lb/hr/hp	Weng inlet, lb/sec	Wcool[1], lb/sec	Wcool[2], lb/sec	Wcool[3], lb/sec
90,000	0.48	100	96.7	163.3	300	0.394	1.064	1.107	1.098	1.096
90,000	0.48	75	89.5	122.4	225	0.423	0.963	0.965	0.960	0.959
90,000	0.48	50	78.4	81.7	150	0.465	0.807	0.789	0.768	0.766
90,000	0.48	25	63.8	40.8	75	0.522	0.626	0.574	0.550	0.547
90,000	0.5	100	96.3	163.3	300	0.394	1.071	1.107	1.099	1.096
75,000	0.33	100	74.4	163.3	300	0.394	1.335	1.254	1.216	1.096
60,000	0.27	100	53.0	163.3	300	0.394	1.473	1.390	1.333	1.113
45,000	0.22	100	35.0	163.3	300	0.394	1.500	1.511	1.462	1.096
30,000	0.2	100	26.8	163.3	300	0.394	1.469	1.633	1.582	1.096
15,000	0.17	100	23.7	163.3	300	0.394	1.387	1.741	1.713	1.102
0	0.125	100	27.9	163.3	300	0.394	1.251	1.852	1.826	1.112

The LP compressor was set up with 14.5% surge margin and the IP and HP compressors were set up with 17.5% surge margin at the 90,000 ft design point condition. At the lower altitudes it was necessary to use compressor bleed on both the LPC and IPC to maintain at least 10% surge margin. This is necessary due to the degree that the compressors are spooled back in speed at the lower altitudes. It was discovered that a more optimum cycle resulted if this bleed was dumped overboard.

Both the parasitic and heat loss power extractions were input as a function of IPC and HPC spool speeds. Therefore, whenever the engine is spooled back in speed at the lower altitudes, these two losses have been decreased accordingly.

3.6.5 Coleman Engine - NT Technology

The Coleman engine poses unique off-design analytical challenges. Methods that can be used to model the Coleman engine in the off-design mode include selecting the "typical" operation/control variables for varying power such as spool speed (rpm), turbine rotor inlet temperature (RIT), and exhaust area. Due to the feedback feature of the Coleman engine, however, several more variables are present over a conventional gas turbine cycle, including work split between the turbines and feedback flow ratio (FFR). Based on the results of that study, fixed geometry components were selected with a constant turbine work split defined by enthalpy drop, $\%\Delta H$. Power is controlled by varying RIT, rpm, and FFR. This method not only retains an optimum part power SFC characteristic; it is also desirable because fixed geometry configurations equate to lower engine weight and higher reliability, and reduced rpm and RIT equate to improved life. Low energy feedback flow (with just sufficient pressure to recirculate) was essential and thus necessitated a single spool (or turbine load transferring) arrangement.

An assumption of constant $\%\Delta H$ was made to fix the work split and allow FFR to be varied to maintain this work split. This method was chosen over a method of fixing work split defined by horsepower (including flow), $\%\Delta HP$, because the latter method required variable turbine geometry and had less desirable part-power SFC characteristics. The constant $\%\Delta H$ assumption is similar to that of a stage loading in a multistage turbine. Future studies should address multiturbine off-design performance characteristics on a single shaft. The $\%\Delta H$ at the design point is 54.38% as noted in section 3.1.5.

Due to the complexity of the Coleman cycle, several off-design simplifications were assumed. Both the intercooler and recuperator were assumed to have constant effectiveness throughout the operating range and pressure losses default to a function of flow parameter (or Mach number) squared. The maximum power SFCs at lower altitudes (below 30,000 ft) will be lower than if the model included variable heat exchanger effectiveness. Combustion efficiency and pressure loss were simplified accordingly. More

research is needed in studying the combustion process of the Coleman engine because the combustion process uses recirculated flow that contains partially combusted products, and the combustion is near stoichiometric. Due to higher pressures from the higher compression ratio, and higher temperatures from the recirculated flow, the burner loading is lower than the turboshaft configurations (higher efficiency) without having to increase burner size.

The same approach to Reynolds number corrections as discussed in section 3.6.1.1 applies to this configuration.

The feedback flow re-entry into the mainstream flow path is modeled as an in-flow bleed. An energy balance is used to calculate the mixed temperature, but the pressure is not calculated through an appropriate "mixing". It is simply "dumped" and assumes the pressure of the mainstream.

The first phase of the off-design analysis involved analyzing maximum power points from sea level up to the design altitude of 90,000 ft. A flat rating of 1600 hp was imposed until the 2500°F BOT limit was reached. Figure 117 shows a SFC versus altitude plot for maximum power at several Mach numbers (Mach = 0.0, 0.2, 0.4, and 0.6). The second phase of the off-design analysis involved developing power hooks at 90,000 ft. Figure 118 shows SFC versus power at 90,000 ft for Mach = 0.2, 0.4, and 0.6.

Table 21 contains a summary of the Coleman engine powerplant performance for both 90,000 ft, 0.48 Mach part power and a typical climb at maximum power. The maximum power setting was defined as an HPT RIT of 2500°F. The engine was limited to 1600 shp at the lower altitudes. Section 3.6.1.1 has a more detailed discussion of the contents of Table 21.

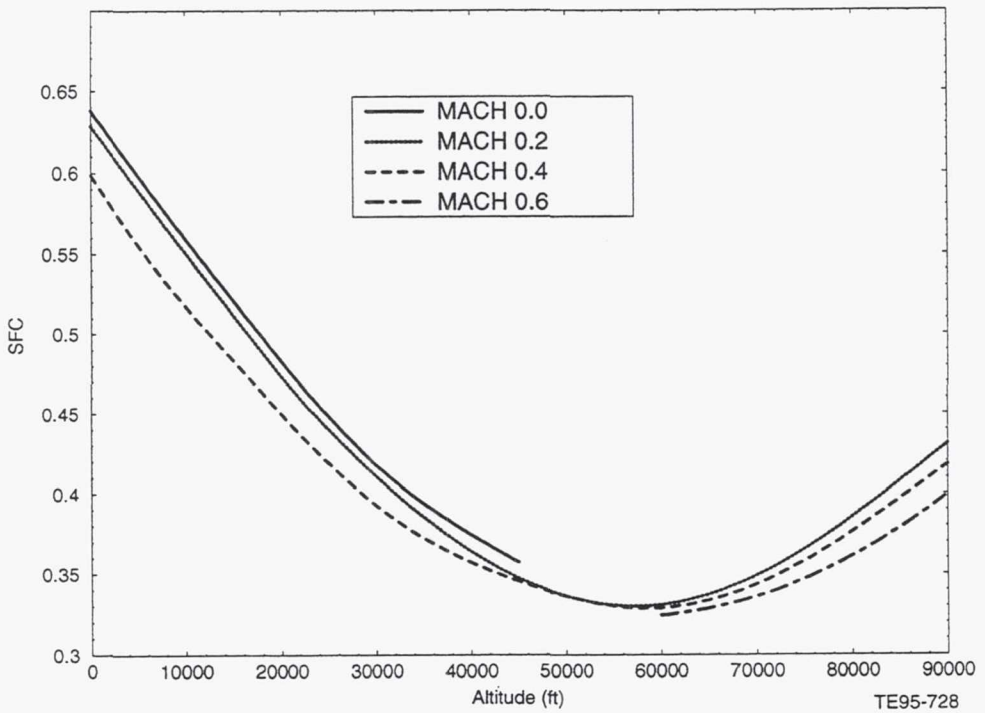

Figure 117. ERAST Coleman engine off-design analysis: maximum power (1600 shp flat rating).

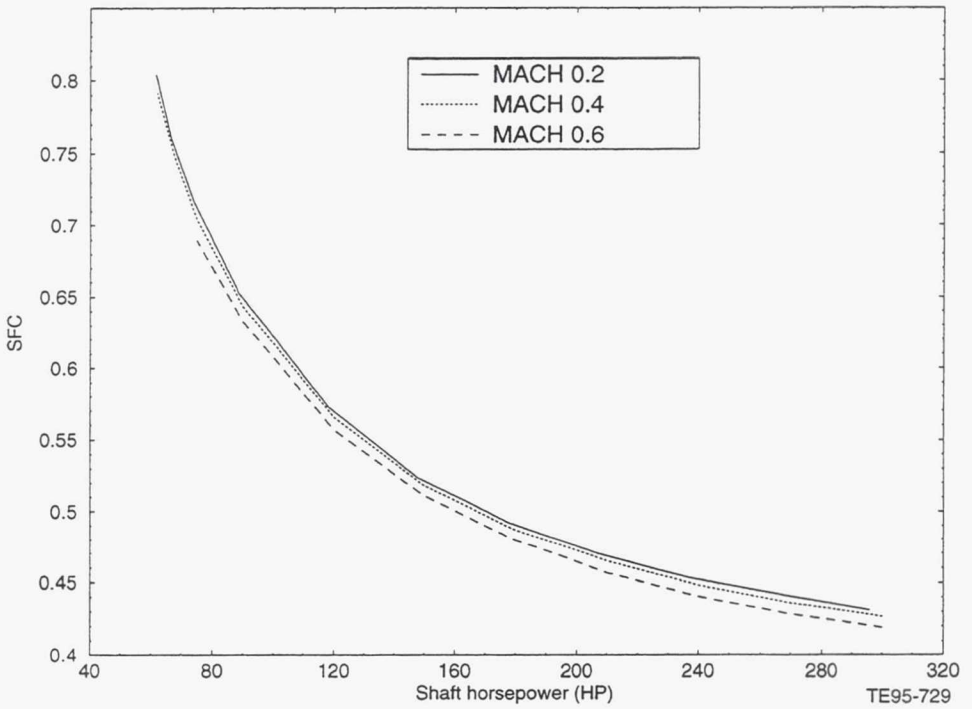

Figure 118. ERAST Coleman engine off-design analysis: part power performance, 90,000 ft/ISA.

Table 21.
Fuel consumption and airflow requirements for Coleman engine, 90,000 ft, 0.48 Mach load line and typical climb at maximum power standard day, uninstalled.

Altitude, ft	Mach	Power setting, %	% corrected N LPC	Shp, hp	SFC, lb/hr/hp	Weng inlet, lb/sec	Wcool, lb/sec
90,000	0.48	100	101.9	354.6	0.411	0.648	1.940
90,000	0.48	75	96.4	266.0	0.435	0.579	1.610
90,000	0.48	50	90.3	177.3	0.486	0.504	1.278
90,000	0.48	25	81.5	88.6	0.644	0.409	0.898
90,000	0.5	100	101.9	357.0	0.409	0.651	1.951
75,000	0.33	100	101.8	721.2	0.366	1.189	3.426
60,000	0.27	100	100.3	1600	0.331	2.387	6.768
45,000	0.22	100	83.8	1600	0.348	3.157	6.994
30,000	0.2	100	69.9	1600	0.410	4.564	7.881
15,000	0.17	100	59.1	1600	0.512	6.466	8.956
0	0.125	100	53.1	1600	0.630	10.648	12.589

Future analysis of the Coleman engine should address a more detailed discussion of the aspects that were simplified, such as combustion, off-design heat exchanger characteristics, and feedback flow mixing. Other factors, such as engine operability, engine starting, shaft dynamics, the HPT acting more like a power turbine (operating point moves significantly on the map), and engine control, should be addressed.

3.6.6 Turboshaft Engine - SOA and NT Technology

To model the ERAST turboshaft engine configurations for off-design analysis, the individual components are modeled individually and integrated using TERMAP. Component performance maps for

the compressor, gas generator turbine, and power turbine were obtained from the HALE engine model and scaled according to design point conditions described in sections 3.1.6.1 through 3.1.6.3. Combustion efficiency calculated as a function of burner loading parameter was also taken from the HALE engine and is derived from AE 3007 combustor data. Parasitic horsepower losses consisting of bearing, sump, and windage losses were modeled as a linear function of corrected gas generator speed. Parasitic losses associated with waste heat rejection were modeled as a function of RIT for each model. The recuperated model has a larger loss, as discussed in sections 3.1.6 and 3.3.3.

The power turbine for all three configurations was kept at 100% open at the 90,000 ft maximum power design point to allow maximum turbine efficiency but was closed to 70% open at lower altitudes and part power conditions to keep RIT elevated and thus provide better SFC. This was especially apparent with the recuperated turboshaft model, which was much more efficient at very high temperatures. The engine limits imposed during the off-design analysis were a corrected compressor speed of 105%, an RIT of 2500°F, a corrected gas generator turbine speed of 118%, and a corrected power turbine speed of 118%. The power turbine speed was held constant at 15,000 rpm and the engine was flat rated to 1600 hp throughout all the off-design analysis.

In addition to the off-design component modeling mentioned, the recuperated turboshaft engine required that the recuperator be modeled for off-design operation (see section 3.3.2 for discussion). Off-design effectiveness as well as hot and cold side pressure losses were calculated and included in the cycle matching. Two different fuels were used in the off-design analysis: JP-5, which has a fuel heating value (FHV) of 18,500 Btu/lbm, and hydrogen, which has a FHV of 51,593 Btu/lbm. The first part of the off-design analysis consisted of running maximum power points from sea level up to the design point altitude of 90,000 ft. Figures 119 through 122 show plots of SFC versus altitude for all three turboshaft configurations for Mach numbers 0.0, 0.2, 0.4, and 0.6. Figures 123 through 125 show plots of SFC versus power at 90,000 ft for the part power portion of the off-design analysis. All plots show the results of using JP-5 and hydrogen fuels on the same plot.

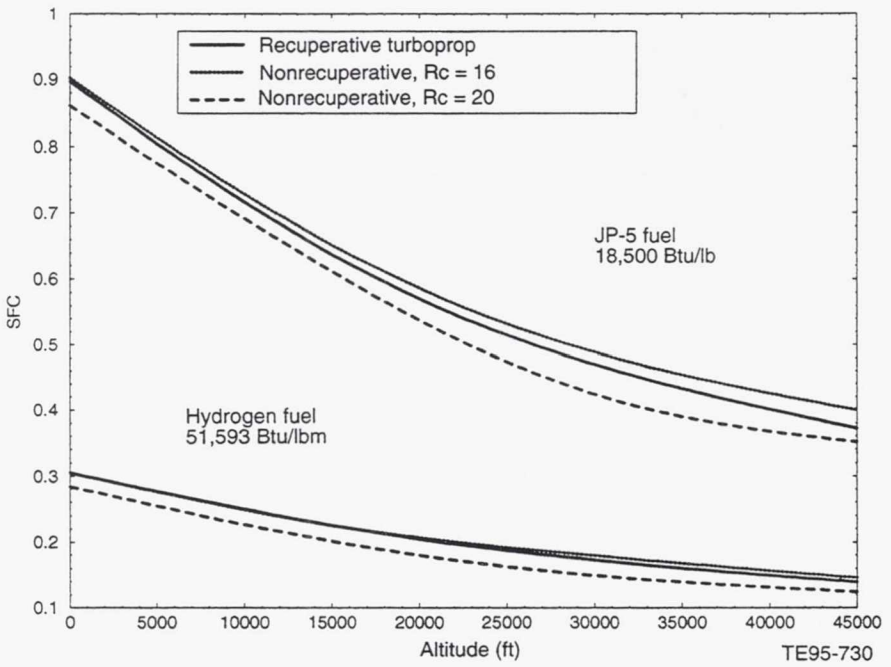

Figure 119. ERAST turboshaft off-design analysis: maximum power (1600 shp flat rating), Mach 0.0 ISA.

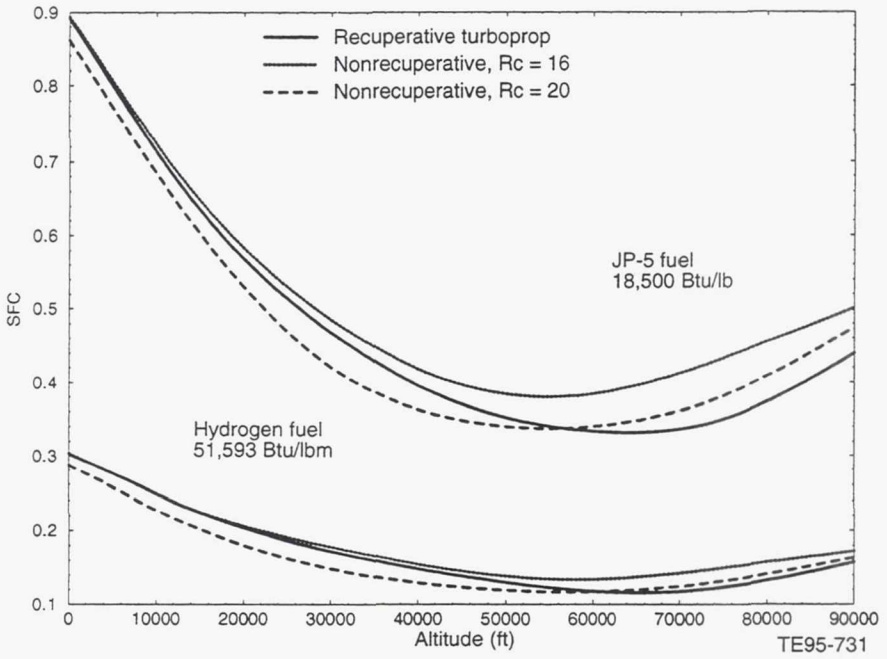

Figure 120. ERAST turboshaft off-design analysis: maximum power (1600 shp flat rating), Mach 0.2 ISA.

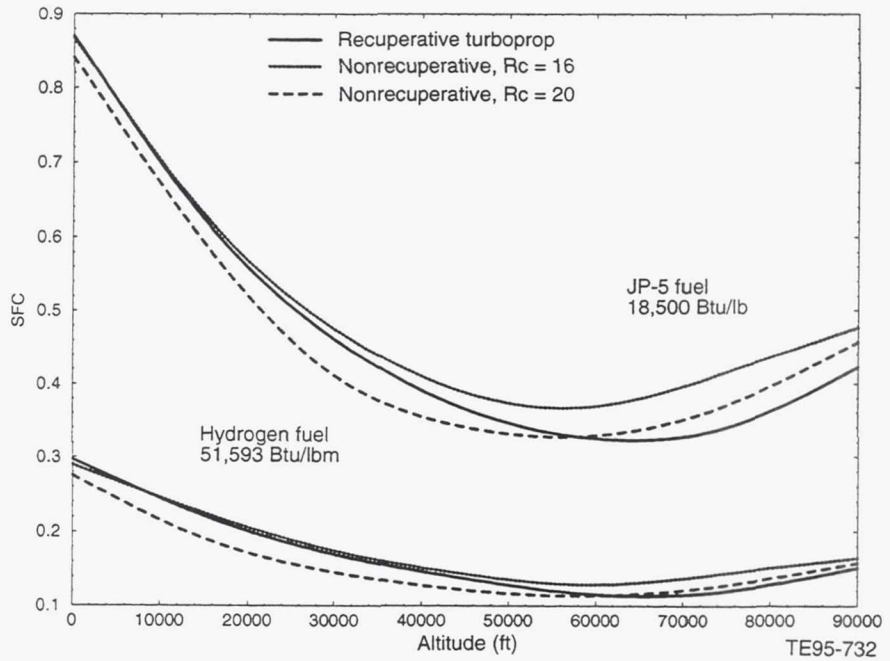

Figure 121. ERAST turboshaft off-design analysis: maximum power (1600 shp flat rating), Mach 0.4 ISA.

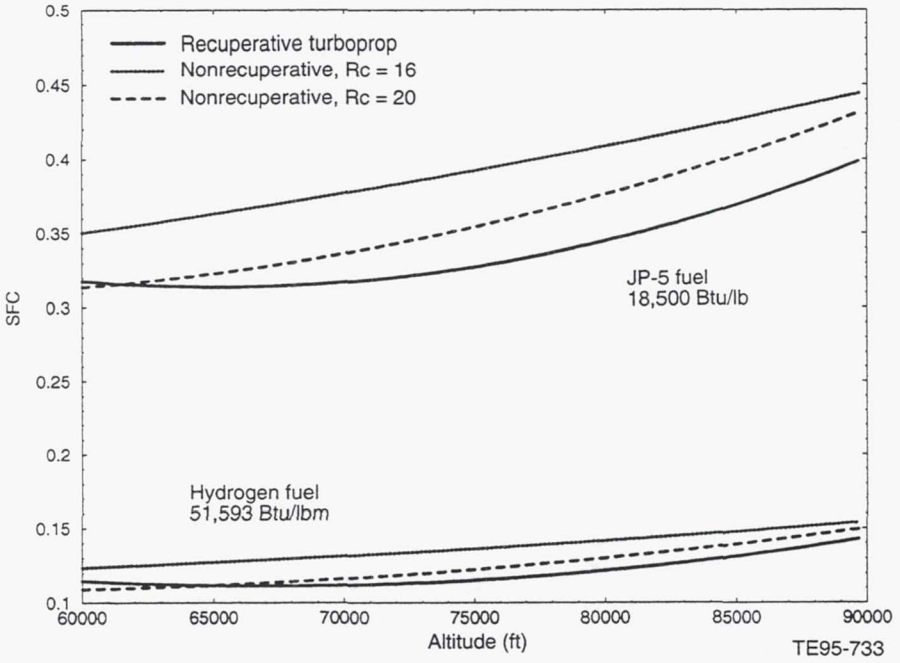

Figure 122. ERAST turboshaft off-design analysis: maximum power (1600 shp flat rating), Mach 0.6 ISA.

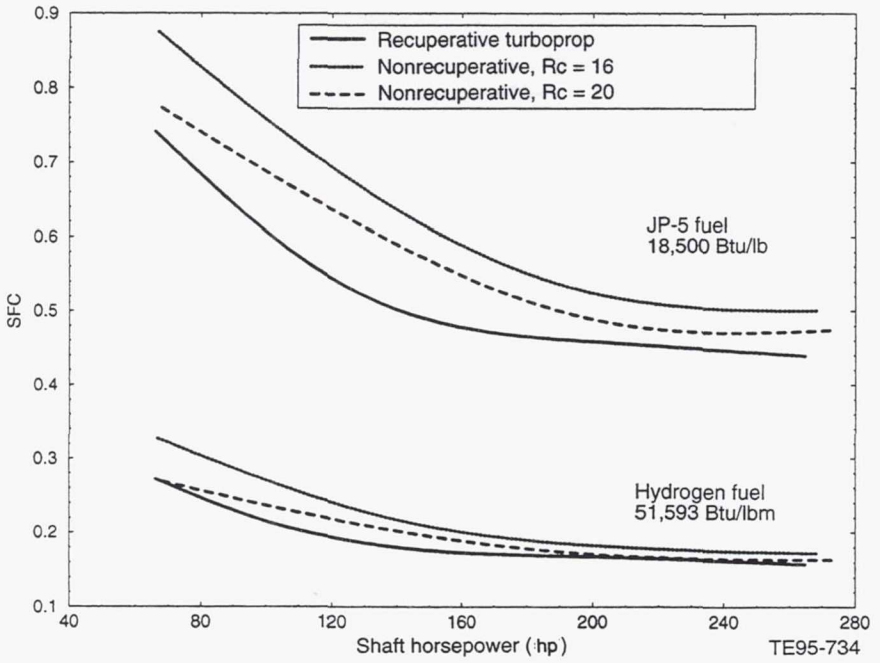

Figure 123. ERAST turboshaft off-design analysis: part power performance, 90,000 ft/0.2 Mach/ISA.

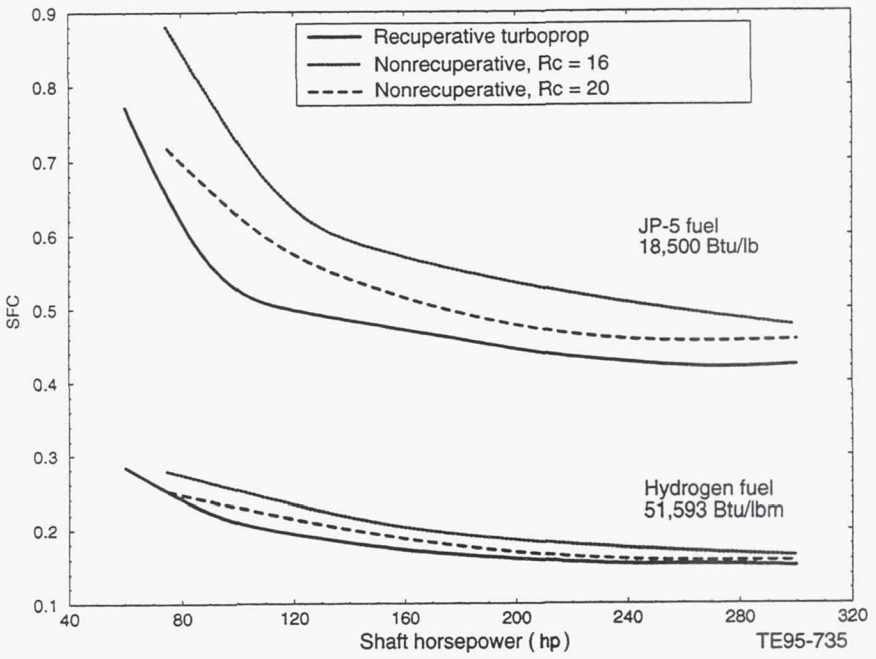

Figure 124. ERAST turboshaft off-design analysis: part power performance, 90,000 ft/0.4 Mach/ISA.

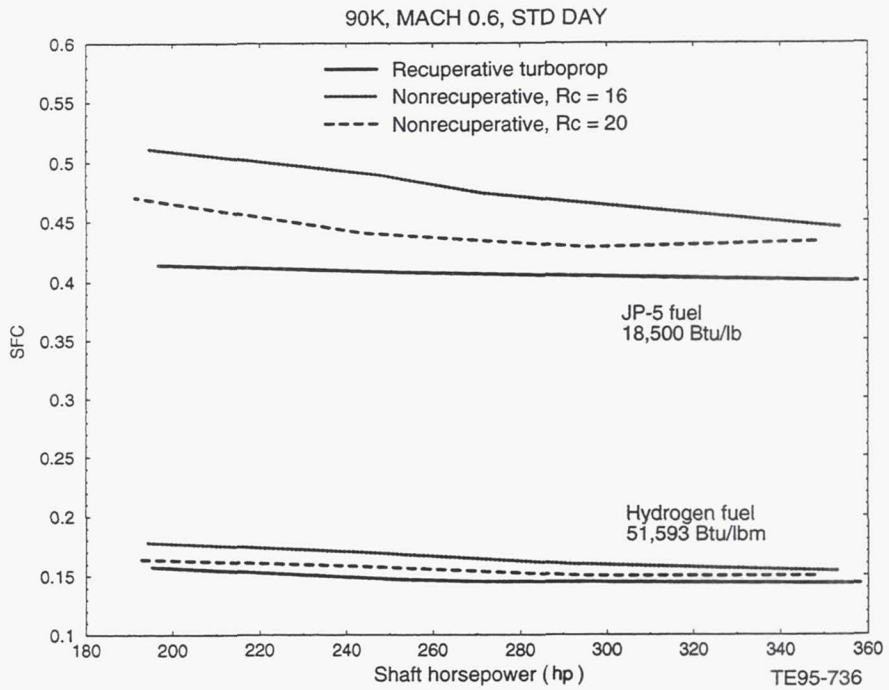

Figure 125. ERAST turboshaft off-design analysis: part power performance, 90,000 ft/0.6 Mach/ISA.

Tables 22 through 25 contain a summary of the turboshaft engines performance for both 90,000 ft, 0.48 Mach part power and a typical climb at maximum power. The maximum power setting was defined as an HPT RIT of 2500°F. The engines were limited to 1600 shp at the lower altitudes.

Table 22.
Fuel consumption and airflow requirements for recuperated turboshaft, Rc = 16:1, 90,000 ft, 0.48 Mach load line and typical climb at maximum power standard day, uninstalled.

Altitude, ft	Mach	Power setting, %	% corrected N LPC	Shp, hp	SFC, lb/hr/hp	Weng inlet, lb/sec
90,000	0.48	100	101.8	319.3	0.414	1.710
90,000	0.48	75	97.2	239.5	0.430	1.554
90,000	0.48	50	87.6	159.7	0.447	1.034
90,000	0.48	25	79.7	79.8	0.643	0.732
90,000	0.5	100	101.8	325.1	0.412	1.729
75,000	0.33	100	99.0	728.3	0.345	3.141
60,000	0.27	100	105.0	1560.8	0.331	6.908
45,000	0.22	100	94.8	1600	0.370	11.614
30,000	0.2	100	88.5	1600	0.468	18.695
15,000	0.17	100	83.3	1600	0.635	27.462
0	0.125	100	79.9	1600	0.894	39.476

Table 23.
Fuel consumption and airflow requirements for nonrecuperated turboshaft, Rc = 16:1, 90,000 ft, 0.48 Mach load line and typical climb at maximum power standard day, uninstalled.

Altitude, ft	Mach	Power setting, %	% corrected N LPC	Shp, hp	SFC, lb/hr/hp	Weng inlet, lb/sec
90,000	0.48	100	101.7	317.8	0.465	1.424
90,000	0.48	75	97.1	238.3	0.481	1.287
90,000	0.48	50	87.6	158.9	0.561	0.867
90,000	0.48	25	79.9	79.5	0.764	0.625
90,000	0.5	100	101.7	323.3	0.462	1.440
75,000	0.33	100	98.3	650.5	0.423	2.572
60,000	0.27	100	105.0	1441.7	0.380	5.758
45,000	0.22	100	95.3	1600	0.396	9.882
30,000	0.2	100	88.6	1600	0.485	15.657
15,000	0.17	100	83.0	1600	0.648	22.647
0	0.125	100	79.4	1600	0.899	32.151

Table 24.
Fuel consumption and airflow requirements for nonrecuperated turboshaft, Rc = 20:1, JP-5 fuel, 90,000 ft, 0.48 Mach load line and typical climb at maximum power standard day, uninstalled.

Altitude, ft	Mach	Power setting, %	% corrected N LPC	Shp, hp	SFC, lb/hr/hp	Weng inlet, lb/sec
90,000	0.48	100	101.9	316.8	0.448	1.429
90,000	0.48	75	96.7	237.6	0.452	1.271
90,000	0.48	50	87.6	158.4	0.511	0.869
90,000	0.48	25	80.2	79.2	0.687	0.638
90,000	0.5	100	101.8	321.3	0.446	1.444
75,000	0.33	100	100.3	730.4	0.375	2.689
60,000	0.27	100	105.0	1497.5	0.337	5.767
45,000	0.22	100	94.7	1600	0.348	9.653
30,000	0.2	100	87.8	1600	0.421	15.192
15,000	0.17	100	82.7	1600	0.612	22.217
0	0.125	100	79.2	1600	0.860	31.606

Table 25.
Fuel consumption and airflow requirements for nonrecuperated turboshaft, Rc = 20:1, hydrogen fuel, 90,000 ft, 0.48 Mach load line and typical climb at maximum power standard day, uninstalled.

Altitude, ft	Mach	Power setting, %	% corrected N LPC	Shp, hp	SFC, lb/hr/hp	Weng inlet, lb/sec
90,000	0.48	100	101.9	316.2	0.155	1.304
90,000	0.48	75	96.6	237.1	0.159	1.156
90,000	0.48	50	87.1	158.1	0.178	0.779
90,000	0.48	25	79.4	79	0.241	0.559
90,000	0.5	100	101.9	321.0	0.154	1.319
75,000	0.33	100	100.3	728.6	0.130	2.457
60,000	0.27	100	105.0	1488.5	0.116	5.265
45,000	0.22	100	94.6	1600	0.123	8.768
30,000	0.2	100	87.4	1600	0.149	13.681
15,000	0.17	100	82.7	1600	0.204	19.492
0	0.125	100	79.1	1600	0.282	28.078

The same approach to Reynolds number corrections as discussed in section 3.6.1.1 applies to this configuration. In addition to Reynolds corrections on compressor efficiency, corrections were also applied to airflow and pressure ratio.

3.6.7 Fuel Cell Engine - Advanced Technology

An off-design analysis was not conducted for the fuel cell engine.

3.7 WEIGHT ANALYSIS

Previous work on the High Altitude Long Endurance (HALE) program established general engine configuration and sizing of components required to condition the ambient air at high altitudes. The ERAST study extends the HALE UAV mission to an altitude of 90,000 ft and expands the number of propulsion system configurations being evaluated in this program to 11. From a weight analysis standpoint the 11 configurations were divided into 3 fundamental categories and they are turbocharged pistons, turboshafts, and a combination of turbocharged pistons and turboshafts. The detailed weight

analysis was performed on all propulsion systems designed for 300 shp. The final propulsion system weight was dictated by and scaled from the mission analysis results.

3.7.1 Core Engine

The two-stroke diesel propulsion core weight was obtained from a previous study. The four-stroke diesel core weight was scaled from previous outside studies on engine arrangements (V, in-line, opposed). The four-stroke spark ignition core weight was obtained from open literature for the Teledyne Continental Motors TSIO 520 configuration. Additional weight was added for the liquid cooled cylinders and manifolds. The rotary engine weight was obtained from RPI.

The fuel cell core engine weight was estimated using a projected power density ratio of 5.0 lb/hp for a mid-1995 time frame. This density ratio was increased by a factor of 1.5 to account for air filtration (oil free agent), heat exchangers, and piping. Therefore, the core engine estimated weight was 2250 lb (7.5 x 300). A DC motor weight was estimated based on a starter/generator for an advanced military turbojet engine drawing and assumed density plus control weight function. The estimated weight (210 lb) was added to the turbomachinery external weight number shown later in Table 27.

3.7.2 Turbomachinery Core

Turbomachinery weights for the four spool turbo-compounded, two-stroke diesel concept were calculated from the design layout and used as the baseline for the remaining piston and rotary engines. The turboshaft engine turbomachinery is based on the Allison T406 turboshaft engine, scaled to the ERAST altitude operating condition. Adjustments to the basic T406 engine had been made in the HALE study and these adjustments were carried on into the ERAST program. Once the recuperated turboshaft engine was sized for ERAST, the remaining two nonrecuperative turboshaft engines were scaled using this as the base design.

Intercoolers and recuperators were sized and interconnecting ducting and structures were estimated from the dimensioned layouts and performance cycle parameters. As a check, where Allison production axial and centrifugal modules were similar, scaled comparisons were made. The following paragraphs present much of the detail concerning component weight scaling as follows.

1. The form of the weight scaling equations will be given. In general, weights are functions of performance parameters that are obtained from design point cycle performance sheets provided for each of the 11 engines and that were also available from component hardware design point cycle performance sheets.
2. The new or desired component performance parameter and the reference component performance parameter form a ratio that is raised to some exponential power. In the scaling equations the precise exponent values will not be given, but an indication of the exponential impact will be implied by using the letter "n" for exponents less than unity and "m" for exponents equal to or greater than unity. Since temperature is not explicitly used, reference engine/component performance at new cycle RITs were predicted for consistency in scaling.
3. Reference weights are usually actual components weights and the reference engines will be stated for the various components.

3.7.2.1 Inlet/Forward Support

The inlet support weights were T406/HALE weights. Weight scaling assumed that the new inlet weight varied as the corrected air mass flow entering the inlet.

$$\text{Inlet weight} = \text{Ref inlet weight} * \left[\frac{\text{New Wa in}}{\text{Ref Wa in}}\right]^{(m)}$$

3.7.2.2 Compressor (Case and Rotor)

At least three reference compressor weights were used in the study. The high pressure ratio all axial compressors for the three turboshaft engines used the T406/HALE 14-stage all axial compressor. The low-pressure axial compressor for the rotary and the fuel cell engines used Model 250-C20 four- and six-stage all axial compressors. All of the centrifugal compressors used Model 250-C30 impellers and cases. The same weight scaling equations were used in each scaling case.

$$\text{LP compressor weight} = \text{Ref LPC weight} * \left[\frac{\text{New Wa LPC in}}{\text{Ref Wa LPC in}}\right]^{(m)} * \left[\frac{\text{New LPC Rc}}{\text{Ref LPC Rc}}\right]^{(n)}$$

3.7.2.3 Diffuser/Combustor

For the Coleman, fuel cell, and turboshaft engines the HALE combustor was used for scaling.

$$\text{Combustor weight} = \text{Ref combustor weight} * \left[\frac{\text{New Wa comb in}}{\text{Ref Wa comb in}}\right]^{(m)} * \left[\frac{\text{New Rcoa}}{\text{Ref Rcoa}}\right]^{(n)}$$

3.7.2.4 Turbine

The turbines used in the program were all of axial flow design. The 11 ERAST engines used turbines having one to four stages. The high pressure and intermediate pressure turbine rotors were scaled from one- or two-stage turbines. The low pressure turbines were scaled from existing two- to three-stage turbines. Power turbines were scaled from three-stage turbines with adjustments made to account for four-stage turbines. For high RIT turbines the HALE HP turbine was used for scaling. Lower temperature one- and two-stage turbines used for scaling were from T406 and Model 250 engines depending on flow size. For three- and four-stage LP and power turbines, the three-stage HALE turboshaft power turbine and three-stage AE 3007 turbofan LP turbine were used for weight scaling. Turbine weight scaling parameters included inlet and outlet corrected air mass flows, enthalpy extracted, and percent cooling air used.

$$\text{Axial HP turb weight} = \text{Ref HPT weight} * 0.5 * \left[\left[\frac{\text{New Wa HPT in}}{\text{Ref Wa HPT in}}\right]^{(m)} * \left[\frac{\text{New Wa HPT out}}{\text{Ref Wa HPT out}}\right]^{(m)}\right] *$$

$$\left[\frac{\text{New HPT (h in} - \text{h out)}}{\text{Ref HPT (h in} - \text{h out)}}\right]^{(m)} * \left[\frac{\text{Ref (100} - \%\text{ HPT cool air)}}{\text{New (100} - \%\text{ HPT cool air)}}\right]^{(m)}$$

3.7.2.5 Rear Turbine Bearing Support/Aft Support

The rear support is sized by the corrected airflow out of the final turbine stage and the absolute pressure at the final turbine stage discharge. The T406/HALE rear turbine support was the reference component for all of the ERAST engines.

$$\text{RTBS weight} = \text{Ref RTBS weight} * \left[\frac{\text{New Wa LPT out}}{\text{Ref Wa LPT out}}\right]^{(m)} * \left[\frac{\text{New LPT Press}}{\text{Ref LPT Press}}\right]^{(n)}$$

3.7.3 Turbomachinery Externals

The turbomachinery externals included the following items or systems: fuel system, ignition system, lubrication system, air system, controls/electronics system, engine monitoring system (EMS), accessory gearbox, full authority digital electronic control (FADEC), and starter. The externals were based on T406 engine externals.

3.7.3.1 *Fuel System*

The fuel system is comprised of the fuel pump and metering unit (FPMU), which varies in weight with the maximum fuel flow anywhere in the operating cycle (e.g., climb out), the weight of the fuel nozzles and hardware, and the remaining hardware (lines, manifolds, brackets, nuts, bolts, etc). The fuel nozzle weights were assumed to be the same as the T406 fuel nozzles. The balance of the weight is the hardware that was assumed to vary with combustor corrected inlet air mass flow. The sum of these items constituted the fuel system weight.

Fuel system

$$\text{FPMU weight} = \text{Ref FPMU weight} * \left[\frac{\text{New fuel rate, lbm/hr}}{\text{Old fuel rate, lbm/hr}}\right]^{(n)} +$$

$$\text{Fuel nozzle weight} = \_\_\_\_\_ +$$

$$\text{Fuel manifold and wt remainder} = \text{Ref weight} * \left[\frac{\text{New Wa comb cor in}}{\text{Old Wa comb cor in}}\right]^{(n)}$$

Total fuel system weight = _____ lbm

3.7.3.2 *Ignition System*

The ignition system was also estimated from T406 ignition system weights. Igniters and exciters were assumed to be the same weight as the T406 parts. Leads and hardware were assumed to vary in weight with combustor inlet airflow.

Ignition System

Igniters, qty = (___) Ref igniters:_____
Exciters, qty = (___) Ref exciters:_____

$$\text{Leads qty and hardware} = (\_\_\_) = \text{Ref weight} * \left[\frac{\text{New Wa comb cor in}}{\text{Old Wa comb cor in}}\right]^{(n)}$$

Igniters, qty = (___) * Ref igniter wt (_____) = _____
Exciters, qty = (___) * Ref exciter wt (_____) = _____

$$\text{Leads qty and hardware} = (\_\_\_) = \_\_\_\_\_ * \left[\frac{\text{lb/sec}}{\text{lb/sec}}\right]^{(n)} = \_\_\_\_\_$$

Total ignition system weight _____ lbm

3.7.3.3 *Lubrication, Air, and EMS*

The weights of these T406 systems were determined as a percentage of the T406 core engine components. For the ERAST weights these percentages were multiplied times the weights determined for the 11 core engines. The percentages of core engine weights were as follows:

- lubrication system—7.07%
- air system—1.49%
- engine monitoring system—1.64%

3.7.3.4 Controls/Electronics, Accessory Gearbox, Starter, and FADEC

For these systems it was decided that there should be practical minimum weights. Therefore, for eight of the engines (all but the three turboshaft engines), these accessory or system minimum weights were defined as follows:

- controls/electronics—10.0 lbm
- accessory gearbox—20.0 lbm
- starter—15.0 lbm
- FADEC—8.0 lbm

For the turboshaft engines, the FADEC and accessory gearbox weights were set at the current T406 weights of 11.2 lbm and 31.7 lbm, respectively. The controls/electronics and starter weights were T406 weights scaled by the ratio of inlet airflow to an exponential.

3.7.4 Weight Summaries

Table 26 shows a summary of the ERAST engine turbomachinery configurations for each of the 11 propulsion systems. Turbomachinery weights for these components are summarized in Table 27. Included in this summary are the weights of the turbomachinery modules, the external systems for the turbomachinery, and the ducting to and from intercoolers and recuperators. Refer to Table 4 for the weights of the complete propulsion systems.

3.8 MISSION ANALYSIS

The mission analysis conducted for this program included modeling the aircraft, assessing the installation factors for each engine configuration, performing a mission simulation, and sizing the engines and aircraft to perform the design mission. For this analysis, Allison used a computer program, called the mission analysis program (MAP), that is designed specifically to correctly size an engine/aircraft configuration to perform a specified design mission.

3.8.1 Aircraft Modeling

Allison uses a complete geometric, weight, and aerodynamic description of an aircraft configuration to conduct mission analysis studies. Geometric constraints are tracked and configuration drag incremented, or decremented, due to changes in maximum cross-sectional area, wetted area, and wing area. The aircraft weight breakdown is modeled in MAP so that components may be scaled as the engine and aircraft change size. This weight breakdown is important since some components, such as landing gear weight, will scale with aircraft takeoff gross weight (TOGW); some, such as engine mount weight, scale with engine weight. Other components, such as fuel system weight that changes with fuel required, vary with values other than the aircraft or engine, and there are also components such as the payload that do not vary during the sizing exercise.

3.8.2 Baseline Aircraft Source

The baseline aircraft description was obtained from a model of the aircraft constructed by NASA-Ames using the ACSYNT aircraft design and analysis program. This is a program developed through Government and industry sponsorship that is able to optimize an aircraft configuration for specified mission requirements and technology level. Allison does not utilize ACSYNT, but NASA-Ames provided Allison with a detailed description of the aircraft design that they obtained using a simulation of a turbocharged piston engine.

3.8.3 Baseline Aircraft Description

The Stratolite baseline aircraft is geometrically similar to, and a growth version of, the Aurora Perseus high altitude unmanned vehicle. It has a high aspect ratio wing, short fuselage, containing the engine, payload, and fuel, and weighs about 3000 lb at takeoff. The wing is mounted high and the propeller is a pusher configuration with the drive shaft extending through the aft fuselage and attaching to the

Table 26.
ERAST candidate engine turbomachinery configurations.

		Initial Scale	<---------Scaled from 4-Spool, 2-Stroke, TurboCompounded Diesel---------->							<---------No Intercoolers--------->		
Engine		4-Spool	3-Spool	3-Spool	4-Spool	4-Spool	3-Spool	2-Spool	3-Spool	T/S Rc=16	T/S Rc=16	T/S Rc=20
Module	Axial/Centrif	2StD-TC	2StD-NTC	4StD-NTC	4StSI-TC	4StSIH2-TC	Rotary	Coleman	Fuel Cell	Recup	N-Recup	N-Recup
Turbomachinery Core												
LP Compressor	Axial/Centrif	Centrif	Centrif	Centrif	Centrif	Centrif	Axial	Centrif	Axial	-	-	-
	No. Stages	1	1	1	1	1	5	1	4	-	-	-
IntrCool/Recup	From->To	LPC->IPC	LPC->IPC	LPC->IPC	LPC->IPC	LPC->IPC	LPC->IPC	-	-	-	-	-
	No Units:Sides	4:4	4:4	2:2	2:2	2:2	6:2	-	-	-	-	-
IP Compressor	Axial/Centrif	Centrif	Centrif	Centrif	Centrif	Centrif	Centrif	-	Axial	-	-	-
	No. Stages	1	1	1	1	1	1	-	4	-	-	-
IntrCool/Recup	From->To	IPC->HPC	IPC->HPC	IPC->HPC	IPC->HPC	IPC->HPC	IPC->HPC	-	-	-	-	-
	No Units:Sides	4:4	4:4	2:2	2:2	2:2	6:2	-	-	-	-	-
HP Compressor	Axial/Centrif	Centrif	Centrif	Centrif	Centrif	Centrif	Centrif	Centrif	Centrif	Axial	Axial	Axial
	No. Stages	1	1	1	1	1	1	1	1	14	14	15
AftrCool/Recup	From->To	-	-	HPC->Eng	HPC->Eng	HPC->Eng	HPC->Eng	HPC->Com	-	HPC->Diff	-	-
	No Units:Sides	-	-	2:2	2:2	2:2	6:2	6:6	-	6:6	-	-
Combustor	Yes/No	No	No	No	No	No	No	Yes	Yes	Yes	Yes	Yes
HP Turbine	Axial/Centrif	Axial	Axial	Axial	Axial	Axial	Axial	Axial	Axial	Axial	Axial	Axial
	No. Stages	1	1	1	1	1	1	2	2	2	2	2
Recuperator	From->To	-	-	-	-	-	-	HPT->I/C	-	-	-	-
	No Units:Sides	-	-	-	-	-	-	6:6	-	-	-	-
IP Turbine	Axial/Centrif	Axial	Axial	Axial	Axial	Axial	Axial	-	Axial	-	-	-
	No. Stages	1	1	2	1	1	2	-	2	-	-	-
InterCooler	From->To	-	-	-	-	-	-	Recup->HP	-	-	-	-
	No Units:Sides	-	-	-	-	-	-	10:2	-	-	-	-
LP Turbine	Axial/Centrif	Axial	Axial	Axial	Axial	Axial	Axial	Axial	Axial	-	-	-
	No. Stages	2	3	2	2	2	2	2	2	-	-	-
IntrCool/Recup	From->To	-	-	-	-	-	-	-	-	PT->Exit	-	-
	No Units:Sides	-	-	-	-	-	-	-	-	6:6	-	-
P Turbine	Axial/Centrif	Axial	-	-	Axial	Axial	-	-	-	Axial	Axial	Axial
	No. Stages	3	-	-	3	4	-	-	-	3	3	3

Table 27.
ERAST engine candidate weights configurations.

Engine Module	Source		Initial Scale 4-Spool 2StD-TC	<--------Scaled from 4-Spool, 2-Stroke, TurboCompounded Diesel----------> 3-Spool 2StD-NTC	3-Spool 4StD-NTC	4-Spool 4StSI-TC	4-Spool 4StSIH2-TC	3-Spool Rotary	2-Spool Coleman	3-Spool Fuel Cell	<--------No Intercoolers---------> T/S Rc=16 Recup	T/S Rc=16 N-Recup	T/S Rc=20 N-Recup
Turbomachinery Core		Spools->	3+PT	3	3	3+PT	3+PT	3	1	3	1+PT	1+PT	1+PT
Inlet	T406 > Al		--	--	--	--	--	89.4	--	361.2	144.6	120.6	120.8
LPC Case	C30 > Al		24.4	33.9	42.3	22.9	23.1	84.9	35.8	442.3	--	--	--
LPC Rotor	C30 > Al		31.9	44.4	55.3	30.0	30.3	65.0	46.8	338.6	--	--	--
LPC Exit Scroll	C30 > Al		--	--	11.5	6.2	6.3	18.4	13.0	--	--	--	--
LPC->I/C Duct	Al		20.6	21.2	14.8	11.4	11.6	21.5	--	--	--	--	--
I/C->IPC Duct	T800 Ti > Al		20.7	20.8	39.5	36.5	14.0	64.3	73.3	--	--	--	--
IPC Case	C30 > Ti		7.5	7.6	11.7	8.3	8.4	18.0	--	69.0	--	--	--
IPC Rotor	C30		9.8	9.9	15.4	10.8	10.9	23.6	--	52.8	--	--	--
IPC Exit Scroll	C30 > Ti		--	--	3.2	2.2	2.3	5.1	--	--	--	--	--
IPC->I/C Duct	Al		11.7	11.8	7.6	14.7	7.4	5.5	11.2	--	--	--	--
I/C->HPC Duct	T800 Ti > Al		19.9	19.9	27.7	27.8	28.0	15.3	6.5	--	--	--	--
HPC Case	C30 > Ti		1.6	1.6	2.2	2.1	2.1	3.5	32.2	40.3	--	--	--
HPC Rotor	C30		2.1	2.1	2.9	2.7	2.7	4.5	42.1	14.6	576.0	467.5	500.8
HPC Exit Scroll	C30 > Ti		0.6	0.6	0.6	0.6	0.6	1.0	11.7	19.7	--	--	--
HPC->A/C Duct	Al		--	--	0.9	1.1	1.1	1.3	9.8	--	--	--	--
Cold Side->Core Engine			1.4	1.4	1.7	2.2	2.2	1.0	9.8	--	--	--	--
Combustor			--	--	--	--	--	--	133.7	178.8	340.3	208.1	186.5
Core Engine->Hot Side			2.5	5.3	2.6	3.9	3.9	3.5	6.5	--	--	--	--
HPT Inlet Scroll	C30		4.6	4.6	6.6	7.0	7.5	6.4	--	--	--	--	--
HPT Case	C30 HPT1		7.0	6.7	9.3	8.5	8.8	12.4	109.0	73.7	--	--	--
HPT Rotor	C30 HPT1		2.8	2.7	3.2	2.9	3.0	4.3	187.5	126.8	714.1	554.0	529.5
IPT Case	C30 HPT2		2.7	2.6	5.9	2.8	2.6	36.5	--	154.7	--	--	--
IPT Rotor	C30 HPT2		7.2	7.2	8.4	4.0	3.7	14.5	--	329.2	--	--	--
LPT Case	C30 PT		24.1	11.0	34.2	21.9	18.0	19.7	43.9	179.2	--	--	--
LPT Rotor (2)	C30 PT		9.6	--	--	8.7	7.1	32.6	72.5	296.0	--	--	--
LPT Rotor (3)	PT Rotor (3)		--	13.7	42.4	--	--	--	--	--	--	--	--
PT Case	3007a > Ti		40.1	--	--	45.7	63.6	--	--	--	--	--	--
PT Rotor (3)	3007a > Ti		49.8	--	--	56.8	79.0	--	--	--	695.6	735.5	705.5
RTBS	3007a > Ti		17.2	9.0	21.7	17.9	18.2	32.1	29.4	206.5	127.9	115.1	112.4
Core Total Weight, lbm			**319.9**	**238.1**	**371.7**	**359.6**	**366.5**	**584.3**	**874.6**	**2,883.6**	**2,598.5**	**2,200.8**	**2,155.5**
Turbomachinery Externals		Fuel+Ign	--	--	--	--	--	--	--	50.0	40.0	56.6	55.1	53.4
Lube	3007a x	7.07%	22.6	16.8	26.3	25.4	25.9	41.3	61.8	203.9	74.6	62.2	62.3
Air	3007a x	1.49%	4.8	3.5	5.5	5.4	5.5	8.7	13.0	43.0	30.3	27.7	27.7
Controls/Elect	est.		10.0	10.0	10.0	10.0	10.0	10.0	10.0	10.0	29.7	27.1	27.1
Acc. GB	est.		20.0	20.0	20.0	20.0	20.0	20.0	20.0	20.0	31.7	31.7	31.7
Starter	est.		15.0	15.0	15.0	15.0	15.0	15.0	20.2	15.0	52.0	43.4	43.4
EMS	3007a x	1.64%	5.2	3.9	6.1	5.9	6.0	9.6	14.3	47.3	20.3	18.5	18.5
FADEC	est.		8.0	8.0	8.0	8.0	8.0	8.0	8.0	8.0	11.2	11.2	11.2
Externals Total Weight, lbm			**85.6**	**77.3**	**90.9**	**89.7**	**90.4**	**112.6**	**197.4**	**387.1**	**306.4**	**276.9**	**275.4**

propeller behind the tail. The baseline aircraft included minimal landing gear. The propellers locked in place horizontally after the mission was completed and before landing to prevent damage. The design details of this aircraft are shown in Tables 28 and 29. A three view drawing of the baseline aircraft is shown in Figure 126. This aircraft proved a useful baseline as the final engine/aircraft configurations sized both higher and lower than the baseline.

Table 28.
Aircraft weight breakdown.

Qmax:	5.8
Design load factor:	4.7
Ultimate load factor:	7
Structure and material:	Composite skin, stringer

Component	Pounds	Kilograms	Percent
Airframe structure	*1142.8*	*518.4*	*38.07*
Wing	688.3	312.2	22.93
Fuselage	315.8	143.2	10.52
Horizontal tail (low)	28.3	12.8	0.94
Vertical tail	51.7	23.4	1.72
Nacelles	0	0	0
Landing gear	58.7	26.6	1.96
Propulsion	*864.7*	*392.2*	*28.81*
Engines (1)	816.8	370.5	27.21
Fuel system	47.9	21.7	1.6
Fixed equipment	*192.6*	*87.3*	*6.41*
Hyd & pneumatic	23.5	10.6	0.78
Electrical	56.1	25.5	1.87
Avionics	17	7.7	0.56
Instrumentation	4.4	2	0.15
De-ice & air cond	75.2	34.1	2.51
Auxiliary gear	0	0	0
Furnish & equipment	3.3	1.5	0.11
Flight controls	13.1	5.9	0.44
Empty weight	*2200.1*	*998*	*73.29*
Operating items	*15*	*6.8*	*0.5*
Flight crew	0	0	0
Crew baggage and provisions	0	0	0
Unusable fuel and oil	15	6.8	0.5
Operating weight empty	*2215.1*	*1004.8*	*73.79*
Fuel	*566.1*	*256.8*	*18.86*
Payload	*220.5*	*100*	*7.35*
Total weight	***3001.7***	***1361.6***	***100***

Table 29.
Aircraft characteristics.

General		Weights	
Weight, lbm	3002	Structure, lbm	1143
W/S	7.4	Propulsion, lbm	865
Thrust/weight	0.46	Fixed eq, lbm	193
N(z) ult	7	Fuel, lbm	581
Crew	0	Payload, lbm	221
Passenger	0	Oper IT, lbm	15
Engine		Fuselage	
Number	1	Length, ft	24.4
Length, ft	5.6	Diameter, ft	3
Diameter, ft	2.9	Volume, ft^3	135.9
Weight, lbm	816.8	Wetted area, ft^2	214.6
Thrust SLS, lbf	1371	Fineness ratio	8.1
Specific fuel consumption SLS	0.21		
ESF	0		

	Wing	Htail	Vtail
Area, ft^2	405.4	38.2	50
Wetted area, ft^2	818.7	76.7	100.3
Span, ft	97.3	15.1	12.4
LE sweep, deg	0.9	5	5
C/4 sweep, deg	0.4	3.2	2.3
Aspect ratio	23.33	5.96	3.08
Taper ratio	0.69	0.68	0.55
Thickness/chord root	0.14	0.08	0.08
Thickness/chord tip	0.14	0.08	0.08
Root chord	4.9	3	5.2
Tip chord	3.4	2.1	2.9
MA chord	4.2	2.6	4.1
Location of LE	12.6	29.3	28.7

The aerodynamic and weight characteristics of the aircraft were established by NASA Ames through studies outside this contract. Their assistance in establishing our baseline aircraft was invaluable as Allison has little aircraft design experience in the field of high altitude, unmanned aerial vehicles.

3.8.4 Baseline Aircraft Modeling

Allison's MAP accepts input of an aircraft's aerodynamic, geometric, and weight characteristics. The baseline aircraft geometric and weight characteristics were input to the program without modification from the data given previously. The aerodynamic characteristics, specifically Cd versus Cl, are input in as a function of Mach number. NASA-Ames supplied drag polar (Cd as a function of Cl) data for the aircraft at Mach numbers from 0.05 to 0.50, all at sea level. These data were used by the program with a provisions for a correction to the drag for altitude. Good agreement of aircraft drag and mission fuel burn was obtained using MAP to NASA-Ames final design results.

3.8.5 Engine and Aircraft Modeling Unique to This Program

Certain items unique to the ERAST propulsion system study required modifications to the basic sizing process of Allison's MAP. Specifically, the propeller and gearbox needed individual sizing algorithms. To provide proper sizing of these components, propeller and gearbox weight could not be scaled simply with engine size. Correct scaling was not linear, and there was a difference in scaling for the turbo-

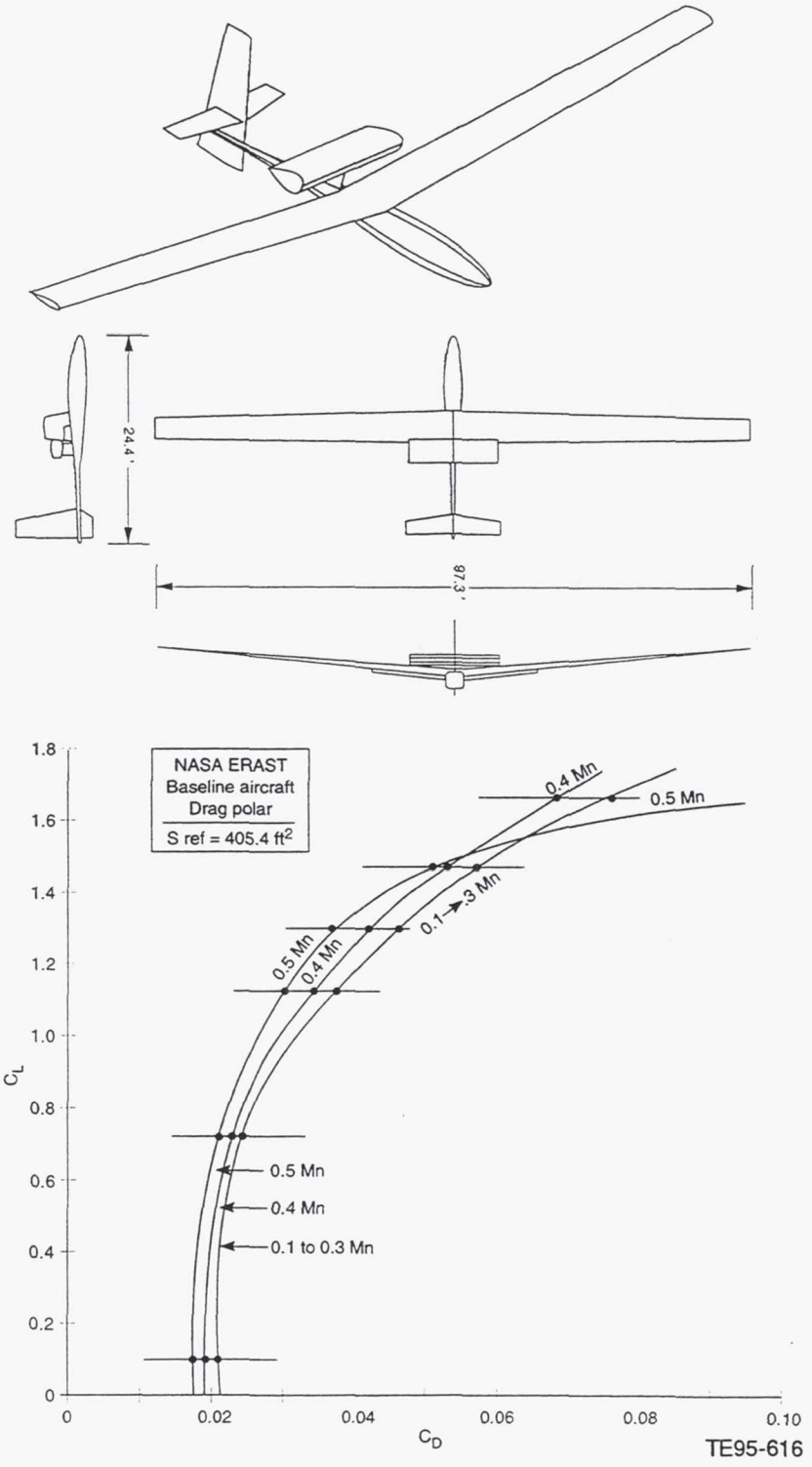

Figure 126. Stratolite reference airplane.

compounded spark ignition and diesel engines and the turboshaft engines due to the driving speed difference and additional hardware for turbo-compounding between the different engine types.

3.8.5.1 Propeller

The propeller unity size weights were derived by the same scaling laws as used inside MAP to determine the propeller weight for the sized engine and aircraft. The propeller used as a baseline for this process is designed for 135 hp at 0.4 Mach and 90,000 ft. The diameter is 18.75 ft with a Cli of 0.583 and an activity factor of 124 that provides an 80% propeller efficiency. Additionally, the propeller is designed to handle 300 hp as a maximum. This propeller weighs 200 lb. These data were provided to Allison by Hamilton Standard under subcontract.

It is noted that Allison assumed an 80% efficient propeller at climb and cruise conditions for all candidate engines to provide an equitable or "referee" propeller to convert shaft power to thrust.

To scale this propeller for changes in maximum and cruise horsepower requirements, the weight was varied using two different equations: one for propeller diameter and the other for maximum horsepower. Propeller diameter is determined by holding constant the cruise prop shaft horsepower (pshp) loading function, which is cruise power divided by the diameter squared. The equations are as follows:

$$PL_{cruise} = (\text{base cruise pshp})/(\text{base prop dia})^2 = 135/(18.75)^2 = 0.384 = \text{const}$$
$$PL_{max\ base} = (\text{base max pshp})/(\text{base prop dia})^2 = 300/(18.75)^2 = 0.853 = \text{const}$$

in scaling: $\text{Prop dia} = (\text{cruise pshp}/PL_{cruise})^{1/2}$

$$\text{Prop wt } (\Delta \text{ dia}) = 4.27*(\text{prop dia} - 18.75) + 200 \text{ (lb)}$$
$$\text{Prop wt } (\Delta \text{ dia \& max PL}) = [\text{prop wt } (\Delta \text{ dia})]\ (PL_{max}/PL_{max\ base})^{0.34}$$

The unity engines varied in the amount of maximum horsepower produced, so this in itself causes changes in the propeller weight before engine and aircraft sizing.

3.8.5.2 Gearbox

The gearbox weight is a function of the mechanical arrangement as well as the power handling requirements. The gearbox scaling is broken into three categories based on the type of engine. The turbo-compounded engines, due to the additional mechanical arrangement required to combine power output of the main engine and the turbomachinery, are heavier and scaled by maximum horsepower. For turbo-compounded diesels, the equation is given as follows:

$$\text{Gearbox weight} = (pshp_{max} * 35)^{0.59} \text{ pounds}$$

The spark ignition, turbo-compounded engine gearbox weight is given in the following equation:

$$\text{Gearbox weight} = (pshp_{max} * 52)^{0.59} \text{ pounds}$$

The difference in scaling constants is due to the speed difference between the diesel and spark ignition systems.

All the other non-turbo-compounded systems used a common scaling law for the gearbox weight. This equation is as follows:

$$\text{Reduction gearbox weight} = 430\ [(pshp_{in}/rpm_{in})*(pshp_{out}/rpm_{out})]^{.3333} \text{ pounds}$$

These algorithms for gearbox weight were developed at Allison by the weights and mechanical design groups that have extensive experience in designing gearboxes for a wide range of aviation, marine, and industrial applications.

3.8.6 Main Engine Inlet and Exhaust

The baseline aircraft, as designed by NASA-Ames, included an inlet and exhaust to supply the engine. These components were sized for a triple turbocharged spark ignition system. The main engine inlet is sized to accommodate the airflow requirements of the turbomachinery. The inlet drag of this system, not including the ram drag, is negligible for systems such as this, operating subsonically. The ram drag of the system is accounted for in the installed thrust calculations for the engine. The inlet ducting for all the various propulsion systems is short and the weight not accounted over and above that provided for in the baseline aircraft.

3.8.7 Radiators and Intercooler Air Handling

The nonturboshaft engines all had additional air handling requirements in the form of radiators, oil coolers, and intercoolers. The general arrangement drawings of the engines, which have already been presented, and the weights were included in the engine weight buildup. In addition to accounting for the weight of these components, there is also a drag penalty to assign. This drag addition is based on the frontal area of the component, therefore assuming a constant pressure drop through the heat exchanger, and also assuming that the inlet is properly designed for subsonic operation. A reasonably designed subsonic inlet will not incur a measurable drag penalty other than the momentum loss of the captured airflow.

3.8.8 Engine Descriptions for Installation

The engine installations take into account the weight and physical dimensions of the various complete propulsion systems. A compilation of the unity size engine weights, including propeller, gearbox, additional cooling components, and envelope dimensions are shown in Table 30. Frontal areas were minimized for each propulsion system installation.

3.8.9 Mission Modeling

The ERAST mission is modeled by the definition of three phases of flight: an engine warm-up period, climb to altitude, and cruise as illustrated in Figure 127. Climb and cruise are the significant segments of the flight and determine how the engine and aircraft will size. The warm-up period is 20 sec at maximum horsepower to simulate engine start, warm-up, and takeoff.

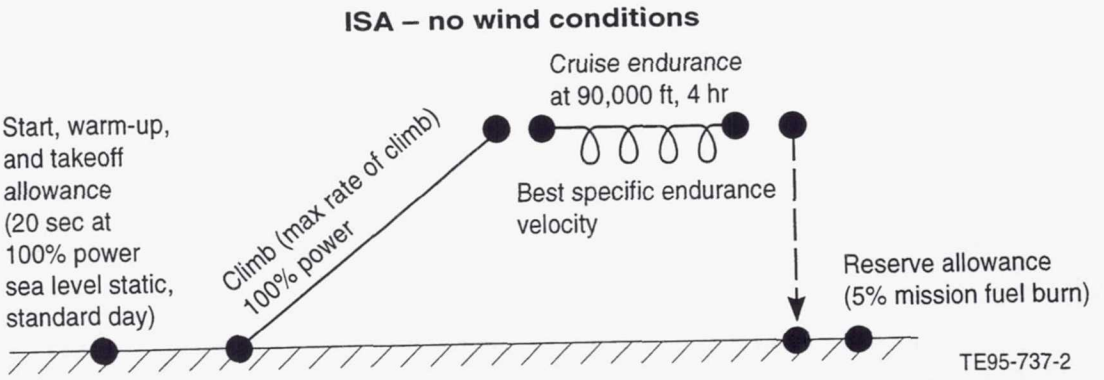

Figure 127. ERAST mission profile.

Table 30.
Unity size engine characteristics—designed for 300 shp.

Technology Level	ADV	ADV	SOA	SOA	NT	NT	NT	NT	SOA	NT
Engine	2 Stroke	2 Stroke	4 Stroke	4 Stroke	4 Stroke	Rotary	Coleman	Recup TS	Non Recup	Non Recup
Identification	Turbocomp	Non TC	Non TC	Turbocomp	Turbocomp	Non TC	Rc = 35	Rc = 16	Rc = 16	Rc = 20
	Diesel	Diesel	Diesel	Spark Ign	Spark Ign		Turboshaft	Turboshaft	Turboshaft	Turboshaft
Fuel Type	Diesel	Diesel	Diesel	Avgas	H2	Avgas	JP	JP	JP	JP
Power										
PSHP @ 0.4M/90K	300	300	300	300	300	300	300	300	300	300
PSHP, Max	860.1	638.5	304	475	565	300	1600	1600	1600	1600
Propeller Diameter, ft	27.96	27.96	27.96	27.96	27.96	27.96	27.96	27.96	27.96	27.96
Weights										
Core (if piston), lb	230	230	610	486	486	420	----	----	----	----
Turbomachinery, lb	541.4	472.1	830.7	715.2	695.2	1023.5	1521.6	4237.6 *	2539.1	2492.3
Gearbox, lb	439	214.5	196.7	391	433	130.6	266.8	293.3	293.4	293.5
Propeller, lb	261	235.8	183.2	213.2	227	182.5	319.5	322.4	322.4	322.3
Total, lb	1471.4	1152.4	1820.6	1805.4	1841.2	1756.6	2107.9	4853.3	3154.9	3108.1
SFC @ 0.4M/90K	0.242	0.303	0.342	0.371	0.097	0.394	0.427	0.423	0.477	0.457
Dimensions										
Max Diameter, ft	3.06	3.26	4.41	4.17	4.17	4.17	6.25	6.07	3.76	3.73
Length, ft	8.04	6.61	9.63	9.42	9.42	13	10.3	15.14	10.84	10.89
Volume, cu ft	59.13	55.17	147.09	128.65	128.65	177.54	316	438.12	120.4	119
Auxillary air handling Area (Frontal)										
Intercooler 1, sq in	730.4	978.8	1109.8	651.2	651.2	1780.8	4804	----	----	----
Intercooler 2, sq in	847.2	1168.4	1024	598	598	2113.2	----	----	----	----
Intercooler 3, sq in	----	----	1217.4	696.8	696.8	1993.8	----	----	----	----
Radiator, sq in	481.1	609.6	1241.5	1084.3	728	2018.6	----	----	----	----
Oil Cooler, sq in	30.6	107.4	327.4	343.2	329.1	349.4	----	----	----	----
Total, sq in	2089.3	2864.2	4920.1	3373.5	3003.1	8255.8	4804	----	----	----
Total, sq ft	14.51	19.89	34.17	23.42	20.85	57.33	33.36	----	----	----
DRAG, ~(Δ fe), sq ft	1.54	2.11	3.63	2.49	2.21	6.09	3.54	----	----	----

* incl. recup

3.8.9.1 Climb

The climb is performed from sea level to 90,000 ft and at the airspeed that gives maximum rate of climb. This is a unique value for each engine and aircraft combination as shown in the mission summaries. Because each engine was designed to provide about 300 hp at the aircraft design cruise point of 0.4 Mn/90,000 ft, the horsepower produced at lower altitudes during the climb is significantly different for the various engines. For example, the turboshaft engines can produce approximately 9,000 hp at sea level while the rotary engine produces only 300 hp. It was decided that the engines that could produce more horsepower at lower altitudes should not be limited to 300 hp in climb. Engines were optimized for "flat rated" horsepower, that is the maximum horsepower that the engine would be allowed to produce, by calculating the flat rated horsepower that gave the lowest aircraft TOGW.

The trade-off is that with more horsepower, the aircraft is able to climb more quickly to altitude; but to handle the increase in horsepower, both the gearbox and propeller become heavier, thus increasing the propulsion system weight. There are fuel burn savings, compounded by a decrease in aircraft weight and thus sizing horsepower required, but offset by the weight gain. The result of this optimization, conducted on a turboshaft engine, is that about 1,600 hp, over five times the design cruise power only a sixth of the thermodynamic power available, is optimum for lowest TOGW. The nonturboshaft engines are also allowed to flat rate at a higher horsepower if this additional power is available. Note from Table 30 that the nonturboshaft engines have only limited increased horsepower available.

3.8.9.2 Cruise

Cruise is 4 hr in duration and is conducted at the flight speed that gives best lift over drag ratio. This is typically at a fairly low airspeed, in this case about 0.47 Mach. At the end of the 4 hr duration the fuel is expended and it is assumed that the aircraft glides back to sea level. There is no requirement or provision for a powered descent.

3.8.10 Engine and Aircraft Sizing

The engine and aircraft are sized during the iteration steps performed by MAP. Engine sizing is normally obtained by defining a maneuver requirement, such as a specific excess power at a given flight condition, or by specifying a maximum takeoff distance requirement. For ERAST, a rate of climb requirement at the initial cruise aircraft weight and flight condition was specified. This gave a specific requirement such that the engine would be scaled up or down, depending on the aircraft weight, and so that the system would have a reasonable rate of climb at the top of climb. This prevents the engine from being sized just large enough to asymptotically approach the cruise altitude, and unreasonably extending the climb phase.

The aircraft is sized such that the fuel required, based on mission fuel burn calculations, matches the fuel available, based on a weight and volume analysis of the aircraft. The process is iterative, with good convergence achieved in three to five passes. The engine sizing and aircraft sizing loops interact with more engine power required when fuel available is increased, and additional fuel required when the engine size increases.

The results of this sizing process obtained from MAP are summarized in Table 31. This table shows the resulting aircraft takeoff gross weight for each candidate powerplant along with aircraft maximum length and diameter. Also contained in this table is powerplant scaled horsepower for cruise, maximum horsepower level, and weights for the engine, reduction gearbox, and propeller. The initial and final optimum endurance velocities, percent thrust, and TSFC levels for the 4-hr phase are also summarized.

A mission analysis for the recuperative turboshaft and the fuel cell powerplant was not possible due to their excessive weight. The MAP program would not converge when simulating these powerplants in the ERAST aircraft.

Table 31.
Mission analysis summary.

Technology Level	ADV	ADV	SOA	SOA	NT	NT	NT	SOA	NT	NT	NT	ADV
Engine Description	2 Stroke Diesel Turbo	2 Stroke Diesel	4 Stroke Diesel	4 Stroke Spark Turbo	4 Stroke Spark Turbo	Rotary	Coleman Recup	Turboshaft Rc = 16	Turboshaft Rc = 20	Turboshaft Rc = 20	Turboshaft Rc = 16 Recup	Fuel Cell
Fuel Type	Diesel	Diesel	Diesel	Avgas	H2	Diesel	JP-5	JP-5	JP-5	H2	JP-5	H2
Aircraft Characteristics :												
Aircraft TOGW, lb	1956	1532	2639	2656	3325	3203	2486	3302	3166	4069		
Wing Area, sq ft	264	207	356	359	449	433	336	446	428	550		
Fuselage Length, ft	22.0	21.7	24.4	24.0	24.6	26.1	25.2	23.6	23.5	24.1		
Fuselage Diameter, ft	2.7	2.7	3.0	3.0	3.0	3.2	3.1	2.9	2.9	3.0		
Powerplant Characteristics :												
Engine Scale (Sized SHP/Unity SHP)	0.297	0.220	0.410	0.399	0.506	0.500	0.294	0.344	0.334	0.447		
Sized SHP (@0.4M/90K), hp	89	66	123	120	152	150	98	103	100	134		
Max Power Level, hp	256	140	125	190	286	150	470	551	534	716		
Engine Weight, lb	246	170	637	516	631	785	442	865	823	1106		
Reduction Gearbox Weight, lb	214	61	94	227	290	73	96	121	118	150		
Propeller Weight, lb	202	173	150	174	194	156	245	256	254	269		
Total Propulsion System Weight, lb	662	404	881	917	1115	1014	783	1242	1195	1525		
Propeller Diameter, ft	15.2	13.1	17.9	17.7	19.9	19.8	15.9	16.4	16.2	18.7		
Max Endurance Cruise @ 90K (4 hrs) :												
Initial Mn	0.49	0.48	0.48	0.49	0.50	0.46	0.48	0.51	0.51	0.52		
Final Mn	0.48	0.47	0.46	0.47	0.50	0.44	0.46	0.49	0.49	0.51		
Percent Thrust, %	83	84	87	83	84	85	96	100	100	100		
TSFCavg, lb/hr/hp	0.258	0.274	0.355	0.374	0.107	0.410	0.422	0.489	0.473	0.167		
Mission Fuel Burn, lb	128	114	274	261	94	430	255	344	313	148		

No solution

No solution

4.0 RANKING OF CONCEPTS

The 11 powerplant configurations evaluated in this ERAST study were ranked according to three categories consisting of mission suitability, risk, and cost within their respective technology levels. Each powerplant candidate was given a ranking from 1 to 10, with 10 being the best possible. Mission suitability was given a weighting factor of 0.5, risk a weighting factor of 0.3, and cost a weighting factor of 0.2. Each ranking was then multiplied by the weighting factor in each of the three categories and then all three category numbers were added to get a total. A final ranking was then done based on this total with the number one candidate being identified for each technology level. The results are presented in Table 32.

The mission suitability part of the rankings is based on the mission analysis results presented in Table 31. For example, the advanced two-stroke, non-turbo-compounded diesel has the lowest TOGW of all the advanced powerplant candidates and therefore was given the highest possible ranking of 10. The ADV 2 stroke, turbo-compounded diesel followed in having the lowest TOGW and was given a ranking of 9. This ranking continues on down to the NT recuperative turboshaft and advanced fuel cell, both of which were very heavy concepts. Because of their very large weight, the aircraft/recuperated turboshaft engine propulsion systems would not produce a converged mission solution. The fuel cell engine was considerably heavier than the recuperated turboprop; therefore, no mission analysis effort was focused on the fuel cell. Both of these candidates were given a ranking of 1, the lowest possible.

The risk part of the rankings took into account the complexity, technology level, and uniqueness of each powerplant candidate and how that might affect the development and reliability of each candidate. Since the SOA nonrecuperative, Rc=16 turboshaft, JP-5 candidate is merely a flow up scale of a current production engine, it was given the highest ranking of 10. The advanced two-stroke, non-turbo-compounded diesel received a ranking of 6 in the risk category due to its advanced technology level. The turbo-compounded version of this powerplant received a lower ranking of 5 due to the additional gearboxes required. The advanced fuel cell was ranked the lowest in this category due to its leading edge technology level and the potential development problems that could arise for this particular application.

The cost part of the rankings was based on perceived development and production costs. A high score here implies low cost. The piston and rotary engines rate higher than the turboshaft candidates. The highest ranked candidate is the SOA four-stroke, turbo-compounded, aviation gas, spark ignition powerplant. The advanced fuel cell ranked the lowest in this category.

After taking into account all three category rankings and their corresponding weighting factors, a total was calculated. The powerplant candidates were ranked based on these totals with the highest total receiving the highest ranking of one. The propulsion system employing SOA technology that was best matched for this mission was the four-stroke, non-turbo-compounded diesel. The best matched NT technology concept was the Coleman engine and the best advanced concept was the two-stroke, non-turbo-compounded diesel engine.

Table 32.
ERAST propulsion system concept ranking.

Technology Level Engine Description		SOA 4 Stroke Diesel	SOA 4 Stroke Spark Turbo	SOA Turboshaft Rc=16	NT Coleman	NT Rotary	NT Turboshaft Rc=20	NT 4 Stroke Spark Turbo	NT Turboshaft Rc=20	NT Turboshaft Rc=16 Recup	ADV 2 Stroke Diesel	ADV 2 Stroke Diesel Turbo	ADV Fuel Cell
Fuel Type		Diesel	Avgas	JP-5	JP-5	Diesel	JP-5	H2	H2	JP-5	Diesel	Diesel	H2
Mission Suitability (Weighting Factor=0.5)	Rank	7	7	5	8	6	6	5	3	1	10	9	1
	Sub Total	3.5	3.5	2.5	4	3	3	2.5	1.5	0.5	5	4.5	0.5
Risk (Weighting Factor=0.3)	Rank	8	7	10	6	7	9	5	6	9	6	5	1
	Sub Total	2.4	2.1	3	1.8	2.1	2.7	1.5	1.8	2.7	1.8	1.5	0.3
Cost (Weighting Factor=0.2)	Rank	9	10	4	7	8	4	6	4	4	7	6	1
	Sub Total	1.8	2	0.8	1.4	1.6	0.8	1.2	0.8	0.8	1.4	1.2	0.2
	Total	7.7	7.6	6.3	7.2	6.7	6.5	5.2	4.1	4	8.2	7.2	1
	Group Ranking	1	2	3	1	2	3	4	5	6	1	2	3
	Overall Ranking	2	3	7	4	5	6	8	9	10	1	4	11
		I<------- SOA = State of the Art ------->I			I<---------- NT = Near Term technology ----------->I						I<--- ADV = Advanced tech -->I		

5. CONCLUSIONS

A series of propulsion system concepts in three technology levels (SOA, NT, and advanced) were designed to carry a 100 kg sensor package to 90,000 ft and perform measurements for 4 hr. Spark ignition, diesel, rotary, gas turbine, and fuel cell propulsion system concepts were interrogated. Aircraft performance characteristics were provided by the NASA Ames Research Laboratory. Diesel, spark ignition, rotary, and fuel cell performance models were developed outside of this project. A preliminary design analysis, where all turbomachinery, heat exchangers, engine core concepts were sized for near optimum performance and weighed along with a detailed mission analysis, was completed on each propulsion system concept. Aircraft minimum TOGW was selected as the prime figure of merit in evaluating the various propulsion system concepts. Based on the preliminary design/mission analysis results and a ranking process for all propulsion systems investigated, the following conclusions have been reached:

1. Propulsion system weight was the predominate design variable.
2. Aircraft TOGW varied nearly directly with propulsion system weight.
3. Because of the relatively short mission flight duration (4 hr), specific fuel consumption did not exert a strong influence on aircraft TOGW.
4. Power levels ranged from about 65 to 150 shp for the various propulsion systems to complete the required mission.
5. Aircraft TOGW ranged from 1530 lb with the advanced two-stroke, non-turbo-compounded propulsion system to over 4000 lb with the NT hydrogen fuel turboshaft propulsion system.
6. Propeller performance information was provided by the Hamilton Standard Division of UTC. Results showed that propeller diameter would range from 13.5 to 18.7 ft, depending on the propulsion system and attendant power requirements.
7. A ranking process that considered mission suitability, risk, and cost resulted in the following ranking of propulsion system concepts:

Best in Technology	Concept
• State of the Art	Four-Stroke, Non-Turbo-Compounded Diesel
• Near Term	Coleman
• Advanced	Two-Stroke, Non-Turbo-Compounded Diesel

8. It is recommended that the top ranked concepts be further investigated for improved performance, detailed installation size, and arrangement limitations and subsequent weight analysis.
9. Had the mission analysis required a much longer cruise leg, where specific fuel consumption exerted a strong influence on TOGW, or required a larger payload, the resulting ranking of concepts might have produced different results.

6.0 REFERENCES

1. Benson, Rowland S., and Whitehouse, N. D., "Internal Combustion Engines," Vols I & II, Pergamon Press, 1st Edition, 1979.

2. Winsor, R. E., VanderBok, A. J., Hammer, W. G., "The New DEDEC Series 60 Diesel Engine," SAE Paper 870616 presented at the International Congress and Exposition, Detroit, February 23-27, 1987.

3. Wilkinson, R. E., "Design and Development of the Voyager 200/300 Liquid Cooled Aircraft Engine," USA: Society of Automotive Engineers, Inc, 1987.

4. Stroh, K. R., McFarland, R. D., Hedstrom, J. C., Inbody, M. A., and Vanderborgh, N. E., "FCSYS —A Steady-State Simulation Code for Fuel-Reforming Fuel-Cell Power Systems," Los Alamos National Laboratory report LA-UR-93-xxx, September 30, 1993.

5. Goldstein, S., "On the Vortex Theory of Screw Propellers," Proceedings of the Roy Soc, A123, 440, 1929.

6. Kays, W. M., and London, A. L., "Compact Heat Exchangers," McGraw-Hill, Inc, 2nd Edition, 1955.

REPORT DOCUMENTATION PAGE

Form Approved
OMB No. 0704-0188

1. AGENCY USE ONLY (*Leave blank*)	2. REPORT DATE	3. REPORT TYPE AND DATES COVERED
	May 1995	Final Contractor Report

4. TITLE AND SUBTITLE

Propulsion System Assessment for Very High Altitude UAV Under ERAST

5. FUNDING NUMBERS

WU–537–10–20
C–NAS3–25950

6. AUTHOR(S)

James L. Bettner, Craig S. Blandford, and Bernie J. Rezy

7. PERFORMING ORGANIZATION NAME(S) AND ADDRESS(ES)

Allison Engine Company
P.O. Box 420
Indianapolis, Indiana 46206–0420

8. PERFORMING ORGANIZATION REPORT NUMBER

E–9653

9. SPONSORING/MONITORING AGENCY NAME(S) AND ADDRESS(ES)

National Aeronautics and Space Administration
Lewis Research Center
Cleveland, Ohio 44135–3191

10. SPONSORING/MONITORING AGENCY REPORT NUMBER

NASA CR–195469
EDR 17199

11. SUPPLEMENTARY NOTES

Project Manager, Paul Senick, NASA Lewis Research Center, Aeropropulsion Analysis Office, organization code 2430, (216) 977–7024.

12a. DISTRIBUTION/AVAILABILITY STATEMENT

RESTRICTED DISTRIBUTION DOCUMENT
Distribution available only with approval of issuing office: Aeropropulsion Analysis Office, Lewis Research Center, Cleveland, Ohio 44135
Subject Category 07

12b. DISTRIBUTION CODE

13. ABSTRACT (*Maximum 200 words*)

A series of propulsion systems were configured to power a sensor platform to very high altitudes under the Experimental Research Advanced Sensor Technology (ERAST) program. The unmanned aircraft was required to carry a 100 kg instrument package to 90,000 ft altitude, collect samples and make scientific measurements for 4 hr, and then return to base. A performance screening evaluation of 11 propulsion systems for this high altitude mission was conducted. Engine configurations ranged from turboprop, spark ignition, two- and four-stroke diesel, rotary, and fuel cell concepts. Turbo- and non-turbo-compounded, recuperated and nonrecuperated arrangements, along with regular JP and hydrogen fuels were interrogated. Each configuration was carried through a preliminary design where all turbomachinery, heat exchangers, and engine core concepts were sized and weighed for near-optimum design point performance. Mission analysis, which sized the aircraft for each of the propulsion systems investigated, was conducted. From the array of configurations investigated, the propulsion system for each of three different technology levels (i.e., state of the art, near term, and far term) that was best suited for this very high altitude mission was identified and recommended for further study.

14. SUBJECT TERMS

Unmanned aerial vehicle (UAV); Environmental Research Aircraft and Sensor Technology (ERAST); High altitude propulsion

15. NUMBER OF PAGES

156

16. PRICE CODE

A08

17. SECURITY CLASSIFICATION OF REPORT	18. SECURITY CLASSIFICATION OF THIS PAGE	19. SECURITY CLASSIFICATION OF ABSTRACT	20. LIMITATION OF ABSTRACT
Unclassified	Unclassified	Unclassified	